

PHOTOSTIMULATED OXYGEN AND WATER VAPOR REACTIONS  
ON  
SEMICONDUCTING TITANIUM DIOXIDE SURFACES

by

THOMAS JOHN O'NEILL, Jr.

B.A., University of California, San Diego  
(1977)

M.Sc., University of California, Berkeley  
(1979)

SUBMITTED TO THE DEPARTMENT OF  
MATERIALS SCIENCE AND ENGINEERING  
IN PARTIAL FULFILLMENT FOR THE DEGREE OF

Doctor of Philosophy

at the

MASSACHUSETTS INSTITUTE OF TECHNOLOGY

JUNE 1984

© Massachusetts Institute of Technology, 1984

Signature of Author.....  
Department of Materials Science and Engineering  
May 4, 1984

Certified by.....  
Prof. Harry C. Gatos  
Thesis Supervisor

.....  
Dr. Jacek Lagowski  
Thesis Supervisor

Accepted by.....  
Prof. Bernhardt J. Weunsch  
Chairman, Departmental Graduate Committee

MASSACHUSETTS INSTITUTE  
OF TECHNOLOGY

Archives

JUN 29 1984

LIBRARIES

## ABSTRACT

### PHOTOSTIMULATED OXYGEN AND WATER VAPOR REACTIONS ON SEMICONDUCTING TITANIUM DIOXIDE SURFACES

by

Thomas John O'Neill, Jr.

Submitted to the Department of Materials Science and Engineering on May 4, 1984 in partial fulfillment of the requirements for the degree of Doctor of Philosophy.

The photostimulated surface phenomena and their relationship to the electrical, optical and chemical properties of real titanium dioxide surfaces were investigated. Variations in the  $TiO_2$  work function, the activity of surface electronic states and the surface bonding configurations due to the adsorption and desorption of oxygen and water vapor species have been identified. These changes can be attributed to the charge transfer chemisorption of electronegative species with unoccupied donor surface states. Adsorbate interactions with  $TiO_2$  surfaces were found to be irreversible, although the original surfaces could be reclaimed by the photo-depopulation of surface states and the desorption of adsorbed species in UHV.

For the present studies, single crystal  $TiO_2$  with no intentional impurities was doped n-type by vacuum and hydrogen reductions. This resulted in differing bulk donor defects which in turn influenced the surface behavior. A procedure for producing reproducible experimental surface conditions, without resorting to rigorous clean surface preparation, was developed and utilized as a basis for monitoring those surface changes due to adsorbate interactions. The results of this investigation thus provide information applicable to the behavior occurring in  $TiO_2$  photoelectrochemical cells, but at a level more basic and less ambiguous than can be derived from wet electrochemical cell measurements.

Contact potential difference measurements were employed to monitor the charge transfer occurring at the semiconductor surface during adsorbate interactions. The results of these measurements are first phenomenologically presented in terms of  $TiO_2$  work function fluctuations, and then analyzed to yield information on the change in surface charge associated with surface state populations and the surface electron affinity. X-ray photoelectron spectroscopy was used to monitor changes in the surface bonding arrangements of chemisorbed species.

The initial effect of ambient exposures to  $\text{TiO}_2$  surfaces is to decrease the work function of the material. This decrease is interpreted in terms of the simultaneous charge transfer chemisorption of electronegative species and the surface electron-hole recombination. The amount of exposure necessary to saturate such chemisorption surface reactions varies with bulk defect type, illumination conditions, and interacting ambient. These exposures spanned the range from  $10^3$  to greater than  $10^{12}$  Langmuirs. Optical stimulation of energy greater than that of the  $\text{TiO}_2$  band gap was necessary to produce surface state depopulation and desorption reactions. Optical stimulation alone could not produce flat band conditions, due to the high density of surface states.

Modelling of the photostimulated adsorbate interactions involved the delineation of three different sets of surface states: Ti surface states similar to conduction band states,  $\text{Ti}^{3+}$  defect states associated with surface oxygen depletion and, Ti states effected by chemisorbed species. Adsorbate interactions were confined to the Ti surface states. Fluctuations in their densities occurred with ambient exposure, bulk defect type and illumination conditions.

Ti states on the semiconductor were continuously distributed in energy below the conduction band, had short relaxation times and large effective hole capture cross sections, similar to conduction band states.  $\text{Ti}^{3+}$  defect and adsorbate-effected states both had long relaxation times (several minutes). Shockley-Read recombination analysis revealed hole capture cross sections of  $10^{-18} \text{ cm}^2$  and  $5 \times 10^{-19} \text{ cm}^2$  for the  $\text{Ti}^{3+}$  defect states and the adsorbate-effected states, respectively.

Thesis Supervisors:

Dr. Harry C. Gatos, Professor of Electronic Materials.

Dr. Jacek Lagowski, Senior Research Associate.

## TABLE OF CONTENTS

	<u>page</u>
Abstract.....	2
Table of Contents.....	4
List of Figures.....	7
List of Tables.....	11
Acknowledgements.....	12
Chapter 1. Introduction.....	13
Chapter 2. Literature Survey.....	18
2.1 TiO <sub>2</sub> Photoelectrochemical Cells.....	18
2.2 Semiconductor-Liquid Interfaces.....	21
2.2.1 Double Layers.....	23
2.2.2 Interfacial Interactions.....	25
2.2.2.a Surface States.....	25
2.2.2.b Fluctuating Solution Energy Levels.....	28
2.2.2.c Adsorption.....	31
2.3 Defects in TiO <sub>2</sub> .....	33
2.3.1 Surface States.....	33
2.3.2 Bulk Defect and Electromigration Effects.....	35
2.4 Vacuum Studies.....	38
2.4.1 Clean TiO <sub>2</sub> Surfaces.....	39
2.4.2 Real TiO <sub>2</sub> Surfaces.....	43
2.5 Theoretical Considerations.....	46
2.5.1 Photostimulated Semiconductor Behavior near Surfaces.....	46
2.5.2 Charge Transfer at Semiconductor Surfaces.....	48
2.5.2.a Classical Surface Recombination.....	48

## TABLE OF CONTENTS

	<u>page</u>
2.5.2.b Semiconductor-Liquid Charge Transfer.....	50
2.5.2.c Charge Transfer Chemisorption.....	52
Chapter 3. Motivation and Scope.....	55
Chapter 4. Experimental Procedures.....	57
4.1 Sample Preparation.....	57
4.2 Apparatus.....	60
4.3 Experimental Techniques.....	63
4.3.1 Measurement of Semiconductor Work Function.....	63
4.3.2 Measurement of Surface Potential.....	66
4.3.3 Measurement of Surface Electronic States.....	69
4.3.4 Measurement of Charge Transfer Activity.....	69
4.3.5 Measurement of Surface Bonding Arrangements.....	73
4.4 Procedure.....	82
4.4.1 Control Surface Conditions.....	82
4.4.2 Light Ambient Cycling.....	85
4.4.3 Dark Ambient Cycling.....	88
4.4.4 XPS Experimentation.....	90
Chapter 5. Results and Discussion.....	91
5.1 Results.....	91
5.1.1 Preliminary Bulk and Surface Information.....	91
5.1.2 Ambient Cycling.....	98
5.1.2.a Phenomenological Work Function Changes.....	101
5.1.2.b Surface Charge Changes.....	103
5.1.3 XPS Information.....	105
5.2 Discussion.....	115
5.2.1 Control Surface Characteristics.....	115

## TABLE OF CONTENTS

	<u>page</u>
5.2.2 Influence of Ambients.....	121
5.2.2.a Adsorption.....	121
5.2.2.b Desorption.....	130
5.2.3 Surface State Modelling.....	137
5.2.4 Electronic Surface Transitions.....	148
5.2.5 Surface Recombination.....	149
5.2.6 Charge Transfer Chemisorption.....	151
5.2.7 Surface Degradation.....	154
Chapter 6. Conclusions and Recommendations.....	156
Appendices.....	164
A: Selected Properties of TiO <sub>2</sub> (rutile).....	164
B: Growth and Reduction of TiO <sub>2</sub> (rutile).....	168
C: Derivation of Equations.....	172
D: CPD Ambient Cycling Data.....	178
Bibliography.....	203
Biographic Note.....	210

## LIST OF FIGURES

	<u>page</u>
1.1 Schematic Photoelectrochemical Cell and Energy Diagram.....	14
2.1 TiO <sub>2</sub> Photoelectrochemical Cell Energy Diagram.....	19
2.2 Possible Mediation of Charge Transfer by Surface States.....	22
2.3 Double Layers at the Semiconductor-Electrolyte Interface.....	24
2.4 Simplistic Model for Water Adsorption on TiO <sub>2</sub> .....	32
2.5 Bulk Defect Energy Levels in TiO <sub>2</sub> .....	37
2.6 Energy Level Schematic for Contact Potential Difference.....	45
4.1 Sample Mounting and Carrousel Arrangement.....	61
4.2 Vacuum System.....	62
4.3 Contact Potential Difference Electronics.....	65
4.4 Contact Potential Difference Energy Schematic.....	67
4.5 Surface Potential Transients.....	72
4.6 Schematic Photoelectron and Auger Processes.....	75
4.7 XPS Spectrum for TiO <sub>2</sub> .....	76
4.8 High Resoultion XPS spectra for Ti (2p) Photoelectrons.....	79
4.9 Escape Depth of Photoelectrons as a Function of Kinetic Energy.....	80
4.10 Energy Schematic for Control Surface Preparation.....	84
4.11 Light Cycling Procedure.....	86
4.12 Dark Cycling Procedure.....	89
5.1 Bulk Donor Density <u>vs.</u> Reduction Parameters.....	92
5.2 White Light Intensity Dependance of CPD.....	97
5.3 Wavelength Dependance of CPD.....	99
5.4 TiO <sub>2</sub> Work Function Changes: Hydrogen annealed samples during Oxygen Light Cycling.....	102

## LIST OF FIGURES

	<u>page</u>
5.5 Surface Charge Changes: Hydrogen annealed samples during Oxygen Light Cycling.....	104
5.6 Hydrogen Annealed Samples, O (1s) XPS peak, with and without Adsorbates.....	107
5.7 Hydrogen Annealed Samples, Ti (2p) XPS peak, with and without Adsorbates.....	108
5.8 Hydrogen Annealed Samples, O (1s) XPS peak, Control Surface before and after Ambient Cycling.....	109
5.9 Vacuum Annealed Samples, O (1s) XPS peak, with and without Adsorbates .....	111
5.10 Vacuum Annealed Samples, Ti (2p) XPS peak, with and without Adsorbates.....	112
5.11 Vacuum Annealed Samples, O (1s) XPS peak, Control Surface before and after Ambient Cycling.....	113
5.12 Vacuum Annealed Samples, Ti (2p) XPS peak, Control Surface before and after Ambient Cycling.....	114
5.13 Surface State Repopulation Transient and Elovitch-Type Behavior Comparison.....	117
5.14 Simplified Model of Dipolar Physisorption of Water.....	129
5.15 Amount of Physisorbed Water Vapor Removed During Pumpdown (H <sub>2</sub> annealed samples, light cycle).....	131
5.16 Charge Transfer Difference (relative to control) During O <sub>2</sub> Desorption, H <sub>2</sub> annealed samples.....	134
5.17 Adsorbate Charge Transfer Rate, Desorption, H <sub>2</sub> annealed samples, O <sub>2</sub> ambient Cycling.....	135
5.18 Surface State Modelling (1).....	138
5.19 Surface State Modelling (2).....	140
5.20 Surface State Modelling (3).....	141
5.21 Surface State Concentrations <u>vs.</u> Previous O <sub>2</sub> Exposure.....	143
5.22 Surface Charge Changes: Vacuum annealed samples during Oxygen Light Cycling.....	146
5.23 Vacuum Annealed Samples: Photovoltage Inversion.....	147



## LIST OF FIGURES

	<u>page</u>
5.24 Degradation of Vacuum Annealed Control Surface.....	155
A-1 Crystal Structure of Rutile.....	165
A-2 Room Temperature Refractive Index of Rutile.....	165
A-3 Resistivity of Reduced Rutile.....	165
A-4 Absorption Coefficient of Rutile (unreduced).....	167
A-5 Absorption Coefficient of Reduced Rutile.....	167
A-6 Mobility <u>vs.</u> (1/T) for n-type Rutile.....	167
D-1 H <sub>2</sub> annealed samples, light cycling, O <sub>2</sub> exposures, $\Delta\phi(\text{TiO}_2)$ ....	179
D-2 H <sub>2</sub> annealed samples, light cycling, (O <sub>2</sub> +H <sub>2</sub> O) exposures, $\Delta\phi(\text{TiO}_2)$ ..	180
D-3 H <sub>2</sub> annealed samples, light cycling, H <sub>2</sub> O exposures, $\Delta\phi(\text{TiO}_2)$ ...	181
D-4 H <sub>2</sub> annealed samples, dark cycling, O <sub>2</sub> exposures, $\Delta\phi(\text{TiO}_2)$ .....	182
D-5 H <sub>2</sub> annealed samples, dark cycling, (O <sub>2</sub> +H <sub>2</sub> O) exposures, $\Delta\phi(\text{TiO}_2)$ ..	183
D-6 H <sub>2</sub> annealed samples, dark cycling, H <sub>2</sub> O exposures, $\Delta\phi(\text{TiO}_2)$ .....	184
D-7 H <sub>2</sub> annealed samples, light cycling, O <sub>2</sub> exposures, $\Delta n_s$ .....	185
D-8 H <sub>2</sub> annealed samples, light cycling, (O <sub>2</sub> +H <sub>2</sub> O) exposures, $\Delta n_s$ ...	186
D-9 H <sub>2</sub> annealed samples, light cycling, H <sub>2</sub> O exposures, $\Delta n_s$ .....	187
D-10 H <sub>2</sub> annealed samples, dark cycling, O <sub>2</sub> exposures, $\Delta n_s$ .....	188
D-11 H <sub>2</sub> annealed samples, dark cycling, (H <sub>2</sub> O+O <sub>2</sub> ) exposures, $\Delta n_s$ ....	189
D-12 H <sub>2</sub> annealed samples, dark cycling, H <sub>2</sub> O exposures, $\Delta n_s$ .....	190
D-13 Vacuum annealed samples, light cycling, O <sub>2</sub> , $\Delta\phi(\text{TiO}_2)$ .....	191
D-14 Vacuum annealed samples, light cycling, (O <sub>2</sub> +H <sub>2</sub> O), $\Delta\phi(\text{TiO}_2)$ ....	192
D-15 Vacuum annealed samples, light cycling, H <sub>2</sub> O, $\Delta\phi(\text{TiO}_2)$ .....	193
D-16 Vacuum annealed samples, dark cycling, O <sub>2</sub> , $\Delta\phi(\text{TiO}_2)$ .....	194
D-17 Vacuum annealed samples, dark cycling, (O <sub>2</sub> +H <sub>2</sub> O), $\Delta\phi(\text{TiO}_2)$ .....	195
D-18 Vacuum annealed samples, dark cycling, H <sub>2</sub> O, $\Delta\phi(\text{TiO}_2)$ .....	196
D-19 Vacuum annealed samples, light cycling, O <sub>2</sub> , $\Delta n_s$ .....	197

LIST OF FIGURES

	<u>page</u>
D-20 Vacuum annealed samples, light cycling, $(O_2+H_2O), \Delta n_s$ .....	198
D-21 Vacuum annealed samples, light cycling, $H_2O, \Delta n_s$ .....	199
D-22 Vacuum annealed samples, dark cycling, $O_2, \Delta n_s$ .....	200
D-23 Vacuum annealed samples, dark cycling, $(O_2+H_2O), \Delta n_s$ .....	201
D-24 Vacuum annealed samples, dark cycling, $H_2O, \Delta n_s$ .....	202

## LIST OF TABLES

	<u>page</u>
2.1 Surface Reconstructions on Clean TiO <sub>2</sub> Surfaces.....	41
4.1 Binding Energies of Photoelectron and Auger Peaks using a Mg X-ray Source.....	77
5.1 Ambient Cycling Pressures and Exposures.....	100
5.2 Transient Turning Points During Ambient Exposures.....	125
5.3 Surface State Populations.....	144
5.4 Surface State Capture Cross Sections and Relaxation Times.....	152

## ACKNOWLEDGEMENTS

I would like to express my deepest gratitude to Professor Harry Gatos for his support, interest, advice and consideration during the course of my studies and research. I am similarly grateful for the encouragement, assistance and patient attention paid to me by Dr. Jacek Lagowski during this work. The guidance and expertise of these mentors has been critical in the progress of this research.

My thanks also extend to Professors Ron Latanision and Harry Tuller for their helpful and insightful comments and criticisms during the preparation of this document.

The assistance, advice, friendship and support of many members (or past members) of the Electronic Materials Group have been greatly appreciated, and I cannot begin to adequately thank or repay these individuals for their consideration: Drs. J. Parsey, T. Kazior, A. Morawski, P. Becla, C. Wang and M. Wargo; Mssrs. J. DiMaria, C. Boucher, L. Pawlowicz, C. Brandt and D.G. Lin; Mlles. P. Merrick and G. Landahl. Particular thanks go to Drs. W. Walukiewicz and H. Ruda for several helpful and many interesting conversations. The assistance of Dr. J. Martin in XPS measurements has been greatly appreciated. I congratulate all of my friends (particularly Mssrs. Taylor and Walker) on enduring my irascible behavior during the course of this research.

This research was funded by a grant (#CPE-82-08939) from the National Science Foundation This support is gratefully acknowledged.

To my wife Susan and daughter Audrey I owe great appreciation, for their love, understanding and patient confidence. The support and encouragement of my family during this sometimes difficult period, shall always be gratefully and fondly remembered.

## Chapter 1: INTRODUCTION

Recently, wide gap semiconductors, among them titanium dioxide, have received considerable attention as potential electrodes in photoelectrochemical fuel cells.<sup>1-15</sup> Such cells show promise of inexpensively converting solar energy into electrical energy or storable chemical fuels. In the case where the photoelectrochemical cell employs an aqueous solution, hydrogen gas may be derived as a storable product. Difficulties in understanding the mechanisms by which photoelectrochemical cells operate, and the limitations by which these operating mechanisms are constrained, have hindered the development of such cells.

To illustrate the present understanding of how a photoelectrochemical cell (PEC) functions, a simplified cell apparatus and accompanying energy diagram are shown in Figure 1.1<sup>8-10</sup> This cell consists of an n-type semiconductor anode and a metallic cathode immersed in an aqueous electrolyte and connected externally. Because of the difference in work functions between the semiconductor and electrolyte, and the presence of electrically active surface states on the semiconductor, an analogue of a Schottky barrier is formed at semiconductor-electrolyte interface. Electron-hole pairs generated by light of energy greater than the band gap of the material are separated by the field of the barrier. Photogenerated electrons move away from the surface, into the bulk and then by the external circuit to the metallic cathode. Photogenerated holes in the semiconductor accumulate at the semiconductor-electrolyte interface. The charge carriers thus separated may be used to drive electrochemical reactions at the interface.

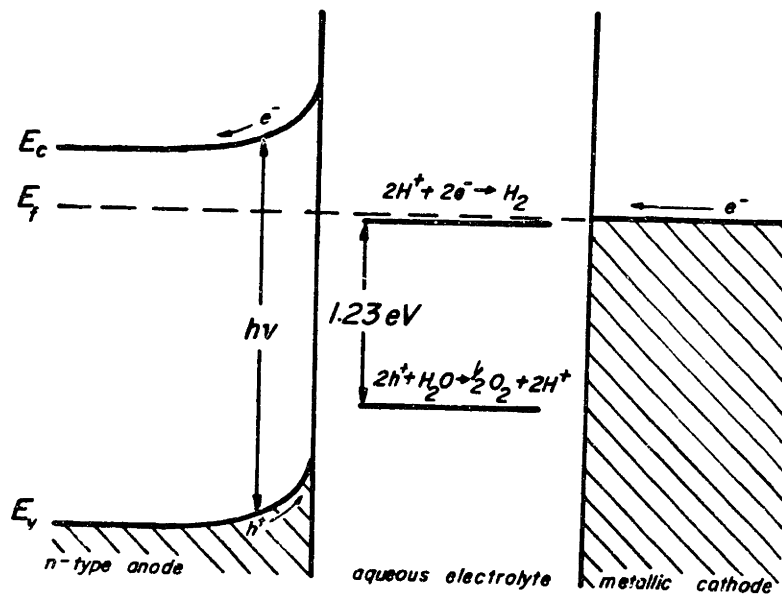
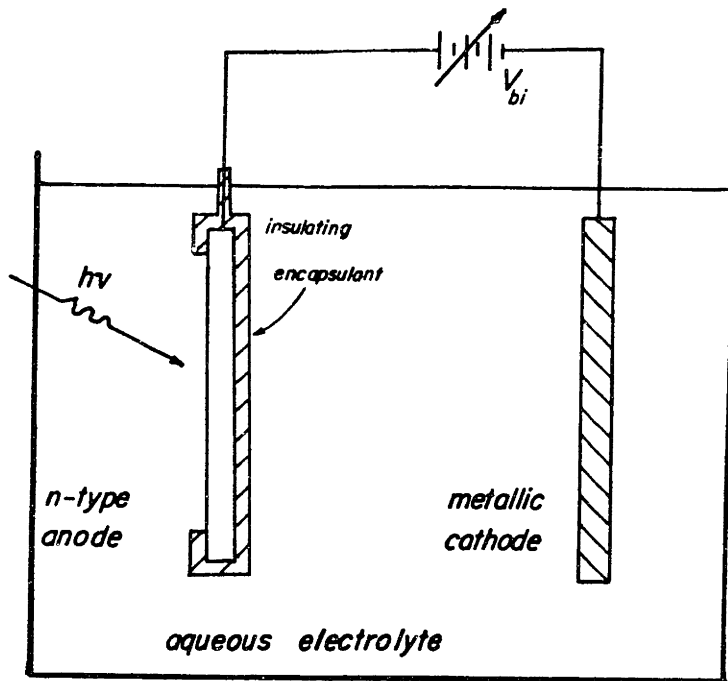


Fig. 1.1 Schematic Photoelectrochemical Cell and Energy Diagram

The reactions which occur in the electrolyte determine whether electrical or chemical energy is produced by the cell.<sup>11-13,15</sup> At the anode, holes may be transferred from the semiconductor surface to the (H<sub>2</sub>O/O<sub>2</sub>) solution level where O<sub>2</sub> is liberated according to the reaction

$$2h^+ + H_2O \rightarrow 1/2 O_2 + 2H^+. \quad (1-1)$$

Simultaneously, electrons injected into the electrolyte at the cathode may drive either of two reactions:



If reaction (1-2) occurs, then the overall cell reaction is



and hydrogen is produced as a storable product. If, on the other hand, reaction (1-3) occurs at the cathode, no change in electrolyte composition will be realized. In this case, the only usable energy produced is that made available by current flow in the external circuit.

In addition to these productive reactions occurring in the electrolyte, further reactions are possible which may cause the degradation of the cell materials, particularly the semiconductor anode. For this reason, the semiconductor anodes most often used in these photoelectrochemical cells are oxide materials.<sup>7-9,12,14,16</sup> This class of materials generally exhibits long term stabilities in the harsh conditions of oxygen evolution in electrolytes having a large range of pH. Unfortunately, these materials have band gaps too large to effectively utilize much of the solar spectrum. Furthermore, the band bending occurring at the semiconductor-electrolyte interface is often insufficient to readily separate all the photoexcited carriers created in the surface region. Despite these efficiency limiting constraints,

photoelectrochemical cells show promise as alternative energy sources, primarily because of their modest system requirements and their ease of fabrication with readily available materials. Moreover the understanding of the reaction mechanisms of photoelectrochemical cells employing oxide semiconductor anodes will provide a basis critical to the development of materials better suited for use as electrodes in such cells.

In this investigation, non-standard techniques for surface analysis will be utilized in an attempt to elucidate information concerning the reactions of water vapor and oxygen on  $\text{TiO}_2$  surfaces. By using these techniques, the changes in the  $\text{TiO}_2$  surface electronic properties are unambiguously monitored during photostimulated oxygen and water vapor interactions. The reference surfaces to be used in these studies are to be created by means less rigorous than those employed in common vacuum characterization studies (LEED, UPS, etc.). Thus, the reactions occurring on these reference, or control surfaces provide a bridge between  $\text{TiO}_2$  vacuum studies and wet electrochemical cell investigations. At the same time, the utilization of such control surfaces provides information on the adsorption and desorption of oxygen and water vapor on  $\text{TiO}_2$  at a level more basic than can be derived from wet electrochemical cell measurements. In this fashion, the nature of photo-catalyzed reactions at semiconducting  $\text{TiO}_2$  surfaces is to be investigated.

This thesis reports on the investigations of light stimulated reactions involving oxygen and water vapor on single crystal, n-type titanium dioxide ( $\text{TiO}_2$ ) surfaces. The present chapter serves to introduce the historical context in which these investigations have



been carried out, namely, in relation to photoelectrochemical cell applications.

The second chapter of this thesis presents a survey of previous investigations on  $\text{TiO}_2$  surfaces. Also included in this chapter are important data generated from wet, photoelectrochemical test cells, and a brief review of the chemical physics of the semiconducting  $\text{TiO}_2$ -liquid interface. This chapter is intended to provide a pertinent background in the properties of  $\text{TiO}_2$  surfaces and the reaction mechanisms of these surfaces as they are presently understood.

Chapter three is a statement of the motivation and scope of this thesis.

Chapter four is a description of the sample preparation, apparatus, measurement techniques, experimental and data analysis procedures used in this research.

The fifth chapter presents the results of experimentation. A phenomenological presentation of the data is first made, wherein changes in the surface electronic parameters are reported. The findings are then discussed in terms of microscopic effects where changes in the surface electronic structure, surface recombination velocity, and surface state capture cross sections are presented.

Chapter six presents the conclusions resulting from this work, and recommendations for further work based upon the results of this investigation.

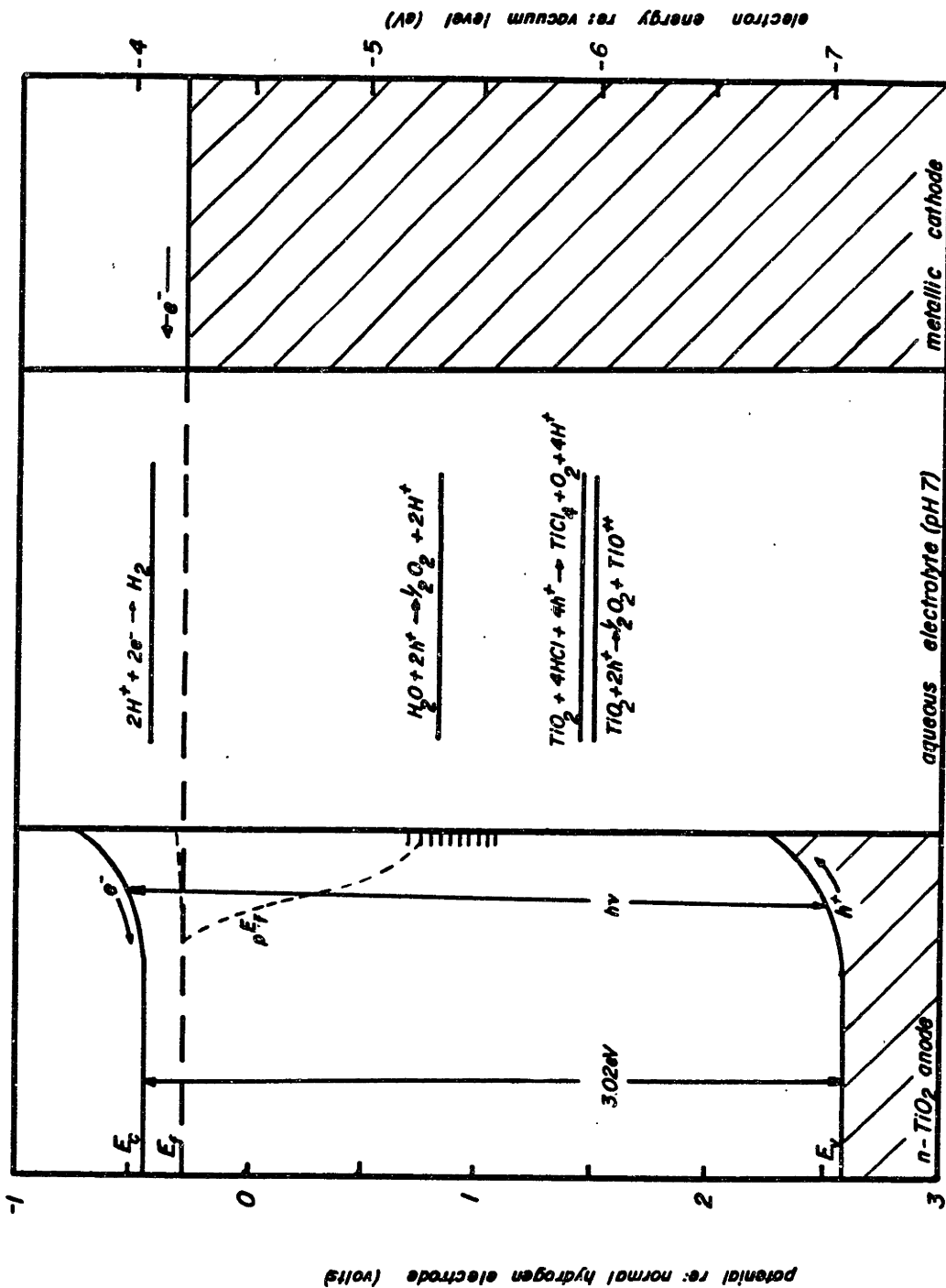
## Chapter 2: LITERATURE SURVEY

In this chapter information regarding the photoelectrochemical reactions catalyzed by semiconductors, particularly  $\text{TiO}_2$ , is briefly reviewed. Findings from previous  $\text{TiO}_2$  photoelectrochemical cell investigations are first summarized and the importance of surface states on the semiconductor is indicated. The electrochemistry at the  $\text{TiO}_2$ -electrolyte interface is then reviewed. The influence of surface states, and of impurity states in the semiconductor bulk are next discussed. Surface phenomena observed in vacuum studies of  $\text{TiO}_2$  are presented. Theoretical considerations concerned with the photostimulated behavior and charge transfer at generalized semiconductor surfaces are outlined. It is necessary to review these topics in order to clarify the nature and impact of this research.

### 2.1 $\text{TiO}_2$ Photoelectrochemical Cells

The energy diagram of Figure 2.1, as determined by previous investigations, shows a photoelectrochemical cell (PEC) wherein n-type  $\text{TiO}_2$  is employed as the semiconductor anode. Contrasting this diagram with that of Figure 1.1 illustrates the difficulties involved in using this material for the conversion of solar energy to electric current or hydrogen. The band gap of 3.02 eV allows the semiconductor to use only the ultraviolet portion of the light spectrum to create photogenerated carriers. The separation of these carriers by the electric field of the Schottky barrier is limited by the small amount of band bending which occurs at the semiconductor surface.<sup>9,11,12,14,17</sup> The reaction for the production of  $\text{H}_2$  by the reduction of protons lies very near the semiconductor band edge and generally above the Fermi level of the

Fig. 2.1 TiO<sub>2</sub> Photoelectrochemical Cell Energy Diagram



semiconductor.<sup>9,17</sup> Hence it is unlikely that without external bias the electrons from the metallic cathode can be used to drive the reaction to produce hydrogen as a chemical product.<sup>17,18</sup> Electrons from the cathode will more likely be involved in the reduction of oxygen and protons according to reaction (1-3), particularly if there is oxygen present in the electrolyte near the cathode. This mode of operation generates a current in the external circuit which is available for electric work.

The discharge of photogenerated holes from the  $\text{TiO}_2$  anode to the electrolyte determines the stability of the semiconductor against corrosion and may also be the rate determining step in the operation of the photoelectrochemical cell.<sup>11-13,19</sup> As shown in Figure 2.1, several reactions may compete with the oxidation of water according to reaction (1-1) for the consumption of photogenerated holes. The stability of  $\text{TiO}_2$  in aqueous electrolytes, as reported by many researchers,<sup>7-9,13-16,20,21</sup> is due to the prevention of holes interacting with the dissolution reactions detrimental to the semiconductor.

Under illumination, the driving force for anodic reactions occurring at the  $\text{TiO}_2$ -electrolyte interface can statistically described be described by the lowering of the quasi-Fermi level for holes,  $pE_f^*$ . Under steady state, non-degenerate conditions this is given by

$$pE_f^* = E_v - kT \ln(p_i/N_v) - kT \ln(p^*/p_i) \quad (2-1)$$

where  $p_i$  is the intrinsic, bulk hole density;  $p^*$  the local concentration of photogenerated holes; and  $N_v$  is the density of states in the valence band. If, under illumination,  $pE_f^*$  at the surface drops to below the reaction level for the oxidation of water, but is still above the energy levels for the dissolution reactions, corrosion of the semiconductor will not occur while the desired oxidation becomes

possible.<sup>11,12,22</sup> Thus, Gerischer has postulated that the stability of  $\text{TiO}_2$  against photodecomposition is due to kinetic, rather than thermodynamic conditions: the  $\text{H}_2\text{O}$  oxidation by holes at the surface occurs so fast that  $p E_f^*$  at the surface does not exceed the critical energy level where the crystal decomposition may occur.<sup>11</sup>

The mediation of charge (photogenerated holes) at the  $\text{TiO}_2$ -electrolyte interface by surface states may also explain the stability of  $\text{TiO}_2$  against photocorrosion. As shown in Figure 2.2, several transitions may occur by which these acceptor surface states may become populated by holes. Illumination with light of energy greater than that of the band gap may produce holes in the valence band which are transferred to the surface states. It may alternatively be possible to excite electrons trapped at the surface states to the conduction band with less energetic light. Due to their different generation mechanisms, it is expected that these processes will occur at different rates. In particular, the nature of the surface states on  $\text{TiO}_2$  may influence the charge transfer mechanism at the semiconductor surface.

## 2.2 Semiconductor-Liquid Interfaces

The chemical physics which underlie the phenomena occurring at  $\text{TiO}_2$  interfaces in photoelectrochemical cells will, in this section, be briefly outlined. Such a review is necessary in order to visualize the photostimulated reactions of interacting species on the  $\text{TiO}_2$  surface. A comprehensive review of the electrochemistry occurring at generalized semiconductor-liquid interfaces is provided by the texts of Morrison<sup>23,24</sup> and the references cited therein. This section summarizes some of the key features of the semiconductor-electrolyte interface as they have been presented in these works.

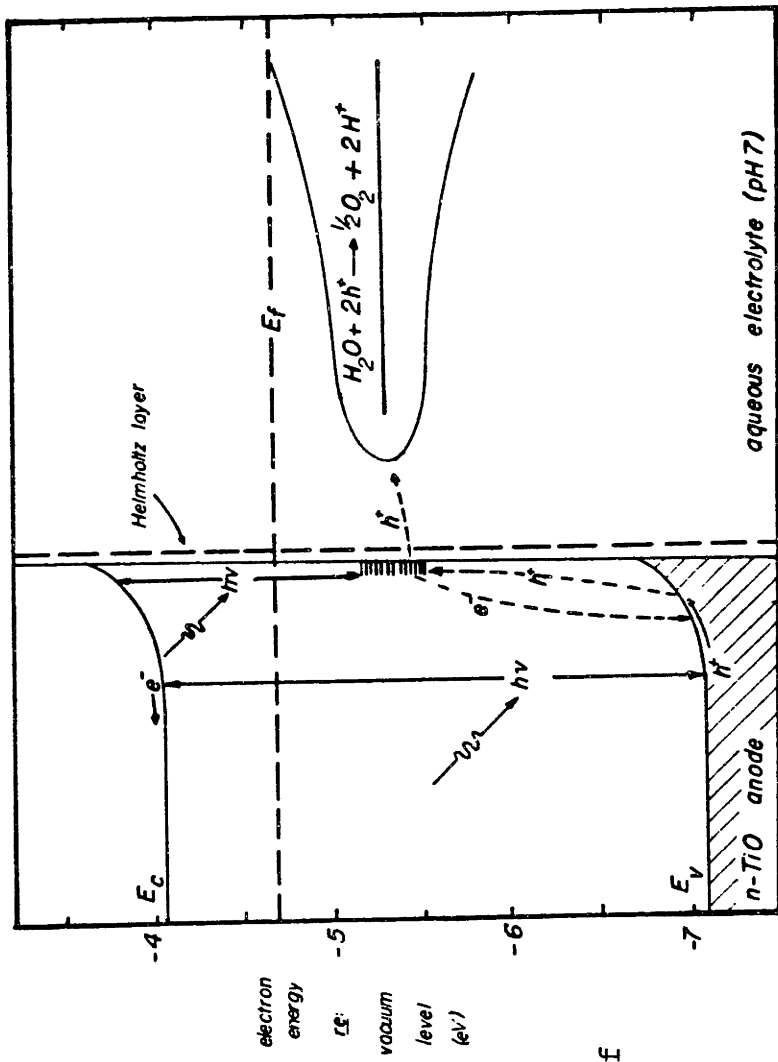


Fig. 2.2 Possible Mediation Of Charge Transfer by Surface States

### 2.2.1 Double Layers

Charged planes or space charge layers almost inevitably form at any interface including the semiconductor-liquid juncture. These lead to electrical double layers, consisting of layers of positive and negative charge, with regions of high electric field between or within these charged layers. Such double layers dominate the electrical and chemical processes occurring at the surface, such as carrier recombination, photovoltaic effects and the charge exchange at the surface. Three distinct double layers appear at the semiconductor-electrolyte interface, each involving charged planes or space charge layers and each characterized by a double layer voltage. The origins of these double layers are now described.

The three double layers occurring at the semiconductor-electrolyte interface are indicated in Figure 2.3. They include first a semiconductor space charge double layer; second, a Helmholtz double layer, between the solid and the "outer Helmholtz plane", the distance of closest approach by non-adsorbed ions to the surface; and third, the Gouy-Chapman double layer in the solution in which an excess of ions of one sign exists.

Corresponding to these three double layers are four regions of excess charge. First we have the space charge region in the semiconductor. In the case of  $n\text{-TiO}_2$ , the excess positive charge is in the form of uncompensated donor defects due to the electrons being captured by surface states or transferred to species in the electrolyte. This results in a depletion layer near the surface of the  $n\text{-TiO}_2$  and the formation of a Schottky barrier analogue at the surface. The physics and analysis of this semiconductor space charge region is not unique to electrochemical applications and is dealt with in detail

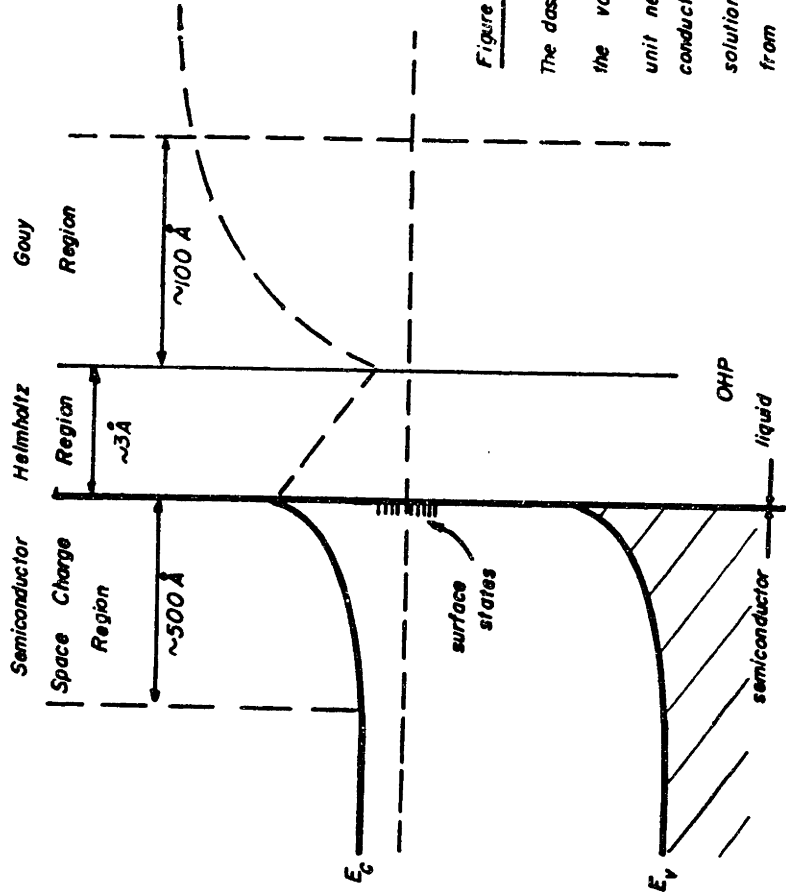


**Figure 2.3**

The dashed line through the liquid indicates the variation in potential energy of a unit negative charge as it moves from the conduction band of the solid into the solution. from reference 24



by most semiconductor texts. A review of the photostimulated behavior of this region is given in section 2.5.1. The next region of excess charge appears on the solid side of the Helmholtz double layer. In the case of non-degenerate  $\text{TiO}_2$ , the charge at this inner Helmholtz plane arises due to bulk electrons trapped at the surface states, and the charge associated with adsorbed ions or dipoles. The actual location of charge at the inner Helmholtz plane may not be distinguishable, with the charge in each case residing in the same bonding orbitals of the surface atoms. The outer Helmholtz layer presents the next layer of charge, which originates in the accumulation of mobile ions from the liquid at the distance of closest approach to the semiconductor. Due to the attraction of the sheet of negative charge at the inner Helmholtz plane, this outer Helmholtz plane will be positive in charge. The ions attracted to the outer Helmholtz plane do not suffice to compensate all the charges on the electrode, and the residual electric field directed normal to the surface results in a final charged region referred to as the Gouy-Chapman layer. The width of this region depends on the concentration of ions in the solution, and becomes appreciable only for dilute solutions.

## 2.2.2 Interfacial Interactions

### 2.2.2.a Surface States

Localized energy levels at the semiconductor surface stem from several sources: states intrinsic to a uniform surface, Lewis sites (orbitals that can share electron pairs, which can be acidic or basic), and surface states arising from foreign adsorbing species.

On reasonably covalent semiconductors, intrinsic surface states arising due to dangling surface bonds are termed Shockley surface

states. These states arise from a symmetric termination of the electric potential at the surface. A significant overlap occurs between neighboring dangling orbitals causing the splitting of the resulting "molecular orbitals" into bonding and antibonding states to which acceptor and donor activity, respectively, can be attributed. The broadening of such levels into bands is expected by quantum effects because of orbitals overlapping with each other or with the bands of the solid. Surface heterogeneity can also give rise to a spectrum of energy levels appearing as a band.

The surface of a more ionic compound semiconductor will have ionic surface states, or Tamm states, intrinsic to the surface. These Tamm states are associated with an asymmetric termination of electronic potential at the surface. A surface lattice oxygen ion of  $\text{TiO}_2$ , surrounded by less than its normal complement of cations will give rise to surface electrons of energy higher than that of the bulk (valence band) electrons simply because of the lowered electrostatic attraction from neighboring cations. When the surface is neutral, these states are occupied, hence they represent donor levels. These levels are essentially valence band orbitals perturbed by the electrostatic interaction into the energy gap at the surface. They will probably form a band of levels for the same reasons discussed above for the Shockley states. Analogously, unoccupied energy levels for the titanium surface cations will be acceptor states which will be located below the conduction band simply because the surface cation has fewer neighboring anions than a bulk cation.

Lewis sites are another type of surface states on an ionic semiconductor which are important because of their chemical reactivity with the adjoining electrolyte. A Lewis acid site is attractive to

electron pairs from an adsorbing molecule; a Lewis base site is able to donate electron pairs to an adsorbing species. These Lewis sites are not normally considered to be electronic surface states inherent to the ionic semiconductor. They are distinguished from ionic (Tamm) surface states in that for ionic states we are interested in the exchange of unpaired electrons between both the energy bands of the solid, the surface states and the adsorbing species. Measurements of the properties of Lewis sites requires the adsorption of electron pair donor or acceptor molecules and hence are not observable on clean surfaces. Although Lewis acid/base interactions do not themselves accept or donate electrons from the bands of a semiconductor, their effect at the semiconductor-liquid is significant in two ways. First, they contribute to an ionic double layer at the surface (Helmholtz layer) such that a surface with a high density of Lewis acid sites will, for example, become negatively charged. Second, Lewis activity causes adsorption and passivation of surface sites that would otherwise be active ionic (Tamm) surface states. For example, surface  $O^-$  would tend to be intrinsic ionic donor states, but the presence of a proton interacting with the electron pair of this Lewis base site will tend to stabilize an electron at the  $O:H^+$  complex site.

Adsorbed electronegative species, species which tend to give up or accept charge, form a third class of surface states. They can act as donors or acceptors and they will have surface state energy levels associated with their bonding and antibonding levels. For example, weakly bound  $O_2$  molecules on a semiconductor will form strong acceptor states characteristic of the free molecule. If, on the other hand, a strong bond forms between the surface and the adsorbed species, the

resultant surface states are determined by the complex formed and need not be closely related to the properties of the isolated adsorbing species. The broadening of adsorbate surface states may not be appreciable if there is little physical overlap of the wave functions of the adsorbate-surface complexes. The adsorbate levels may however appear to form a band because of surface heterogeneities, making the energy of each adsorbate molecule somewhat different from that of its neighbors.

#### 2.2.2.b Fluctuating Solution Energy Levels

Mobile ions in solution which are within tunnelling distance of the semiconductor can exchange electrons with the energy bands of the solid. The correspondance between the equilibrium solution energy level for an ion, and the adjacent active energy levels of a semiconductor may not always be appreciable, as is shown in Figure 2.2. The mechanisms by which the energies of ions in solution are modified, so that isoenergetic electron tunnelling may occur between the semiconductor and the solution ions, involves the modification of either the ions surroundings or its charge.

The description of energy levels associated with ions in solution is more complex than is encountered in semiconductor physics because of the effect on electronic levels of the ions by their surrounding polar solvent. The dipoles associated with the solvent molecules are able to move and rotate much more easily than in solids. As a result of thermal fluctuations of the solvent dipoles, the potential at the ion fluctuates and the energy level of the ion fluctuates about some most probable value.

Consider the energy  $\Delta E_p$  necessary to cause fluctuations from the equilibrium polarization of the dielectric around the ion, without

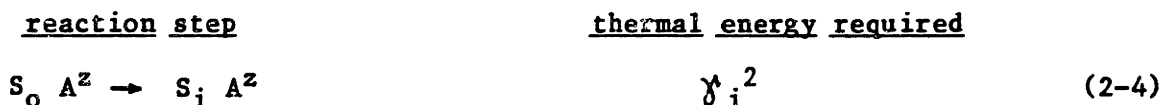
changing the charge on the ion, such that the charge of the solvated ion ensemble changes by  $q(Z \pm \delta)$ , where  $Z$  is the actual charge on the ion. With this polarization energy, the energy  $E_p$  is given to a good approximation by

$$\Delta E_p = \gamma^2 \lambda \quad \text{where} \quad (2-2)$$

$$\lambda = \frac{q^2}{8\pi\epsilon_0 a} \left( \kappa_{op}^{-1} - \kappa_s^{-1} \right) \quad (2-3)$$

is a "reorganizational energy" containing the factors  $\kappa_{op}$ , the optical dielectric constant;  $\kappa_s$ , the static dielectric constant of the liquid;  $a$ , the ionic radius and;  $\epsilon_0$  the permittivity of free space. Corrections can be made to this expression using quantum mechanics, but for the sake of clarity, they are omitted here.

Using the energy of polarization fluctuation, we can calculate the energy necessary to reduce an ion in solution in three steps. The prepolarization shifts the ion's energy level from its equilibrium position to an intermediate, and as yet, unspecified activated energy level,  $E_i$ . Electron transfer from the conduction band ensues with an energy change of  $E_{cb} - E_i$ . The ion now has a new charge, and we let the polarization of the solvent dielectric to relax to its equilibrium value, releasing the associated thermal activation energy. Utilizing the subscript  $i$  for for the intermediate activated state of the solvent dielectric, the three steps of the reduction can be written as:



The total energy change required to transfer an electron to an ion in

solution is then, with the appropriate changes in the dielectric polarization,

$$\Delta = \gamma_i^2 - (1 - \gamma_i)^2 + E_i - E_{cb} \quad (2-7)$$

The energy  $\Delta$  must be independent of the intermediate energy level during charge transfer,  $E_i$  and we can thus use this relation to determine a relation between  $E_i$  and  $\Delta E_p$ . By determining  $\Delta$  for the case where  $\gamma_i = 0$  and  $E_i = E_t$  where  $E_t$  is the mean energy of the activated reaction level in solution we find that  $\Delta = -\lambda + E_t - E_{cb}$ . Inserting this value into (2-7), and solving for  $\gamma_i$  we have  $\gamma_i = (E_t - E_i)/2$ , whence the energy needed to thermally activate an ion by polarizing its surrounding dielectric [equation (2-4)] is

$$\Delta E_p = (E_t - E_i)^2/4 \quad (2-8)$$

Equating this energy with the available thermal energy,  $kT$ , of the system,

$$(E_t - E_i)^2 = 4 \lambda kT. \quad (2-9)$$

An evaluation of the value of  $\lambda$  for an ion with a  $3\text{\AA}$  radius solvated by water molecules is of the order of 1eV. Substituting this value of  $\lambda$  into equation (2-9), it is seen that fluctuations in the energy levels of ions in solution by the amount of 0.3eV or more may be anticipated.

Fluctuations of the energy levels of ions in solution are also associated with the change of charge on the ion. If we neglect for the moment the temporal thermal fluctuations of the energy levels, the transfer of an electron from the semiconductor to an oxidized species in solution will result in the dipoles of the solvent dielectric slowly reorienting themselves around the ion and the removal of some of the negative poles from the polarization dielectric. This will cause the potential of the central ion to increase (be more attractive to electrons) and the electronic energy of the solvated ion moves slowly

to a lower level on a band model.

#### 2.2.2.c Adsorption

In general, any oxide surface will have adsorbed water vapor present in the form of adsorbed protons and hydroxide ions before immersion into any solution. In the case of adsorption from the vapor phase, the surface concentrations of  $H^+$  and  $OH^-$  are approximately equal. Upon immersion into liquid water however, the equal adsorption of  $H^+$  and  $OH^-$  may no longer be the case. Particular surfaces will adsorb an excess of one or the other of these species and become charged positive and negative.

Figure 2.4 indicates the simplest picture of adsorption of water vapor on  $TiO_2$ . The  $OH^-$  groups are attracted to the Ti surface ions, the Lewis acid sites of the surface; and the  $H^+$  ions are attracted to the oxygen surface anions, the Lewis base sites. Upon immersion into aqueous solutions,  $TiO_2$  tends to adsorb more  $OH^-$  ions at the surface than  $H^+$  ions, with a pH of 6 necessary to balance the adsorbate charge at the surface.<sup>25</sup> This indicates that a significantly higher concentration of  $H^+$  ions ( a factor of 100 times more than  $[OH^-]$ ) is necessary to balance the populations of  $H^+$  and  $OH^-$  species at the  $TiO_2$ -liquid interface. With this information, one may surmise that the activity associated with the  $OH^-$ -surface Ti ions should be considerably less than the  $H^+$ -surface O ions.<sup>26</sup>

The above is a somewhat oversimplified model of the  $TiO_2$  surface in that it ignores surface heterogeneity. More complex and stronger adsorption of water and its fragments can occur associated with sites of extra chemical activity on the oxide surface, or at sites of active ionic (Tamm) surface states. Such sites are to be expected on a

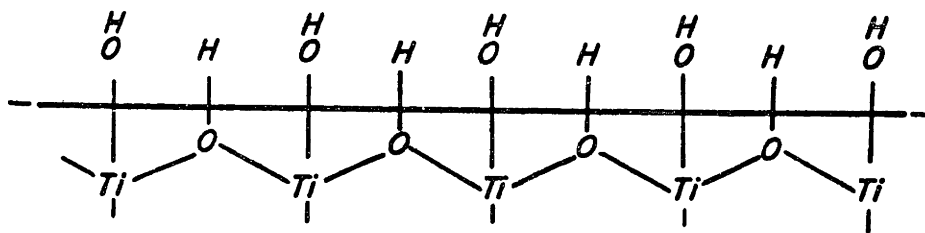


Fig. 2.4 Simplistic Model for  
Water Adsorption on  
TiO<sub>2</sub>



heterogeneous surface. For example, in catalysis studies at the gas-solid interface it is recognized<sup>23</sup> that poorly coordinated oxygen ions at the surface, say at surface steps, provide strong ionic donor surface states. That is, they tend to give up electrons (or capture holes) more easily than the more completely coordinated oxygen ions associated with the valence band.

## 2.3 Defects in TiO<sub>2</sub>

### 2.3.1 Surface States

The quantum efficiency with which photocurrent is discharged from the TiO<sub>2</sub> anode in photoelectrochemical test cells has been reported to be anomalously high.<sup>9,13,17,27,28</sup> In these TiO<sub>2</sub> PEC's, the transfer of photogenerated holes at the semiconductor-electrolyte interface to the oxygen production level [equation (1-1)] has been assessed to be too large to be simply accounted for by the injection of holes from the valence band edge into the electrolyte. As seen in Figures 2.1 and 2.2, little communication is expected between the valence band and the oxygen production level in the electrolyte since they are separated in energy by about 1 eV. Thus, to explain the large observed photocurrent in TiO<sub>2</sub> test cells, several authors have suggested the mediation of charge by surface states on the TiO<sub>2</sub>.<sup>9,13,17,22,27-29</sup> These surface states were postulated to lie about 1.7 eV above the valence band, and act to isoenergetically transfer photogenerated holes trapped from the valence band to the oxygen production level. It has been pointed out however, that surface reaction intermediaries in the electrolyte may alternatively account for the transfer of holes from the valence band to various reaction levels in the solution.<sup>29,30</sup> Such surface charge intermediaries are to be expected in aqueous electrolytes, particularly

if there is oxygen dissolved in the solution.<sup>27,29</sup> Thus, the high quantum efficiencies of current discharged at TiO<sub>2</sub> anodes in aqueous PEC's cannot be uniquely be ascribed to the presence of semiconductor surface surface states.

More substantial evidence for the existence of TiO<sub>2</sub> surface states can be offered on the basis of the electrochemical behavior of a broad range of redox couples in aqueous and non-aqueous electrolytes. After making such studies, Bard et.al.<sup>30,31</sup> have concluded that active surface states are located about 1.8 eV above the valence band of TiO<sub>2</sub>. These states were hypothesized by Bard to be donor states activated at high temperatures and associated with oxygen vacancies or Ti<sup>3+</sup> surface atoms.

The presence of these surface states has hindered attempts to characterize TiO<sub>2</sub> PEC electrodes by wet electrochemical techniques. In particular, Mott-Schottky plots have exhibited considerable non-linearities which are attributable, at least in part, to the presence of partially populated surface states.<sup>31,32</sup> Rigorous surface preparation procedures have been used to produce Mott-Schottky plots wherein the influence of surface states, as well as other extraneous factors, such as surface roughness and doping inhomogenieties, have been minimized.<sup>33,34</sup> Despite these efforts, it is recognized that variations in the reported values of some surface parameters, such as flatband voltage, may be large and attributable to both bulk defect levels and surface preparation procedure.

The influence of surface modification has been investigated by Tomkiewicz, who has analyzed the capacitance values for Mott-Schottky plots in terms of an equivalent electric circuit to determine the distribution of states at the TiO<sub>2</sub>-electrolyte interface.<sup>35-37</sup> In

aqueous electrolytes, the capacitance values have yielded a broad Gaussian distribution of surface states centered at 1.8 eV above the valence band, in agreement with Bard's results. But, upon modifying the surface with alkylsilanes, a different set of surface states, located near the bottom of the conduction band, is produced. It is seen by these analyses that the distribution of surface states at the  $\text{TiO}_2$ -electrolyte interface is critically dependant upon the surface preparation and environment of the  $\text{TiO}_2$  electrode. Defects in the bulk may also influence the behavior of the semiconductor surface, and we turn now to review the literature concerned with this topic.

### 2.3.2 Bulk Defect and Electromigration Effects

The electronic defects in bulk  $\text{TiO}_2$ , introduced in order to make the crystal semiconducting, exert an influence on both the response of the material to optical and thermal stimulation, and the behavior of the material as employed in photoelectrochemical cells. The basic defect reactions which occur upon growth and reduction of  $\text{TiO}_2$  (rutile) crystals are discussed in Appendix B. In this section, the response of donor defects to optical and thermal excitation as well as photoelectrochemical cell testing is reviewed.

Bulk defect energy levels within the bandgap of  $\text{TiO}_2$  were first observed by Cronmeyer<sup>38</sup> who attributed optical absorption peaks to the presence of cationic substitutional impurities and oxygen vacancy defects. In this analysis, a simple atomic modelling based upon hydrogen and helium atoms' ionization energies predicted well the observed ionization energies as derived from optical absorption spectra. These conclusions were substantiated by further work,<sup>39,40</sup> although complications in the optical spectra were also observed in

highly reduced samples.

Thermoluminescence and thermally stimulated current measurements made by Ghosh et.al.<sup>41</sup>, utilizing a wide range of TiO<sub>2</sub> crystals, orientations and reductions reproducibly observed a weak luminescence band deep within the gap of the material, and also eight distinct shallow (less than 0.9 eV) donor levels. These results were later analyzed<sup>42</sup> and it was determined that the luminescence center, located ~1.46 eV below the conduction band, was associated with interstitial Ti<sup>3+</sup> ions, in agreement with EPR results (see Appendix B). These interstitial ions act as donors, producing n-type semiconduction according to the reaction:



The ionization of Ti<sup>3+</sup> interstitial ions is to be expected as the lattice titanium ions in rutile have a 4+ valency. Subsequent analysis of the photostimulated kinetics of this luminescence center yielded an excited lifetime of 3.6x10<sup>-5</sup> sec and a capture cross section of 5x10<sup>-18</sup> cm<sup>2</sup>.<sup>43</sup> One of the shallow defects was also identified with the first ionization of vacant oxygen sites according to the reaction:



This defect was found to have a thermal ionization energy of 0.48 eV while its optical ionization energy was measured with less confidence as 1.18 eV. Although more investigation is necessary to reconcile these values, the tentative results of defect levels in TiO<sub>2</sub> are summarized in the band diagram of Figure 2.5.<sup>42</sup>

The substitution of trivalent cationic species into TiO<sub>2</sub> photoanodes has been theoretically analyzed and compared with experimental results.<sup>44</sup> The effect of Al<sup>3+</sup> substitutional impurities

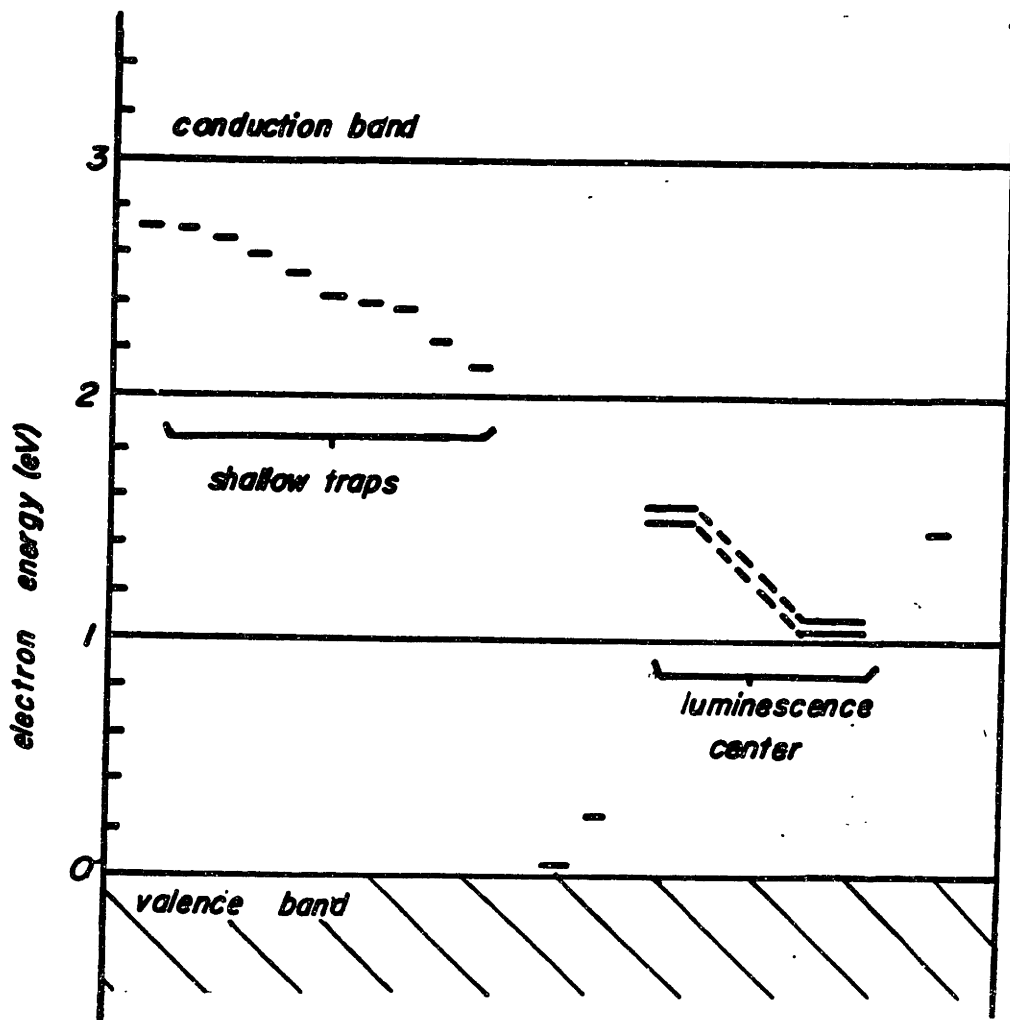


Fig. 2.5 Bulk Defect Energy Levels  
in  $\text{TiO}_2$

Data from Reference 42.

was found by this method to increase the hole diffusion length by a factor of four to  $\approx 4$   $\mu\text{m}$ , while  $\text{Cr}^{3+}$  impurities improved the wavelength response of the photoanodes towards the visible portion of the spectrum. Investigations to substantiate these claims have not yet been carried out however. As discussed in Appendix B, the effect of trivalent cationic substitutional impurities is to introduce an acceptor band in the bulk of the material, compensating for the n-type activity normally associated with  $\text{TiO}_2$ .

Donor defects produced by both vacuum and hydrogen reductions of  $\text{TiO}_2$  have been found to electromigrate during photoelectrochemical cell testing,<sup>44-47</sup> although there has been some discussion as to the extent of this phenomenon.<sup>48</sup> In general, a gradual reduction in the conversion efficiencies, and an accompanying deterioration of the surface morphology of  $\text{TiO}_2$  anodes in PEC's have been observed with continuous testing. It has been envisioned that this deterioration of  $\text{TiO}_2$  device performance is due to the electromigration of positively charged donor defects (primarily  $[\text{Ti}]_i^{3+}$ , but also hydrogen related defects) under the influence of the space charge field, to the surface.<sup>45-47</sup> Besides reducing the donor density and thereby changing the space charge field, the migration of donors to the electrolyte interface has also been noted to effect the flatband voltage and the  $\text{TiO}_2$  work function.<sup>49</sup> All of these effects suggest that substitutional rather than interstitial doping is preferred in  $\text{TiO}_2$  anodes.

#### 2.4 Vacuum Studies

In this section, literature concerned with surface studies on  $\text{TiO}_2$ , as performed under vacuum, is reviewed. A delineation must first be made, however, between clean and real surfaces.

Clean surfaces are those produced in UHV either by cleavage or by argon ion bombardment and subsequent annealing. These procedures seek to produce atomically perfect surfaces without defects, reconstructions or contaminants as a basis for further study. While these clean surface studies may provide fundamental information at an atomic level, they are limited in their applicability by the severe preparation procedures rarely encountered in engineering situations.

In contrast to these clean surfaces studies, investigations of "real" surfaces may employ less rigorous preparation procedures, and thus may have a broader range of applicability. The criteria that "real" surfaces must fulfill is that they must be procedurally reproducible and also sensitive to the employed experimental stimuli. These less stringent requirements for real surface studies introduce increased experimental flexibility and also serve to enhance the applicability of the experimental results to a broader range of engineering situations. Difficulties in the production of surfaces that are reproducible from an electronic standpoint have hampered such studies on  $\text{TiO}_2$ .

### 2.3.1 Clean $\text{TiO}_2$ Surfaces

Clean surface vacuum studies on  $\text{TiO}_2$  have been hampered by the instability of these surfaces to the standard preparation procedures, and also to the stimulating radiation used in these analysis techniques. The control surfaces used in Auger electron spectroscopy (AES), low energy electron spectroscopy (LEED), electron energy loss spectroscopy (EELS), and ultraviolet photoemission spectroscopy (UPS), are most often produced by  $\text{Ar}^+$  ion bombardment and subsequent annealing in vacuum, resulting in oxygen deficient surfaces.<sup>50-59</sup> Moreover, the

ionizing radiation used in the forementioned analysis techniques is also detrimental to the  $\text{TiO}_2$  surfaces, causing a loss of oxygen with prolonged exposure.<sup>50-55,57,58</sup> Nonetheless, vacuum studies on clean  $\text{TiO}_2$  surfaces do provide useful information helping to analyze surface reactions under real conditions.

As determined by LEED patterns,  $\text{TiO}_2$  surfaces undergo surface reconstructions during  $\text{Ar}^+$  ion milling and and annealing (see Table 2.1).<sup>50,53,54</sup> The consolidation of surface dangling bonds produced by the  $\text{Ar}^+$  bombardment is generally accepted as the driving force behind these reconstructions.<sup>50,53,54,56,58</sup> The rearrangement of such dangling bonds results in the formation of electronic surface defect states within the band gap of the material. On perfect, vacuum cleaved crystals, where no such rearrangement of bonds occur, such surface states do not exist.<sup>59</sup>

Henrich<sup>56</sup> notes that low levels of  $\text{Ar}^+$ -induced defect densities give rise to surface states located  $\sim 0.7$  eV below the conduction band; higher defect densities increase the number of these surface states, and further bombardment produces ordering into a metallic  $\text{Ti}_2\text{O}_3$ -like surface overlayer. While moderate oxygen depletions result in an UPS peak  $\sim 2.5$  eV above the valence band, EELS measurements indicate that the same states lie  $\sim 0.7$  eV lower in energy.<sup>50,53,54,56</sup> It has been suggested that the energy loss spectra is more sensitive to the electronic structure of the top surface layer, and the assignment of surface states to a level  $\sim 1.8$  eV above the valence band is more correct.<sup>62</sup> This would energetically correlate those surface states found by these clean surface studies with those surface states found by the modification of electrolytes in PEC's and by photoresponse measurements. Intermittent testing of these oxygen depleted surfaces in



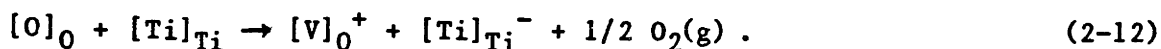
**TABLE 2.1: TiO<sub>2</sub> Surface Reconstructions**

<u>surface</u>	<u>structure</u>	<u>reconstruction conditions</u>
(110)	(1x1) <u>ie.</u> : stable	600°C anneal in vacuum
(001)	unstable: facets to (110) and (100)	600°C anneal in vacuum
(100)	(1x3)	600°C anneal in vacuum
	(1x5)	800°C anneal in vacuum
	(1x7)	1200°C anneal in vacuum

Data from references 50, 53 and 54.

aqueous test cells has shown that reoxidation of the surfaces does occur, and that the density of surface states associated with oxygen depletion is thereby reduced.<sup>55</sup> The oxygen exposure necessary to eradicate these defect surface states has been calculated to be about  $10^6$  L.<sup>50,56</sup>

There is general agreement among researchers that the mid-gap surface states on  $\text{TiO}_2$  are attributable to  $\text{Ti}^{3+}$  ions which result from the oxygen depletion of the surface.<sup>50,53,56,58,59</sup> The formation of these surface states has been formulated by Chung et.al.<sup>53</sup> as



In this equation the valences of the oxygen and titanium lattice sites are 2- and 4+, respectively, so that the  $[Ti]_{Ti}^-$  is a triply positive ion. With this reaction, the reduction in the density of  $\text{Ti}^{3+}$  surface states upon exposure to oxygen is understood to be the reversible exchange of charge between surface anions and cations upon the re-incorporation of oxygen into the lattice.

The adsorption of oxygen and water vapor onto  $\text{TiO}_2$  surfaces result in changes in the UPS and EELS spectra, indicating the interaction of adsorbates with surface states.<sup>50,51,54,56-58</sup> It has been found that on oxygen depleted surfaces on which  $\text{Ti}^{3+}$  surface states are present the initial chemisorption of oxygen occurs dissociatively, and at higher exposures, molecular adsorption follows.<sup>50,51,54,56,57</sup> The exposure at which the dissociative adsorption is saturated has been recorded as about 100L.<sup>54,56</sup> Similarly,  $\text{H}_2\text{O}$  chemisorption is found to occur dissociatively at low exposures, but molecularly at higher (up to  $\sim 10^8$ L) exposures, in the presence of  $\text{Ti}^{3+}$  surface states.<sup>50,51</sup> It has been noted that the oxygen and water vapor adsorption scheme depends on the presence of cationic

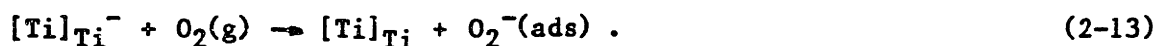
defects: if  $Ti^{3+}$  surface states are not present, such as on vacuum cleaved surfaces, dissociative chemisorption does not occur.<sup>50,51,58,59</sup>

Calculations performed to determine the position and character of surface states formed on surfaces of  $TiO_2$  have indicated that antibonding orbitals are responsible for the mid-gap surface states.<sup>60-62</sup> These orbitals largely result from perturbed Ti conduction band states. Consequently, they are in agreement with the  $Ti^{3+}$  surface states observed in UPS and EELS spectra.<sup>50</sup> Calculations have also shown that oxygen vacancies located several lattice planes beneath the surface can also result in the production of these defect states on the surface.<sup>62</sup>

#### 2.4.2 Real $TiO_2$ Surfaces

The preparation procedures used in the production of real, reproducible surfaces on  $TiO_2$  are not so rigorous as those utilized in clean  $TiO_2$  investigations. While these studies admit to some ambiguity in the exact atomic nature of the surfaces under study, their results are quite useful in determining the surface reactions occurring under conditions more realistic than those of clean surface studies. Moreover, correlations can often be drawn between clean and real surface studies.

Electron spin and paramagnetic resonance studies on vacuum reduced  $TiO_2$  powders have indicated that the formation of  $Ti^{3+}$  lattice ions are responsible for the mid-gap surface states.<sup>63,64</sup> These states are formed by a reaction such as (2-12). Moreover, the initial adsorption of oxygen on these surfaces was shown to occur according to:



The charge transfer occurring during this adsorption could occur via

direct (surface state→adsorbate) or indirect (surface state→conduction band→adsorbate) mechanisms. Through the ESR and EPR measurements, an assessment of the maximum negative electronic charge on the surface of  $\text{TiO}_2$  doped to  $n_b \approx 5 \times 10^{18} \text{ cm}^{-3}$  was calculated as  $7 \times 10^{12} \text{ cm}^{-2}$ .

Photocurrent studies coupled with oxygen reactions on slightly reduced rutile single crystals were made by Addiss and Wakim.<sup>65</sup> This study suggests that adsorbed oxygen acts as a recombination center with a very large (many minutes) relaxation time, and that part of the observed photocurrent can be associated with the photodesorption of oxygen. Although the detailed shapes of the photoresponse behavior were not reproducible in these studies, it was ascertained that Elovitch-type kinetics were not followed by the  $\text{TiO}_2$ . It was also found that the exposures of oxygen to  $\text{TiO}_2$  single crystal surfaces increased the resistivity of the sample relative to those surfaces held in vacuum or exposed to inert gases. The temperature dependence of this resistivity change up to  $\sim 200^\circ\text{C}$  conformed to a linear plot of  $\log_{10}(\rho)$  vs.  $1000/T$ . Using this data, an activation energy for the resistivity change associated with oxygen exposure can be determined to be 70 meV.

Contact potential difference (CPD) measurements were made on  $\text{TiO}_2$  films by Vohl<sup>66</sup> with limited success. His photovoltage results can be summarized as follows: 1) upon illumination with band-gap light, a positive photovoltage is produced (see Figure 2.6); 2) the photovoltage is proportional to light intensity and; 3) the photovoltage produced in vacuum was greater than that in air. It was also reported that the contact potential difference increased in darkened conditions under vacuum over illuminated conditions in air.

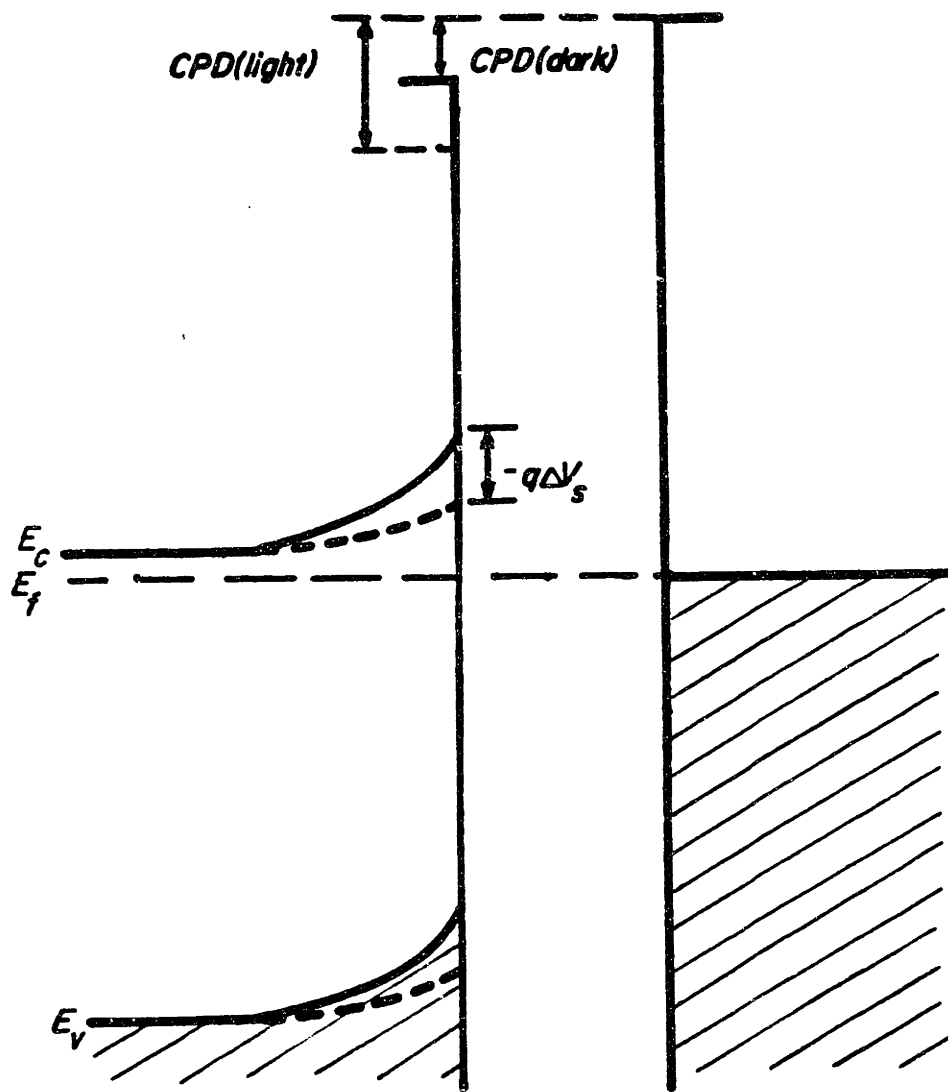


Fig. 2.6 Energy Level Schematic  
for Contact Potential  
Difference

Physisorbed species were found to be desorbed by vacuum and chemisorbed adsorbates were removed by illumination.<sup>67</sup> In this analysis, Vohl interpreted the results in terms of a depletion layer barrier at the  $\text{TiO}_2$  surface with several types of surface states present on the surface. No attempt was made to further analyze the data in terms of charge transfer activity, electronic surface parameter modifications or surface state characteristics. The nature of the real surface under study, namely a colloidal film of  $\text{TiO}_2$  particles with an unknown surface area prevented such assessments.

## 2.5 Theoretical Considerations

It has been shown that photoelectrochemical reactions occurring on semiconductor surfaces depend primarily upon the accumulation of photogenerated minority carriers at the semiconductor surface, and the transference of these carriers from the semiconductor to the adjoining reaction levels in the electrolyte. In this section the physics pertaining to these processes will be reviewed, and the properties and parameters of importance will be made clear.

### 2.4.1 Photostimulated Semiconductor Behavior near Surfaces

Theory from semiconductor physics is readily applicable to photostimulated processes occurring within semiconductors adjacent to interacting mediums. Recombination at the surface of the semiconductor in the absence of adsorbate interactions can also be described using solid state theory. These topics are treated in turn below.

The theory of photoconduction of minority carriers through a Schottky barrier analogue of Figure 1.1 was first developed by Gartner,<sup>68</sup> and has since been reaffirmed, with minor modifications, by different approaches to the problem.<sup>14,15,69-71</sup> It was recognized that

the total minority carrier current reaching the surface of the semiconductor under steady state conditions was due to both the carriers generated in the depletion layer, and the carriers which diffuse from the bulk to the surface without recombining. As a result, the total photocurrent density at the surface of a semiconductor under illumination and constant reverse bias is given by (see Appendix C for derivation):

$$J_{\text{tot}} = -qI_0 \left\{ 1 - \frac{\exp(-\alpha W)}{1 + \alpha L_p} \right\} \quad (2-14)$$

where  $I_0$  is the incident light intensity of band-gap photons,  $\alpha$  is the absorption coefficient at energies greater than  $E_{\text{gap}}$ ,  $W$  is the depletion layer width,<sup>72</sup> and  $L_p$  is the diffusion length of holes. Attempts have been made to modify this equation to account for the surface recombination of holes, and carriers transferred to the electrolyte.<sup>70</sup> These modifications however introduce additional parameters without physical significance, the values of which have yet only been derived to fit experimental data.

An additional current due to defect electromigration to the surface has been observed and modelled by Butler.<sup>47</sup> This effect is however secondary in photostimulated semiconductor behavior, and is not considered here.

Several factors influence the amount of photovoltage supported by the illuminated semiconductor. Gerisher<sup>73</sup> has derived the change in voltage due to illumination under the condition of constant current as (see Appendix C for details):

$$\Delta V_{\text{ph}} = (kT/q) \ln \left\{ 1 - (L_p/D_p p_0) [I - I_{\text{sr}}] \right\} \quad (2-15)$$

where  $I$  is the absorbed light intensity [ $I = I_0 \exp(-\alpha/d)$ ],  $I_{\text{sr}}$  is the surface recombination rate,  $D_p$  is the diffusion coefficient of holes,

$P_0$  is the equilibrium hole concentration (bulk), and  $L_p$  is the diffusion length of holes. While the condition of constant current may not be satisfied in the system under study, the above equation serves to indicate those parameters of importance in determining the reaction of the semiconductor, in the region adjacent to the surface, to illumination. As is seen, the parameters associated with the photogenerated minority carriers are critical in determining the behavior of the semiconductor, as would be expected in light of equation (2-1).

### 2.5.2 Charge Transfer at Semiconductor Surfaces

The exchange of charge at the semiconductor surface between active electronic states of the semiconductor and interacting ions from either liquid solutions or gaseous ambients is fundamental to the nature of the semiconductor-catalyzed chemical reactions occurring at the surface. Photogenerated holes at the semiconductor surface can participate in two events: they can either recombine with unlike charges at the semiconductor surface, or they can be transferred to interacting species at the surface. Surface recombination can be thought of as a special case of charge transfer wherein minority carriers move to recombination centers at the surface, recombining with majority carriers.

#### 2.5.2.a Classical Surface Recombination

It is normally assumed in semiconductor physics, as well as in semiconductor electrochemistry, that the net rate of capture of conduction band electrons by a surface energy level can be expressed as

$$dn_t/dt = \langle c \rangle A_n [n_s(N_t - n_t) - n_1 n_t] \quad (2-16)$$



where  $n_s$  is the surface density of electrons [ $n_s = n_b \exp(-qV_s/kT)$ ] in the conduction band at the surface,  $n_t$  is the density of electrons (per unit area) in surface state traps,  $N_t$  is the total density of surface traps,  $n_1$  is a temperature dependant emission constant for the surface traps determined by applying the condition that at equilibrium,  $dn_t/dt = 0$ .<sup>23,24,74</sup> The product of the thermal velocity of electrons,  $\langle c \rangle$ , and the capture cross section of surface traps for electrons,  $A_n$ , is referred to as the rate constant or capture probability. The two terms in the above equation represent the flows of electrons from the bulk to the surface trapping levels and vice-versa. The mechanisms of charge transference are not specified. A similar equation for the net rate of hole transfer to surface traps is given by

$$dp_t/dt = \langle c \rangle A_p (p_s n_t - p_l p_t). \quad (2-17)$$

In this equation, the influence of photogenerated holes is felt through the surface density of holes,  $p_s = p_i \exp [(p E_f^* - E_i)/kT]$ , which is defined in terms of the quasi-Fermi energy for holes (Equation 2-1). Under steady state conditions where the net electron and hole currents to the surface are equal, equations (2-16) and (2-17) may be equated, and an expression for  $n_t$  in terms of the above variables may be obtained. Utilizing this expression for  $n_t$  in equation (2-16) yields

$$\frac{dn_t}{dt} = \frac{\langle c \rangle^2 A_p A_n N_t (n_s p_s - n_b p_b)}{\langle c \rangle A_n (n_s + n_l) + \langle c \rangle A_p (p_s + p_l)}. \quad (2-18)$$

Using this expression, one can find the surface recombination velocity (SRV), which is defined as the ratio of electron (or hole) flow into a surface area to the excess carrier density (of each respective type, electrons or holes) in the bulk just beneath the surface. Such an expression for the SRV can be made in the case of photogenerated holes recombining at electron occupied surface states on n-TiO<sub>2</sub> as:

$$(SRV) = \frac{n_b \langle c \rangle A_p n_t}{n_i \left[ \exp\left(\frac{E_t - E_i}{kT}\right) + \exp\left(\frac{E_{f,s}^* - E_t}{kT}\right) \exp\left(\frac{E_{f,s}^* - E_i}{kT}\right) \right]} \quad (2-19)$$

In this equation,  $n_b$  is the bulk donor density,  $\langle c \rangle$  is the thermal velocity of holes,  $A_p$  the surface state capture cross section for holes,  $n_t$  the total number of surface traps,  $E_i$  the intrinsic Fermi level,  $E_t$  the surface trap energy level, and  $E_{f,s}^*$  is the Fermi level at the surface under illumination (see Appendix C). Thus the value of the surface recombination velocity, and in turn the behavior of the potential distribution in the space charge region (SCR) and at the surface are dependant upon the surface state capture cross section and the thermal velocity of holes interacting with these surface states. The above expression pertains to a steady state situation where the population of electron occupied surface states existing at a discrete energy level remains constant. This Shockley-Read expression was first derived to describe bulk recombination processes, although it was extended to address surface phenomena.

#### 2.5.2.b Semiconductor-Liquid Charge Transfer

The fundamental idea that catalyzed reactions on semiconductors may involve the transfer of charge between the semiconductor and the surface reactants was first put forth by Wagner and Hauffe.<sup>75</sup> Further investigation<sup>76</sup> demonstrated that the adsorption of molecules at semiconductor surfaces involves charge transference which results in the modification of the surface potential barrier. Quantitative models of charge transfer chemisorption utilizing Fermi-Dirac statistics for surface donor and acceptor states due to adsorbed molecules have been developed<sup>77,78</sup> and, under steady state conditions, have resulted in the

recombination analyses governed by equations such as (2-19).

There are fundamental differences between the steady state evaluation of net surface recombination processes according to equations such as (2-19) and the description of charge transfer processes occurring at semiconductor-liquid interfaces. Charge transfer processes cannot be described by steady-state modelling (indeed in steady state, no net processes occur), and the processes which do occur are limited by the slowest step in the sequence of occurring events. The process by which the rate of adsorption on semiconductor surfaces may be limited is the transference of conduction band electrons to species in solution. These charged species may subsequently interact with electroactive adsorption sites on the semiconductor surface.

An approximation can be made for the capture of conduction band electrons by oxidized species in solution adjacent to the semiconductor.<sup>23,24</sup> Utilizing an integration in the thermal energies of conduction band electrons from  $E_{cb}$  to  $(E_{cb} + 2kT)$ , and adapting equation (2-16) to the situation of a semiconductor-electrolyte interface wherein the energies of the oxidized species in solution fluctuate according to the mechanisms discussed in section 2.2.2.b, Morrison has expressed the rate of conduction band electron transfer to oxidized surface species as

$$\frac{dn}{dt} = \langle c \rangle A_n n_b \exp(-qV_g/kT) d[ox] (kT/\pi\lambda)^{1/2} \exp\left[-\frac{(E_{cb} - E_{ox})^2}{4\lambda kT}\right]. \quad (2-20)$$

Here,  $[ox]$  is the solution concentration of oxidized species,  $E_{ox}$  their equilibrium energy level in solution, and  $d$  is the distance to which the electrons can tunnel into the solution and combine with the oxidized species. A preferred value of  $d$  is about 15 Å. The capture cross section in this case pertains to that of the oxidized species

which subsequently bonds at an active surface site.

### 2.5.2.c Charge Transfer Chemisorption

The interactions between a gaseous ambient and the semiconductor surface during adsorption roughly parallel those of liquid interactions. Some important distinctions are to be made however. The gaseous oxidized species are not solvated, nor are they in continuous physical contact with the surface. These species arrive at the surface at some rate determined by the pressure of the system, becoming temporarily physisorbed to the surface. Also the fluctuations in energy of these species do not involve the repolarization of the solvent dielectric; their fluctuations are related to the thermal energy of the physisorbed species themselves.

A simple equation for the charge transfer rate developed by Many<sup>74</sup>, and applied to the adsorption of oxygen on surfaces of II-VI compounds is of the form

$$dn_t/dt = M_p \langle c \rangle A_n n_s \quad (2-21)$$

where  $M_p$  is the density of physisorbed molecules,  $\langle c \rangle$  is the thermal velocity of electrons,  $A_n$  is the surface state capture cross section for an electron and  $n_s$  is the surface density of electrons. The density of physisorbed molecules is reasoned to be constant at a given pressure throughout the chemisorption process since physisorption rates are many times faster than chemisorption rates. Thus, charge transfer chemisorption occurs between a semiconductor and an inexhaustible supply of physisorbed molecules proportional to pressure of the interacting ambient.

As applied to the chemisorption of oxygen on CdS and ZnO<sup>79</sup>, equation (2-8) yields unphysically small capture cross sections in the

range from  $10^{-29}$  to  $10^{-22}$   $\text{cm}^2$ . Consequently, Weber<sup>80</sup> has suggested that chemisorption depends on the overcoming of an activation barrier such that only physisorbed molecules which are activated by sufficient thermal energy is isoenergetically capture conduction band electrons may participate in the chemisorption process. This model was verified by Lagowski et.al.<sup>81</sup> for the chemisorption of oxygen on ZnO, and resulted in more realistic capture cross sections of  $10^{-16}$   $\text{cm}^2$  for activated surface states. This thermal activation model is discussed and developed from first principles in Appendix C. The rate of charge transfer between adsorbing species and the semiconductor surface is given by the equation

$$\frac{dn_t}{dt} = c P_{O_2}^{n\beta/2} \exp(-q\phi/kT) \langle c \rangle A_n (n_{tot} - n_{occ}) n_b \exp(-qV_s/kT) \quad (2-22)$$

where  $P_{O_2}$  is the oxygen pressure,  $\langle c \rangle$  is the thermal velocity of electrons,  $A_n$  is the electron capture cross section of the activated surface state,  $n_{tot}$  is the total number of surface states participating in chemisorption,  $n_{occ}$  is the number of surface states occupied by electrons,  $(-q\phi/kT)$  is the thermal activation energy term,  $n_b$  is the bulk electron density,  $(-qV_s/kT)$  is the surface potential energy barrier term and  $c$  is a proportionality constant.

Comparing and contrasting equations 2-20 and 2-22 serves to draw correlations between the charge transfer modelling of the semiconductor when in contact with solutions and ambients. Many of the terms in these equations are similar. The number of thermally activated species present at the surface can, for example, be delineated in each case. It is only the ambient interaction modelling which indicates a dependance on the number and occupation of surface states however. The investigation of the photostimulated ambient interactions can thus

serve to provide an increased knowledge and improved understanding of the reactions occurring at semiconductor surfaces. While this information may be of immediate importance in photoelectrochemical cell applications, it is, in a larger sense, important in the fundamental understanding of reactions catalyzed at semiconductor surfaces.

### Chapter 3: **MOTIVATION AND SCOPE**

The electronic surface properties of semiconductors are prominent as factors critical in the reactions catalyzed at such surfaces. As has been mentioned in previous chapters, the photostimulated behavior of semiconductors can be exploited in solar energy collectors, such as photoelectrochemical cells, to provide desirable chemical fuels. More important than this immediate technological impact is the basic understanding of the nature of reactions catalyzed at semiconductor surfaces. It is only through this basic understanding that we can hope to more gainfully utilize semiconductors as catalysts in chemical reactions. The role of the electronic surface properties of semiconductors are thus of paramount importance in the determination and manipulation of the processes which occur at such surfaces.

The study of the role of semiconductor behavior in the reactions occurring at their surfaces has largely proceeded along two fronts: the direct study of semiconductor-electrolyte interfaces in solutions containing electroactive species; and the investigations of ambient interactions on clean, vacuum prepared surfaces. Both of these methods provide a wealth of information within their own regimes, but each suffer from limitations inherent to their particular approach to the problem. Wet electrochemical cell studies suffer from ambiguities arising from the interactions of a surface dipole layer, and the constant altering of the exact status of the surface by ongoing reactions. Clean surface studies are limited by their rigorous preparation techniques which may produce surfaces bearing little resemblance to those encountered in engineering situations. Also these

clean surface studies employ ambient exposures low small to adequately describe those processes occurring in situations of technological importance.

The motivation behind this thesis is to identify the effects of illumination and adsorbates upon the properties of useful, reproducible surfaces of semiconducting titanium dioxide, to present the physics of ongoing surface reactions occurring in such situations, and to discover more of the true nature of real  $\text{TiO}_2$  surfaces and their properties.

In addressing these objectives, this thesis is the next logical step in semiconductor surface research. This thesis seeks to investigate the behavior of  $\text{TiO}_2$  surface reactions, which will provide insights not possible by either the wet electrochemical cell or clean vacuum approaches. The approach to be taken here will be to use reproducible titanium dioxide surfaces on which the variations in the surface electronic properties due to illumination and a wide range of ambient exposures are measured via the contact potential difference technique. Correlations between clean surface studies and wet electrochemical cell measurements will be made, and attempts to reconcile information both of these methods will be undertaken. The photostimulated ambient interaction effects upon the surface potential, electron affinity, surface electron energy states, surface recombination velocity, and the surface bonding arrangements are the relationships to be measured and analyzed.



## Chapter 4: EXPERIMENTAL PROCEDURE

### 4.1 Sample Preparation

The sample preparation procedure utilized in this study, particularly the surface preparation technique, has been critical to this research insofar as the ensuing experimental procedures and results are dependant upon routinely obtaining a reproducible surface to be used as a basis for experimentation. The sample preparation outlined in this section is not a haphazard recounting of the procedures used. Rather, the steps utilized in this preparation have been painstakingly developed in order to obtain a surface which is reproducible, sensitive to illumination and ambient exposures, and can be reclaimed after photostimulated reactions.

Single crystal titanium dioxide crystals (rutile) as grown by the Verneuil flame fusion technique were utilized in this study. A nominally stoichiometric rutile boule containing no intentional impurities was obtained from Commercial Crystal Laboratories.<sup>82</sup> Subsequent chemical analysis of the boule revealed the following trace impurities (by weight percent): 0.30% Al; 0.03% Cr; 0.009% C and less than 0.01% Si. The aluminum and chromium impurities act to introduce acceptor levels in the energy gap of the material, partially compensating for the vacant oxygen (donor) activity (see Appendix B). As recieved, the crystal was translucent with a slight yellowish tint.

Samples were oriented using the back-reflection Laue technique<sup>83</sup> and cut perpendicular to the c-axis ( $\pm 2^\circ$ ) using a guillotine wire saw and a cutting slurry of 600 grit (20  $\mu\text{m}$ ) SiC powder in light oil. Typical sample dimensions were 1cm x 1cm x 0.1cm. To minimize the

impact of impurity concentration fluctuations within the as received boule, all samples were cut from the same region of the crystal. Samples were reduced in various pressures of hydrogen to induce n-type conductivity (see Appendix B). The reduction of samples under one atmosphere of hydrogen was done in a carbon filament furnace using a continuous flow of purified hydrogen. Reduction of samples in reduced pressures of hydrogen was done by back-filling quartz ampoules containing the samples with the requisite pressures of hydrogen. The ampoules were sealed and subsequently heated in a tube furnace. All samples were held at the reducing temperature for 48 hours to insure sample homogeneity, and they quickly cooled to prevent the out diffusion of donor defects. The temperatures and pressures of reduction ranged from 350°C to 700°C and from 1 atm to  $10^{-8}$  atm, respectively. The coloration of the samples thus treated changed to a translucent light bluish-green. This color was retained by the samples throughout the following polishing, cleaning and surface testing.

All samples were polished prior to any characterization procedure. An acetone-soluble thermoplast wax (Crystalbond) was used to affix the sample to a flat metal disc which was then mounted onto a polishing block assembly. Rough lapping of the samples was performed first by use of 20 $\mu$ m sandpaper and then by the use of a 5 $\mu$ m optical garnet powder slurry on a flat plate. Rough polishing was done on a Rodel type-204 synthetic polishing pad on a polishing wheel using a 0.5 $\mu$ m alumina slurry. Between each step of this polishing procedure, the polishing assembly was thoroughly cleaned with DI water to remove any residual polishing grit. Each step of this mechanical polish was continued until all traces of previous steps were removed from the surface. During mechanical polishing, approximately 200 $\mu$ m of surface

material was removed. The removal of this amount of surface material insures the removal of any surface layers from which donor defects may have out-diffused during the cooling of the samples after reduction.

The final polishing of the samples was done on a polishing wheel, again with a Rodel-204 polishing pad, and a solution of Nalcoag 1030 colloidal silica from the Nalco Chemical Company.<sup>84</sup> The colloidal silica was diluted 1:2 with DI water. Samples were polished until all surface damage, as inspected at 140x magnification by Nomarski interference contrast, was removed, and a mirror finish was produced. Typical final polish times were 40-60 minutes.

After achieving a mirror finish, the samples were removed from the metal discs by gentle heating ( $\sim 80^{\circ}\text{C}$ ) and the residual wax removed with EG acetone. The samples were then cleaned by repeated rinses in DI water, EG trichloroethylene, EG acetone and EG isopropyl alcohol. Samples were dried in a room temperature nitrogen gas stream. Gross surface contaminants were then removed from the samples by a 30 minute cleaning in a 5N NaOH solution at  $80^{\circ}\text{C}$ . Following this cleaning, samples were again rinsed in DI water and EG isopropyl alcohol, and dried in nitrogen.

Four ohmic contacts made with clean In metal were symmetrically soldered at the sample periphery. Gold wires (0.003" dia.) were soldered to the contacts. Contacts were tested for ohmic (resistive) behavior with an I-V curve tracer. The specific resistivity of the samples was determined using the van der Pauw technique.<sup>85</sup>

Gold wires and indium contacts were then removed and the surfaces of the samples were then again polished (both sides of the samples were polished at this time), rinsed, cleaned, rinsed again and dried per the

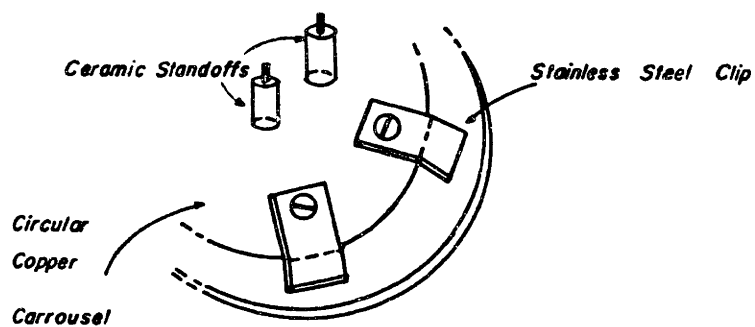
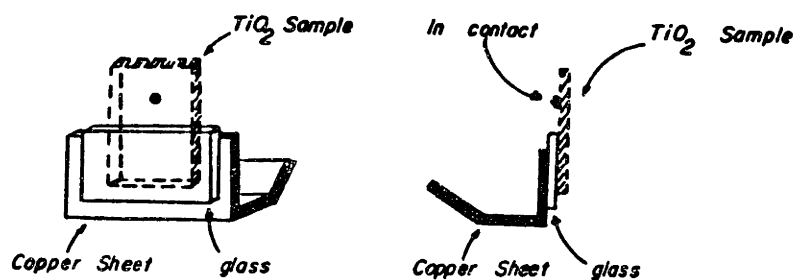
above procedure.

The samples were cantilevered from a small piece of glass using a silver paste (conductive epoxy). The glass acted as a insulator and a spacer such that the metal of the sample manipulator would not influence the contact potential difference measurements. The glass standoffs were then attached, again by means of silver paste, to a piece of malleable copper sheet (see Figure 4.1). Care was taken not to allow any electrical shorting to occur between the  $\text{TiO}_2$  samples and the copper sheet via the silver paste. The copper sheet-glass- $\text{TiO}_2$  assemblies were then mounted on a copper carrousel. Indium contacts were soldered to the back sides of the cantilevered  $\text{TiO}_2$  samples. Gold lead wires from the samples were connected to adjacent terminals to minimize the strain on the contacts. Further connections were made using anodically anodized aluminum wire. The sample carrousel was placed into the vacuum chamber via a 6" OD port. Further electrical connections to the samples were made via the electrical feedthroughs on the sample manipulator to which the carrousel was attached. The copper carrousel was grounded through one of these feedthroughs so that interfering effects on the measurements were minimized.

#### 4.2 Apparatus

The vacuum system used in the contact potential difference measurements, with the exception of the main chamber itself, is the Varian model 981-1000 low-energy electron diffraction (LEED) system (Figure 4.2). This system is composed of a 140 liter/second ion pump which is throttled by a butterfly valve, a zeolite charged sorption pump, a roughing manifold which is isolated from the chamber by a sealed bakeable valve and a copper-sapphire seal variable leak valve

Fig. 4.1 Sample Mounting and  
Carrousel Arrangement



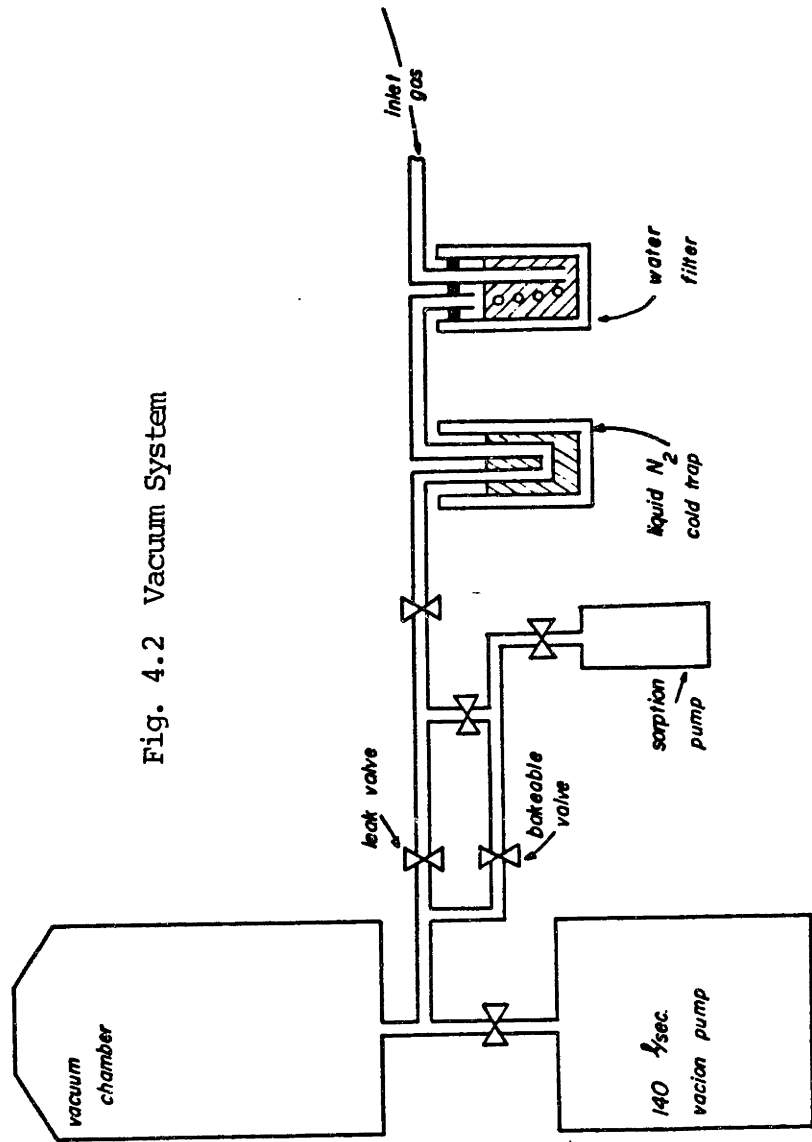


Fig. 4.2 Vacuum System

between the gas manifold and the chamber. Using this system, controlled ambient pressures in the ranges from  $10^{-8}$  to  $5 \times 10^{-5}$  torr, and  $10^{-2}$  to 0.5 torr could be obtained. Atmospheric pressure of desired ambients could also be admitted into the chamber. The pressures in the chamber were monitored with Varian ionization and thermocouple gauges.

The vacuum chamber used is an ULTEK model with two 8" ports, three 6" ports and seven 2-3/4" ports. All vacuum ports were sealed by copper gasket-conflat flange seals. All instrumentation and samples were introduced into the chamber via the conflat feedthroughs. The chamber also had a twelve pin electrical feedthrough, a viewport on an 8" OD flange, a viewport on a 2-3/4" OD flange, and a sapphire window with an 80% transmission from  $0.34\mu\text{m}$  to  $2.5\mu\text{m}$  on a 2-3/4" OD flange. All external equipment interacted with the sample through these feedthroughs. A stainless steel bracket was welded to the inner wall of the chamber so that a Kelvin probe apparatus could be installed for contact potential difference (CPD) measurements. This apparatus was placed below the sapphire window such that an optical path was established for illumination of the sample during CPD measurements. The copper carousel was mounted onto a stainless steel rod beneath a Huntington PM 600-XYZR manipulator secured to the chamber on a 6" OD flange. With the manipulator, samples could be placed into a position adjacent to the Kelvin probe apparatus. Several samples mounted on the carousel could be rotated into position by using the manipulator.

### 4.3 Experimental Techniques

#### 4.3.1 Measurement of Semiconductor Work Function

The semiconductor work function,  $\phi_{\text{TiO}_2}$ , the energy difference between the semiconductor Fermi level and the vacuum level, is measured

by the contact potential difference technique.<sup>86</sup> A gold reference electrode and the TiO<sub>2</sub> sample are connected externally and brought into close proximity such that they form a capacitor. A field exists between the two "plates" of this capacitor that is proportional to the difference in work functions between the two materials, and inversely proportional to the distance between the two plates. As the plates are moved closer together, a current is generated that is equal to the difference between the work functions times the rate of change of the capacitance (Equation 4-1).

In the vibrating Kelvin probe CPD measurement technique, the gold probe is attached to a stiff ferromagnetic reed which is vibrated at its natural frequency by an electromagnet driven by a sinusoidal function generator (H.P. 3310B, see Figure 4.3). In this manner, the capacitance is varied sinusoidally, which results in an AC current flowing between the electrodes. The equation to describe this AC current is

$$i = (\phi_{\text{TiO}_2} - \phi_{\text{Au}}) \frac{dC}{dt} \quad \text{wherein} \quad (4-1)$$

$$(\phi_{\text{TiO}_2} - \phi_{\text{Au}}) = \text{CPD} = \text{contact potential difference, and} \quad (4-2)$$

$$\frac{dC}{dt} = \frac{\epsilon A w \Delta d \cos(wt)}{[d_0 + \Delta d \sin(wt)]^2} \quad (4-3)$$

where  $\epsilon$  is the permittivity between the capacitor plates, A is the effective area of the capacitor plates,  $d_0$  is the equilibrium spacing of the plates and,  $\Delta d$  and  $w$  are the amplitude and frequency of vibration, respectively. The area sampled in these measurements is the effective physical cross section of the boss on the gold probe, approximately 1 mm<sup>2</sup>. In all the measurements taken, the equilibrium



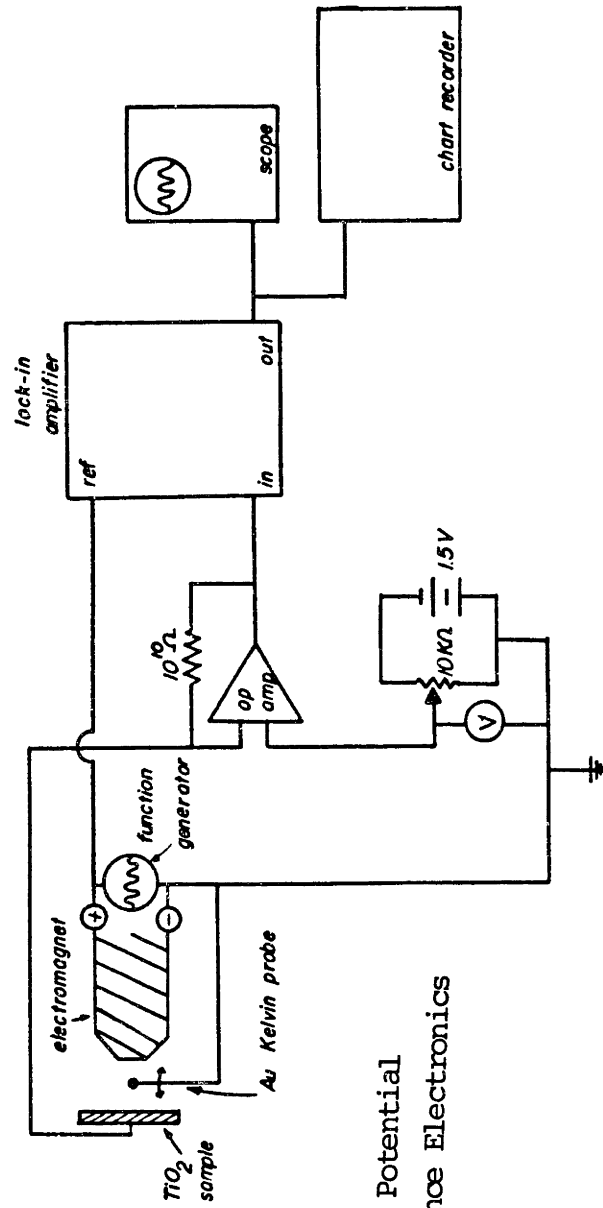


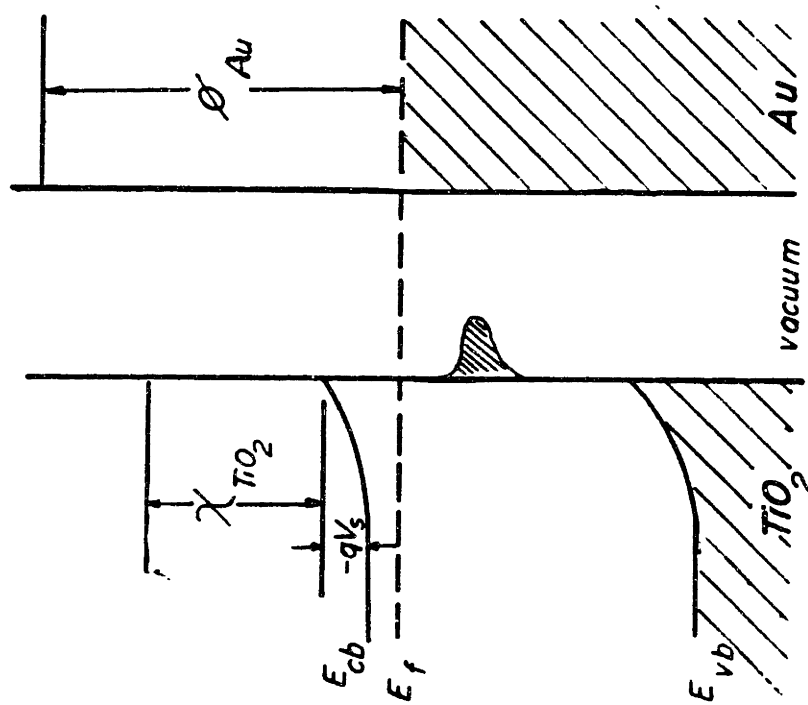
Fig. 4.3 Contact Potential Difference Electronics

spacing, amplitude and frequency of vibration were held constant at values of 0.35mm, 0.11mm, and 94.4 hz, respectively. Thus the time rate of change of capacitance was the same for all tested samples, and direct comparison of CPD changes for different samples was possible.

The AC signal from the  $\text{TiO}_2$  sample a high input impedance, low noise perational amplifier (Burr-Brown 3542J). The ensuing signal analysis is shown in Figure 4.3. The signal is calibrated using the operational amplifier in the differential input mode. A variable bias voltage supply with a digital readout (Keithly 177) is used as an opposing input to the operational amplifier. The AC signal from the operational amplifier is subsequently amplified by a lock-in amplifier (PAR 124A with 117 pre-amp) driven at the same frequency as that of the gold probe vibration. Thus, when the output of the lock-in amplifier is nulled, the bias voltage supply is equal to  $-(\text{CPD})/q$ . The CPD value of the  $\text{TiO}_2$ -Au pair can thus be read from the digital readout to within 2 meV. The output signal from the lock-in amplifier is monitored with an oscilloscope (Tektronix 5110), and the variation in the CPD is continuously monitored pen chart recorder (H.P. 7044A). Changes in the CPD are interpreted as changes in the  $\text{TiO}_2$  work function since gold's work function is not considered to change under these treatments.<sup>87</sup> The changes in the contact potential are then due to changes in the semiconductor's electron affinity,  $\chi_{\text{TiO}_2}$ , and surface potential (see Figure 4.4). Periodically, calibration marks are made on the chart recorder, by using the variable bias voltage supply, and off null measurements can be made by linear interpolation.<sup>88</sup>

#### 4.3.2 Measurement of Surface Potential

When the  $\text{TiO}_2$  sample is illuminated with light of energy greater



$$CPD = \phi_{TiO_2} - \phi_{Au}$$

$$CPD = \chi_{TiO_2} - qV_s + (E_{cb} - E_f) - \phi_{Au}$$

$$\Delta CPD \approx -q\Delta V_s + \Delta\chi_{TiO_2}$$

Fig. 4.4 Contact Potential Difference Energy Schematic

than that of the band gap ( $\lambda < 0.41 \text{ um}$ ), photogenerated minority carriers accumulate at the semiconductor surface, recombine with electrons and depopulate surface states. The absorption of light energy by the semiconductor thus has the influence of reducing the surface potential barrier by inducing a flux of photogenerated holes to the surface which depopulate occupied surface states. Under the conditions where no ambient interactions are allowed at the semiconductor surface (surface stabilized in UHV), the change in contact potential difference with illumination thus reflects the change in the surface potential (see Figure 4.4,  $\Delta\chi = 0$ ). By increasing the intensity of illumination, the hole flux to the surface increases until flat band conditions are reached at the semiconductor surface. Consequently, the contact potential difference should change with increasing illumination intensity until a saturation occurs where  $-\text{CPD}/q = V_{\text{barrier}}$  and flat band conditions are obtained. If a saturation of contact potential difference does occur, photoconductivity measurements should also be made under identical experimental conditions, to ascertain if the photovoltage saturation is consistent with the numbers of free carriers being generated, and complications due to the heating of the sample do not arise.<sup>79,88</sup>

Illumination of the  $\text{TiO}_2$  samples while being monitored for CPD measurements within the vacuum chamber, was provided by a 150 watt Xenon arc lamp (Osram XBO 150W/1 powered by an Oriel 8500 DC supply). The integrated intensity of this lamp was measured with a Moletron pyroelectric radiometer (PR200) to be  $10^{17}$  photons/cm<sup>2</sup>-sec. Using Ziess and Oriel optical bench equipment, the light was focussed onto a 1 cm<sup>2</sup> with intensities of up to  $\sim 150 \text{ mw/cm}^2$ , as detected with an Oriel radiometer (7084).

### 4.3.3 Measurement of Surface Electronic States

Surface photovoltage spectra, the spectral response of the surface potential under illumination with light of various energy, can be used to locate in energy the optical thresholds for electronic transitions between the valence and conduction bands and the active surface states. Thus, the energy positions of active surface states can be located with respect to the band edges.<sup>89</sup> A double prism monochromator (Ziess 12MM, with #814 quartz prisms) was in conjunction with the Xenon lamp to provide a continuous range of monochromatic light from 2 $\mu$ m to 0.25 $\mu$ m. To increase the intensity of the monochromatic light to the sample, a narrow range light filter ( 0.5 $\mu$ m  $\pm$  0.005 $\mu$ m from Thin Film Products) was used to excite most sub-gap optical processes (processes with energies less than 2.48 eV).

The effects of ambient exposures on the surface electronic structure can be revealed by the comparison of surface photovoltage spectra before and after such exposures.

### 4.3.4 Measurement of Charge Transfer Activity

The semiconductor space charge region is characterized by its surface potential barrier,  $V_s$ . This surface potential is found by using Gauss' law at the surface to be

$$V_s = \frac{Q_s^2}{2\epsilon_0 q n_b} \quad (4-4)$$

where  $Q_s$  is the surface charge per unit area ( coul-cm<sup>-2</sup> ),  $\epsilon$  is the dielectric constant of the semiconductor perpendicular to its surface,  $\epsilon_0$  is the permittivity of free space, and  $n_b$  is bulk free carrier density. The nature of the surface space charge layer is determined by the sign and amount of the charge trapped on its surface: with majority

carriers trapped on its surface, a depletion layer occurs (An inversion layer may also occur, but the equations developed here treat only the depletion layer situation). An expression for the amount of charge at the surface can be found in terms of the surface potential,  $V_s$ , by substituting  $Q_s = n_s q$  into the above equation to yield

$$n_s = \left( \frac{\epsilon \epsilon_0 n_b V_s}{q} \right)^{1/2} . \quad (4-5)$$

Consequently, the amount of surface charge change,  $n_s$ , associated with various processes (changes in illumination conditions, ambient exposures, etc.), can be found to be

$$\Delta n_s = \left( \frac{\epsilon \epsilon_0 n_b}{q} \right)^{1/2} [ V_{s,f}^{1/2} - V_{s,i}^{1/2} ] \quad (4-6)$$

where  $V_{s,f}$  and  $V_{s,i}$  are the final and initial surface potentials, respectively, associated with the process involved. By monitoring the changes in the contact potential difference under conditions where  $\phi = 0$ , changes in the surface potential can be determined (see Figure 4.4). Consequently, the change in surface charge population can be determined.

The rate at which charge is transferred to the surface of the semiconductor can be determined by utilizing the time derivative of equation (4-6). Presuming steady state initial conditions whereby the time rate of change of surface potential is zero, the surface charge transfer rate can be expressed as

$$\frac{dn_{s,t}}{dt} = \left( \frac{\epsilon \epsilon_0 n_b}{4q} \right)^{1/2} \left| V_{s,t} \right|^{-1/2} \frac{dV_{s,t}}{dt} \quad (4-7)$$

where  $V_{s,t}$  is the surface potential measured at a particular time  $t$  during the studied process.

To illustrate the use of equations (4-6) and (4-7) in determining the amount and rate of charge transferred to the surface, consider the change in surface charge accompanying the illumination of two surfaces under ultra high vacuum, one being a surface with no associated adsorbates, the other being the same surface upon which interactions with some electronegative species are allowed. Under strong illumination, the surface potential is measured via the off null-technique described in section 4.3.1. Upon termination of illumination, different processes may occur. First, both surfaces regain an amount of surface potential due to the repopulation of surface states by conduction band electrons. In addition to this crystal relaxation process, the second surface interacts with the electronegative species and charge transfer chemisorption proceeds. The amount of transferred charge associated with the chemisorption process can be determined by the comparison to the two CPD or surface potential transients ( $V_s = -\text{CPD}/q$ ). The crystal relaxation transient (the surface charge change associated solely with the repopulation of surface states with conduction band electrons) of the surface potential (Figure 4.5) is recorded as a CPD transient on the pen chart recorder. The total amount of charge transferred is determined from the initial and final surface potential values [equation (4-5)]. The amount of charge associated with ambient chemisorption is found by subtracting the surface potential change under vacuum conditions from that measured in the presence of an interacting ambient:

$$\Delta n_s(\text{ads}) = \left( \frac{\epsilon \epsilon_0 n_b}{q} \right)^{1/2} \left\{ [V_{s,f}(\text{amb})]^{1/2} - [V_{s,f}(\text{vac})]^{1/2} \right\}. \quad (4-8)$$

Similarly, the chemisorption rate associated with an interacting ambient can be found by comparing the slope and value of the CPD

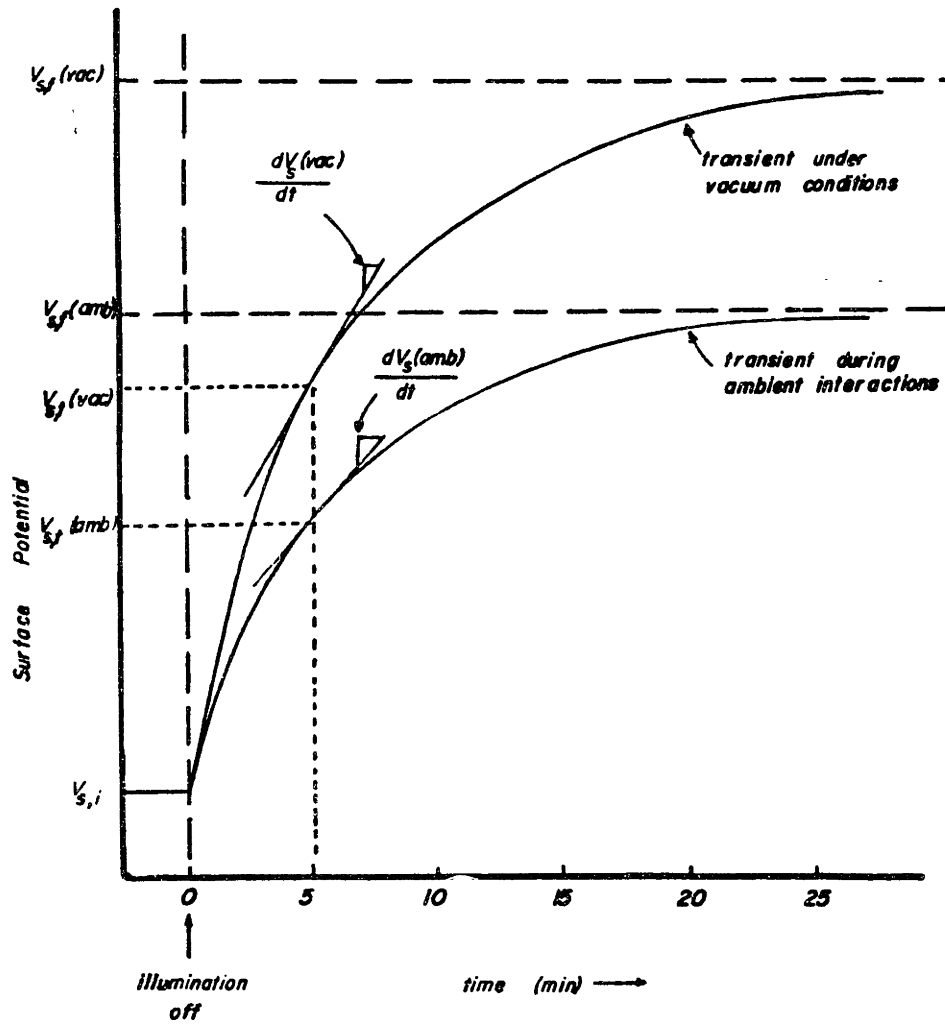


Fig. 4.5 Surface Potential Transients



transient in the presence of an interacting ambient with the slope and value of the CPD transient in vacuum. The comparative chemisorption rate at some time  $t$  is given as

$$\frac{dn_{s,t}}{dt} = \left( \frac{\epsilon \epsilon_0 n_b}{4q} \right)^{1/2} \left\{ [V_{s,t}(\text{amb})] \frac{-1/2 dV_{st}(\text{amb})}{dt} - [V_{s,t}(\text{vac})] \frac{-1/2 dV_{st}(\text{vac})}{dt} \right\}. (4-9)$$

As is seen in Figure 4.5, the change in the CPD during ambient interactions is larger and occurs more quickly than the CPD change with no ambient interactions. In the former case, the CPD transient reflects the processes occurring due to both the crystal relaxation and ambient interactions. This change is consequently larger and faster than solely the crystal relaxation transient when the ambient interactions act to reinforce those changes.

It should be reiterated here that this approach to the determination of charge transfer activity is dependant upon the assumption that the electron affinity of the semiconductor surface does not change during the chemisorption process. Under conditions where large ambient exposures are allowed to interact with the surface, particularly in cases where the ambient contains chemical species different from those of the semiconductor material, changes in electron affinity may become appreciable. Consequently the comparison of several surface potential transients, employing a range of interacting ambient exposures, illumination and vacuum conditions, is necessary to delineate the surface potential and electron affinity effects, as will be discussed in sections 4.4.2 and 4.4.3.

#### 4.3.5 Measurement of Surface Bonding Arrangements

X-ray photoelectron spectroscopy ( XPS; also known as ESCA, electron spectroscopy for chemical analysis) has been the primary

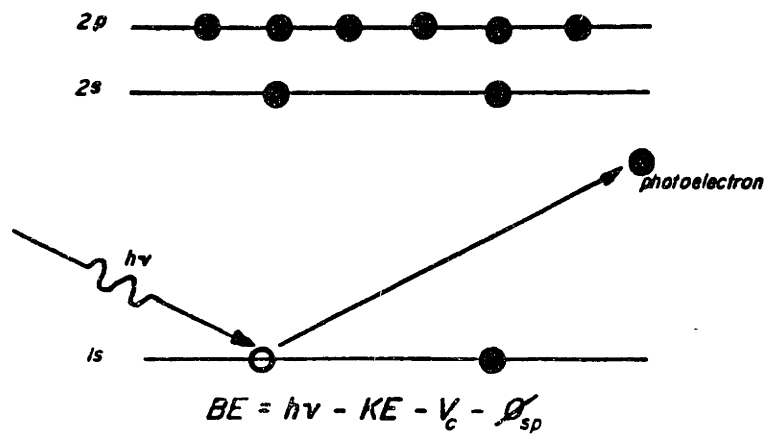
source of atomic and molecular information within the surface region ( $\approx 50 \text{ \AA}$ ). XPS experiments utilize characteristic x-rays ( Mg  $K\alpha_{1,2}$ , 1253.7 eV ) to photoionize core-type electrons from atoms in this surface region. This process is schematically shown in Figure 4.6 for the element neon. The photoionization process produces an excited, ionized atom and an electron. If the kinetic energy of the ejected electron is determined, then the binding energy of the electron to its atomic core can be calculated as:

$$\text{Binding Energy} = (\text{X-ray Energy}) - (\text{Kinetic Energy}) - V_c - \phi_{sp} \quad (4-10)$$

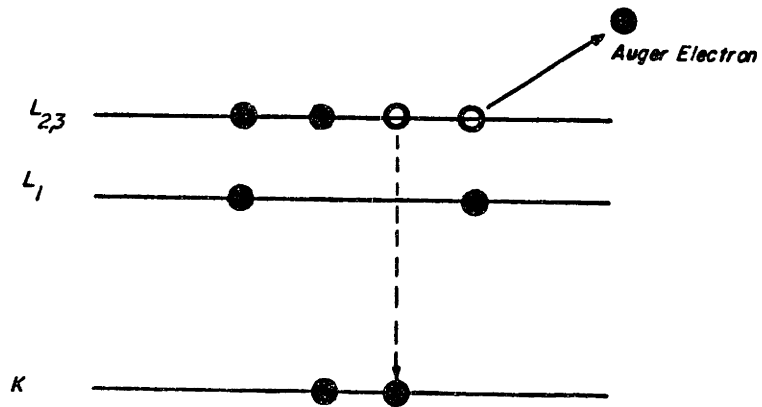
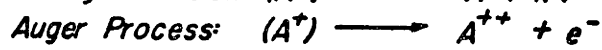
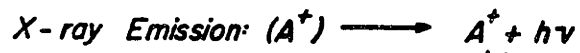
where  $V_c$  is a correction term for the positive charging which occurs on the surfaces of insulators (typically a few eV) and  $\phi_{sp}$  is the work function of the spectrometer, a known constant ( $\approx 3 \text{ eV}$ ). The binding energies of these photoelectrons are characteristic of the elements from which they have originated. Thus the binding energy can directly related to atomic species.

The XPS process generates an excited ionized ion. These species can "relax" by one of two processes: X-ray emission or the Auger process. In the Auger process, a valence electron drops in energy to fill a core vacancy while ejecting another electron to create a doubly ionized atom (Figure 4.6). This Auger electron has a characteristic energy equal to the difference in energy between the initial and final energies of the atom. Thus, when a survey scan of binding energy (1000-0 eV, 100 eV pass energy) is acquired, two different types of electron peaks can be observed: photoelectrons and Auger electrons. A sample spectrum is shown in Figure 4.7 for titanium dioxide. The photoelectron peaks and the Auger peaks are labelled, and are listed in Table 4.1.

PHOTOIONIZATION



RELAXATION PROCESSES



$$KE = E(A^+) - E(A^{++})$$

Fig. 4.6 Schematic Photoelectron and Auger Processes

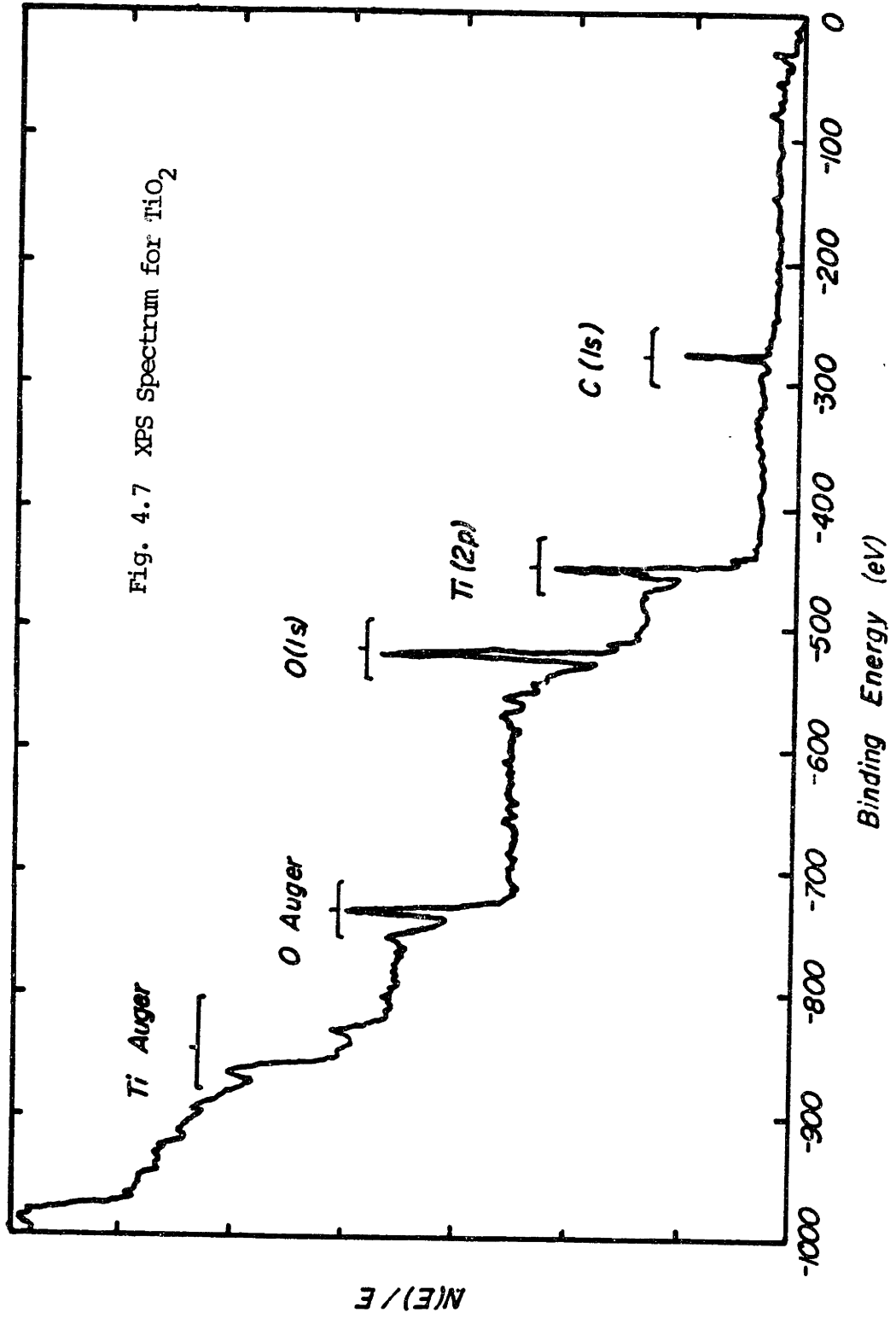


Fig. 4.7 XPS Spectrum for TiO<sub>2</sub>

**Table 4.1** Binding Energies of Primary Photoelectron and Auger Peaks of TiO<sub>2</sub> Surfaces using a Mg X-ray Source.

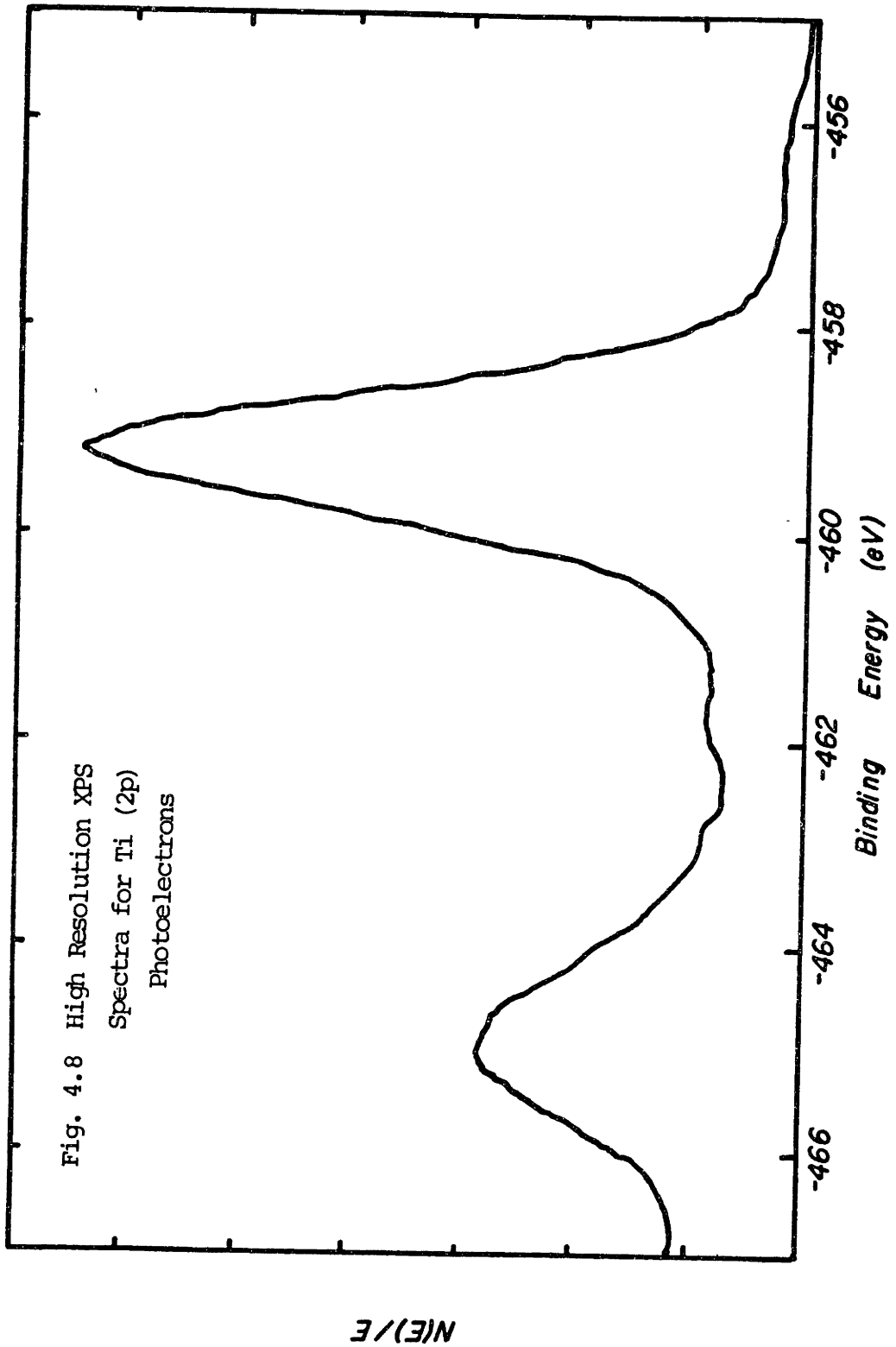
<u>element</u>	<u>photoelectron peak (eV)</u>	<u>Auger peak (eV)</u>
C	287 (1s)	993 (KLL)
O	531 (1s)	743 (KLL)
Ti	458 (2p)	839 (LMM)

data from reference 90.

Particular portions of the XPS spectra can be scanned to provide information on the binding energies of particular species (Figure 4.8). In this high resolution mode, a lower pass energy (25 eV) is used to increase the resolution of the XPS peaks and a 20 eV region about the peaks of interest are scanned. By measuring the area under the major photoelectron peaks of each element present, and using appropriate machine and element dependant correction factors,<sup>91,92</sup> the atomic composition of the surface region can be determined. Unfortunately, the error in the atomic compositions as determined by this method is  $\pm 10\%$ . Since the variations in chemisorbed oxygen species used in this study was less than 10% of the surface oxygen ( $\text{TiO}_2$ ) species, compositional determination using XPS was not pursued.

Using the high resolution XPS mode, information concerning the binding of various species at the surface can be obtained. Shifts in the exact position of these peaks result from a change in the chemical environment of the atom. These chemical shifts are of the order of 0.5 to 10 eV. Chemical shifts are to be anticipated upon the chemisorption of species onto the surface. In particular, those surface ( $\text{TiO}_2$ ) species most effected by the chemical binding of adsorbates are are expected to undergo large shifts in energy positions in the XPS spectra.

The surface sensitivity of XPS can be explained as follows. X-rays can induce ionization to a depth greater than a micron in semiconductors. However, the photoelectrons escaping from the semiconductor may undergo inelastic collisions which effectively erase their characteristic energy. The mean free path of electrons between inelastic collisions is a function of their Kinetic energy (see Figure 4.9), and is below  $\sim 20 \text{ \AA}$ . Thus  $\sim 95\%$  of the signal detected for XPS



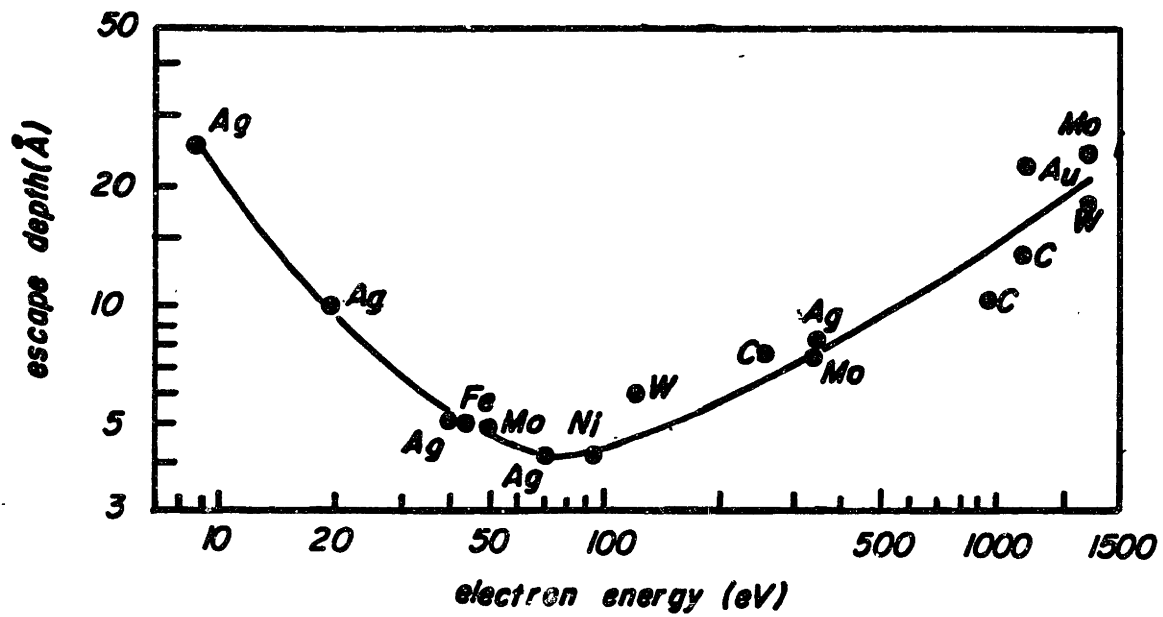


Fig. 4.9 Escape Depth of Photoelectrons as a Function of Kinetic Energy

Data from Reference 79.



peaks is produced by the top 60 Å of the semiconductor. This is the electron energy loss phenomenon which is responsible for the the surface sensitivity of XPS.

When an insulating sample is examined with XPS, positive charging (a few eV) occurs at the surface due to the emission of photoelectrons. The nature of this phenomena and an absolute referencing technique are still being debated. To eliminate the binding energy shifts caused by such surface potential buildup and return the binding energy difference to the Fermi level of the conducting standard, the standardization method of Landis and Martin<sup>93</sup> has been employed. This method determines precisely the exact energy location of the Au 4f<sub>7/2</sub> photoelectron peak from a sample reference dot and calculates a shift factor by noting the difference between the 4f<sub>7/2</sub> peak under biased (XPS operating) conditions and its reference value of 84.0 eV. Such a shift factor is then applied to the TiO<sub>2</sub> sample peaks under the same operating conditions.<sup>94</sup> In practice, the Au reference scans are taken both before and after the actual XPS sampling is done in order to account for and monitor any drifting that might occur due to changes in the surface charging.

To prepare samples for XPS measurements, a 2mm gold dot was affixed to the TiO<sub>2</sub> samples as prepared by the procedure described in section 4.1. The gold was deposited in a vacuum evaporator using a stainless steel mask. The gold decorated samples were then attached to small pieces of glass using silver paste. These glass standoffs were used to insure that the XPS data taken pertained to the same electrical conditions as those employed in CPD measurements. The TiO<sub>2</sub>-glass assemblies were set and clamped on stainless steel holders for XPS analysis.

The  $\text{TiO}_2$  samples were examined in a Physical Electronics model 548 XPS, Auger and LEED spectrometer maintained at high vacuum ( $10^{-9}$ - $10^{-10}$  torr) and interfaced to a Physical Electronics Multiple Technique Analytic Computer System (MACS). As digitized by the the computer system, the XPS information can be mathematically massaged to produce smoothed spectra, and to remove spurious data. Samples are admitted into his XPS chamber through a low vacuum ( $760 > P > 10^{-3}$  torr) entry chamber which is evacuated by a turbo-molecular pump. This chamber can be back-filled with gaseous ambients and maintained at pressures in the range of  $10^{-2}$  to 0.5 torr. The ability to expose samples to selected ambients was exploited, as will be explained in section 4.4.4.

#### 4.4 Procedure

In this section the procedures used in the study of the charge transfer reactions involving oxygen and water vapor on  $\text{TiO}_2$  will be discussed. It is first necessary to describe the control surface to be employed in this research, as it is this reproducible surface which serves as a basis for the the ensuing experimentation.

##### 4.4.1 Control Surface Conditions

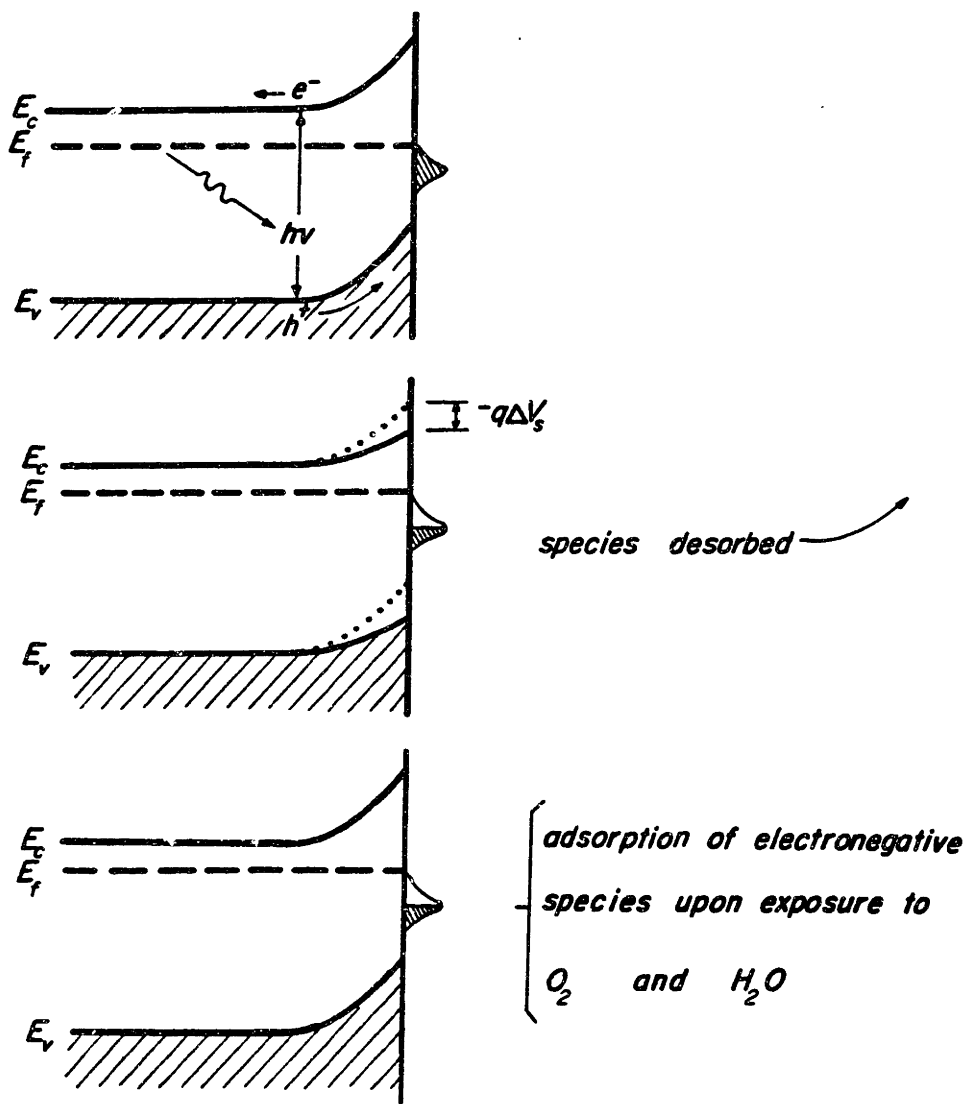
For the study of the charge transfer reactions on  $\text{TiO}_2$  surfaces, the semiconductor samples were prepared and admitted into the vacuum chamber as described in section 4.1. The vacuum chamber was pumped to a pressure of less than  $10^{-8}$  torr (typically  $P \sim 10^{-9}$  torr). Prolonged illumination of the samples under white light of and intensity of  $\sim 150 \text{ mw-cm}^{-2}$  (one hour illumination) serves to depopulate electron occupied surface states by the flux of photogenerated holes to the surface. During this process, any chemisorbed electronegative species which are

associated with the surface states will be released from the surface and drawn off into the vacuum. Illumination under high vacuum thus serves to prepare the sample for ensuing ambient interactions with surface states (Figure 4.10).

Upon termination of the illumination in vacuum, repopulation of the surface states by conduction band electrons occurs. However, a portion of this surface repopulation process occurs very slowly. Preliminary CPD measurements have indicated that it is necessary to "relax" the semiconductor for a period of greater than 10 hours following illumination in order to obtain reproducible CPD transients. This phenomena may be attributable to both the reappearance of the surface potential barrier upon termination of illumination, or the existence of states of differing characteristics at the surface. The nature of these surface states will be discussed in Chapter 5.

The reproducible control surface to be utilized in this study as a reference is that surface as prepared according to the procedure outlined in section 4.1, inserted into a vacuum of pressure less than  $10^{-8}$  torr and subjected to prolonged illumination with white light of an intensity of  $\sim 150$  mw/cm<sup>2</sup>. In this illuminated, evacuated condition, the surface is reproducible and is sensitive to changes in illumination and ambient interactions. The employment of such a reproducible surface as a basis for investigation is significant inasfar as it represents a departure from traditional methods of semiconductor surface study. It does not employ preparation procedures as rigorous as those used in clean surface studies (Ar<sup>+</sup> bombardment and vacuum anneal, etc.), nor does it employ wet electrochemical cell testing wherein the monitoring of surface reactions is complicated by the presence of surface dipole

Fig. 4.10 Energy Schematic for Control Surface Preparation



layers. At the same time, the as-prepared surface reflects conditions that would be encountered in actual engineering devices. Thus, study of this control surface can draw on and correlate information from both clean surface and electrochemical cell studies, attempt to reconcile differences between the two approaches, and be applied to engineering situations.

In this research, two cycling procedures have been employed to study the charge transfer reactions occurring on the  $\text{TiO}_2$  semiconductor surface. Both of these control cycling procedures are initiated by the production of the real, control surface. They are described in turn below.

#### 4.4.2 Light Ambient Cycling

A schematic diagram depicting the light cycling procedure is shown in Figure 4.11. The title of this procedure reflects the fact that ambient interactions are allowed during illumination of the semiconductor. The procedure is initiated by the production of a control surface according to the the procedure of the previous section. Two transients are shown in Figure 4.11: one pertaining to a control standard where no ambient interactions with the surface are allowed; one pertaining to the interaction of a hypothetical ambient species with the surface. The transient for the control standard undergoes processes which are related only to photostimulation: no intentional physisorption or chemisorption of species is allowed, although a controlled amount of photodecomposition of the  $\text{TiO}_2$  surface does occur. The quantity to be measured in this cycling procedure is the contact potential difference of the  $\text{TiO}_2$ - gold probe test cell.

After the control surface on the  $\text{TiO}_2$  surface has been prepared,

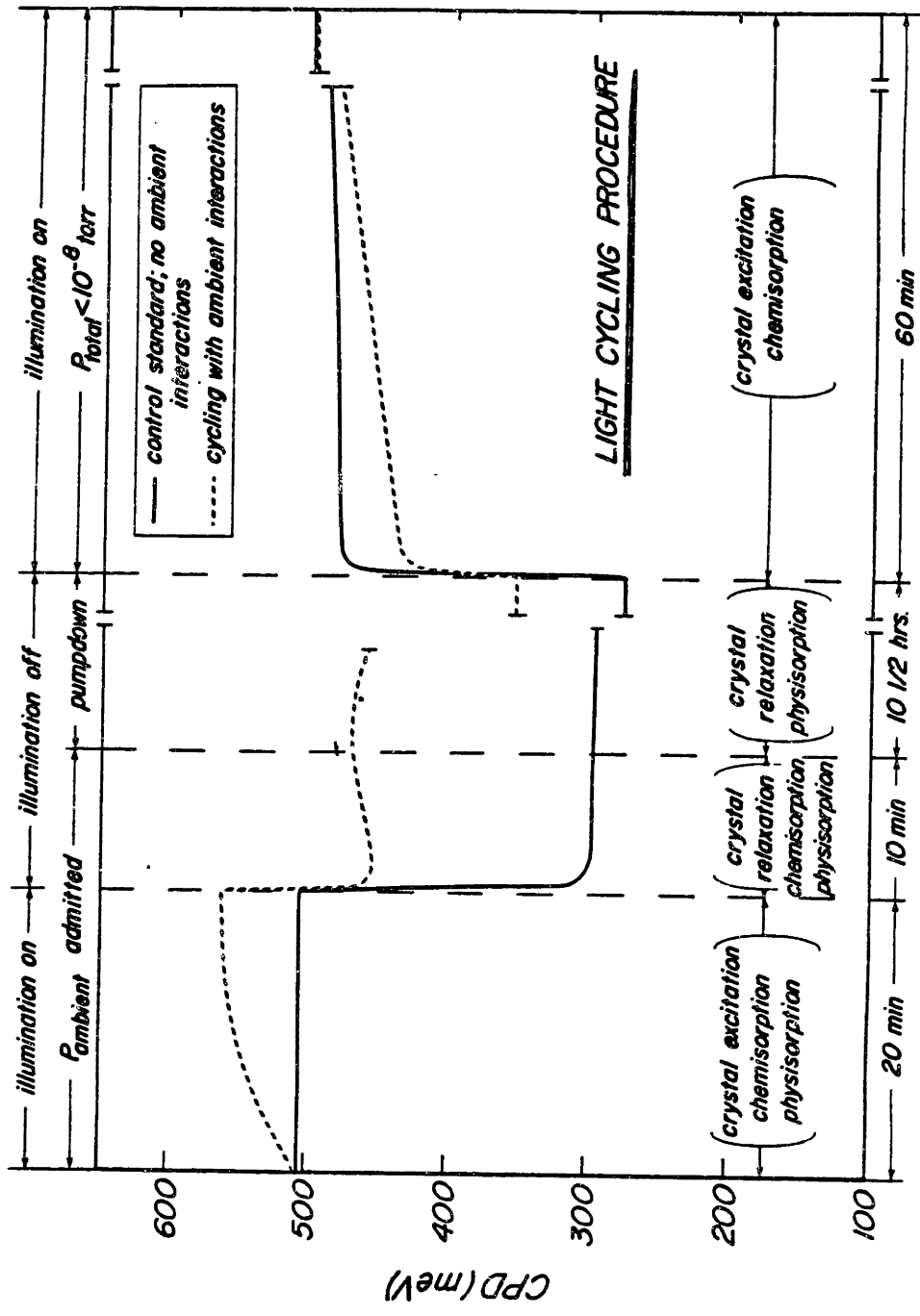


Fig. 4.11 Light Cycling Procedure

a controllable pressure of ambient is admitted into the vacuum chamber. While illumination is on, the CPD value reflects the chemisorption and physisorption processes occurring at the surface due to the interacting ambient, and also the depopulation of surface states due to the flux of photogenerated holes to the semiconductor surface. After 20 minutes the illumination is terminated, and the CPD transient reflects the chemisorption and physisorption processes, as well as the relaxation processes associated with the repopulation of surface states by conduction band electrons. After 30 minutes, the chamber is pumped, and the ambient is removed. During this pumping, all physisorbed species are removed. The relaxation response of the crystal continues through this pumpdown period. The pumping time of 10-1/2 hours allows relaxation of the semiconductor to occur completely, and also reduces the pressure within the chamber to less than  $10^{-8}$  torr. As shown in Figure 4.11, the removal of physisorbed species by the vacuum does not result in a CPD response identical to that of the control standard. This indicates that irreversible processes due to the interacting ambient have occurred, and that further steps must be taken to return the surface to a condition where the effects of adsorbates are eliminated.

After relaxation and pumping of the chamber have been completed, attempts were made to observe a photovoltage response of the  $\text{TiO}_2$  surfaces under monochromatic sub-bandgap illumination ( $\lambda = 0.5 \text{ um}$ ). No response was observed, and consequently this sub-gap illumination procedure has been omitted from the schematic diagram of Figure 4.11. The significance of this lack of sub-gap illumination response will be discussed in Chapter 5.

The final portion of the light cycling procedure involves illumination of the  $\text{TiO}_2$  surface under vacuum. During this period, the

CPD response corresponds to the depopulation of surface states on the  $\text{TiO}_2$  by the photogenerated holes, and the desorption of any chemisorbed species which were associated with those states. After one hour of illumination in vacuum, all species have been desorbed and the original control surface has been regained.

The reproduction of the control surface allows the cycle to be repeated, using a different pressure of interacting ambient. The total cycle time of about twelve hours allows the completion of two cycles per day.

#### 4.4.3 Dark Ambient Cycling

A schematic diagram depicting the dark cycling procedure is shown in Figure 4.12. This procedure takes its name from the fact that the ambient interactions are allowed only while the surface is not illuminated. The procedure is again initiated by utilizing the control surface conditions. During the first portion of the cycle, illumination of the surface is terminated and crystal relaxation processes occur while the sample is maintained in UHV. Repopulation of unoccupied surface states by conduction band electrons proceeds during this period. In this portion of the dark cycling procedure, the control standard CPD transient and the ambient interaction transient should be coincident, as no ambient interactions have occurred.

Ten minutes after illumination has been terminated, a controlled pressure of ambient gas is admitted into the vacuum chamber. During this period crystal relaxation and physisorption can occur. Chemisorption involved with surface states can also occur, as not all of the active surface states have been repopulated with conduction band electrons. The subsequent pumpdown of the system allows further crystal



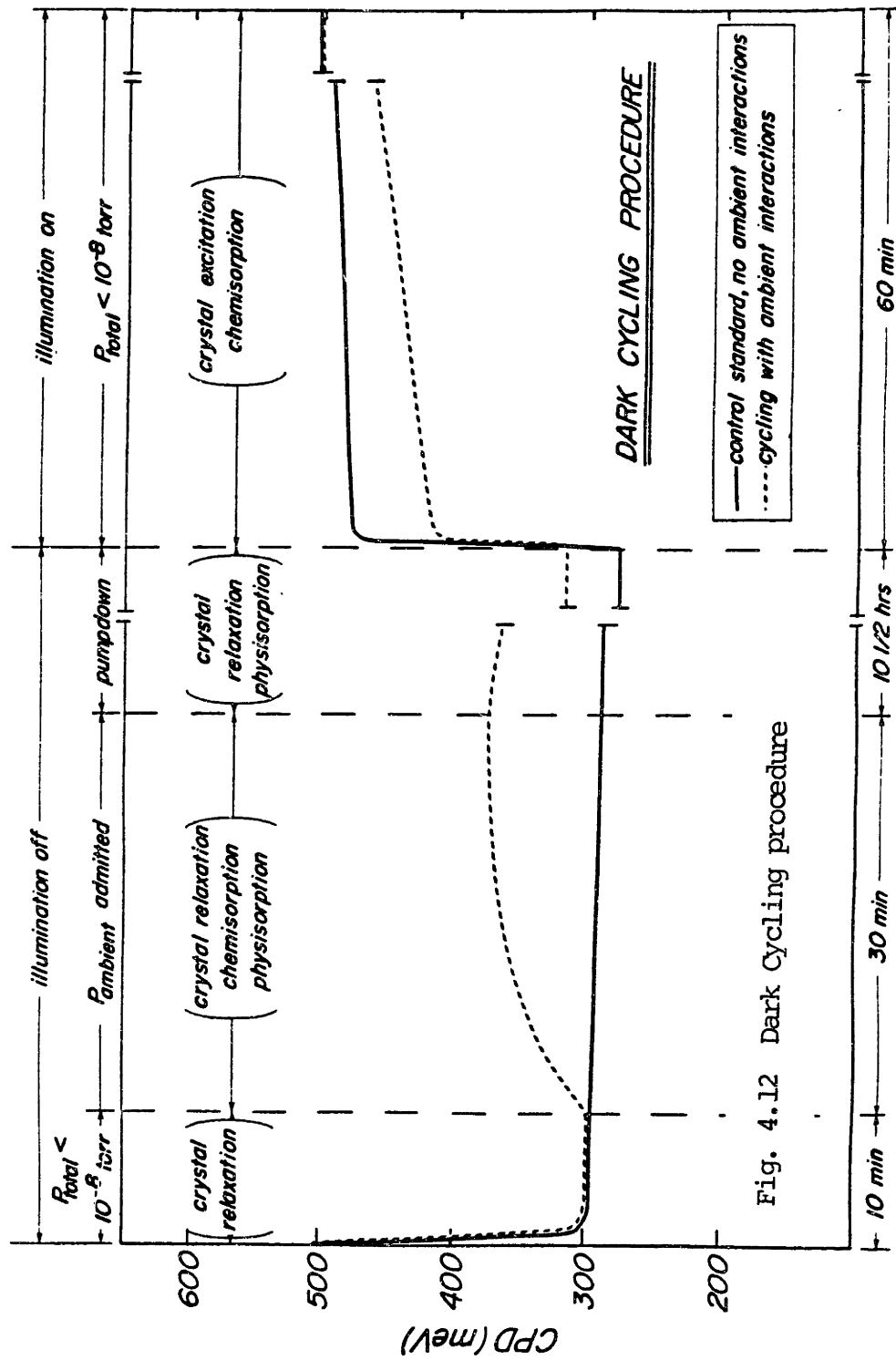


Fig. 4.12 Dark Cycling procedure

relaxation in darkness, and the removal of physisorbed species. After pumpdown and relaxation are completed, the non-coincidence of the control standard and ambient interaction responses indicate irreversible processes associated with the interacting ambient.

Illumination with light of energy less than that of the band gap was again tried without response at this juncture. It is consequently omitted from the cycling procedure schematic.

The final portion of the procedure is identical to that of the light cycling procedure: crystal excitation and desorption of chemisorbed species occurs. After one hour illumination, all species have been desorbed and the original control surface has been regained.

#### 4.4.4 XPS Experimentation

Cycling akin to that of the dark cycling procedure was utilized for the XPS experimentation. Samples were prepared in the XPS vacuum chamber by prolonged illumination in vacuums of less than  $10^{-9}$  torr. The surfaces of these samples were characterized by the collection of high resolution XPS spectra after twelve hours of relaxation in the dark. The samples were then again illuminated for one hour in UHV, the illumination terminated for ten minutes, and the samples withdrawn into the low vacuum entry chamber. In the entry chamber the samples were exposed to ambient pressures in the range from  $10^{-2}$  to 0.5 torr for thirty minutes. The entry chamber was then evacuated, and the samples return to the XPS chamber under ultra high vacuum. The samples were allowed to relax 10-1/2 hours before high resolution XPS spectra were again taken. Comparison of the XPS spectra before and after ambient exposures was facilitated by the digitalized data and computerized data analysis programs.

## Chapter 5: RESULTS AND DISCUSSION

### 5.1 Results

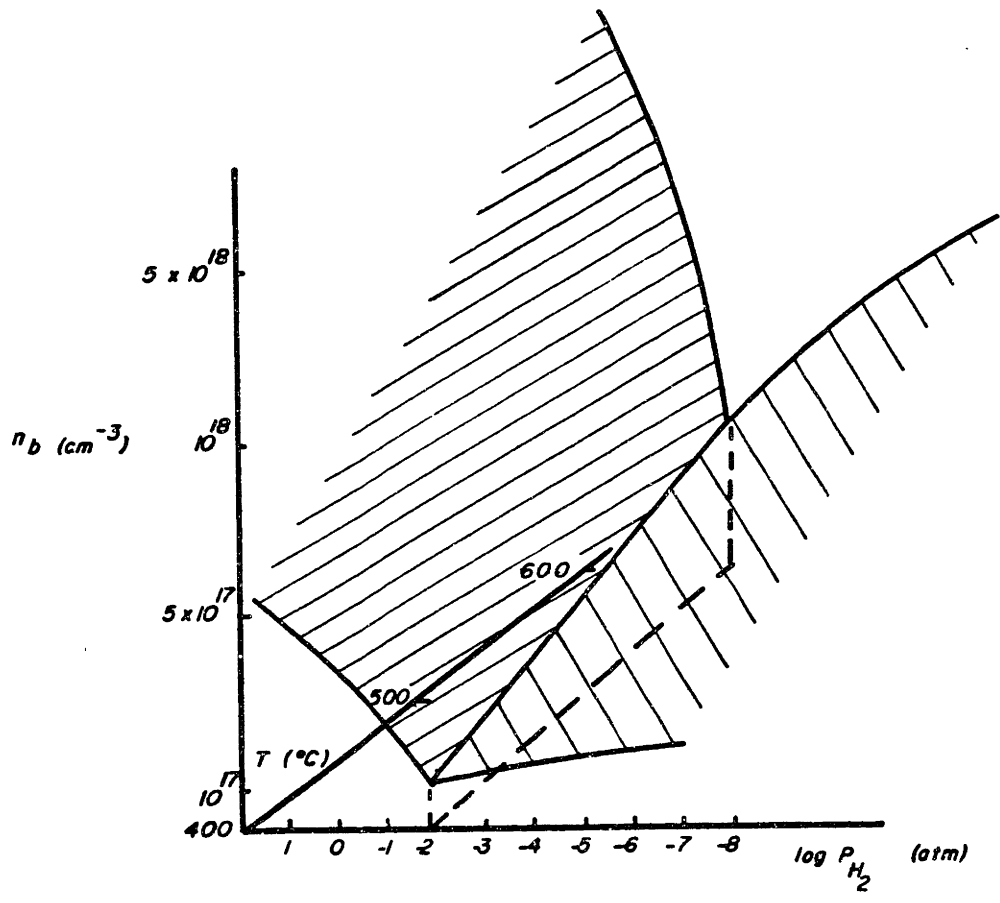
In this section, the results of experimentation are presented. Preliminary information regarding the bulk properties of n-TiO<sub>2</sub> is first reviewed. The behavior common to all tested TiO<sub>2</sub> samples during contact potential difference measurements is also presented. The variations in CPD transients due to interacting ambients are then introduced: first in phenomenological, TiO<sub>2</sub> work function changes, and then more analytically in terms of the changes in surface charge on the semiconductor. Information regarding the changes in the XPS spectra of the surface with ambient cycling are also reviewed.

#### 5.1.1 Preliminary Bulk and Surface Information

TiO<sub>2</sub> samples were reduced by annealing in various pressures of hydrogen at temperatures between 350°C and 700°C. The resistivity of the samples was measured and, using the relation  $(\frac{1}{\rho}) = ne\mu$ , and a value of mobility of 0.4 cm<sup>2</sup>/V-sec,<sup>35</sup> a plot of bulk donor density versus reduction pressure and temperature can be constructed. This plot is shown in Figure 5.1. Because of its importance in dictating the progression of this research, the significance of this plot will be discussed here.

For the two intersecting sheets depicted in Figure 5.1, it is possible to distinguish two defect mechanisms active for the range of reduction temperatures and pressures utilized. The donor defect mechanisms possible are those associated with: 1) the incorporation of hydrogen into the crystal, perhaps as [OH]<sub>O</sub><sup>+</sup> complexes, at high hydrogen pressures; and 2) the loss of oxygen from the crystal at lower hydrogen

Fig. 5.1 Bulk Donor Density vs.  
Reduction Parameters.



pressures, resulting in vacant oxygen sites which ionize to  $[V]_O^\dagger$ . For the production of these different defects, we must consider the diffusivities of hydrogen and oxygen in  $TiO_2$  at the reduction pressures and temperatures employed.

The small size of the diffusing hydrogen species (either molecular or atomic) compared to that of the diffusing oxygen species, allows one to surmise that the diffusivity of hydrogen in  $TiO_2$  will be greater than that of oxygen. Considering then the limiting case of oxygen diffusion in  $TiO_2$ , two possibilities avail themselves for the observed homogeneous dopant distribution. Either the dopant diffusion is truly homogeneous throughout the sample, or the diffusion effected surface layer was removed by the polishing procedure. If we take as an estimate of the depth of the diffused layer the expression

$$l = (Dt)^{1/2} , \quad (5-1)$$

and utilize the sample thickness (0.1 cm), and the amount of material removed by the polishing procedure (200  $\mu$ m) as the pertinent lengths involved for a 48 hour anneal, one may determine the necessary limiting oxygen diffusivities for each of these cases.

The removal of 200  $\mu$ m of oxygen diffusion effected material by polishing would imply an oxygen diffusivity of less than  $2 \times 10^{-9}$   $cm^2/sec$ . For the case of homogeneously effecting a  $TiO_2$  sample of 0.1 cm thickness, an oxygen diffusivity of  $5 \times 10^{-8}$   $cm^2/sec$  or larger would be necessary. The value oxygen diffusivity in the c-direction of  $TiO_2$  (rutile) under the reduction conditions employed in this study is subject to dispute. Several authors suggest values of oxygen diffusivity less than  $10^{-10}$   $cm^2/sec$  in these situations,<sup>95,96</sup> while others<sup>97,98</sup> make assessments in the range of  $10^{-6}$   $cm^2/sec$ . The

effectiveness of producing oxygen related defects by reduction at temperatures and pressures utilized in this study is thus subject to question. The diffusivity of hydrogen in these cases is large enough to homogeneously effect the samples. The retention of the light blue-green color, imparted to the samples during reduction, throughout the polishing procedure substantiates this assessment.

The reduction of  $\text{TiO}_2$  samples under low pressures of hydrogen may not result in donor defects related to the out-diffusion of oxygen. In the reduction of  $\text{TiO}_2$ , it is the ratio of the water vapor to hydrogen pressure which determines the variation in the oxygen/titanium ratio in the material.<sup>96</sup> Also the effective oxygen pressure changes in the range of reduction pressures used may not be large enough to clearly delineate a regime where oxygen related defects may dominate.<sup>99</sup> Nevertheless, the minima in the bulk donor density depicted in Figure 5.1 indicates that there is some change in the dominating bulk donor defect at hydrogen pressures of  $\sim 10^{-2}$  atm. The shallow minima does not necessarily dictate a complete change in the dominating donor defect: it is possible that some amount of phase change within the  $\text{TiO}_2$  samples due to reduction contributes to the variation in donor density.<sup>99</sup> In light of these considerations, it is not possible to uniquely ascribe to those samples reduced under hydrogen pressures of less than  $10^{-2}$  atm any specific dominating donor defect. In lieu of specifying the dominating defect in this regime, those samples reduced at hydrogen pressures less than  $10^{-2}$  atm will henceforth be referred to as "vacuum annealed" samples, reflecting the use of low hydrogen pressures.

The reduction of  $\text{TiO}_2$  in higher pressures of hydrogen also results in n-type conductivity. The dominant defect mechanism responsible for this conduction is however subject to

dispute.<sup>35,41,43,49,100-103</sup> Two active defects are possible:  $Ti_i^{4+}$  and  $[OH]_O^+$ . The formation of these active (ionized) defects is more fully discussed in Appendix B. In all probability, both types of defects should be active, and it may be their additive effect that gives rise to the n-type conductivity present as a result of high hydrogen pressure reduction. Without attempting to specify the dominant donor defect mechanism resulting from high  $P_{H_2}$  reduction, those samples reduced at  $P_{H_2} > 10^{-2}$  atm will be referred to as "hydrogen annealed" samples.

The accuracy of the "hydrogen annealed" and "vacuum annealed" regimes indicated in Figure 5.1 merits comment. The bulk donor densities depicted in the figure are those derived from resistivity measurements. It is recognized that in the formula  $(\frac{1}{\rho}) = ne\mu$ , that fluctuations in the electron mobility,  $\mu$ , could also reflect changes in the donor density. However, changes in the electron mobility would arise only from the activation of new scattering mechanisms in the crystal or the repression of active scattering mechanisms. In any case, the delineation of donor activity into the two regime would still hold. Unfortunately, the use of resistivity data to imply donor densities is limited by the accuracy of the value of mobility used in the calculations. The value of  $\mu = 0.4 \text{ cm}^2/\text{V-sec}$  for  $TiO_2$  slightly reduced in hydrogen is subject to errors of  $\pm 20\%$  (see Appendix A). While this assessment of mobility would be reflected in errors in the value of the donor density of at least  $\pm 20\%$ , the shape and the intersection of the surface depicted in Figure 5.1 would remain the same, with only a change in the scale of the vertical (bulk donor density) axis. Thus, caution should be advised in the application of the data of Figure 5.1.

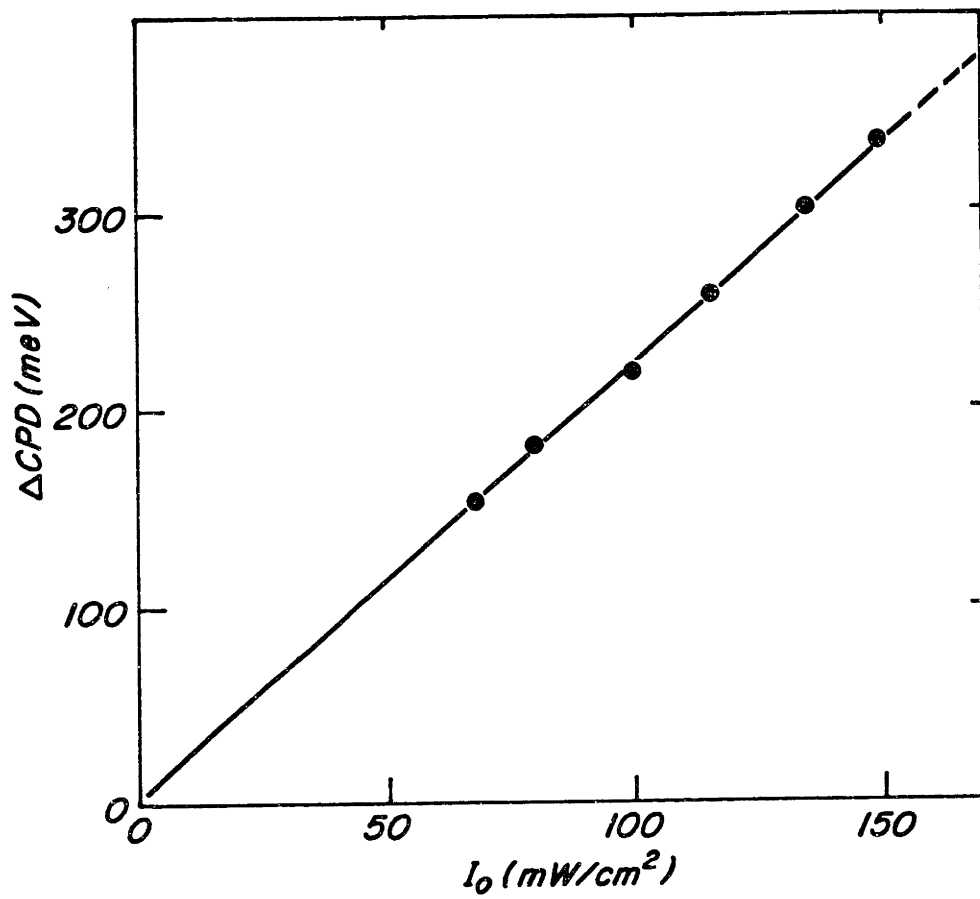
The delineation between the two different types of dominate donor activity remains clear however.

It has been suggested that the type of donor defect present in the  $\text{TiO}_2$  crystal may influence the photostimulated behavior of the surface and the photocatalyzed reactions occurring upon it.<sup>62</sup> The two domains of dominating donor activity, as depicted in Figure 5.1 were subsequently investigated in this research. Hydrogen reduction pressures of 1 and  $10^{-7}$  atm were employed to produce "hydrogen annealed" and "vacuum annealed" samples, respectively. This labelling is intended only to delineate between the two sets of samples utilized in this study; it is not meant to specify the dominant donor defects within each of these regimes.

Constant current photovoltage measurements were employed as a preliminary measure of determining the reduction temperatures to be used to produce maximum photosensitivity of the "hydrogen annealed" and "vacuum annealed" samples. This testing was done in UHV using white light. Maximum photosensitivity was found to occur for "hydrogen annealed" samples reduced at  $400^\circ\text{C}$  and "vacuum annealed" samples reduced at  $600^\circ\text{C}$ . Bulk donor densities associated with these samples were  $4 \times 10^{17} \text{ cm}^{-3}$  and  $2 \times 10^{17} \text{ cm}^{-3}$ , respectively. Samples reduced under these conditions were the subject of further research. Three samples of each type were tested using contact potential difference measurements. All samples of each type were loaded into the vacuum chamber on the CPD measurement carousel. Cyclic ambient testing of each sample was done, with the response of one sample being thoroughly documented (ambient cycling utilizing a wide range of ambient pressures) with measurements from the remaining two samples serving to reinforce the trends identified by the primary sample.



Fig. 5.2 White Light Intensity  
Dependance of CPD



As measured by the contact potential difference technique, the surfaces of all samples, as tested in UHV with no ambient interactions, exhibited two important characteristics. The change in contact potential difference was approximately linear with white light intensity, and no saturation value of CPD was found. Also no change in contact potential difference was exhibited for illumination with light of energy of less than that of the  $\text{TiO}_2$  band gap. These features are reflected in Figures 5.2 and 5.3.

The structure of the semiconductor surface which is consistent with the findings of Figure 5.2 and 5.3 is that the  $\text{TiO}_2$  surface contains a number of surface states that 1) cannot, by sub-band gap illumination, be activated and 2) are present in a density high enough to prevent the generation of flat-band conditions by the absorption of white light of an intensity of  $\sim 150 \text{ mW/cm}^2$  by the semiconductor bulk. As is seen from Figure 5.2, the maximum bulk photovoltage produced by white light of this intensity is  $\sim 300 \text{ mV}$ . Consequently the potential barrier of the depletion region existing at the surface of the semiconductor is at least of this magnitude.

#### 5.1.2 Ambient Cycling

The following ambient cycling sequences were made for both "hydrogen annealed" and "vacuum annealed" samples: light cycling,  $\text{O}_2$  ambients; light cycling,  $\text{H}_2\text{O}$  ambients; light cycling, ( $\text{O}_2 + \text{H}_2\text{O}$ ) ambient; dark cycling,  $\text{O}_2$  ambients; dark cycling,  $\text{H}_2\text{O}$  ambients; and dark cycling, ( $\text{O}_2 + \text{H}_2\text{O}$ ) ambients. The ambient cycling procedures are described in sections 4.4.2 and 4.4.3, and illustrated in Figures 4.11 and 4.12. The ambient pressures used in these cyclings, and the exposures resulting from them are listed in Table 5.1.<sup>104</sup>

Fig. 5.3 Wavelength Dependence  
of CPD

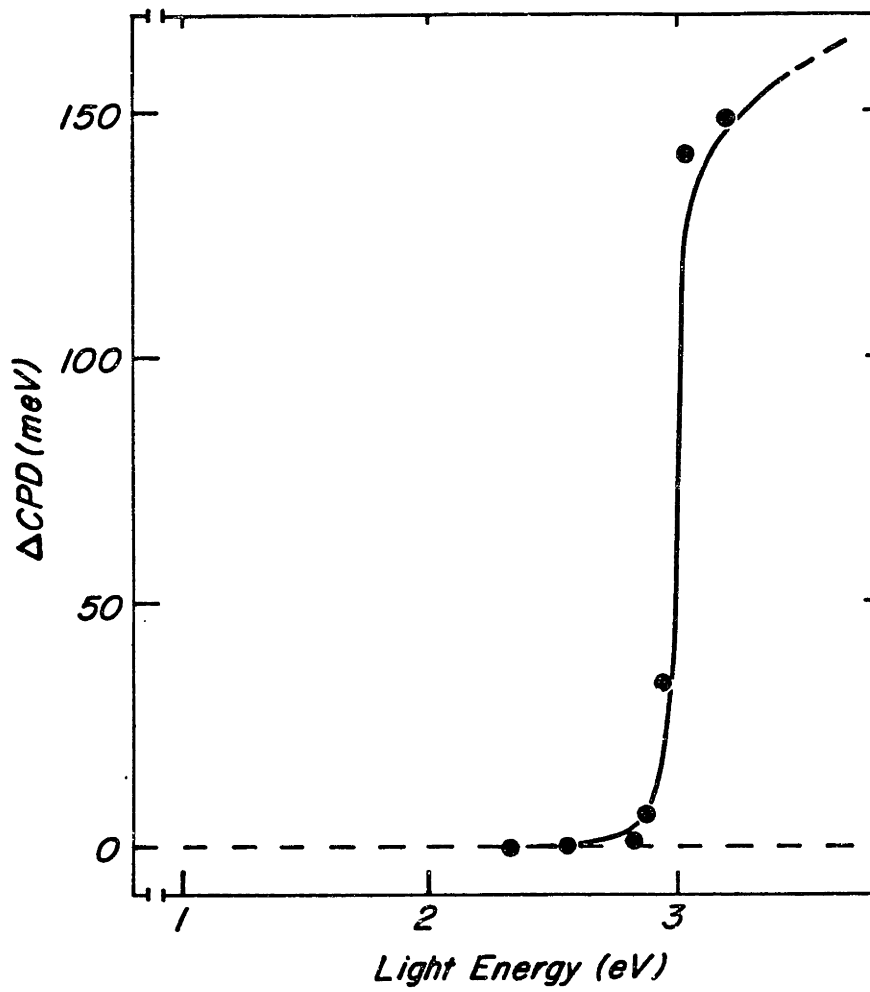


Table 5.1: Ambient Cycling Pressures and Exposures

<u>ambient</u>	<u>Pressure (torr)</u>			<u>Exposure (Langmuir)*</u>	
	<u>P(O<sub>2</sub>)</u>	<u>P(H<sub>2</sub>O)</u>	<u>P(total)</u>	<u>L(O<sub>2</sub>)</u>	<u>L(H<sub>2</sub>O)</u>
oxygen	2x10 <sup>-7</sup>	---	2x10 <sup>-7</sup>	360	---
	2x10 <sup>-6</sup>	---	2x10 <sup>-6</sup>	3.6x10 <sup>3</sup>	---
	10 <sup>-5</sup>	---	10 <sup>-5</sup>	1.8x10 <sup>4</sup>	---
	0.05	---	0.05	9x10 <sup>7</sup>	---
	0.5	---	0.5	9x10 <sup>8</sup>	---
	760	---	760	1.37x10 <sup>12</sup>	---
water vapor	---	5.03x10 <sup>-9</sup>	2x10 <sup>-7</sup>	---	8.8
	---	5.03x10 <sup>-8</sup>	2x10 <sup>-6</sup>	---	88
	---	2.52x10 <sup>-7</sup>	10 <sup>-5</sup>	---	442
	---	1.26x10 <sup>-3</sup>	0.05	---	2.21x10 <sup>6</sup>
	---	1.26x10 <sup>-2</sup>	0.5	---	2.21x10 <sup>7</sup>
	---	19.12	760	---	3.36x10 <sup>10</sup>
oxygen plus water vapor	1.95x10 <sup>-7</sup>	5.03x10 <sup>-9</sup>	2x10 <sup>-7</sup>	351	8.8
	1.95x10 <sup>-6</sup>	5.03x10 <sup>-8</sup>	2x10 <sup>-6</sup>	3.51x10 <sup>3</sup>	88
	9.75x10 <sup>-6</sup>	2.52x10 <sup>-7</sup>	10 <sup>-5</sup>	1.76x10 <sup>4</sup>	442
	4.87x10 <sup>-2</sup>	1.26x10 <sup>-3</sup>	0.05	8.78x10 <sup>7</sup>	2.21x10 <sup>6</sup>
	0.487	1.26x10 <sup>-2</sup>	0.5	8.78x10 <sup>8</sup>	2.21x10 <sup>7</sup>
	741	19.12	760	1.34x10 <sup>12</sup>	3.36x10 <sup>10</sup>

\*: 1 Langmuir (L) = 10<sup>-6</sup> torr-sec, all exposures for 30 minutes.

### 5.1.2.a Phenomenological Work Function Changes

Contact potential difference measurements, as measured in the ambient cycling procedures, can be related to the  $\text{TiO}_2$  work function by the relation  $\Delta\phi_{\text{TiO}_2} = -\Delta\text{CPD}$ . The  $\text{TiO}_2$  work function can then be measured during ambient interactions, as well as during crystal excitation and relaxation processes, by monitoring the CPD fluctuations.

The  $\text{TiO}_2$  work function changes during ambient cycling procedures are depicted in the various plots of Appendix D. The volume of data collected on the  $\text{TiO}_2$  work function changes and its variations due to illumination and ambient interactions precludes the presentation of the material here. An illustrative example of the work function variations on a hydrogen annealed sample during oxygen light cycling is depicted in Figure 5.4

Changes in the work function of the titanium dioxide surfaces represent both changes in the electron affinity of the material, as well as the change in the surface charge associated with surface states. Two general trends in the behavior of the  $\text{TiO}_2$  work function during ambient cycling deserve attention here, without regard to the specific mechanisms by which they are manifested (either electron affinity or surface charge changes). They are 1) upon admittance of any ambient used in this study, the immediate effect of the ambient is to reduce the  $\text{TiO}_2$  work function; and 2) upon desorption of chemisorbed ambient species in UHV, the amount of immediate and gradual work function change is dependant upon the previous ambient exposure, with the immediate work function change upon illumination decreasing with increasing ambient exposure, and the gradual work function change increasing with increasing previous exposure. These general trends will

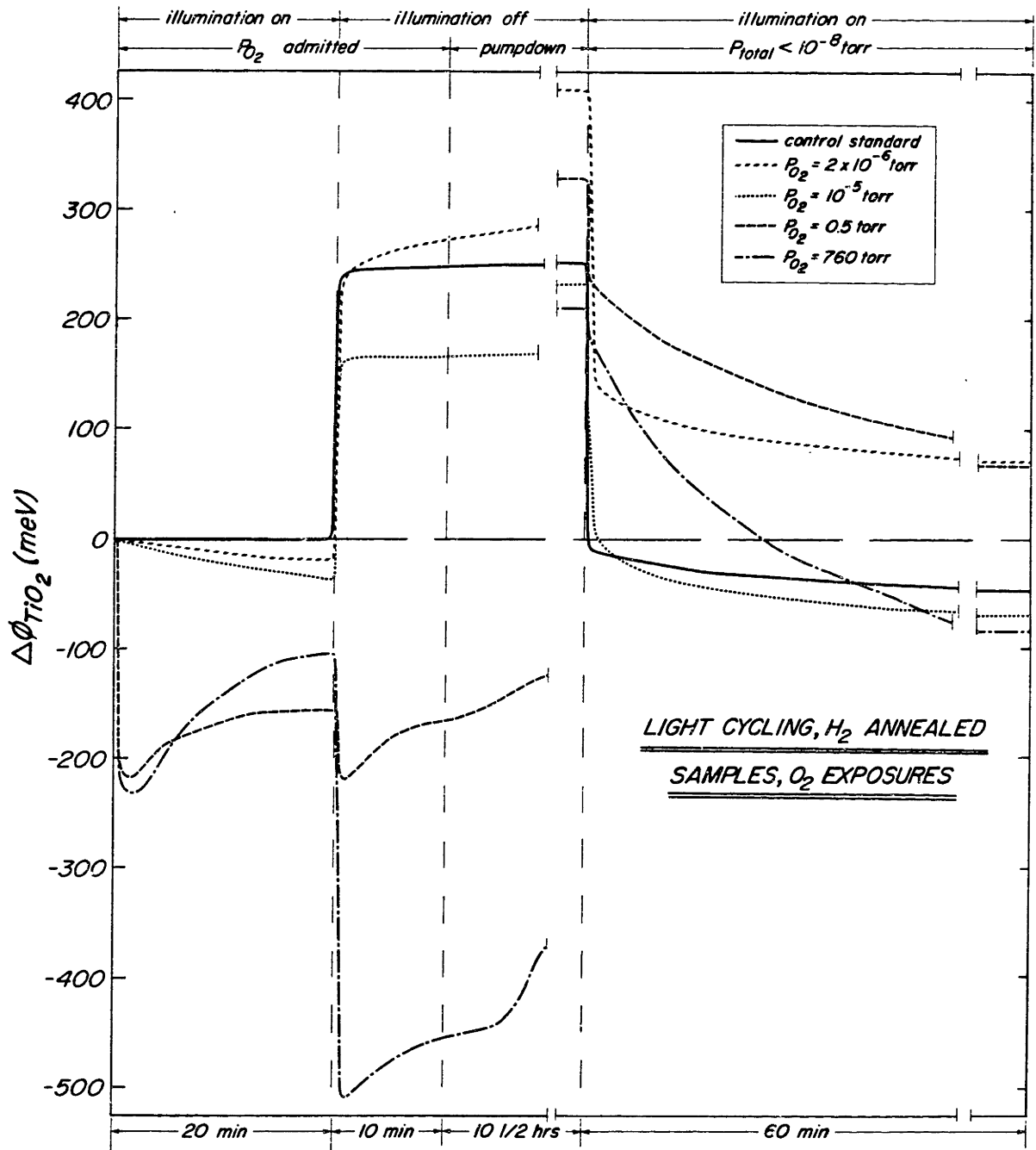


Fig. 5.4  $TiO_2$  Work Function Change  
Hydrogen Annealed Samples  
Oxygen Light Cycling

be discussed more fully in the following sections. Also of note is the range of work function changes due to the interacting ambient. Under illumination, the change in  $\text{TiO}_2$  work function is may be as large as 200 meV during interactions with high pressures of interacting ambients. Under darkened conditions, larger changes in the  $\text{TiO}_2$  work function have been recorded, up to 800 meV with high ambient exposures.

#### 5.1.2.b Surface Charge Changes

Utilizing equation (4-6), which relates the changes in the nulling voltage needed to offset current from the  $\text{TiO}_2$  sample to the change in the surface charge on the semiconductor, the surface charge can be measured during ambient interactions as well as during crystal excitation and relaxation processes, by monitoring the nulling voltage changes of the  $\text{TiO}_2$ -gold probe capacitance cell.

The changes in surface charge on the  $\text{TiO}_2$  surfaces during ambient cycling procedures are depicted in the various plots of Appendix D. The volume of data collected concerning the variation of surface charge during these cycling procedures precludes the presentation of this data here. An illustrative example of the changes in surface charge on a hydrogen annealed sample during oxygen light cycling is depicted in Figure 5.5. The changes in surface charge in this plot, and of all similar plots in Appendix D, result from changes in the surface state populations as well as the changes in charge due to physisorbed overlayers (surface dipole layers). In these figures of  $\Delta n_s$  no attempt has been made to delineate the effects of surface state charge and surface dipole layer charge. An analysis of these components of  $n_s$  will be made in the forthcoming sections.

Changes in the amount of surface charge on the  $\text{TiO}_2$  surface

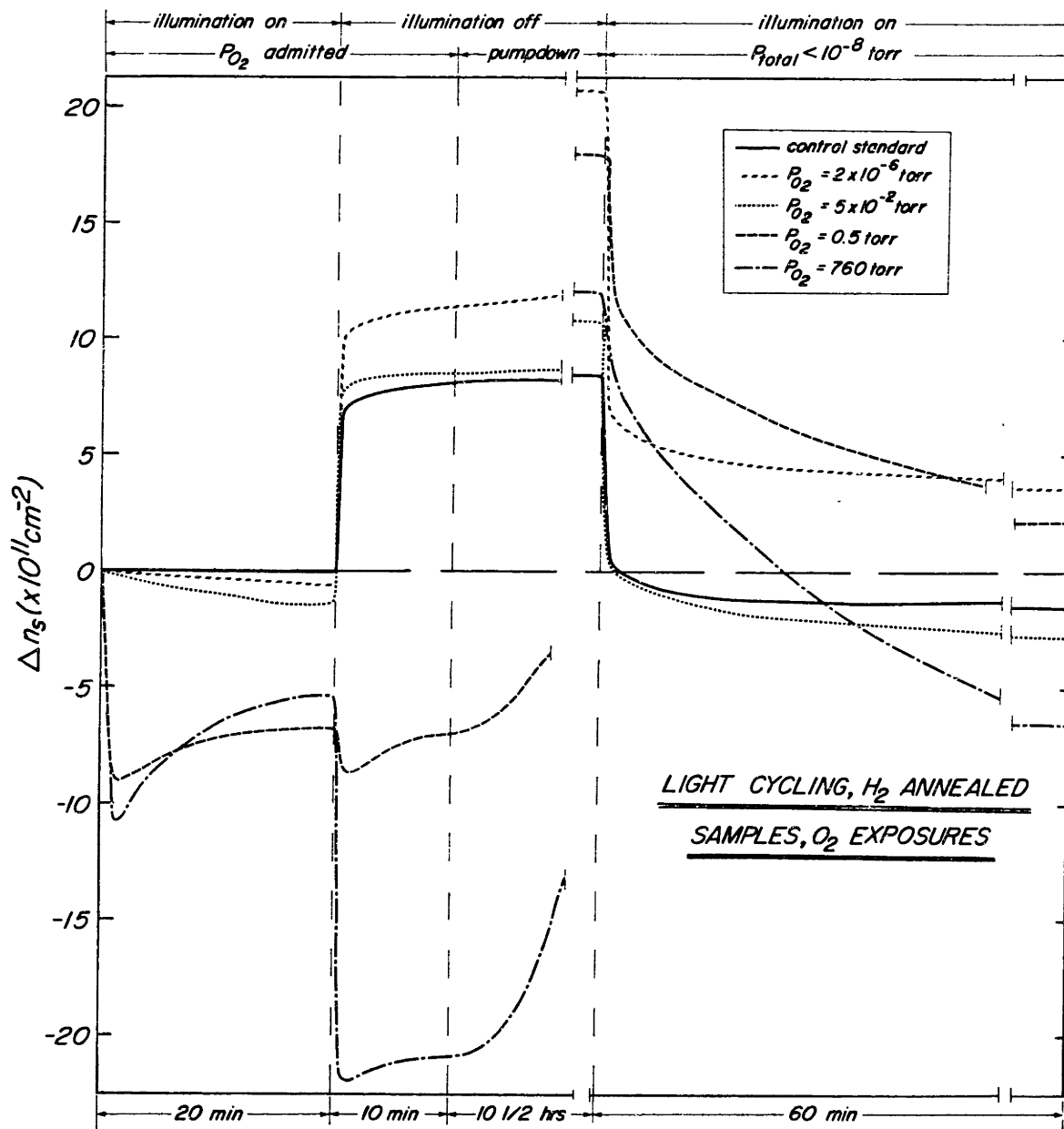


Fig. 5.5 Surface Charge Changes  
Hydrogen Annealed Samples  
Oxygen Light Cycling



roughly parallel changes in the  $\text{TiO}_2$  work function, as can be seen by comparison for Figures 5.4 and 5.5. The changes in each measure are not perfectly similar however, as the surface charge depends on the difference of the square-roots of the nulling voltages (equation 4-6), and the work function change depends only on the difference in their values.

The general trends present in the work function changes are also present in the change in surface charge on the  $\text{TiO}_2$ . Upon admittance of any ambient used in this study, the immediate effect of the ambient is to reduce the surface charge on the semiconductor. Also, upon the desorption of chemisorbed species in UHV, the amount of immediate and gradual charge transferred from the surface depend on the previous exposure of ambient. The immediate amount of charge transferred decrease with increasing ambient exposure.

### 5.1.3 XPS Information

High resolution XPS spectra were collected from several different surfaces of the hydrogen and vacuum annealed samples. XPS spectra in the binding energy range of the O (1s), O (Auger), Ti (2p), Ti (Auger), and the C (1s) [carbon is the primary surface contaminant] peaks were monitored. Sample surfaces could be photocleaned in UHV by prolonged (1 hour) white light illumination of an intensity of  $\sim 150 \text{mw/cm}^2$ . The conditions of the surfaces during XPS monitoring were as follows: photocleaned in UHV followed by 12 hours relaxation; photocleaned, exposed to  $9 \times 10^7 \text{ L O}_2$  (in dark), followed by 12 hours relaxation in darkness and UHV; photocleaned, exposure to  $2.21 \times 10^6 \text{ L H}_2\text{O}$  (in dark), followed by 12 hours of relaxation in darkness and UHV; photocleaned exposure to  $8.78 \times 10^7 \text{ L O}_2$  and  $2.21 \times 10^6 \text{ L H}_2\text{O}$  (in dark), followed by

12 hours relaxation in darkness and UHV. A time lag of 10 minutes was interjected between the termination of illumination and the beginning of ambient exposure to simulate the testing conditions of the dark ambient cycling procedure. The collection of spectra from ambient testing was concluded by the photocleaning of the surface in UHV, and a relaxation in darkness and UHV for 12 hours. A final set of high resolution spectra were then taken for comparison to the initial set where no ambient interactions allowed. This comparison allowed the confirmation of any degradation processes associated with ambient interactions that could not be reversed by illumination in UHV. The lack of any differences in spectra would confirm that the control surface, as prepared by illumination in UHV, was stable under ambient interactions.

Comparitive high resolution XPS spectra for hydrogen annealed samples are shown in Figures 5.6 through 5.8. The influence of adsorbates on the O (1s) peak is to enhance the satellite peaks in the spectra. This indicates that chemisorbing oxygen species have different energy states, and hence differing bonding configurations. The influence of the adsorbing species on the Ti (2p) energy levels is not as pronounced. In both cases, the amount of spectra disruption due to chemisorbed species is relatively minor. It is surmised that the low energy electron flux from the neutralization beam (necessary to accurately determine and adjust for the positive charging of sample under the XPS beam) may be influencing the the chemisorbed species promoting their desorption before completion of XPS measurements. The XPS beam itself may also promote the loss of chemisorbed species from the surface. Consequently the differing bonding configurations associated with chemisorbed species and discernable from XPS

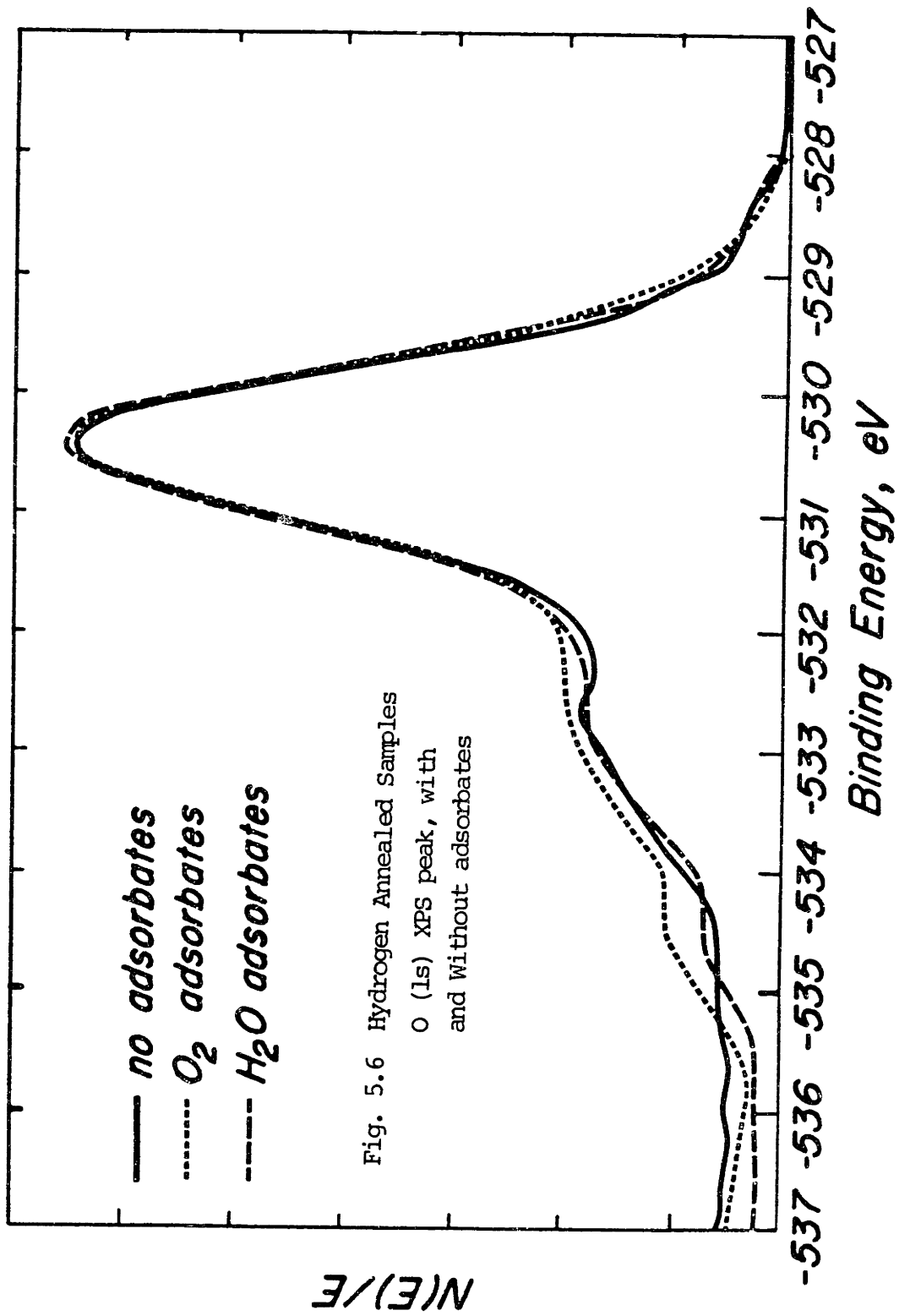


Fig. 5.6 Hydrogen Annealed Samples  
 O (1s) XPS peak, with  
 and Without adsorbates

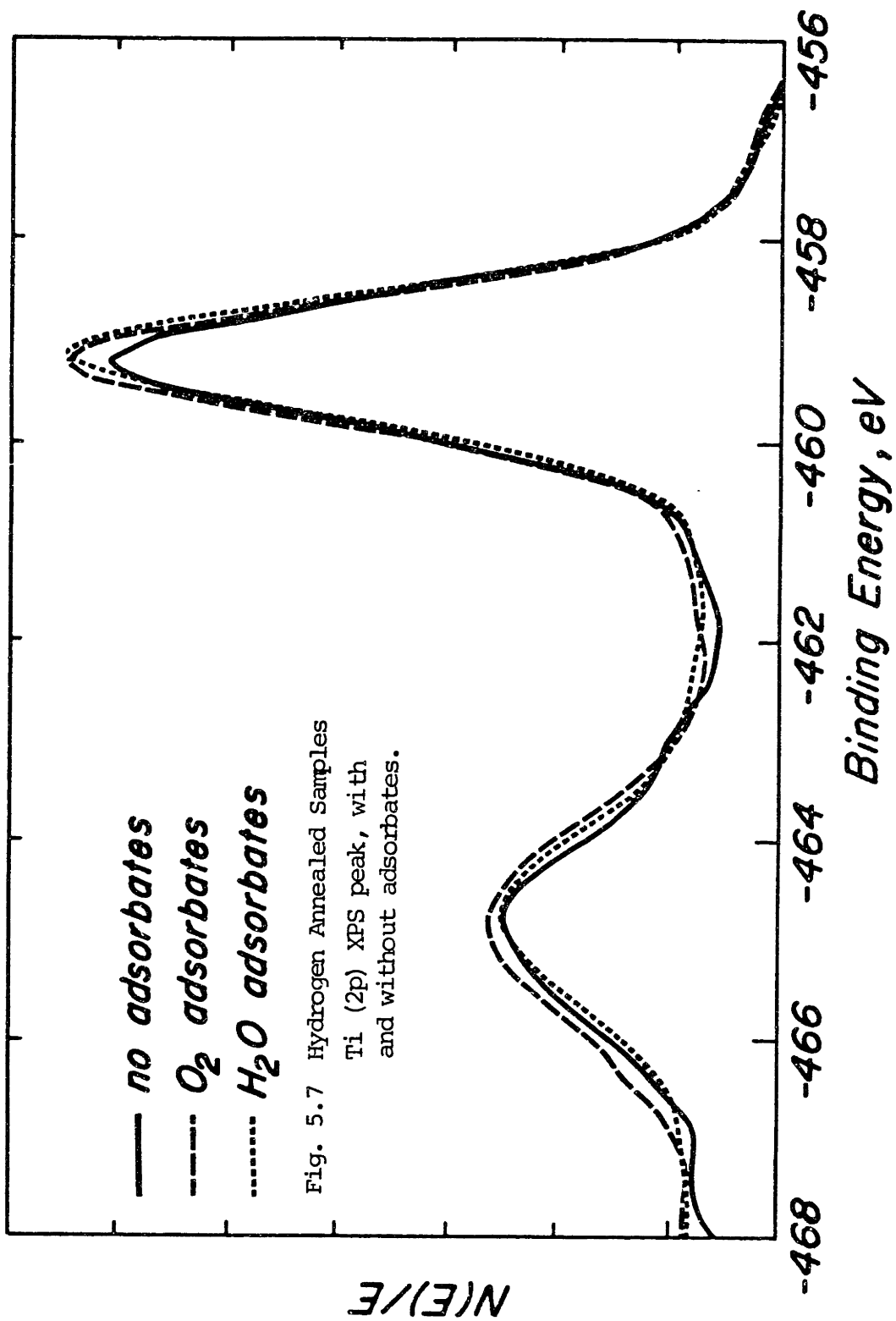


Fig. 5.7 Hydrogen Annealed Samples  
 Ti (2p) XPS peak, with  
 and without adsorbates.

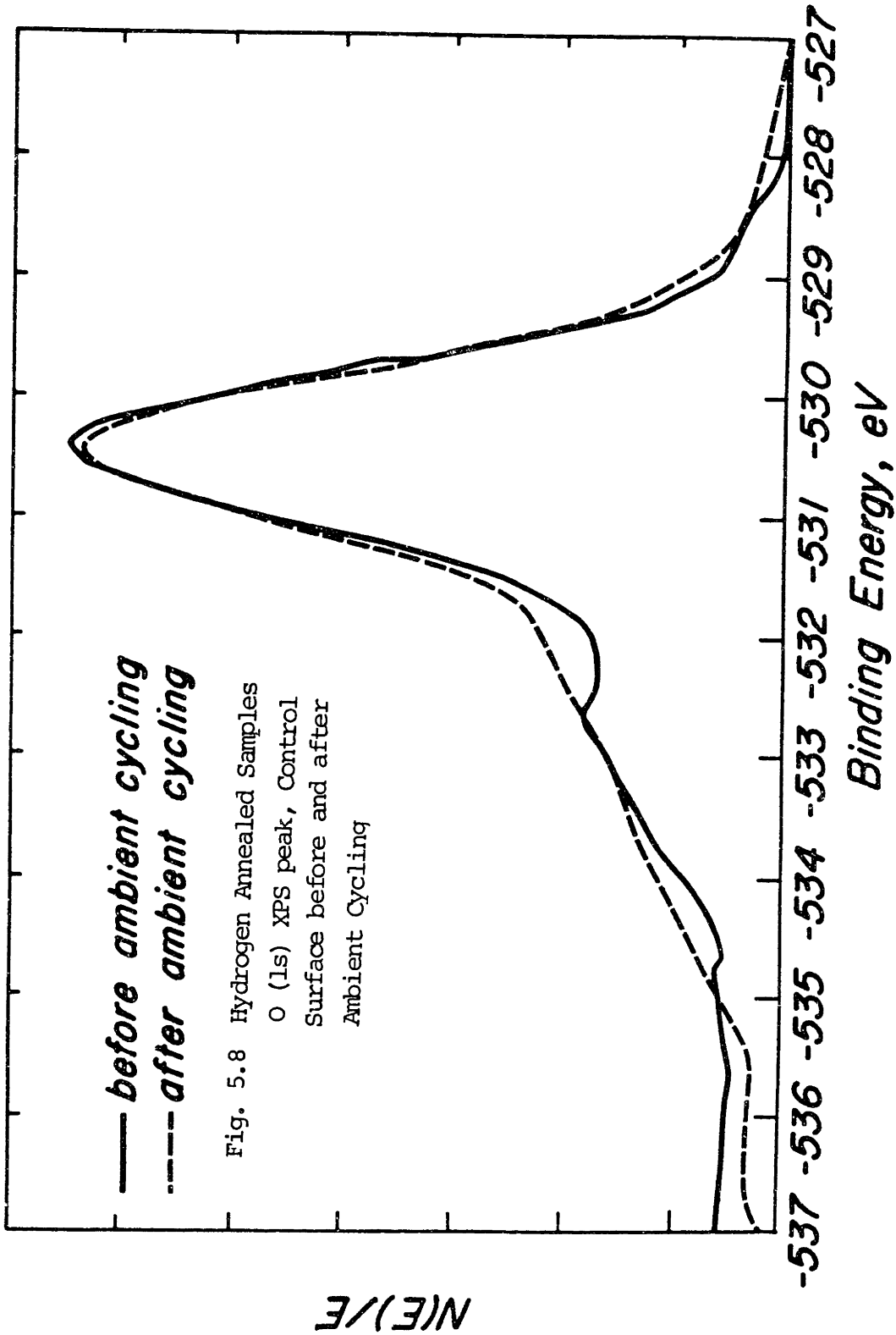


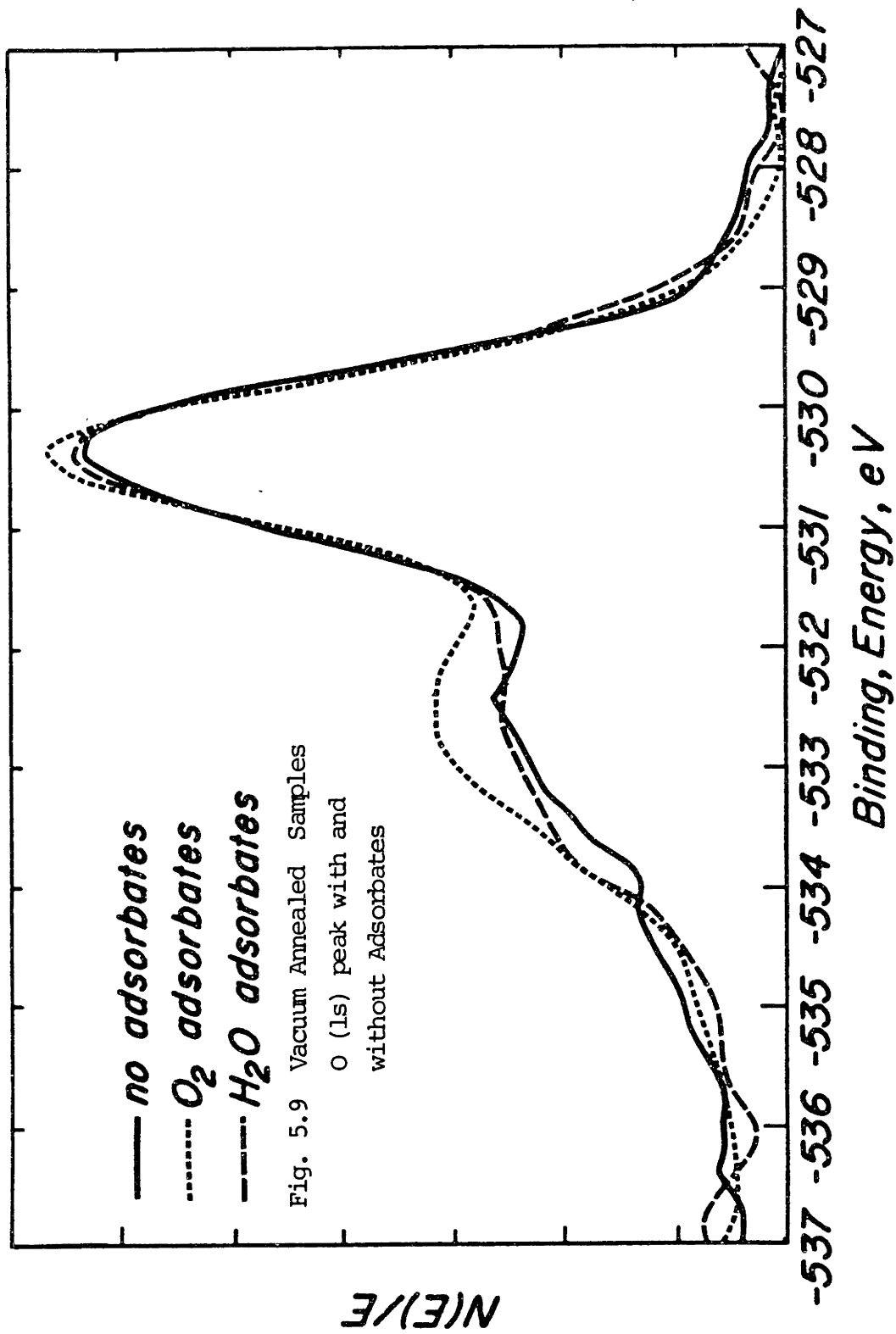
Fig. 5.8 Hydrogen Annealed Samples  
 O (1s) XPS peak, Control  
 Surface before and after  
 Ambient Cycling

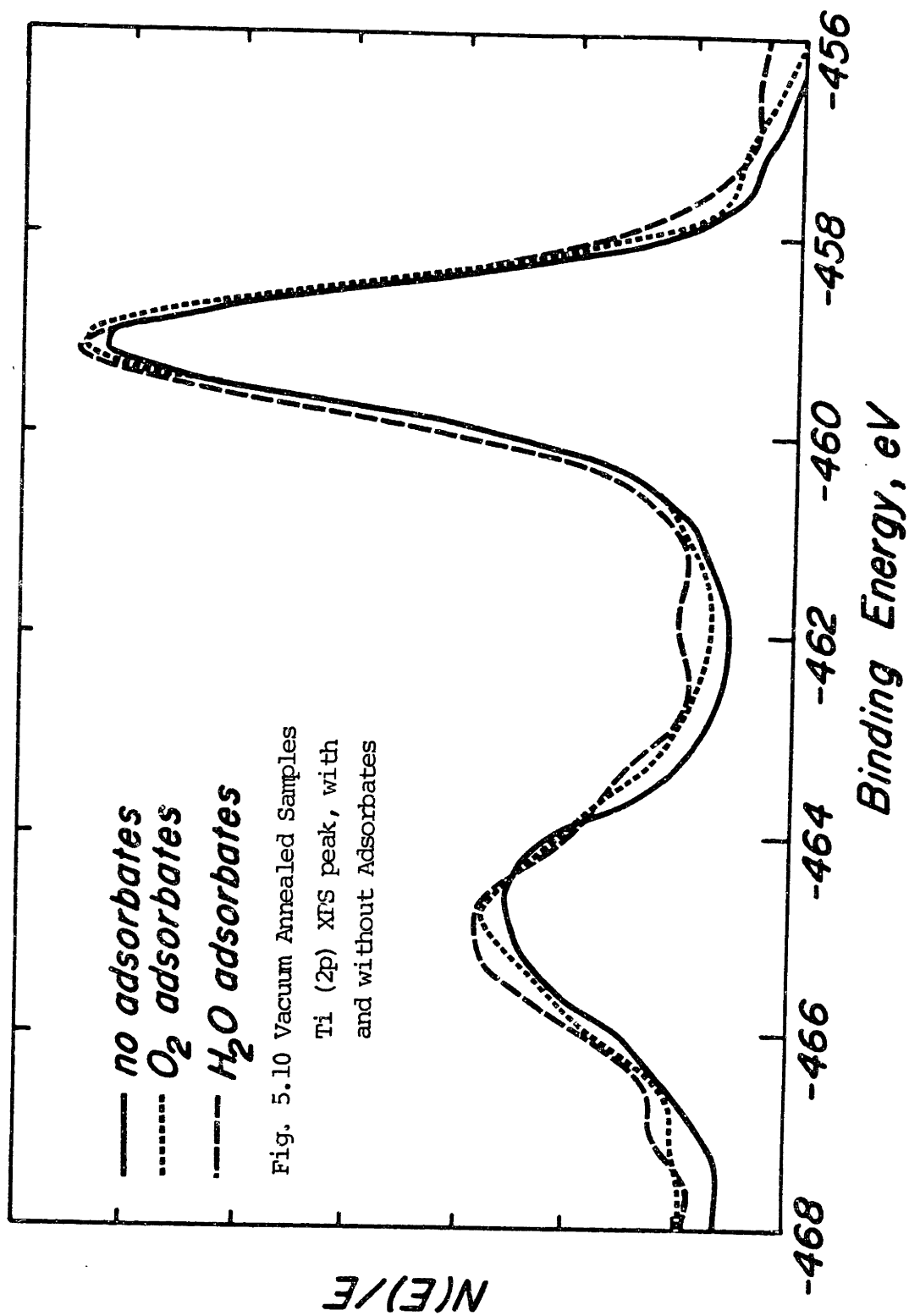
measurements may be significantly enhanced under the actual testing conditions, such as the dark cycling procedure.

The bonding configuration of oxygen on the control surface of hydrogen reduced samples, as produced by illumination and relaxation in UHV, both before and after ambient interactions is shown in Figure 5.8. Here the effect of ambient interactions is to promote the broadening of a satellite peak in the spectra. While it is possible that this feature reflects a permanent disturbance in the surface oxygen bonding configuration, it is felt that the spectra reflects residual oxygen remaining chemisorbed to the surface after photocleaning. The lack of any other discernable changes in the same set of spectra [for Ti (2p), etc.], and the reproducibility of the control surface CPD measurements would support this hypothesis.

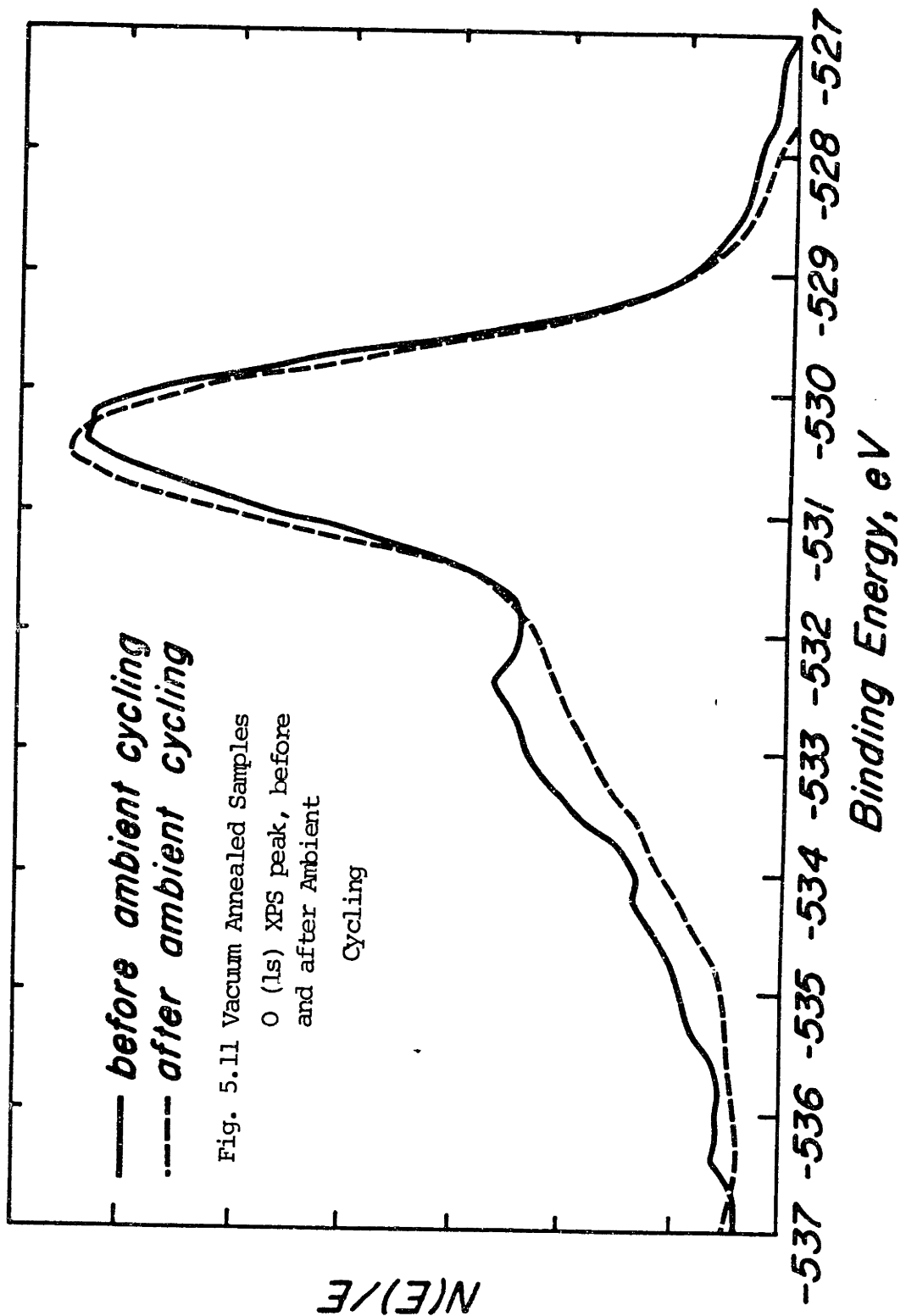
For the surfaces of vacuum annealed samples, the relevant XPS spectra for the interactions with water vapor and oxygen ambients are shown in Figures 5.9 through 5.12. In these cases, the influence of the chemisorbed species is to promote satellite peaks in both the O (1s) and Ti (2p) spectra, which is indicative of the chemisorbing species rearrangement of the titanium and oxygen surface bonding configurations. Comparison of the spectra concerned with the control surface before and after ambient interactions indicate that permanent changes in the bonding configurations of surface Ti and O have occurred. The gradual reduction of the CPD characteristics of this control surface, as indicated in Figure D-13 through D-24, serves to confirm this hypothesis.

The correlation and discussion of XPS and CPD data concerned with the control surfaces used in this study, and the effects of ambient interactions upon them, both for hydrogen and vacuum annealed



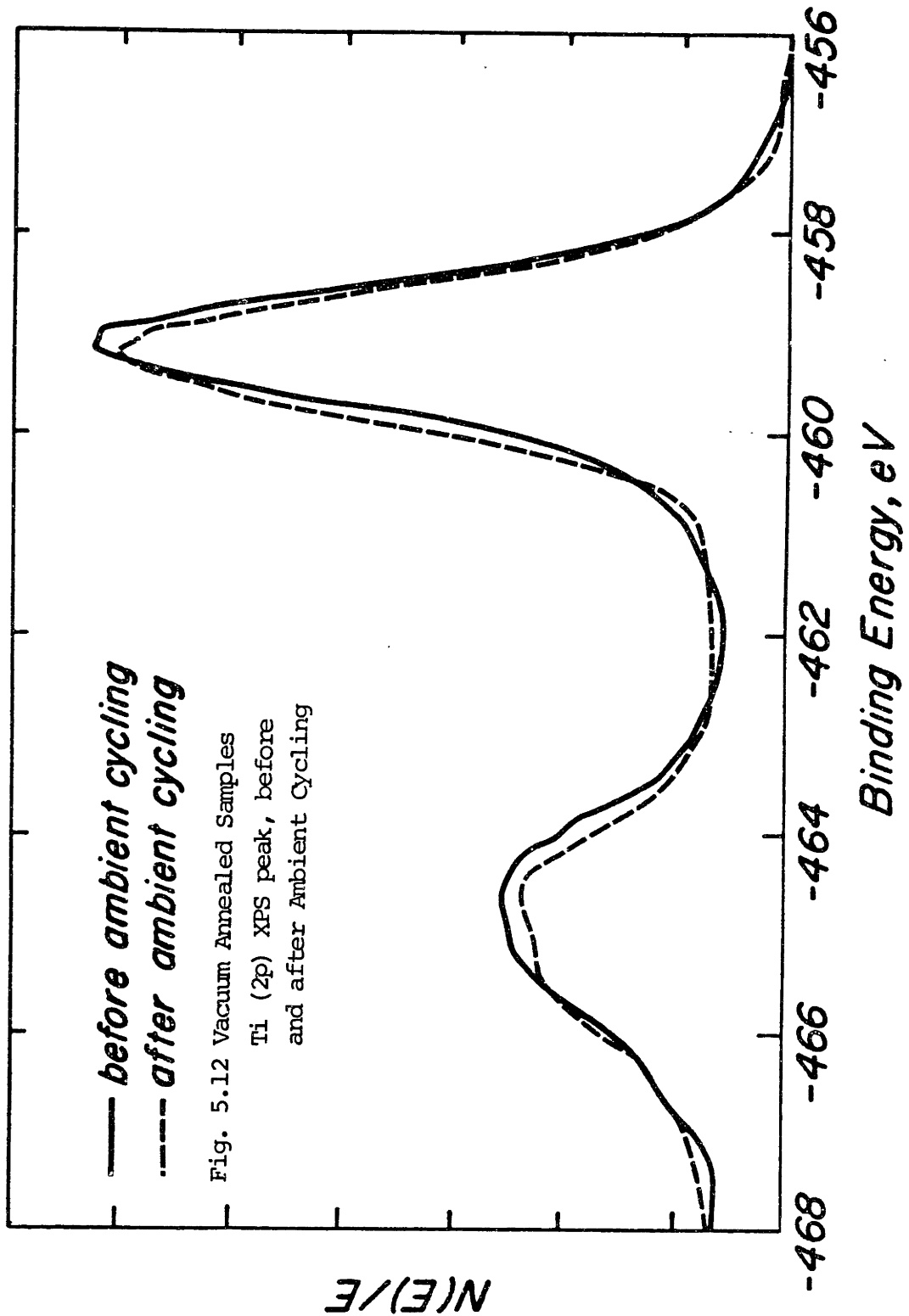






— before ambient cycling  
 - - - after ambient cycling

Fig. 5.11 Vacuum Annealed Samples  
 O (1s) XPS peak, before  
 and after Ambient  
 Cycling



samples, is the topic of the next section.

## 5.2 Discussion

### 5.2.1 Control Surface Characteristics

All ambient cycling data used as a reference a "control standard", which represents the reactions of the real  $\text{TiO}_2$  surface to illumination and termination of illumination. This real surface is prepared according to the procedure of section 4.4.1. Cycling in the presence of ambients produces CPD changes which are the sum total of the changes due to the ambient interactions with the  $\text{TiO}_2$  surface and the changes in CPD inherent to the control surface. By subtracting the amount of change (either  $\Delta\phi_{\text{TiO}_2}$  or  $\Delta n_s$ ) associated with the control standard from the total measured change, the amount of work function or surface charge change associated uniquely with the ambient interactions can be determined. Consequently the amount of photoinduced change in the properties of the control surfaces are of importance and merit further description here. Examples of control surface CPD transients, as they relate to work function and surface charge changes, are shown in Figures 5.4 and 5.5.

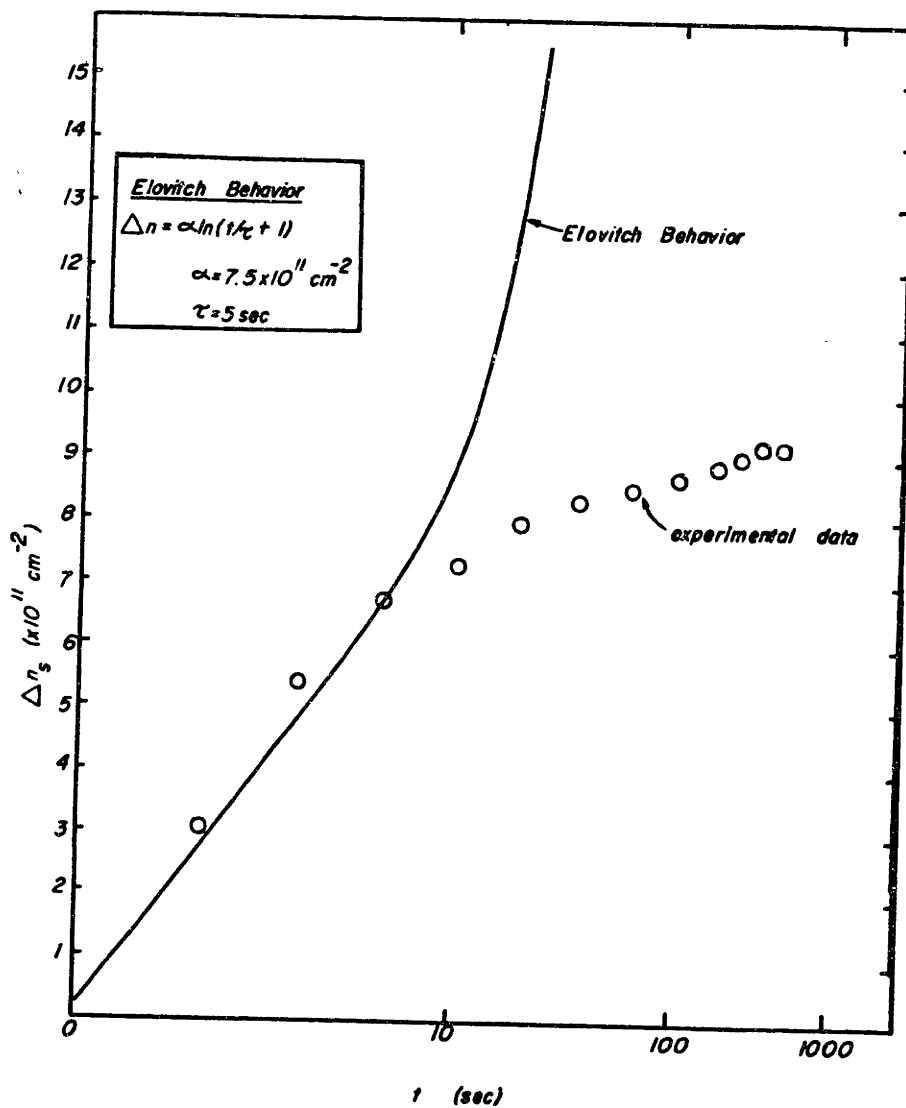
As produced by prolonged illumination in UHV, the values of contact potential difference for the hydrogen and vacuum annealed samples differ. The hydrogen annealed samples have a CPD of  $\sim +500\text{meV}$  in the control surface condition, while the vacuum annealed samples have a CPD of  $\sim -400\text{meV}$ . The same values of equilibrium probe spacing, vibrational amplitude and frequency were used throughout. This indicates that the work function of  $\text{TiO}_2$  is very dependant upon the manner of reduction and the active donor defects in the material. Although there is an offset of the  $\sim 900\text{meV}$  between the CPD values of

the control surfaces on the hydrogen and vacuum annealed samples, the response of these surfaces to illumination conditions is the same: the termination of illumination reduces the CPD to more negative values.

The relaxation response of the control surfaces upon termination of illumination in UHV consists of the repopulation of surface states which, under illuminated conditions, had been depopulated by the flux of photogenerated holes to the surface. The rate at which the conduction band electrons repopulate the surface states does not follow Elovitch-type behavior  $\left\{ \Delta n = \ln[(t/\tau) + 1] \right\}$  beyond about the first ten seconds after the termination of illumination (Figure 5.13). This indicates that there is more than one process occurring on the control surface for the capture of conduction band electrons. An additional reaction proceeds logarithmically at times greater than 10 seconds following the termination of illumination. Attempts to model the entire transient by a single logarithmic process incurs large error ( $\sim 5 \times 10^{11} \text{ cm}^{-2}$ ) in the surface charge at  $t=0$ .

The length of the relaxation period during ambient cycling (Figures 4.11 and 4.12) was chosen to insure that the response of the control surface to illumination was reproducible. Relaxation times of greater than eight hours were necessary to produce repeatable control standard transients. This indicates that those slow processes by which conduction band electrons are captured by surface states continue to play an effect long after the termination of illumination. Still, as reflected in the control standard transients of Figures 5.4 and 5.5, a large change in the surface parameters occurs immediately. Again, at least two processes on the control surfaces, one fast and one slow, are necessary to account for this behavior.

Fig. 5.13 Surface State Repopulation Transient and Elovitch Type Behavior Comparison



In both the light and dark cycling procedures, the samples were illuminated after relaxation under darkened conditions in vacuum. Upon illumination, the control standard transient undergoes both immediate and gradual changes. The depopulation of surface states by the flux of photogenerated holes to the surface again occurs in two stages: a fast depopulation followed by a slower one. Based upon the control standard transient behavior during ambient cycling, and the CPD reactions to light of varying energy and intensity (Figure 5.2 and 5.3), existence of two sets of surface states on  $\text{TiO}_2$  can be postulated.

The first set of surface states activated by illumination are those which are broadly dispersed in energy from the Fermi energy level to  $\sim 150$  meV below it. The immediate change in CPD upon illumination, as realized in the work function and surface charge changes, reflects the depopulation of these fast states. These surface states react quickly to illumination changes: the CPD traverses the 150 meV range of these states within about three seconds upon illumination changes, as determined by standard cycling procedure. By reducing the time constant of the lock-in amplifier however, these changes in CPD were seen to occur within  $10^{-6}$  seconds after the change in illumination. The amount of charge associated with these states were for the hydrogen annealed samples  $\sim 10^{12} \text{ cm}^{-2}$ , and for the vacuum annealed samples,  $\sim 5 \times 10^{11} \text{ cm}^{-2}$ . With the assumption of one charge per surface state, we can assign these values to the surface states densities. These types of surface states will henceforth be referred to as  $n_1$  type surface states.

The second type of surface state on the control surfaces of  $\text{TiO}_2$  as revealed by CPD measurements are located in a narrow energy range beginning about 0.15 eV below the Fermi level at the surface. These surface states are present in a high enough density to prevent their

complete depopulation by the incident illumination. Consequently the Fermi level is pinned at the surface by these states. The density of these states, as measured by CPD analysis, is greater than  $5 \times 10^{-11} \text{ cm}^{-2}$  on both the hydrogen and vacuum annealed samples. The reaction times of these states are considerably slower than the  $n_1$  type states, and typically have relaxation times of about 900 seconds for both hole depopulation and conduction band relaxation processes. The kinetics of these and other surface states during recombination processes will be further discussed in other sections. The slow states present on the control surfaces of  $\text{TiO}_2$  will henceforth be referred to as  $n_2$  type states.

Several pieces of information suggest that the  $n_1$  and  $n_2$  surface states are predominantly titanium in nature. First, their energy location, less than 1 eV below the conduction band edge, would suggest that these states are those of the predominantly Ti (3d) conduction band. Their appearance below the conduction band edge is a consequence of the termination of the lattice and the resulting perturbation in energy for those titanium surface atoms surrounded by less than their normal complement of oxygen atoms.<sup>23,24</sup> This suggestion has been reinforced by calculations of the energy levels occurring on  $\text{TiO}_2$  surfaces which have found that the surface states within the band gap and adjacent to the conduction band are predominantly Ti in nature.<sup>61</sup> Also the XPS spectra of Figures 5.6, 5.7, 5.9, and 5.10 indicate that upon exposure to oxygen containing species, the spectra of the Ti (2p) peaks as well as those of the O (1s) peaks are effected. The interaction of adsorbing oxygen species with surface Ti atoms, as well as the presence of oxygen adsorbates is substantiated by these spectra.

Had only oxygen-affiliated surface states been effected by the adsorbates, changes in only the oxygen spectra would have been noted. This will be discussed more fully in the upcoming sections.

Some authors, generalizing about the ionic defect states on the surface of ionic semiconductors would term such ionic (Ti) states as "Tamm" states.<sup>24</sup> The basis for this distinction however, is the conditions of symmetry in the electron potential at the lattice termination. Since these symmetries are not known for the cationic (Ti) surface states, this labelling has been here avoided.

The energy location of the  $n_2$  surface states correlate well with the surface states determined by UPS and EELS measurements.<sup>50,53,56,58,59</sup> These states are associated with surface  $Ti^{3+}$  ions, which result from the oxygen depletion of the surface. The  $n_2$  type surface states can be tentatively associated with these  $Ti^{3+}$  surface defects.

The energy location of the  $n_1$  surface states below the conduction band edge is to be expected if these defect states are to be considered to be conduction band orbitals perturbed from the conduction band by the less than perfect termination of the lattice. At the same time, the reactions of these states to illumination with energy greater than that of the band gap is very fast, comparable to the reaction times of the bulk conduction band states. With these considerations, the  $n_1$  surface states are tentatively assigned to be cationic (Ti) states. These states have not been detected by UPS and EELS measurements. The surfaces prepared for these vacuum studies are, however, of greater perfection than those utilized in this study. It is thus reasonable to correlate the  $n_1$  surface states found in this study with the residual polishing defects known to be present on the tested samples. These



states would not appear in the more perfect  $\text{Ar}^+$  ion bombarded and annealed surfaces studied by UPS and EELS.

The delineation between the  $n_1$  and  $n_2$  surface states is made on the basis of: 1) the differing responses of these states to illumination of energy greater than that of the band gap, and 2) the known association of the  $n_2$  ( $\text{Ti}^{3+}$ ) states with a particular energy level. The  $n_2$  ( $\text{Ti}^{3+}$ ) states arise from reconstructions on the surface associated with the oxygen depletion of that surface. The  $n_1$  (cationic Ti) states can be correlated with polishing defects which result in reconstructions different from those associated with the  $n_2$  ( $\text{Ti}^{3+}$ ) states. Consequently, the energy levels and illumination reactions of the  $n_1$  (cationic Ti) states would differ from those of the  $n_2$  ( $\text{Ti}^{3+}$ ) surface states.

## 5.2.2 Influence of Ambients

### 5.2.2.a Adsorption

Controlled exposures of ambients were allowed to interact with the  $\text{TiO}_2$  surfaces. The two possible interaction sequences are illustrated in cycling procedures: ambient admittance during illumination of the sample, and ambient admittance following 10 minutes of relaxation in darkness and UHV. In the first case, ambients may interact with all depopulated surface states of the sample, while in the second case, only those surface states which remain active after 10 minutes in darkness have a possibility of undergoing reactions with the ambient. Consequently, it is expected that the ambient-surface interactions during the dark cycling treatment will produce less CPD change than those of its light cycling counterpart.

In order to be attracted to and interact with the surface states that are occupied with photogenerated holes, the ambient species must become negatively charged. The two possible mechanisms for this charging are the dissociation of ambient species, and the capture of electrons by physisorbed species on the semiconductor surface. On clean ( $\text{Ar}^+$  bombarded and annealed) surfaces, dissociative adsorption of oxygen and water vapor has been found to occur up to a saturation exposure of 100L.<sup>50,51,54,56</sup> Beyond this threshold, molecular adsorption occurs. On the real surfaces of the  $\text{TiO}_2$  samples used in this study, it cannot be expected that the dissociative adsorption of species would occur, or if it does, that it would occur to the same extent that it does in clean surface studies. The perfection of the real surfaces employed does not approach that of clean surfaces, and, as prepared, the real surfaces have undergone reactions with solutions and ambients which would have saturated the dissociative reaction limit. The final preparation procedure of prolonged illumination in UHV does not remove all surface contaminants (see C (1s) peak in the XPS spectra of Figure 4.7) and hence the possibility of dissociative reactions similar to those occurring on surface where atomic perfection is approached seems remote.

More plausible is the possibility of the charging of physisorbed molecular species by the capture of conduction band electrons. If the ambient pressure above a surface is maintained at some level P, then the number of physisorbed molecules at the surface can be expressed as some function of this pressure.<sup>79,81</sup> The physisorbed molecular species can interact with the  $\text{TiO}_2$  and accept electrons from the conduction band. The transfer of charge between the  $\text{TiO}_2$  and the physisorbed species may involve thermal activation. This process is discussed more

fully in a following section. Both the surface electrons and the physisorbed electronegative molecular species can interact with surface states occupied by holes. Electrons and holes recombine, but the physisorbed electronegative species, upon exchanging charge with hole occupied surface states, may become chemisorbed at that site. The reactions of these competing processes are



where the subscripts *c* and *s* refer to chemisorbed and surface species, respectively, and  $cP_A^{\alpha-}$  represents the electronegative, thermally activated molecular species after it has gained charge from the conduction band. The population of hole occupied surface states is reduced by the recombination of charge associated with the activated electronegative physisorbed molecules. These activated species interact with the positive charge on the surface being chemisorbed by reaction (5-2). This reaction competes with the electron-hole surface recombination, reducing the forward rate of such recombination. As a result, the concentration of electrons in the  $TiO_2$  which are available for reactions is increased. This raises the bulk electron density, raising the Fermi level and reducing the band bending. The increase in the Fermi level reduces the  $TiO_2$  work function as ambients are admitted into the system (see Figure 5.4). The increase in bulk donor density, and the reducing in the surface potential serves to increase the negative charge on the surface through the equation  $n_s = n_b \exp(-qV_s/kT)$ . Thus, the net surface charge on the  $TiO_2$  is also reduced by the admittance of ambients into the vacuum system, and their

interactions on the  $\text{TiO}_2$  surface (see Figure 5.5). This is the initial reaction of all surfaces under study upon the admittance of oxygen and water vapor into the system.

The amount of chemisorption that occurs on  $\text{TiO}_2$  is expected to vary between light and dark cycling treatments. In the dark cycling procedure, some of the active (hole occupied) surface states accept charge from the conduction band prior to the admittance of ambients into the system. For the  $n_1$  type surface states, little or no interactions are to be expected, as these states react quickly to changes in the illumination conditions. It is the  $n_2$  type surface states that should interact with the ambient species, as it is these states that have very long reaction times, and would remain partially depopulated (hole occupied) during the ten minutes of relaxation in UHV. This scenario precludes the possibility of charge transfer between surface states and also the modification of surface state characteristics by the adsorbing species. Information regarding the possibility of these phenomena can be extracted from desorption data, and will be discussed shortly.

As the exposure of the  $\text{TiO}_2$  surfaces to interacting ambients is increased, reversals in the  $\text{TiO}_2$  work function decrease and the net surface charge decrease are noted. The exposures at which these reversals occur are listed in Table 5.2. The turning points in the cycling transients occur at the same exposures for both the  $\Delta\phi_{\text{TiO}_2}$  and the  $n_s$  transients. In several cases, there are additional turning points in the transients where the now increasing values of  $\Delta\phi_{\text{TiO}_2}$  and  $n_s$  have again reversed, and have begun to decrease.

The significance of the initial turning points in the cycling

Table 5.2 Transient Turning Points during Ambient Exposures

( $\Delta\phi_{\text{TiO}_2}$  and  $\Delta n_s$ )

<u>sample</u>	<u>exposure (Langmuir)</u>	
	<u>L<sub>1</sub></u>	<u>L<sub>2</sub></u>
H <sub>2</sub> annealed, light cycling		
H <sub>2</sub> O	10 <sup>5</sup>	10 <sup>9</sup>
O <sub>2</sub>	10 <sup>7</sup>	---
H <sub>2</sub> O + O <sub>2</sub>	10 <sup>7</sup>	---
H <sub>2</sub> annealed, dark cycling		
H <sub>2</sub> O	10 <sup>3</sup>	10 <sup>4</sup>
O <sub>2</sub>	> 10 <sup>12</sup>	---
H <sub>2</sub> O + O <sub>2</sub>	10 <sup>5</sup>	10 <sup>6</sup>
Vacuum annealed, light cycling		
H <sub>2</sub> O	10 <sup>4</sup>	10 <sup>5</sup>
O <sub>2</sub>	10 <sup>6</sup>	---
H <sub>2</sub> O + O <sub>2</sub>	10 <sup>6</sup>	---
Vacuum annealed, dark cycling		
H <sub>2</sub> O	> 10 <sup>10</sup>	---
O <sub>2</sub>	10 <sup>4</sup>	---
H <sub>2</sub> O + O <sub>2</sub>	> 10 <sup>10</sup>	---

L<sub>1</sub>: first turning point in CPD transient

L<sub>2</sub>: second turning point in CPD transient

transients upon adsorbate interactions is two-fold. First, these are the exposures at which the band bending at the surface is minimized. The surface potential is at its lowest value and this is the closest approach to flat-band conditions that can be produced by the experimental procedures used here. The additional band-flattening effect beyond the of the production of a bulk photo-potential is due to the increase in the bulk Fermi level due to the increase in bulk electron density. This increase in bulk electron density is in turn due to the surface hole trapping of charge associated with activated ambient molecules rather than the trapping of bulk electrons flowing to the surface. The second significant point associated with the first turning point in transient behavior of surfaces exposed to ambients is the change in the surfaces processes. At the exposures listed in Table 5.2, the negative charge on the surface stops accumulating. Several mechanisms are possible for this change. It is possible that the negative charge could be removed from the surface by the desorption of electronegative surface species. Also possible is the gain of positive charge on the surface by the adsorption of electropositive species. A third alternative is the physisorption of dipole overlayers adjacent to the layer of negative charge which would mask the negative charge on the surface, effectively reducing its magnitude. Each of these possibilities will be discussed in turn below.

The interaction of electronegative, activated ambient molecules with the surface states on  $\text{TiO}_2$  allows for the possibility of the molecules charged by electrons from the conduction band, to be desorbed from the surface rather than undergoing charge transfer chemisorption with active surface states. In this case the physisorbed molecules are

activated, receive charge from the conduction band, and then desorb from the surface. It is expected that the negatively charged, physisorbed molecules would desorb only when the positive charge on the surface had been removed by charge transfer chemisorption processes. Thus the exposure at which the first transient turning point occurs would, in this case represent the exposure at which the active surface states on  $\text{TiO}_2$  are saturated. This mechanism of charge removal from the surface of the semiconductor reduces the Fermi level in the bulk of the material, increasing the surface band bending and surface potential. The mechanism does not depend upon the presence of ambient species with an inherent dipole moment, such as water, and would be expected for oxygen ambient interactions. Also, this mechanism would account for the transfer of charge from the semiconductor in spite of chemisorbed species occupying surface state sites which could block current. The mechanism is not photonically driven, and is to be expected under darkened conditions.

It is also possible that holes may be transferred to ambient species making them electropositive. These electropositive species could then be adsorbed to the surface and reduce the negative charge, accounting for the decrease in negative charge and the reversal of the transient. This mechanism is photonically driven, insofar as illumination of the semiconductor is necessary for an appreciable density of holes to appear in the semiconductor and accumulate at its surface. Consequently, this mechanism would not be active under darkened conditions. The reversal of the CPD transients under dark cycling conditions discounts the possibility of this mechanism occurring at the semiconductor surface.

A third possibility of physisorbed dipole overlayers weakly

interacting with the hole occupied surface states may account for the reversal of the CPD transients upon ambient interactions. The negatively charged end of the dipole would be attracted to the positively charged surface states, and would align itself so that its positive pole is directed outward from the surface. The presence of these positive poles would serve to reduce the negative charge on the surface as sensed by CPD measurements. This mechanism is possible in the presence of molecules with an inherent dipole moment (water) or by the creation of activated electronegative molecular species capable of supporting a dipole moment ( $O_2^-$ ). The mechanism is not dependant on illumination conditions and is to be expected for both water vapor and oxygen interactions.

Physisorbed species are removed from the surface by the pumpdown sequence following ambient admission. The difference in the  $TiO_2$  work function between the beginning and the end of the pumpdown procedure reflects the change in the change in electron affinity which can be associated with the presence of physisorbed dipole layers. Considering a physisorbed overlayer of alligned dipoles as a set of parallel planes of opposite charge (see Figure 5.14), the voltage drop across this layer may be expressed as<sup>101</sup>

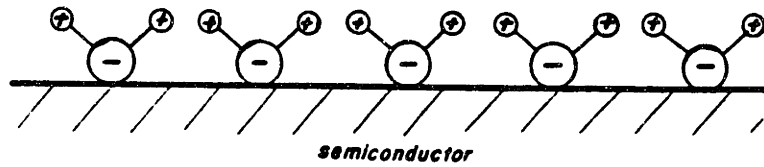
$$-\Delta V = \frac{\Delta\phi_{TiO_2}}{q} = \frac{n M_d}{\epsilon_0} = \frac{\Delta\chi}{q} \quad (5-4)$$

where  $n$  is the surface dipole density,  $M_d$  is the moment of each dipole,  $\epsilon_0$  is the permittivity of free space and  $\chi$  is the semiconductor electron affinity. For an example of equation (5-4), consider the change in work function in a light cycling sequence, such as that depicted in Figure 5.4 wherein the admitted active ambient is water

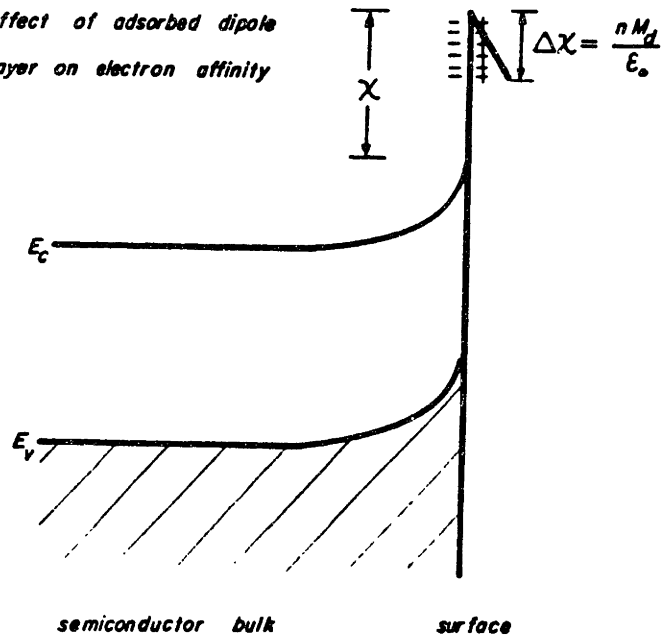


Fig. 5.14 Simplified Model of  
Dipolar Physisorption  
of Water

(a) parallel alignment of adsorbed dipolar molecules.



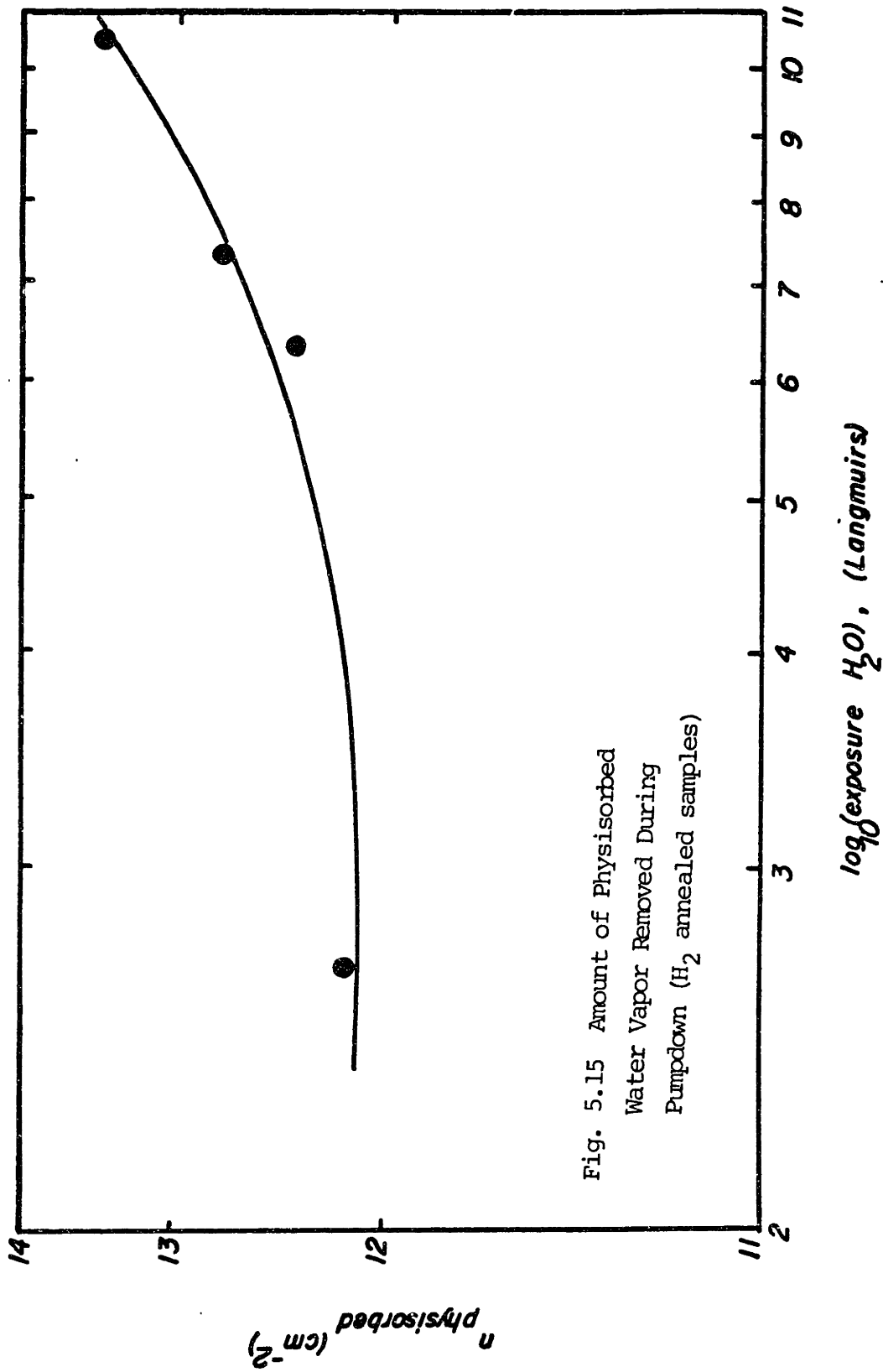
(b) effect of adsorbed dipole  
layer on electron affinity



vapor (re. Figure D-3). The illumination of the surface had been terminated ten minutes prior to the pumping of the chamber. The change in the control surface (no admitted ambient) nulling voltage during the pumpdown was 16 mV. Subtracting this change (inherent to the control surface) from the change in nulling voltage during water vapor ambient cycling, we can find the change in nulling voltage which can be ascribed to the desorption of physisorbed dipole layers. With the value of the dipole moment of a free water molecule as  $6.15 \times 10^{-28}$  coulomb-cm, <sup>88</sup> equation (5-4) can be used to generate the plot of physisorbed dipole moments versus water vapor exposure seen in Figure 5.15. The amount of physisorbed water molecules, particularly at low exposure levels, is much larger than the number of those species which are chemisorbed (as will be discussed in the next section). The number of physisorbed molecules on the surface of the  $TiO_2$  before pumpdown is always at least an order of magnitude larger than the amount of charge ascribed to chemisorption phenomena. This supports the premise that the chemisorption process involves the capture of ambient species from a virtually inexhaustible supply of physisorbed species. The presence of dipole moments in the densities depicted in Figure 5.15 also lends credence to the premise that the reversal in CPD transients following the initial work function decrease upon admittance of ambients is associated with dipole overlayers.

#### 5.2.2.b Desorption

Those species remaining on the surface of the  $TiO_2$  after the pumpdown procedure are assumed to be chemisorbed to it, that is chemical bonds have been made between the adsorbate and the surface. The desorption sequence for these chemisorbed species is the same for



the light and dark cycling procedures. Illumination absorbed by the semiconductor results in the accumulation of holes at the surface of the semiconductor. Consequently, species bonded to the  $\text{TiO}_2$  surface will, as an result of capturing photogenerated holes, have their bonds relieved, and will photodesorbed from the surface.

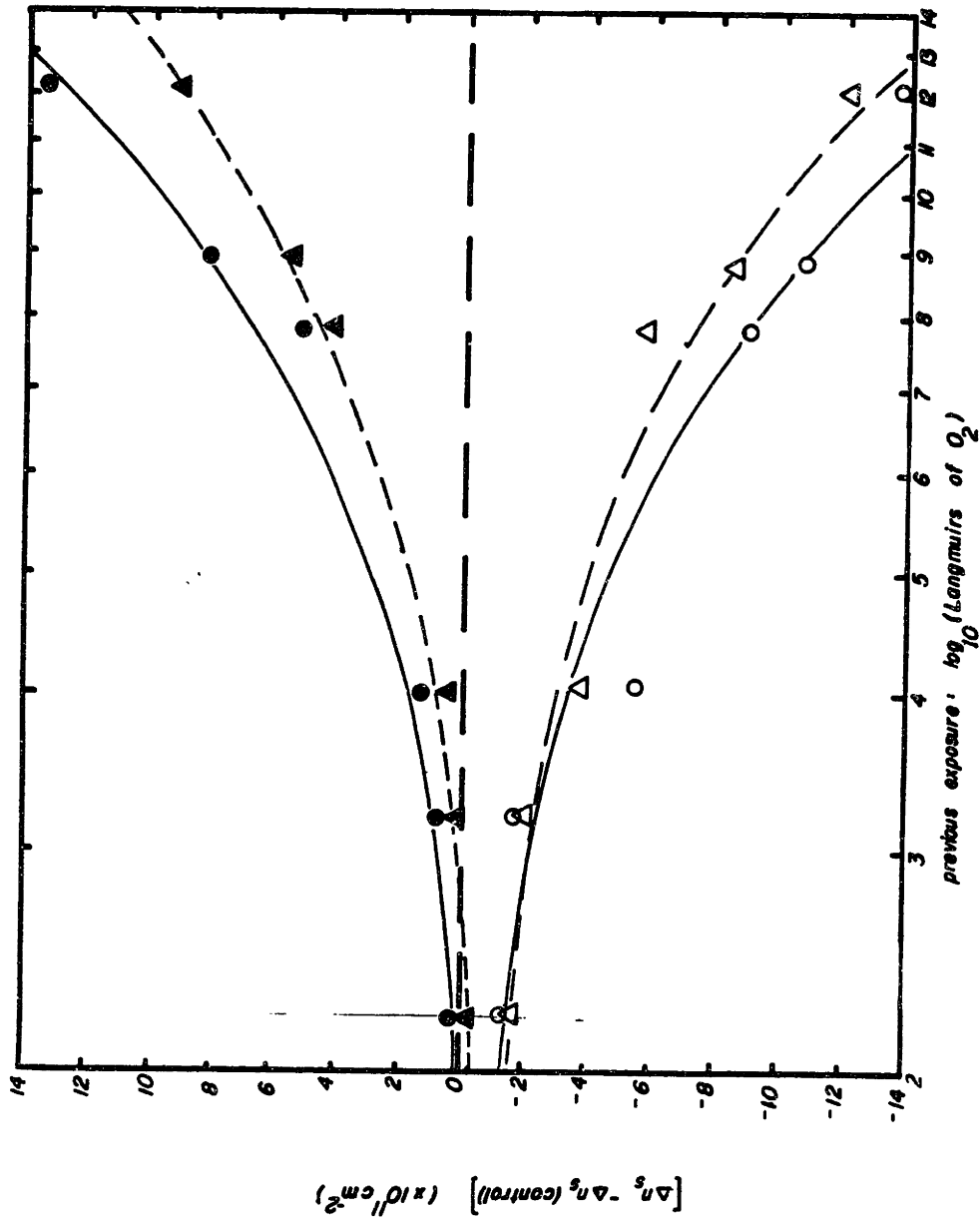
Although it is not indicated on the diagrams for the light and dark cycling procedures, the samples were illuminated with light of energy less than that of the band gap ( $\lambda = 0.5 \mu\text{m}$ ,  $I \approx 150 \text{ mW/cm}^2$ ) for one minute prior to any excitation with light energy greater than that of the band gap. For this sub-gap illumination, no CPD reaction was ever found, both for control (no ambient interactions) surfaces or for surfaces with chemisorbed species present.

The lack of sub-band gap illumination response is not surprising for two reasons. First, the ability of the surface states to absorb sub-band gap radiation is small, due to both the small values of the absorption coefficient in this energy range (see Figures A-4 and A-5), and the thinness of the surface defect layer, with or without chemisorbed species. Also, since the surface bonding configurations, both with and without adsorbates could differ markedly from the bonds of the semiconductor bulk, there is no reason to a priori assume that electrons in these bonds would react in a fashion similar to that of common semiconductors. This notion is particularly significant in the light of the reactions of the surface states which are inherent to the control surfaces utilized in this study. Also, transitions between surface energy levels associated closely with the Ti (3d) conduction band energy levels may not be allowed by momentum transfer rules.<sup>99</sup>

Illumination of the samples with white light (with a portion of the incident light having energy greater than that of the  $\text{TiO}_2$  band

gap) results in CPD changes. The changes are both immediate and gradual. The significance of the changes inherent to the control surface of this study are described in section 5.2.1. The influence of both oxygen and water vapor chemisorbed species is to reduce the amount of immediate CPD change upon illumination in UHV, and also increase the ensuing amount of gradual change in CPD. This is reflected in the changes in the immediate and gradual reductions in the  $\text{TiO}_2$  work functions and surface charge concentrations such as those illustrated in Figures 5.4 and 5.5. Also influenced is the rate at which the CPD changes during the gradual reductions in the  $\text{TiO}_2$  work function. With increasing ambient exposure, the rate of charge transfer during the gradual process increases. The amount of charge transferred during desorption relative to that transferred by the same illumination conditions on a control surface is illustrated in Figure 5.16. The rate at which the gradual component of this change occurs, relative to the rate at which it occurs on the control surfaces, is shown in Figure 5.17. As these Figures illustrate the changes in charge and rate of charge transfer less the amount associated with the same changes under control (no ambients) conditions, they represent changes due solely to the chemisorbed species.

Following the scheme of active surface states on  $\text{TiO}_2$  introduced in section 5.2.1, it is seen that the reduction in the immediate amount of surface charge change upon illumination of adsorbate effected surfaces reflects a reduction in the amount of  $n_1$  (cationic Ti) type surface states. Also, the increase in the rate of change of the gradual desorption processes indicates that surface states other than the  $n_2$  ( $\text{Ti}^{3+}$ ) states are being depopulated by holes at the  $\text{TiO}_2$  surface. The



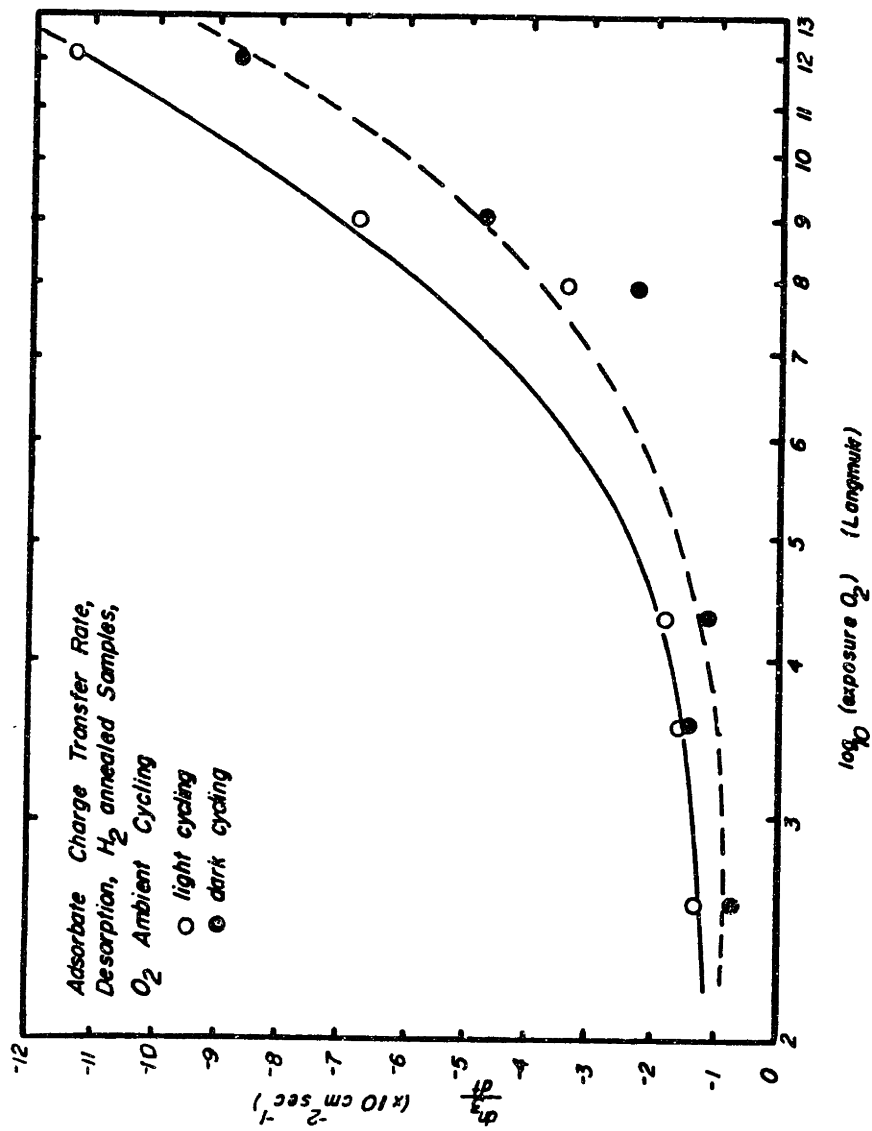
Charge Transfer Difference  
(relative to control)

During  $\text{O}_2$  Desorption,  
 $\text{H}_2$  Annealed Samples

○ immediate, light cycle  
 ● gradual, light cycle  
 △ immediate, dark cycle  
 ▲ gradual, dark cycle

Fig. 5.16 Charge Transfer Difference (relative to control) during  $\text{O}_2$  desorption,  $\text{H}_2$  annealed samples

Fig. 5.17 Adsorbate Charge Transfer  
 Rate, Desorption, H<sub>2</sub> an-  
 nealed samples, O<sub>2</sub> ambient  
 cycling



rate of surface charge change during this gradual depopulation period then represents the sum of the rates at which the various surface states are being depopulated. To account for this observed behavior, it is necessary to postulate a third set of surface states on the  $\text{TiO}_2$ .

The third set of surface states are again cationic in nature, and exist at the expense of the  $n_1$  (cationic Ti) states. The density of these  $n_3$  states present after the pumpdown sequence is related to the amount of previous ambient exposure. As is seen in Figure 5.16, The total of density of surface charge (and hence density of surface states) effected by illumination in UHV remains constant. Due to the lack of evidence to the contrary, it is assumed that the  $n_2$  surface states are not effected by ambient exposure. The  $n_3$  states would then result from some perturbation of the  $n_1$  (cationic Ti) states due to the effects of the chemisorbing species. The correlation of the ionic  $n_1$  states with these adsorbate effected states is substantiated by XPS documentation. The XPS spectra of Figures 5.6 and 5.7 indicate that changes in both the Ti (2p) and O (1s) peaks occur with the chemisorption of oxygen and water vapor species. Changes in the O (1s) peaks are expected as a consequence of the deposition of surface oxygen species. The changes evident in the Ti (2p) peaks indicate that the surface oxygen species are interacting with the surface Ti atoms. This suggests that the third set of surface states are linked to the surface Ti atoms. The third set of states do not, like the  $n_1$  and  $n_2$  surface states, communicate appreciably with the conduction band, as is evidenced by the lack of CPD response upon illumination with light of energy less than that of the band gap. It is necessary to excite a hole in the valence band, which is subsequently transferred to these  $n_3$  surface states, to effect a change in the population in these states.



This again suggests that the  $n_3$  states are Ti in nature, as communication between the predominantly O (2p) valence band and Ti surface states is preferred, as discussed in section 5.2.1. The properties of these  $n_3$  type states are considerably different from the  $n_1$  surface states which they replace. They are much slower in their reactions to band-gap illumination, comparable to the reaction times of the  $n_2$  states. Also interesting is the fact that the rate at which these surface states depopulate during illumination in UHV is related to their density, as is evident from Figure 5.17.

### 5.2.3 Surface State Modelling

Three different sets of surface states have thusfar been proposed to explain the oxygen and water vapor interactions on semiconducting titanium dioxide:  $n_1$ , cationic Ti states due to residual polishing defects;  $n_2$ ,  $Ti^{3+}$  states due to the oxygen depletion of the surface as prepared; and  $n_3$  states arising from adsorbate interactions with the cationic,  $n_1$  states. The effect of ambient exposures and illumination with these proposed surface states is depicted in Figures 5.18 through 5.20.

Consider a control surface (UHV, prolonged illumination) that is permitted to relax in darkness for twelve hours in UHV without ambient interactions. As step (i) of this modelling sequence depicts, only the  $n_1$  and the  $n_2$  states are present on this surface and they are filled by conduction band electrons during the relaxation. The CPD response of this surface upon illumination is both immediate and gradual. The immediate effect is to produce photogenerated holes in the bulk of the material, which, due to the field of the Schottky barrier, accumulate at the surface and depopulate the fast  $n_1$  (cationic Ti) type surface

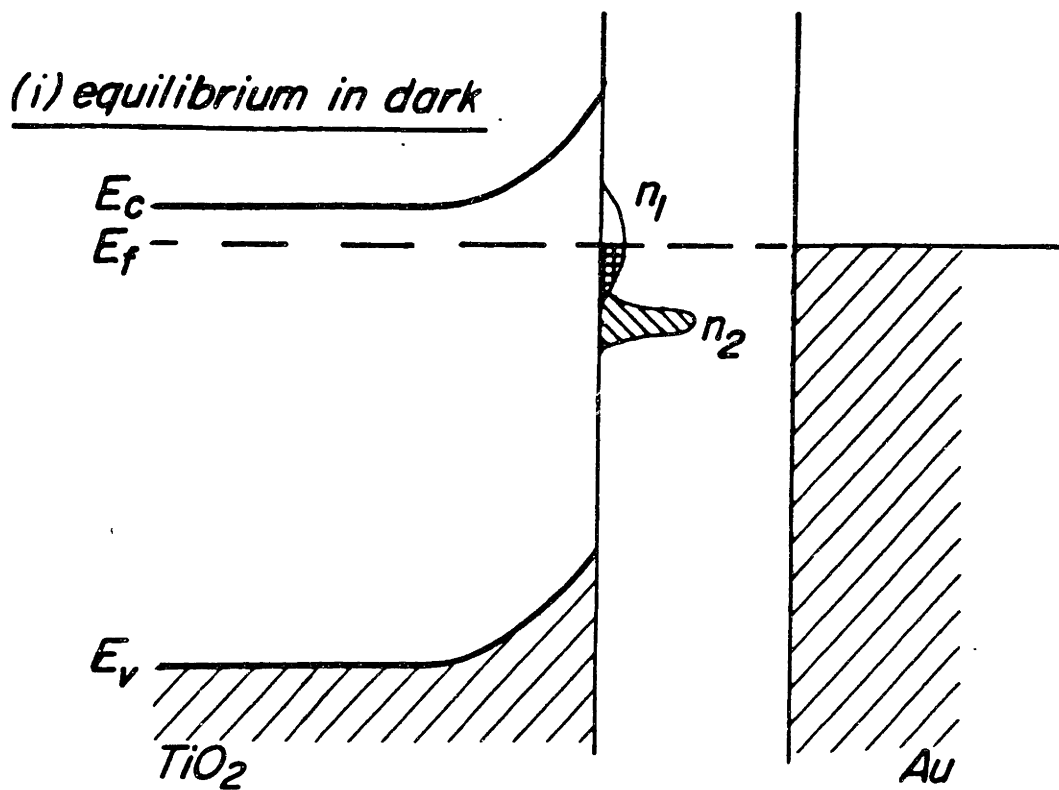
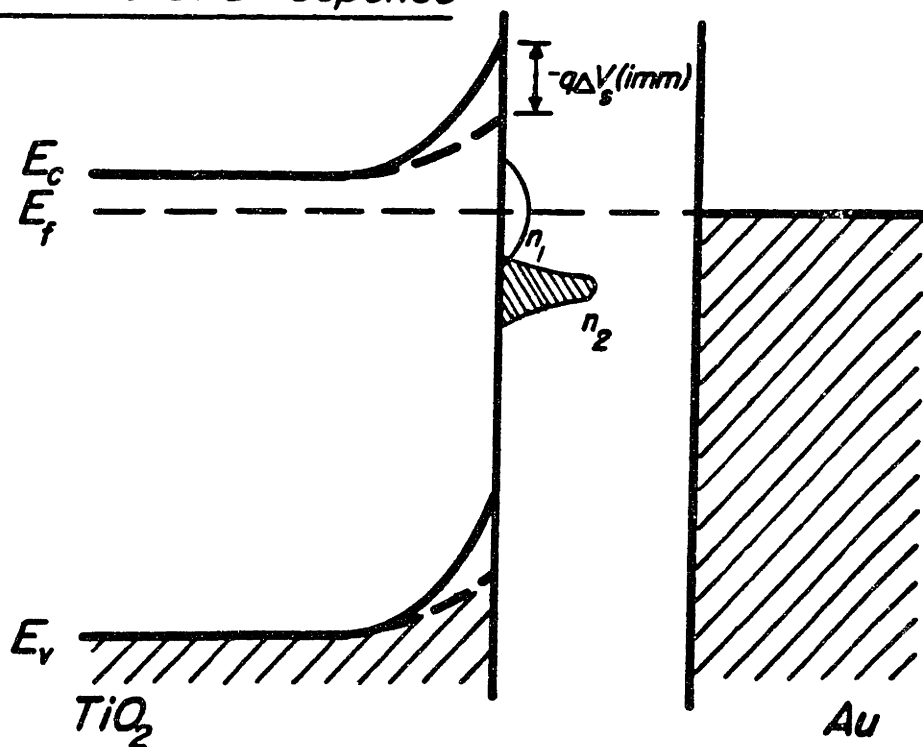


Fig. 5.18 Surface State Modelling

(1)

(ii) immediate CPD response



states [step (ii)]. Prolonged illumination with white light of illumination of  $\sim 150\text{mW/cm}^2$  further relieves some of the band bending, and depopulates some of the  $n_2$  surface states. After one hour of illumination, a steady state condition is reached whereby the  $n_2$  states are partially depopulated, and further depopulation is not possible by simple illumination of the sample [step (iii)]. If the sample is again allowed to relax in vacuum without ambient interactions, the removal of illumination results first in the repopulation of the fast  $n_1$  surface states, and then the slower refilling of the  $n_2$  states by conduction band electrons [step (iv)].

The effects of oxygen and water vapor adsorbates on this sequence of surface conditions is to modify some of the cationic Ti,  $n_1$  surface states, creating at their expense  $n_3$  adsorbate-effected surface states. The recombination of surface holes with the electronegative ambient species result in an increase in the density of conduction band electrons, increasing the Fermi level, diminishing the surface potential and work function. The simultaneous recombination of holes at the surface according to equations (5-2) and (5-3) reflects an increase in the conduction band electrons, and step (v) of the modelling sequence depicts this situation under illuminated conditions. Step (vi) depicts a similar situation wherein ambients are admitted into the system after ten minutes of relaxation of the sample. Under this situation, the  $n_1$  surface states are filled, and only the  $n_2$  surface states remain partially unoccupied (hole occupied). The change in the CPD transients during this dark admittance of ambients indicate that charge is being transferred from the  $n_1$  states to the  $n_2$  states allowing the interaction of ambient species with the  $n_1$  states, modifying them into  $n_3$  adsorbate-effected states. The presence of these

(iii) after 1 hr illumination

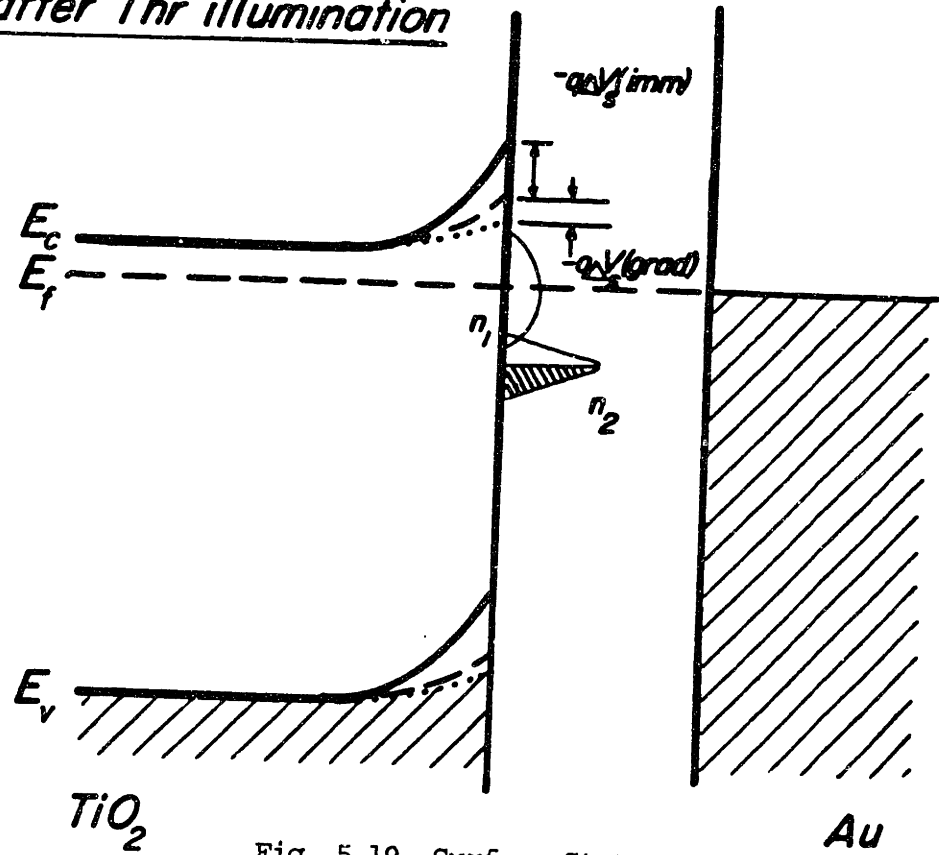
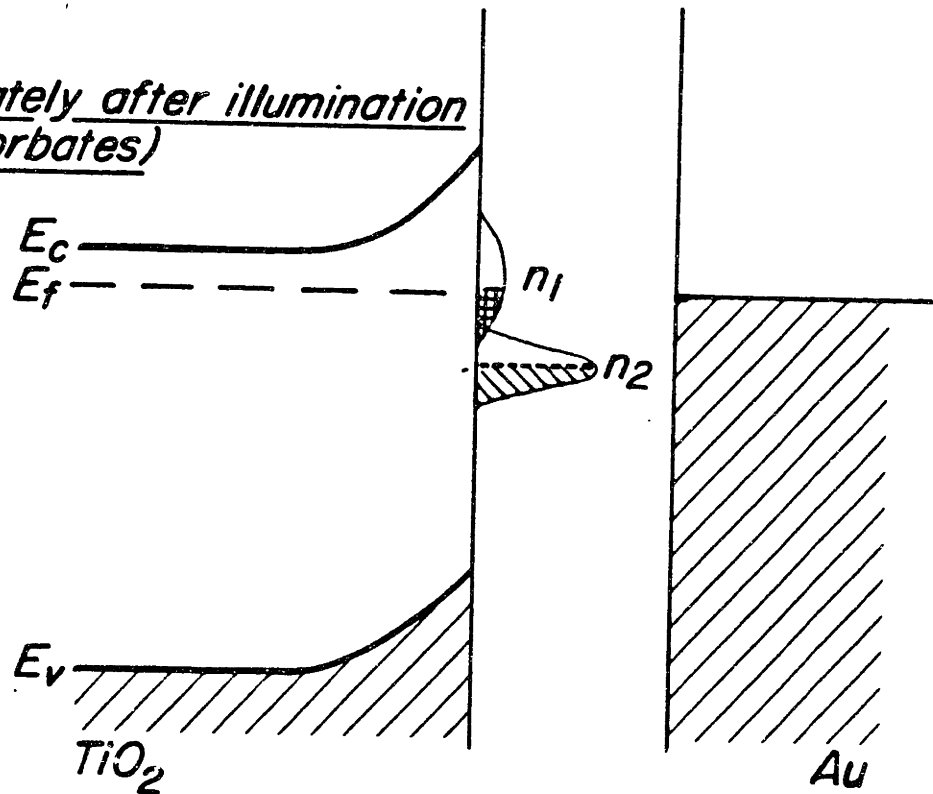


Fig. 5.19 Surface State Modelling

(2)

(iv) immediately after illumination  
(no adsorbates)



(v) illuminated adsorbate interactions

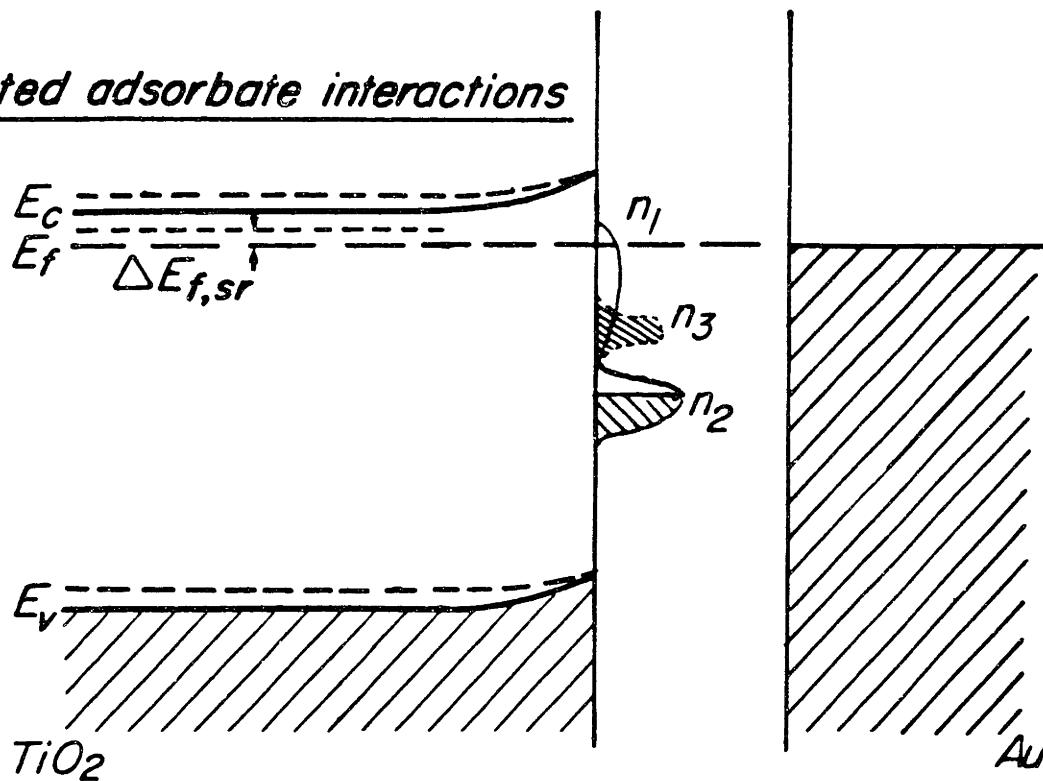
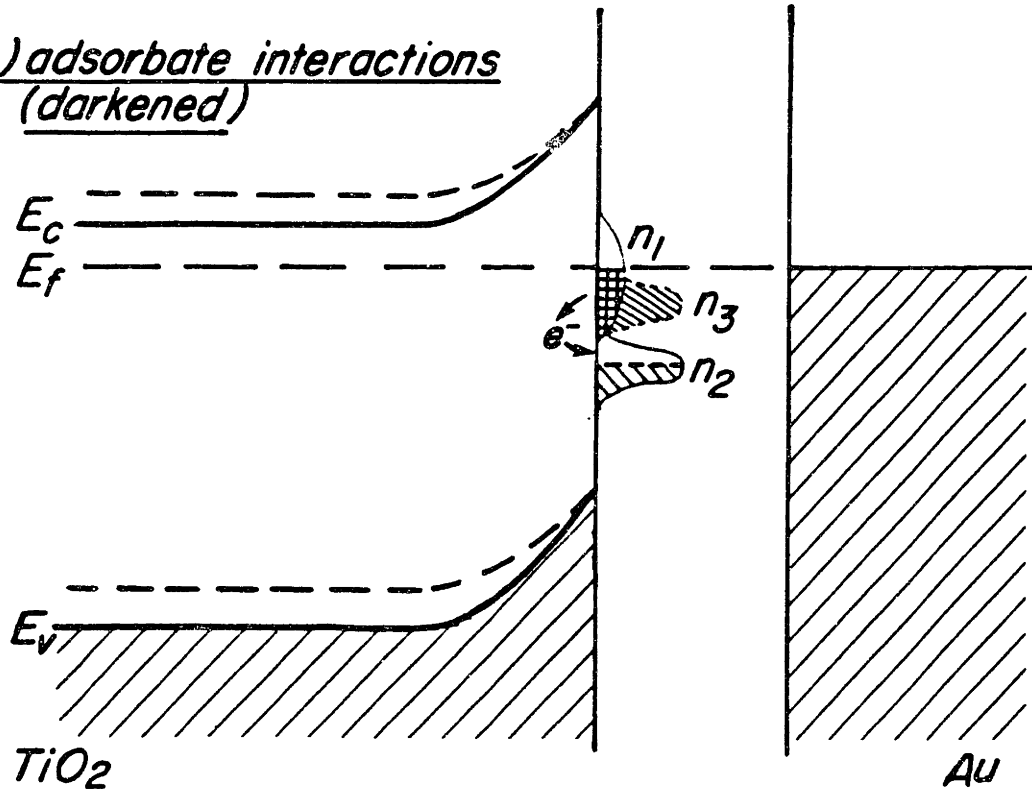


Fig. 5.20 Surface State Modelling  
(3)

(vi) adsorbate interactions  
(darkened)



$n_3$  surface states produced by dark ambient cycling is further supported by the changes in the CPD transients during the ensuing photodesorption sequence.

Using the differences in the CPD transients during the photodesorption sequences, one can determine the changes in the densities of each type of surface state. The difference in the immediate amount of CPD change (relative to control cycling changes) upon illumination can be ascribed to the reduction in the number of  $n_1$  surface states. The difference in the amount of gradual CPD desorption change (again, relative to the change encountered under control cycling conditions) can be ascribed to the  $n_3$  surface states on the surface existing at the expense of the  $n_1$  states. The numbers of surface states present are determined through the use of equation (4-8). In this modelling, the number of  $n_2$  surface states is presumed to remain constant, and is determined by the amount of gradual CPD change upon illumination under control cycling conditions.

Utilizing this model of the surface states on  $\text{TiO}_2$ , the data of Figure 5.16 can, for example, be replotted in terms of the particular surface state populations vs. ambient exposure. Such a restructuring of this data is presented in Figure 5.21 wherein the  $n_3$  states supplant the  $n_1$  states as the exposure of the ambient is increased.

Further data regarding the populations of the particular surface states is listed in Table 5.3. The data concerning the  $n_2$  surface states represents the maximum density of these states which could be probed (depopulated) under the illumination used: it does not represent the total density of these states that may be on the surface. The particular values listed for the surface state densities represent the average of the values found by the CPD ambient cycling procedures.

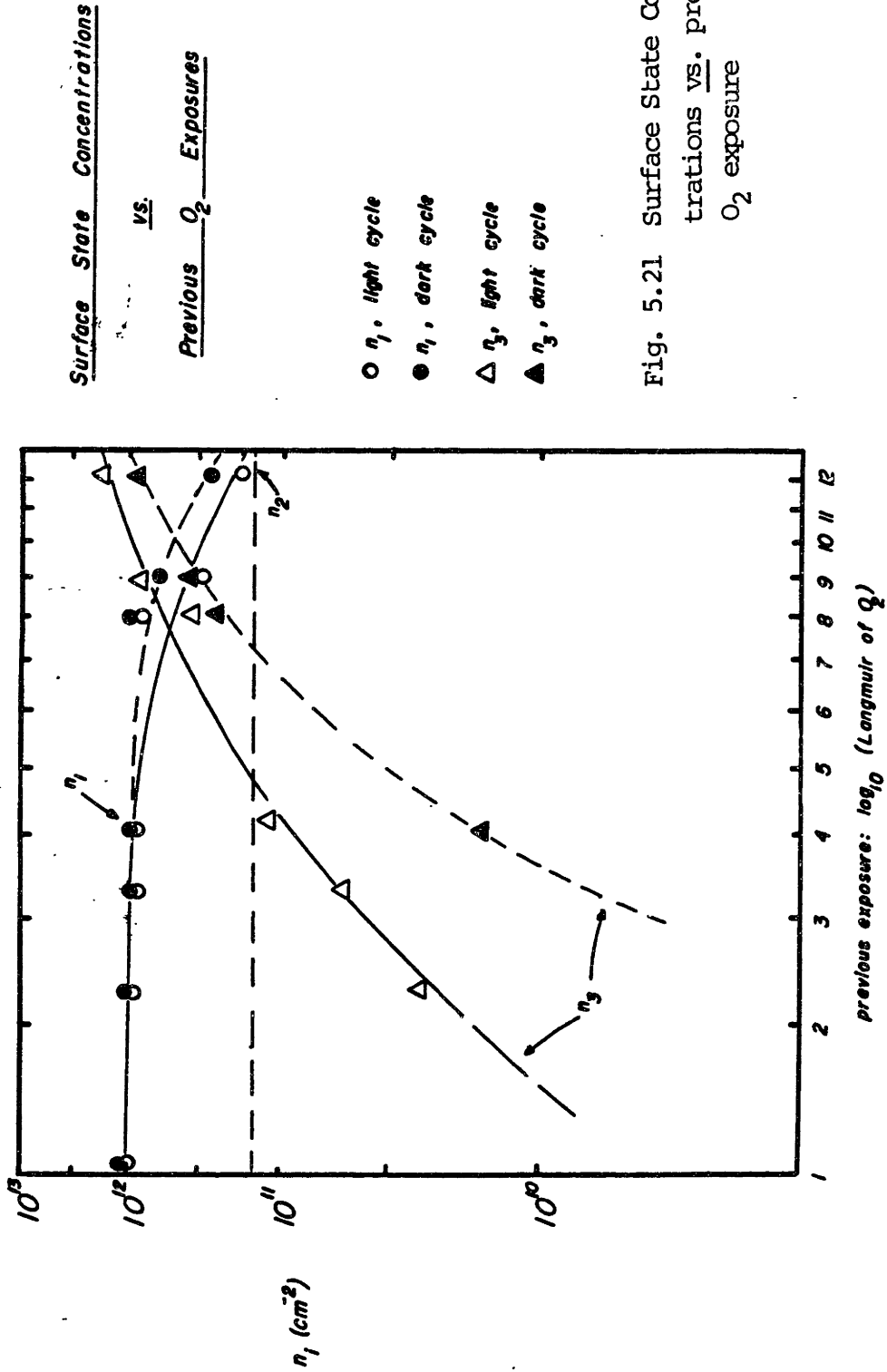


Table 5.3 Surface State Populations(cm<sup>-2</sup>)

<u>sample</u>	<u>n<sub>1</sub></u>		<u>n<sub>2</sub></u>	<u>n<sub>3</sub></u>	
	<u>max</u>	<u>min</u>	<u>min</u>	<u>max</u>	<u>min</u>
<b>H<sub>2</sub> annealed samples</b>					
light cycling: H <sub>2</sub> O	1.2x10 <sup>12</sup>	7.0x10 <sup>11</sup>	>1.9x10 <sup>11</sup>	5.3x10 <sup>11</sup>	0
O <sub>2</sub>	1.6x10 <sup>12</sup>	2.5x10 <sup>11</sup>	>1.9x10 <sup>11</sup>	1.4x10 <sup>12</sup>	0
H <sub>2</sub> O+O <sub>2</sub>	8.0x10 <sup>11</sup>	2.1x10 <sup>11</sup>	>1.9x10 <sup>11</sup>	7.3x10 <sup>11</sup>	0
dark cycling: H <sub>2</sub> O	1.2x10 <sup>12</sup>	7.4x10 <sup>11</sup>	>1.9x10 <sup>11</sup>	2.2x10 <sup>11</sup>	0
O <sub>2</sub>	1.6x10 <sup>12</sup>	4.1x10 <sup>11</sup>	>1.9x10 <sup>11</sup>	9.1x10 <sup>11</sup>	0
H <sub>2</sub> O+O <sub>2</sub>	8.0x10 <sup>11</sup>	2.1x10 <sup>11</sup>	>1.9x10 <sup>11</sup>	4.0x10 <sup>11</sup>	0
<b>Vacuum annealed samples</b>					
light cycling: H <sub>2</sub> O	2.3x10 <sup>11</sup>	7.3x10 <sup>10</sup>	>8.4x10 <sup>10</sup>	1.2x10 <sup>11</sup>	0
O <sub>2</sub>	5.3x10 <sup>11</sup>	4.0x10 <sup>9</sup>	>8.4x10 <sup>10</sup>	1.1x10 <sup>11</sup>	0
H <sub>2</sub> O+O <sub>2</sub>	5.4x10 <sup>11</sup>	4.0x10 <sup>9</sup>	>8.4x10 <sup>10</sup>	1.9x10 <sup>11</sup>	0
dark cycling: H <sub>2</sub> O	2.3x10 <sup>11</sup>	6.1x10 <sup>10</sup>	>8.4x10 <sup>10</sup>	1.2x10 <sup>11</sup>	0
O <sub>2</sub>	5.3x10 <sup>11</sup>	1.7x10 <sup>11</sup>	>8.4x10 <sup>10</sup>	1.7x10 <sup>11</sup>	0
H <sub>2</sub> O+O <sub>2</sub>	5.4x10 <sup>11</sup>	6.0x10 <sup>10</sup>	>8.4x10 <sup>10</sup>	1.6x10 <sup>11</sup>	0



Further complications in the modelling of the ambient interactions on the  $\text{TiO}_2$  surfaces occur when, in the presence of a high ambient pressure, the illumination of samples is terminated. As depicted for the  $\text{O}_2$  ambient, light cycling of a vacuum annealed sample, the termination of light in the presence of a high oxygen pressure results in a decrease in the  $\text{TiO}_2$  work function and an accumulation of positive charge on the surface, as sensed through CPD measurements (Figure 5.22). This increase in positive charge can be associated with the accumulation of a dipole layer on the surface with the positive pole directed outward from the surface, as depicted in Figure 5.14. After the pumpdown sequence, this physisorbed dipole layer is removed. Changes in the CPD transients upon photodesorption do, however, result from the high ambient exposure in these situations. Upon illumination in UHV, the surface first receives negative charge, and after a few minutes illumination, positive charge. The band diagram for this surface during illumination in UHV is shown in Figure 5.23. It consists of a depletion layer extending into the bulk of the semiconductor, but adjacent to the surface, only a small amount of band bending occurs, due to the filling of surface states with charge from electronegative ambient species, rather than by conduction band electrons. Upon illumination, photogenerated electrons can then interact on the surface by surmounting the small surface potential barrier. Interaction with the photogenerated holes accumulating at the surface due to the field of the Schottky barrier would then give rise to the complicated CPD transient depicted in Figure 5.22. The complicated CPD transient behavior observed on vacuum annealed samples upon photodesorption in vacuum is termed photovoltage inversion.

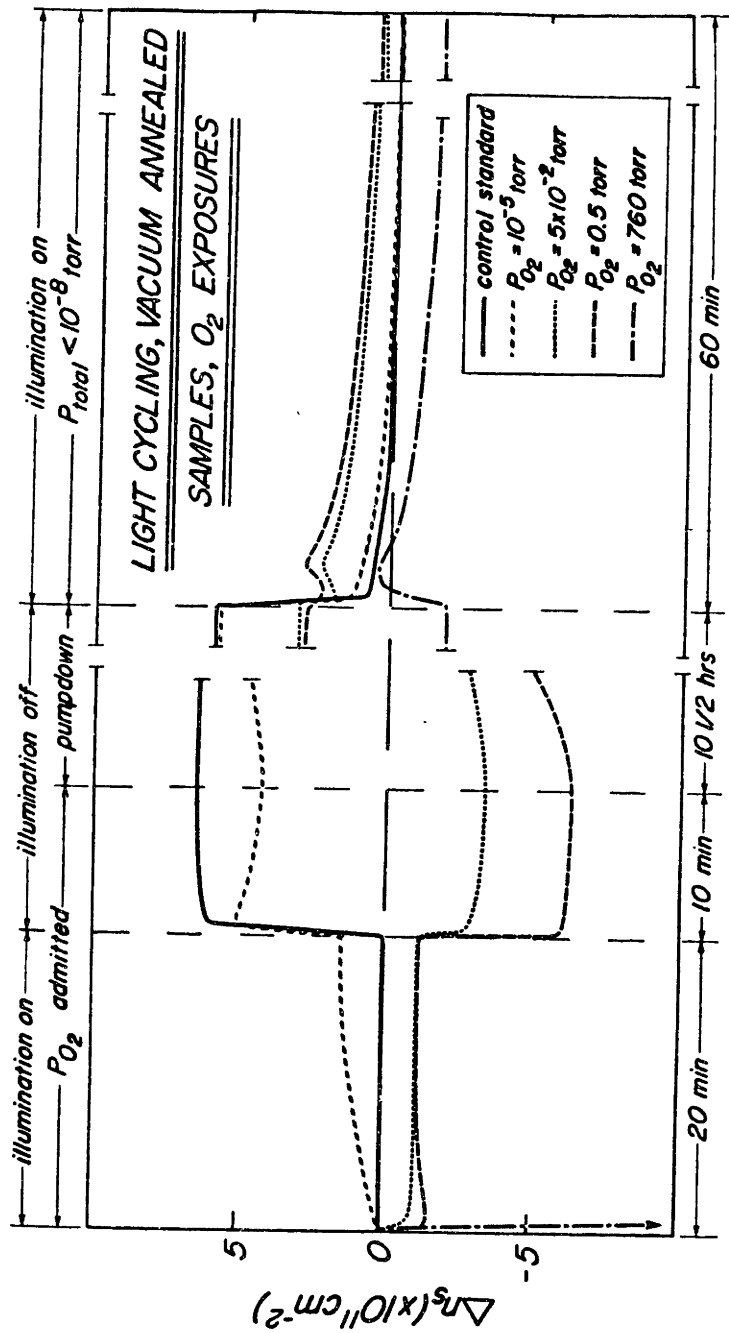


Fig. 5.22 Surface Charge Changes:  
 Vacuum Annealed Samples during  
 Oxygen Light Cycling

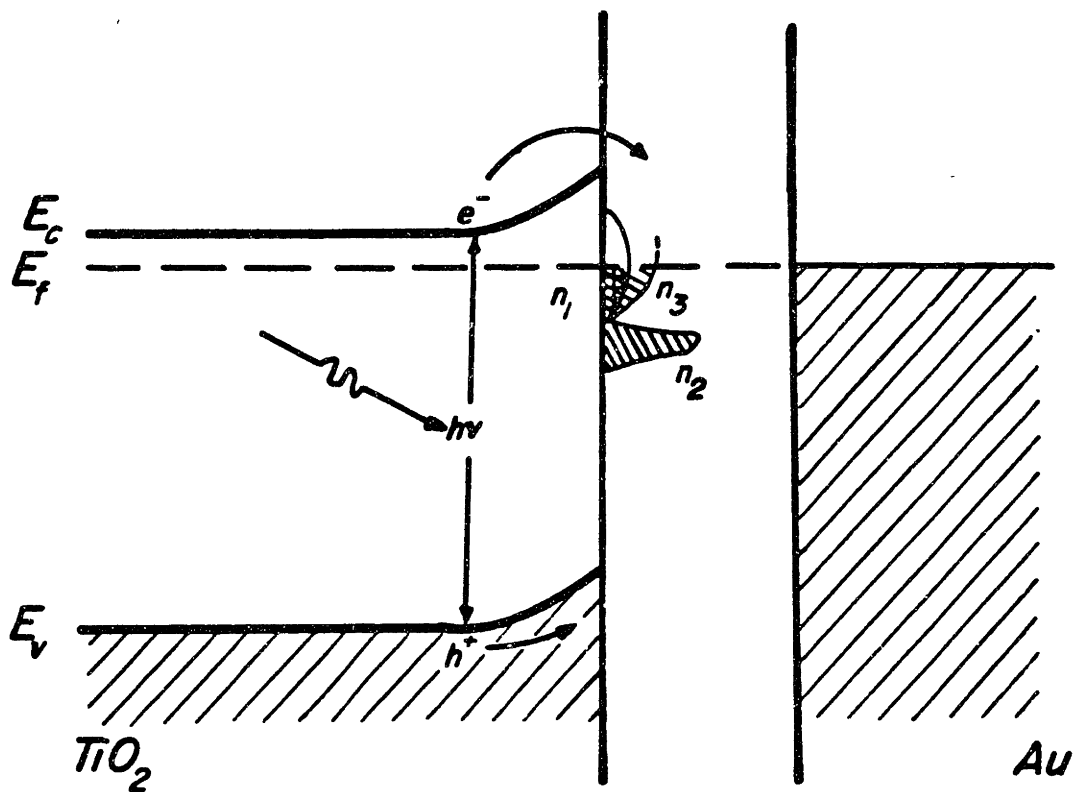


Fig. 5.23 Vacuum Annealed Samples  
Photovoltage Inversion

Another interesting feature of the CPD measurements taken on the vacuum annealed samples is the apparent deviation in the trend that ambient introduction results, at least initially, in the reduction of both the  $\text{TiO}_2$  work function and surface state hole populations. While this does occur for moderate and high ambient exposures, as shown in Figure 5.22, the lower exposure cyclings produce a flux of negative charge to the surface, and an increase in  $\text{TiO}_2$  work function. This deviation is tentatively assigned to a degradation of the control surface, and is discussed further in section 5.2.7

#### 5.2.4 Electronic Surface Transitions

Figures 5.18 through 5.20 depict the changes in the fluctuations in the densities of surface states with illumination and ambient exposures. The transference of charge within these surface states, and also between the surface states and the conduction and valence bands during illumination and ambient exposures deserves clarification.

None of the surface states on the real surfaces of  $\text{TiO}_2$  used in this study communicated effectively with the conduction band. No change in contact potential difference was detected for illumination of the samples with light of energy less than that of the band gap. As has been previously discussed, this information, coupled with changes in the XPS spectra of the  $\text{TiO}_2$  surface indicate that all photo-active surface states encountered in this study are predominantly Ti in nature.

An interchange of charge between surface states has been encountered in the modelling of the surface states. This interchange is substantiated by the production of  $n_3$  surface states in the energy range of the  $n_1$  surface states, in the situation where the  $n_1$  states

had been previously filled [Figure 5.20, (vi)]. The transference of charge between the  $n_1$  and  $n_2$  surface states is thus allowed as the  $n_2$  surface states slowly fill upon relaxation.

#### 5.2.5 Surface Recombination

The rate at which surface holes and electrons recombine is characterized by a parameter known as the surface recombination velocity. It is formally defined as the ratio between the flux of minority carriers (holes) to the surface and the surface population of these carriers. An expression for the surface recombination of a steady state hole population at a discrete energy surface trapping level associated with a single type of defect may be derived using Shockley-Read theory (see section 2.5.2.a and Appendix C). As applied to the case of non-degenerate n-TiO<sub>2</sub>, the generalized expression reduces to that of equation (2-19). Caution must be exercised in the application of this expression to situations encountered in this research: 1) the equation describes the steady state phenomena of the balancing of the hole flux to the surface with the hole recombination at that surface, and 2) discrete energy surface states of uniform capture cross section are involved as recombination centers for hole and electrons at the surface. The applicability of expression (2-19) to the photodepopulation of surface states encountered in this study is thus open to discussion.

An attempt will be made here to apply equation (2-19) to the photodepopulation of the  $n_2$  and  $n_3$  type surface states. While the above criticism of the use of this equation serves to temper the conclusions which may be drawn from its application, it nonetheless may serve to elucidate estimates for the parameters of interest concerning the  $n_2$

and  $n_3$  surface states. For these slow states on  $\text{TiO}_2$ , the deviation from steady state behavior is relatively small, at least compared to the fast  $n_1$  states for which no estimates were attempted.

The estimates of capture cross sections and surface recombination velocities were sought. These parameters were based upon data collected during the desorption sequences. The pertinent time of measurements was five minutes after the beginning of illumination.

The surface recombination velocity is the flux of photogenerated holes to the surface divided by the surface population of holes. The flux of holes to the surface may be determined via the Gartner equation (2-14) knowing the depletion layer width, absorption coefficient at energies greater than that of the band gap of the material, the hole diffusion length and the intensity of photons capable of driving reactions. Under a band-gap illumination of  $8 \times 10^{14}$  photons/cm<sup>2</sup>-sec, the surface potential on the  $\text{TiO}_2$  is estimated as  $\sim 0.1$  Volt. The depletion layer widths for the hydrogen and vacuum annealed samples are  $6.7$  and  $10.6 \times 10^{-6}$  cm, respectively. The absorption coefficient for  $\lambda=350$  nm for  $\text{TiO}_2$  is  $10^4$  cm<sup>-1</sup>, and the hole diffusion length is estimated as  $10^{-4}$  cm.<sup>40</sup> These values, when used in equation (2-14) yield hole fluxes to the surface of  $4.2$  and  $4.4 \times 10^{14}$  holes/cm<sup>2</sup>-sec for the hydrogen and vacuum annealed samples, respectively. The value of the hole surface population can be determined from the expression

$$p_s^* = p_i \exp\left(\frac{E_p^* - E_i}{kT}\right) \quad (5-5)$$

where  $p_i$  is the intrinsic hole density [  $p_i = N_v \exp(-E_g/2kT)$ ;  $N_v \sim N_c \sim 8.78 \times 10^{21}$  cm<sup>-3</sup>;  $p_i \sim 5 \times 10^{-4}$  cm<sup>-3</sup> ]. The hole quasi-Fermi energy is pinned at the level of the surface traps during illumination.

Consequently, the surface hole concentration, and in turn the SRV (=  $F_p/p_s^*$ ) can be estimated. For the control cyclings (no ambient interactions, no  $n_3$  states) the SRV's for solely the  $n_2$  states on the hydrogen and vacuum annealed surfaces are 0.996 and 2.612 cm/sec, respectively.

The Shockley-Read recombination expression (2-19) can now be applied directly to ambient cyclings where both  $n_2$  and  $n_3$  surface states are active. Utilizing a value of  $E_t = 2.58$  eV and  $E_{f,s} = 2.66$  eV (above the valence band), a thermal velocity of  $9 \times 10^5$  cm/sec [ $= (\frac{kT}{*})^{1/2}$ ], and the densities of active  $n_2$  states as listed in Table 5.3, the values of the capture cross sections for the  $n_2$  states can be found during control cycling illumination. These are listed in Table 5.4, as well as the capture cross sections for the  $n_3$  states. The values of the capture cross sections for the  $n_3$  states were found by an equation similar to that of (2-19) but with an additional term in the numerator for the occupancy and cross sections for the  $n_3$  states. The data was taken during the desorption sequences during ambient cycling, when both  $n_2$  and  $n_3$  states are depopulated. Also listed in Table 5.4 are the relaxation times associated with each type of surface state. The time of measurement was again 5 minutes after the beginning of illumination, and the values of  $\tau$  are defined from the expression

$$n(t=5) = n(\text{total}) \exp(-5/\tau) . \quad (5-6)$$

### 5.2.6 Charge Transfer Chemisorption

Inherent in the modelling employed in this study is the mechanism of charge transfer chemisorption. Physisorbed molecules on the surface of the semiconductor are activated, accept charge from the conduction

**Table 5.4 Surface State Capture Cross Sections and Relaxation Times**  
(Shockley-Read Recombination Theory)

<u>sample</u>	$n_2$		$n_3$	
	$\underline{A}_p$ (cm <sup>2</sup> )	$\underline{t}_2$ (sec)	$\underline{A}_p$ (cm <sup>2</sup> )	$\underline{t}_3$ (sec)
<b>H<sub>2</sub> annealed samples</b>				
light cycling: H <sub>2</sub> O	8.4x10 <sup>-19</sup>	550	2.1x10 <sup>-19</sup>	570
O <sub>2</sub>			4.1x10 <sup>-19</sup>	650
H <sub>2</sub> O+O <sub>2</sub>			4.2x10 <sup>-19</sup>	400
dark cycling: H <sub>2</sub> O			4.2x10 <sup>-19</sup>	570
O <sub>2</sub>			8.9x10 <sup>-20</sup>	680
H <sub>2</sub> O+O <sub>2</sub>			5.6x10 <sup>-19</sup>	400
<b>Vacuum annealed samples</b>				
light cycling: H <sub>2</sub> O	1.2x10 <sup>-18</sup>	1530	2.5x10 <sup>-19</sup>	1440
O <sub>2</sub>			7.6x10 <sup>-19</sup>	1330
H <sub>2</sub> O+O <sub>2</sub>			3.1x10 <sup>-19</sup>	2740
dark cycling: H <sub>2</sub> O			2.8x10 <sup>-19</sup>	870
O <sub>2</sub>			8.4x10 <sup>-19</sup>	1270
H <sub>2</sub> O+O <sub>2</sub>			5.7x10 <sup>-19</sup>	1020



band, and with this charge may recombine at active, hole populated surface sites by the exchange of charge between the adsorbate and surface site. The modelling of this process in the case of ambient chemisorption on a semiconductor surface by Lagowski et.al.<sup>81,89</sup> closely resembles the similar situation of conduction band electron transfer to solvated species in solution. Most particularly, the thermal activation terms implicit in both equations (2-20) and (2-22) serve to indicate the constraining mechanism by which charge is transferred to the physisorbed species.

The thermal activation energy during oxygen adsorption has been found by Addiss and Wakim<sup>65</sup> to be 70 meV. Utilizing this value of in equation (2-22) along with the previously mentioned thermal velocity of electrons, surface potential under illumination, oxygen pressures and the total surface state populations listed in Table 5.3, an expression for the capture cross section of the active surface sites in terms of the unoccupied surface state population and the measured rate of charge transfer to the semiconductor surface can be obtained.

The product of capture cross section and a multiplicative constant,  $c$ , can be found by substituting the measured charge transfer rate to the surface and the unoccupied (hole occupied) surface state populations during the adsorption sequences for various oxygen pressures. Using these values, the products of the multiplicative constant and the capture cross section have values in the range of  $10^{-24}$  cm<sup>2</sup>. Although the mechanism of charge transfer chemisorption has been utilized in the modeling of the surface states on TiO<sub>2</sub>, the further pursuit of quantification of the parameters cannot be made with the information at hand.

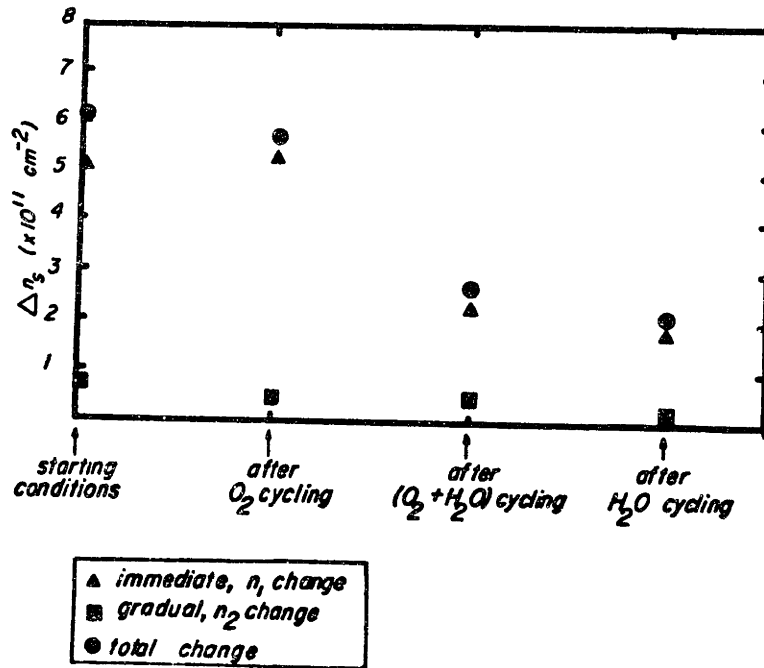
### 5.2.7 Surface Degradation

It has been noted in Figure 5.22 (as well as in Figures D-13, -14, and -20) that the immediate interactions of ambients at low pressures results in an increase in the  $\text{TiO}_2$  work function and negative surface charge, in violation of the apparent trend encountered throughout the remainder of this research. A plausible explanation of this behavior is not the change in the reactions occurring at the semiconductor, but the change in the nature of the real surface due to previous ambient exposures.

The dominant donor species in the vacuum annealed samples are the vacant oxygen sites. Upon exposure to oxygen adsorbates, the diffusion of oxygen into the sample, at least in the highly defected surface layer, may occur. This is equivalent to the diffusion of the vacant donor sites out of the material, resulting in a change in the donor concentration near the surface. This in turn increases the depletion layer width, and effects the flux of holes to the surface upon illumination. It also reduces the density of electrons at the surface.

The deterioration of the control surfaces on the vacuum annealed samples is documented in Figure 5.24. In this figure, the total amount of surface charge change during illumination of control cycling as it varies with previous ambient treatments is depicted. As can be seen, with increasing exposure history, the amount of surface charge associated with the depopulation of surface states decreases. This decrease is not necessarily associated with changes in the surface state densities, but with the photoresponse of the semiconductor.

Fig. 5.24 Degradation of Vacuum  
Annealed Control Surface



## Chapter 6 : CONCLUSIONS AND RECOMMENDATIONS

The photostimulated effects of oxygen and water vapor adsorption and desorption on the surface properties of semiconducting titanium dioxide have been identified. The effects have been attributed to two phenomena: the depopulation of donor surface states by photostimulated minority carriers (holes), and the charge transfer chemisorption of electronegative ambient species interacting with, and modifying the properties of, these donor surface states. Significant changes in the surface recombination velocity, the surface potential and densities of surface electron states have been attributed to 1) the accumulation of photogenerated holes at the semiconductor surface, and 2) the interaction of electronegative oxygen and water vapor species with electronic states at the surface of  $\text{TiO}_2$ . The photostimulated behavior of a subset of these surface states is modified by the charge transfer chemisorption of ambient species.

Based upon the previously explained experimental procedures and results, the following conclusions summarize this thesis research:

### [A.] Bulk and Control Surface Conditions

Single crystal, Verneuil-grown  $\text{TiO}_2$  with no intentional chemical impurities was doped n-type by reduction in various pressures of hydrogen, resulting in different dominating bulk donor defects. Reliable, reproducible control surfaces were produced on n- $\text{TiO}_2$  [001] by polishing, cleaning and finally illuminating with white light ( $\sim 150 \text{ mW-cm}^{-2}$ ) in UHV. Experimentation utilizing these control surfaces as references provides information on the adsorption and desorption of oxygen and water vapor species at a level more basic than can be

derived from wet electrochemical cell measurements.

### [B.] Experimentation

The charge transfer occurring on the  $\text{TiO}_2$  surfaces during the adsorption and desorption of oxygen and water vapor was monitored using contact potential difference measurements. Experiments were designed to cyclically monitor the charge transfer at the surface during the adsorption and desorption of oxygen and water vapor. Ambient exposures spanned the range from 10 to  $10^{12}$  Langmuirs. The effects of adsorbates on the electronic parameters of the  $\text{TiO}_2$  surfaces were quantitatively and unambiguously obtained.

X-ray photoelectron spectroscopy measurements were made using the same cyclical sequences. Large changes in the oxygen 1s spectra were noted with both oxygen and water vapor exposures, indicating the specific chemisorption of oxygen containing species on  $\text{TiO}_2$  surfaces in a configuration differing from that of the bulk or surface oxygen associated with the  $\text{TiO}_2$  crystal.

### [C.] Phenomenological Results

The electronic structure of the semiconductor surface region under control conditions was determined to be that of a depletion layer. The effect of illumination was to generate a photovoltage in the bulk of the material, thereby reducing the surface potential. On control surfaces in UHV, the effects of illumination upon the  $\text{TiO}_2$  work function were both immediate and gradual. Non-Elovitch type behavior was observed suggesting the presence of at least two different simultaneous surface processes. No changes in the  $\text{TiO}_2$  work function were observed with sub-bandgap illumination. This finding, coupled with the results of XPS experimentation suggest that the surface states on the  $\text{TiO}_2$  surfaces are associated with cationic defects and that these

states do not appreciably communicate, at least under optical stimulation, with the predominantly ionic Ti (3d) conduction band. Further, the TiO<sub>2</sub> work function continued to decrease with increasing bandgap illumination intensity without saturation, indicating that flat-band conditions could not be reached using moderate levels of illumination.

The TiO<sub>2</sub> work function is effected by exposure to ambients, both during bandgap illumination and in a period shortly following such illumination. The effect of ambient interactions is to initially decrease the TiO<sub>2</sub> work function relative to those situations where no ambient interactions are allowed. Further interactions with ambients beyond this initial decrease in work function varied with bulk defect type, cycling procedure, and interacting ambient(s).

Physisorbed overlayers were removed from the surface by pumping the test chamber to UHV. Bandgap illumination in UHV again resulted in immediate and gradual decreases in the TiO<sub>2</sub> work function. The immediate change in work function decreased, relative to control conditions, with increasing previous ambient exposures. The amount of gradual TiO<sub>2</sub> work function change increased, relative to control conditions, with the rate of work function decrease during this period also increasing.

#### [D.] Surface State Modelling

Changes in the contact potential difference of the test cell were analyzed via Gauss' Law to reveal fluctuations in the amount of surface charge on the semiconductor. Plots of these charge fluctuations roughly parallel changes in the TiO<sub>2</sub> work function. Changes in the surface charge corresponded to: 1) photostimulated interactions inherent to the

semiconductor, 2) the interaction of chemisorbed species with semiconductor surface states, and 3) to the change in electron affinity due to physisorbed overlayers. Comparison of the charge transfer fluctuations during ambient interactions to control (no ambient interactions) sequences allowed these combined effects to be determined exclusive of the excitation and relaxation processes inherent to the semiconductor. Similarly, after the removal of the physisorbed overlayers, the amount of charge associated with chemisorbed species could be unambiguously determined. Analysis of these measurements has resulted in the following model of  $\text{TiO}_2$  surface states.

Two different sets of surface states appear on all tested  $\text{TiO}_2$  control surfaces. One set, having a low energy density of states, is continuously distributed in energy from about 0.4 eV to 0.7 eV below the  $\text{TiO}_2$  conduction band. These surface states have fast relaxation times ( $\tau \sim 1 \mu\text{sec}$ ), comparable to those of conduction band states. These states are assigned to be cationic states perturbed from the conduction band by surface defects. A second set of surface states, having a large energy density of states lies 0.7 eV below the conduction band and lower. The energy range of this set of surface states could not be fully probed with moderate illumination levels: the high density of these states resulted in the pinning of the hole quasi-Fermi level within their energy distribution. These states have relaxation times of several minutes, and have been assigned to be  $\text{Ti}^{3+}$  defect states in agreement with other investigators.<sup>50,58</sup> The total numbers of these fast and slow surface states are typically  $5 \times 10^{11} \text{ cm}^{-2}$ , and greater than  $10^{11} \text{ cm}^{-2}$ , respectively.

Under illumination, photogenerated holes first depopulate the fast cationic surface states and then slowly depopulate the  $\text{Ti}^{3+}$

states. This continues until a steady state condition is reached wherein the hole flux is matched by surface recombination. Upon termination of illumination, the fast cationic states accept charge from the conduction band first, leaving the depopulated, slow  $Ti^{3+}$  surface states temporarily unoccupied. These slow states gradually accept charge from the cationic states which in turn accept more charge from the conduction band. This surface state repopulation continues until the original equilibrium under darkened conditions is reached.

Charge transfer chemisorption of electronegative species occurs on  $TiO_2$  upon exposure to oxygen and water vapor. Physisorbed molecules are thermally activated to form electronegative species which chemisorb to the  $TiO_2$  surface, interacting with and modifying the properties of the surface states. The adsorption of these species reduce the number of empty (hole occupied) surface states thus reducing the recombination of surface holes and conduction band electrons. This in turn increases the density of electrons in the conduction band, increasing the bulk Fermi level, reducing the surface band bending and the  $TiO_2$  work function. Further ambient interactions beyond the observed initial work function decrease are attributed to surface dipole layer construction effecting the value of the surface electron affinity. Chemisorption adsorbate interactions on the  $TiO_2$  surfaces are irreversible.

Chemisorbed species produce modifications in the properties of the fast cationic surface states. The properties and populations of  $Ti^{3+}$  surface states are not appreciably effected by adsorbates. In the presence of thermally activated electronegative species, the transfer of electrons from occupied cationic states to unoccupied  $Ti^{3+}$  defect states allows the charge transfer chemisorption between electronegative species and cationic surface states. The cationic states with their



associated chemisorbed species now constitute a third class of surface states with photostimulated behavior differing from that of the previously mentioned surface states. The effect of increasing ambient exposures is to increase the number of adsorbate-effected states at the expense of the cationic states. Upon illumination in UHV, the adsorbate-effected states accept photogenerated holes from the valence band more slowly than the original cationic states, at a rate comparable to that of the  $Ti^{3+}$  defect states. Those cationic states at the surface which were not effected by previous chemisorbate interactions accept charge quickly, resulting in a fast initial decrease in the work function. The following gradual decrease in the work function is due to the simultaneous acceptance of charge by both the  $Ti^{3+}$  defect states and the adsorbate-effected states. Consequently the rate of work function decrease during this period is larger than that of the same period during control sequences. During this period, the depopulation of both  $Ti^{3+}$  states and the photodesorption of adsorbates occur simultaneously. The population of the adsorbate-effected states vary with previous ambient exposures between zero and  $5 \times 10^{11} \text{ cm}^{-2}$ . These states display relaxation times of  $\tau \sim 10^3$  sec.

The surfaces of samples reduced at low hydrogen pressures, after exposure to oxygen and water vapor ambients, displayed a photovoltage inversion upon illumination in vacuum. This photovoltage inversion was due to the flux of conduction band electrons, in addition to the flux of photogenerated holes to the surface.

#### [E.] Photostimulated Properties of $TiO_2$ Surfaces

Using the Gartner theory for the hole flux to the semiconductor surface and contact potential difference measurements, the surface

recombination velocities of the  $\text{TiO}_2$  surfaces with and without adsorbates could be determined under illumination. During interactions with cationic surface states, the SRV was too fast to be unambiguously determined. Surface recombination velocities of 1 to 4  $\text{cm}\cdot\text{sec}^{-1}$  were obtained during hole interactions with  $\text{Ti}^{3+}$  defect surface states and with adsorbate effected surface states.

Fluctuations in the surface state populations due to changes in experimental conditions were analyzed using simple Shockley-Read recombination theory and the forementioned surface recombination velocities. Cationic surface states displayed behavior similar to that of the conduction band, and hence had very large effective hole capture cross sections. Surface states associated with  $\text{Ti}^{3+}$  defects had hole capture cross sections evaluated to be  $10^{-18} \text{ cm}^2$ , while the hole capture cross sections for adsorbate-effected surface states were analyzed to be about  $5 \times 10^{-19} \text{ cm}^2$ . The influence of the chemisorbed adsorbates is to modify the surface recombination velocity and the hole capture cross section of the cationic surface states, substantially reducing these parameters by several orders of magnitude.

#### [F.] Recommendations for Future Work

Several recommendations for future work can be made on the basis of this investigation. The feasibility and merits of the study of real  $\text{TiO}_2$  surfaces applicable to photoelectrochemical cell devices have been demonstrated. Extension of the procedures utilized in this investigation to further  $\text{TiO}_2$  real surfaces is in order.

(1.) Surface structure sensitive spectroscopies should be employed to more fully investigate the origin of the surface states discovered in this research. Reproduction of the surfaces utilized in this study would be necessary.

(2.) In an effort to understand the mechanisms of long term stability in  $\text{TiO}_2$  photoanodes, it is recommended that the procedures utilized in this study be extended to  $\text{TiO}_2$  samples wherein the donor defects are due to substitutional, rather than interstitial, defects. Two possible donor defect types avail themselves: pentavalent cationic substitution, and monovalent anionic substitution.

(3.) An attempt should be made to reproducibly oxidize titanium metal foils to produce n-type semiconducting surface layers. Again, the composition of the titanium foil, and/or the oxidizing agent(s) should be modified to allow for substitutional, rather than interstitial n-type defects. These layers should subsequently be investigated by means similar to those used in this thesis investigation to analyze the properties and behavior of surfaces more realistic and applicable actual engineering situations.

## APPENDICES

### A: Selected Properties of TiO<sub>2</sub> (rutile)

Titanium dioxide crystallizes in three modifications: rutile, anatase and brookite. Of these, rutile is tetragonal and is the subject of this study. The crystal growth procedure and the dominant defect reactions effecting the electronic properties of the material are reviewed in Appendix B. A compilation of selected properties of TiO<sub>2</sub> (rutile) useful in this investigation is listed below. A more complete set of information regarding the properties of TiO<sub>2</sub> may be found in the review article by Grant<sup>107</sup> and the references therein.

<u>PROPERTY</u>	<u>VALUE</u>	<u>REFERENCE</u>
Crystal System	✓ tetragonal (see Fig. A-1)	108
Space Group	D <sub>4h</sub> <sup>14</sup>	109
Symmetry	P4/mnm	109
Unit cell parameters	a <sub>0</sub> = 4.492 Å c <sub>0</sub> = 2.830 Å	35
Density	4.26 gm/cm <sup>3</sup>	82
Melting Point	1825°C	110
Hardness	6.5-7.5 on Mohs Scale	107
Bonding	Largely ionic but with a considerable covalent contribution	107
Band Gap	3.02 eV (from the filled O 2p band to the empty Ti 3d band)	111
Refractive Index	see Fig. A-2	112
Resistivity	see Fig. A-3	35

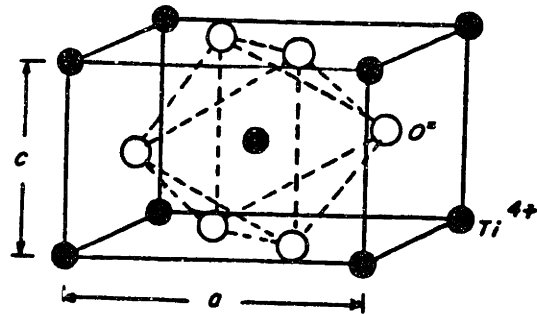


Fig. A-1

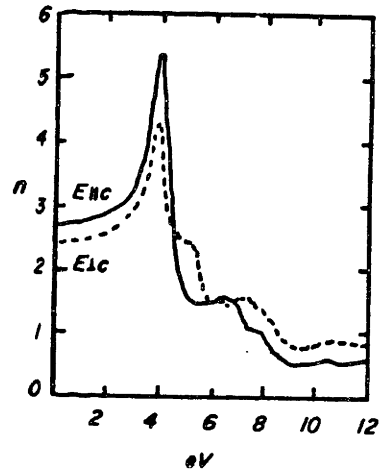


Fig. A-2

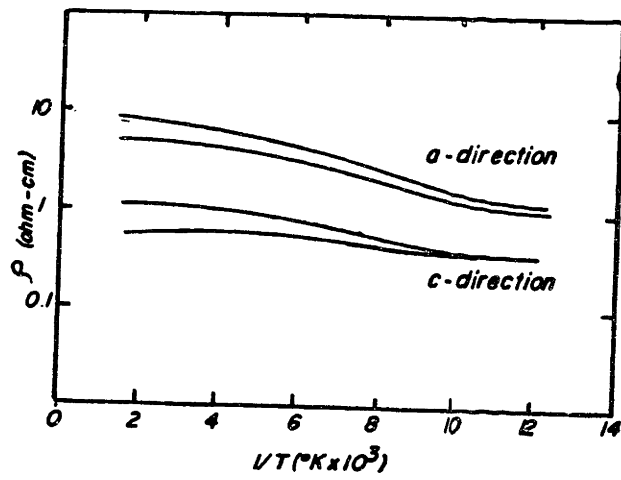
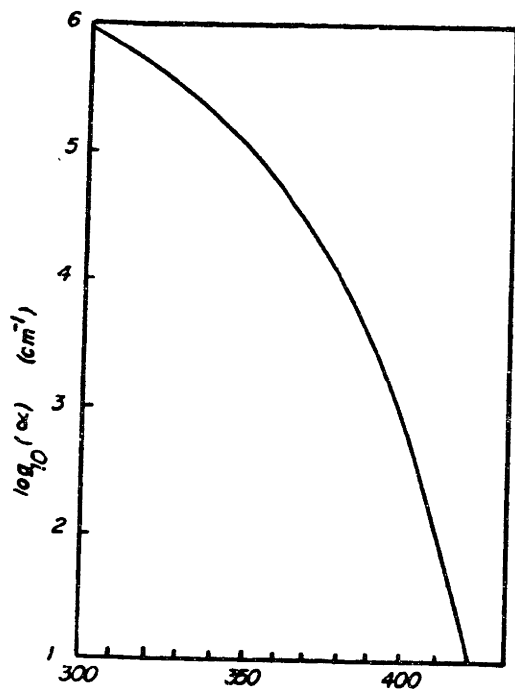


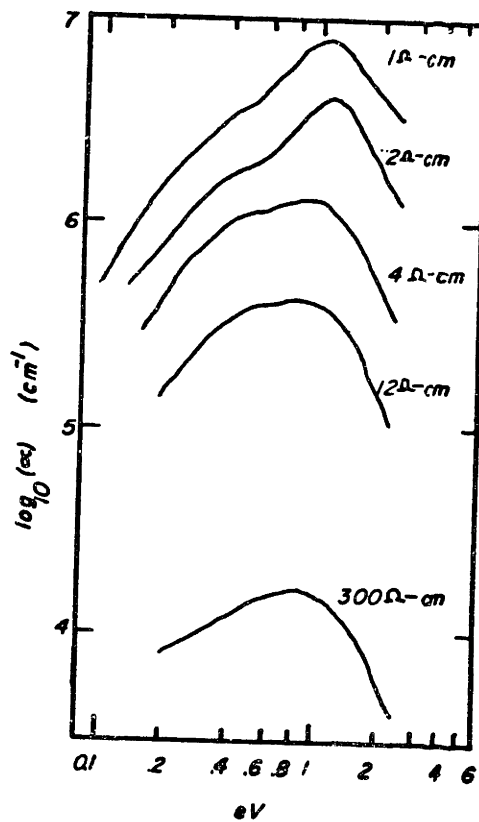
Fig. A-3

<u>PROPERTY</u>	<u>VALUE</u>	<u>REFERENCE</u>
Absorption Coefficient, :		
for unreduced crystals	see Fig. A-4	113
for reduced crystals	see Fig. A-5	114
Mobility	see Fig. A-6	115
Dielectric Constant (300°K, 100khz)		35
parallel to c-axis	173	
perpendicular to c-axis	89	
Effective Mass, $m_e^*$	12-100 $m_0$	95,116
Electron Affinity	4.33 eV (calculated)	15



Wavelength (nm)

Fig. A-4



eV

Fig. A-5

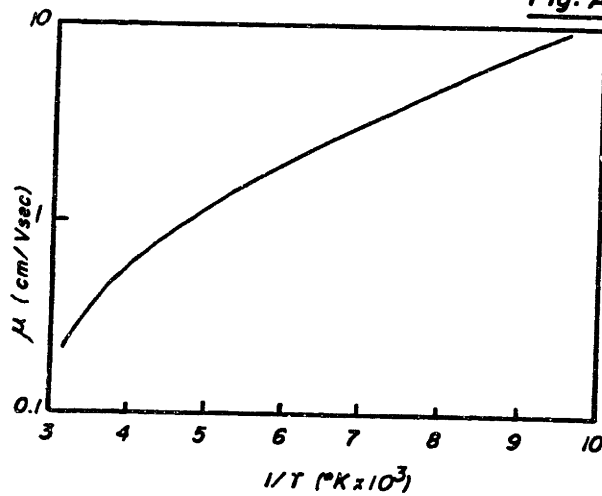


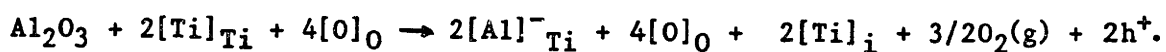
Fig. A-6

## B: Growth and Reduction of TiO<sub>2</sub> (rutile)

### Preparation of TiO<sub>2</sub> Crystals

Rutile single crystals are most commonly grown by the the Verneuil, or flame fusion, technique. Boules are commonly grown in the [001] direction. Growth by this method results in crystals deficient in titanium. Consequently, crystals are reduced in vacuum or inert gas after growth until the proper stoichiometry is reached. To stabilize the crystal stoichiometry, 0.01 wt. % Al<sub>2</sub>O<sub>3</sub> is typically added to the TiO<sub>2</sub> powder before flame fusion, although crystals can be grown without this addition. The effect of the alumina stabilizer is to introduce an acceptor impurity band. This effect can be most easily visualized by the following reaction wherein Al atoms substitutionally replace Ti atoms:

(B-1)



In this equation, we have used the convention that [ ]<sub>Ti</sub> has a quadruple positive charge and [ ]<sub>O</sub> has a double negative charge. This convention physically corresponds to the predominantly ionic crystal structure of rutile wherein Ti<sup>4+</sup> ions are located at the octahedral lattice sites, surrounded by six O<sup>=</sup> ions (see Fig. A-1). The aluminum acceptors act to compensate for the donor activity associated with vacant oxygen lattice sites. These vacant oxygen sites arise due to the loss of oxygen during the reduction following growth. The defect reaction associated with this donor mechanism can be written as:



Other than the intentional Al<sub>2</sub>O<sub>3</sub> stabilizer, impurities normally found in rutile crystals are Al, B, Co, Cr, Cu, Fe, Mn, Mg (typically less than 10 ppm), and Si (20-40 ppm). Defect impurities which exhibit



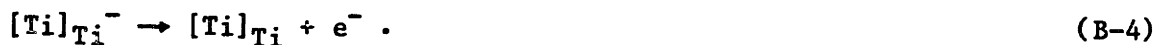
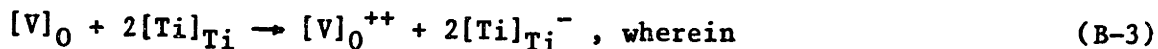
valencies of 3+, such as Al and Cr, are expected to act as acceptor sites. Introduced impurities having valencies of 5+, such as Ta and Nb, are expected to produce donor activity.<sup>117,118</sup> It is anticipated that silicon, which would be amphoteric in most III-V semiconductors, would preferentially occupy oxygen sites, due to size considerations. In this situation, silicon would act to contribute additional acceptor activity. It is also possible to effect the electronic behavior of the material by substitutionally replacing the oxygen anions: replacement of the oxygen atoms with fluorine results in n-type conductivity.<sup>41</sup> Impurity doping has not been utilized in this study, instead, doping of TiO<sub>2</sub> by means of reduction has been used.

#### Semiconducting TiO<sub>2</sub>

TiO<sub>2</sub> is usually made semiconducting by some form of reduction such as heating in vacuum or hydrogen. This produces n-type conduction in the crystal. The nature of the defects responsible for the n-type semiconduction has been the subject of several recent investigations.<sup>41,47,49,97,100-103,117-119</sup> Departures from stoichiometry occur when the oxide is reduced. Studies have shown that the range of existence of point defects extends from TiO<sub>2</sub> to about TiO<sub>1.992</sub>.<sup>117</sup> This change in composition would be produced by vacuum reductions at about 1000°C. Further reductions result in crystallographic shear transitions which generate a family of titanium suboxides known as Magneli phases. For the reductions used in this study (none above 600°C), the TiO<sub>2</sub> is nearly stoichiometric and the electronic behavior of the system can be formulated within the framework of a point defect model.<sup>97,117,119</sup>

Some concern has been raised as to the mechanism of n-type semiconduction in  $\text{TiO}_2$ , particularly in light of the possibility of electron carriers generating plasmons which in turn couple with the phonon modes of the crystal. Thermal and optical investigations have discounted this possibility however, and it can reasonably be assumed that the dominant conductivity mechanism is the activation of carriers between ordinary energy bands.<sup>100,119</sup>

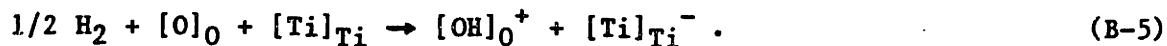
During vacuum reduction treatments, the crystal loses weight due to the loss of oxygen and possibly water. The oxygen vacancies so formed [reaction (B-2)] may ionize and leave some of their adjacent titanium neighbors in a 3+ state which, in turn, may act as donors:



We here have again used the convention that  $[\ ]_0$  is 2-, and  $[\ ]_{\text{Ti}}$  is 4+. Several workers have also observed the appearance of titanium interstitials upon vacuum reduction.<sup>41,49,100-102</sup> EPR studies have indicated that  $[\text{Ti}]_{\text{Ti}}^-$  ions are perturbed from their lattice sites and relocated at the  $(1/2,0,1/2)$  interstices of the rutile structure.<sup>102</sup> These defects contribute donor activity by ionizing according to a reaction similar to (B-4).

The reduction of rutile in hydrogen induces approximately the same amount of n-type conductivity at temperatures  $\sim 200^\circ\text{C}$  lower than those required in vacuum anneals.<sup>103</sup> These lower temperature anneals result in a higher degree of order in the crystal, hence longer hole lifetimes and fewer recombination centers. Infrared absorption peaks due to OH groups are dramatically increased by hydrogen reduction, suggesting the formation of OH bonds.<sup>35,41,102</sup> We may think of the n-type conductivity in hydrogen reduced  $\text{TiO}_2$  crystals as resulting from

the change of divalent  $O^{2-}$  lattice ions to monovalent  $OH^-$  ions which leave the adjacent titanium lattice ions to act as donors:



Again, the preceding convention has been used, and the  $[Ti]_{Ti}^-$  donors ionize according to (B-4).

The effects of the bulk defects in  $TiO_2$ , including oxygen vacancies, titanium donors (both lattice and interstitial) and impurity defects have been discussed in section 2.3.2. Complications in these effects which occur as a result of the use of  $TiO_2$  in photoelectrochemical cells have also been discussed in this section.

### C. Derivation of Equations

#### Equation (2-14)

The total current density through a reverse bias depletion layer is given by

$$J_{\text{tot}} = J_{\text{dl}} + J_{\text{diff}}$$

where  $J_{\text{dl}}$  is the current density due to carriers generated within the depletion layer, and  $J_{\text{diff}}$  is the current density of minority carriers generated outside the depletion layer in the bulk of the semiconductor and diffusing into the reverse bias junction. In the case of monochromatic radiation, absorption and pair generation characteristic is given by the equation

$$g(x) = I_0 \alpha \exp(-\alpha x)$$

where  $g(x)$  is the generation rate,  $I_0$  is the total incident photon flux and  $\alpha$  is the absorption coefficient. With this,  $J_{\text{dl}}$  is found to be

$$J_{\text{dl}} = q \int_0^W g(x) dx = q I_0 (e^{-\alpha W} - 1), \quad (i)$$

where  $W$  is the depletion layer thickness. Under conditions of reverse bias,  $W$  is given by (neglecting thermal effects) :

$$W = (2 \epsilon \epsilon_0 / q n_b)^{1/2} (V - V_{\text{fb}})^{1/2}.$$

For an n-type semiconductor, the hole density diffusion equation is given by

$$D_p \frac{d^2 p}{dx^2} - \frac{p - p_0}{\tau} = g(x)$$

where  $D_p$  is the diffusion coefficient of holes,  $p$  the hole density, and  $\tau$  is the excess carrier lifetime. The solution to this equation subject to the boundary conditions of  $p = p_0$  at  $x = \infty$ , and  $p = 0$  at  $x = W$  yields

$$p = p_0 - (p_0 + Ae^{-\alpha W}) e^{-(W-x)/L_p} + Ae^{-\alpha x},$$

where  $L_p = (D_p \tau)^{1/2}$  and  $A = \left(\frac{I_0}{D_p}\right) \frac{\alpha^2 L_p^2}{\alpha(1-\alpha^2 L_p^2)}$ . The diffusion

current density,  $J_{diff} = qD_p p$ , at  $x = W$  can thus be given as

$$J_{diff} = -q I_0 \frac{\alpha L_p \exp(-\alpha W)}{(1 + \alpha L_p)} - q p_0 \left(\frac{D_p}{L_p}\right) \quad (ii)$$

In large band gap semiconductors where  $p_0 \approx 0$ , the last term is negligible. Combining equations (i) and (ii) and assuming that  $W \gg 1$ , we have

$$J_{tot} = -q I_0 \left\{ 1 - \frac{\exp(-\alpha W)}{(1 + \alpha L_p)} \right\}. \quad (\text{Equation 2-14})$$

The limitations of this equation, aside from those mentioned in this derivation are that effects such as carrier recombination at the interface are ignored, and that the boundary conditions are not adequate near flat band conditions ( $V = V_{fb}$ ).<sup>68</sup>

#### Equation (2-15)

Using Fick's first law to find the surface concentration of holes due to illumination of an n-type semiconductor we have:

$$-D_p \left(\frac{\partial \Delta p}{\partial x}\right) \Big|_{x=0} = I - I_{sr}$$

where  $I$  is the incident band-gap light absorbed by the crystal and  $I_{sr}$  is the surface recombination rate. The result is

$$\Delta p \Big|_{x=0} = \frac{I - I_{sr}}{(D_p/L_p)}$$

or, by dividing this equation by the equilibrium hole concentration in

the bulk,

$$\frac{\Delta P_{\text{surf}}}{P_0} = \frac{L_p}{P_0 D_p} [I - I_{\text{sr}}] \quad (i)$$

Substitution of equation (i) into the quasi-Fermi level for holes [equation (2-1)] ,rearranging and dividing by q yields:<sup>73</sup>

$$V_{\text{ph}} = (kT/q) \ln \left\{ 1 - \left( \frac{L_p}{D_p P_0} \right) [I - I_{\text{sr}}] \right\} . \quad (\text{Equation 2-15})$$

### Equation (2-19)

Consider a homogeneous semiconductor under uniform and steady excitation. The presence of surface recombination in addition to bulk recombination requires a net flow of carriers to the surface. An explicit expression for the surface recombination in terms of surface potential and other pertinent parameters of the surface states involved can be obtained using the recombination theory of Shockley and Read. Many et.al.<sup>74</sup> utilize this theory to obtain an expression for the surface recombination velocity which is the ratio of the rate of minority carrier flow into a unit surface area to the excess minority carrier density in the bulk just below the surface. This expression is

$$(\text{SRV}) = \frac{(n_b + p_b) n_t \sqrt{K_n K_p}}{2n_i^* \left\{ \left( \frac{n_i}{n_s^*} \right) \cosh \left[ \left( \frac{E_t - E_i}{kT} \right) - U_0 \right] + \cosh \left[ \left( \frac{E_{f,s}^* - E_i}{kT} \right) - U_0 \right] \right\}} \quad (i)$$

For the application of this equation to non-degenerate TiO<sub>2</sub>, several simplifications can be made to make this expression less cumbersome. First, considering the large band gap of the material, and the typical doping levels of n-type material ( $n_b \sim 10^{17} \text{ cm}^{-3}$ ), one can assume that the bulk hole density, equal to that of the intrinsic hole density is negligible compared to the bulk electron density. Thus ( $n_b + p_b$ ) can be

approximated as being equal to  $n_b$ . The surface trap capture probabilities,  $K_n$  and  $K_p$ , can, in the absence of any better information be assumed equal. Consequently,  $(K_n K_p)^{1/2} = K_p$  which is related to the capture cross section and hole thermal velocity by  $K_p = A_p \langle c \rangle$ . The parameter  $U_0$  is defined as  $U_0 = \ln (K_p/K_n)$  and hence vanishes when the capture probabilities are equated. Further, when the argument of the cosh functions is greater than 5, as is the case for  $TiO_2$  doped n-type  $10^{17} \text{ cm}^{-3}$ , the function may be approximated without incurring any significant error by;

$$\cosh x \approx 1/2 \exp(x), \quad \text{for } x > 5.$$

With these assumptions, expression (i) above can be simplified to

$$(SRV) = \frac{n_b \langle c \rangle A_p n_e}{n_i \exp\left(\frac{E_t - E_i}{kT}\right) + n_i \exp\left(\frac{E_t^* - E_i}{kT}\right)} \quad (ii)$$

The photogenerated electron density,  $n_i^*$ , can be related to the intrinsic electron density,  $n_i$ , by the difference between the quasi-Fermi levels for hole and electrons:

$$n_i^* = n_i \exp [(E_n^* - E_p^*)/2kT] .$$

Under moderate illumination, the number of photogenerated electrons is much less than the bulk electron density at room temperature, hence the quasi-Fermi level for electrons at the surface is approximately equal to the standard Fermi level,  $E_{f,s}^*$ . Further, if an appreciable density of donor surface traps exist, the quasi-Fermi level for holes will be pinned at the energy level of these surface states.<sup>11</sup> As a consequence, the photogenerated electron density can be written:

$$n_i^* = n_i \exp [(E_{f,s}^* - E_t)/2kT] .$$

Substituting this equation into the denominator of expression (ii) above, one obtains:

$$(SRV) = \frac{n_b(c) A_p n_c}{n_i \left[ \exp\left(\frac{E_c - E_i}{kT}\right) + \exp\left(\frac{E_{fs}^* - E_c}{kT}\right) \exp\left(\frac{E_{fs}^* - E_i}{kT}\right) \right]} \quad (\text{Equation 2-19})$$

Equation (2-22)

Weber<sup>80</sup> has proposed that chemisorption may involve the overcoming of a thermal activation energy barrier. The particular chemisorption process (covalent bonding or ionic charge transfer) is dependant upon the thermal activation of the adsorbate. This model was verified by the charge transfer chemisorption of oxygen on ZnO by Lagowski, Sproles and Gatos.<sup>81</sup> Presently, the model of charge transfer chemisorption of oxygen on TiO<sub>2</sub> will be developed from first principles and compared with the empirical model of Lagowski et.al. Extension of this model to the treatment of water vapor chemisorption on TiO<sub>2</sub> is obvious.

The chemisorption reaction is assumed to be of the form



where physisorbed surface molecular oxygen exchanges charge with the semiconductor, becoming chemisorbed. The rate at which this reaction proceeds is determined from chemical kinetics to be

$$\frac{d[O^-(s)]}{dt} = k_1 [e^-] [O_2(s)]^{\beta/2} - k_2 [O^-(s)]$$

However, experiments show that equilibrium established in a pressure of oxygen which is subsequently evacuated results in no desorption of the chemisorbed species. Consequently, the reverse reaction rate,  $k_2$ , may be ignored.

The term  $[O_2(s)]^{\beta/2}$  represents the amount of oxygen physisorbed to the surface. Typically,  $[O_2(s)]^{\beta/2} = c p n^{\beta/2}$  so that the charge transfer rate, equal to the rate  $O^-$  chemisorption, can be written



$$\frac{dn_t}{dt} = k_1 n_s c P_{O_2}^{n\beta/2}$$

wherein  $n_s$  is equal to  $[e^-]$ . The forward reaction rate is taken from chemical kinetics to be of the form

$$k_1 = \langle c \rangle A_n n_{emp} \exp(-q\phi/kT)$$

where  $n_{emp}$  is the density of empty surface states which interact with the chemisorbing species, *i.e.*  $n_{emp} = (n_{tot} - n_{occ})$ ,  $\langle c \rangle$  is the thermal velocity of electrons,  $A_n$  is the capture cross section of the activated surface states for electrons, and  $(-q\phi/kT)$  is the dimensionless thermal activation energy. With this expression, and the substitution that  $n_s = n_b \exp(-qV_g/kT)$ , the charge transfer rate can be written as

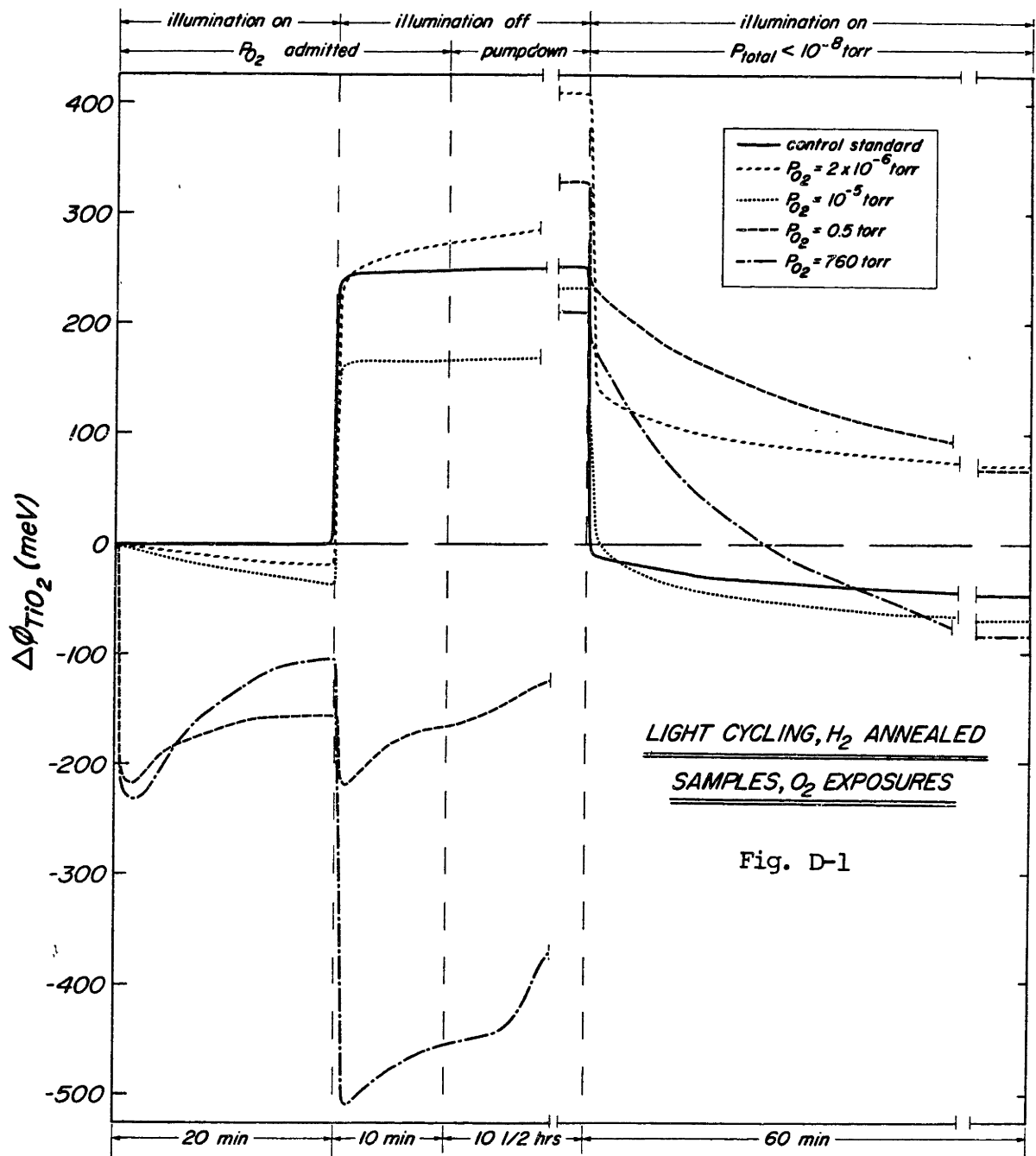
$$\frac{dn_t}{dt} = c P_{O_2}^{n\beta/2} \langle c \rangle A_n (n_{tot} - n_{occ}) \exp(-q\phi/kT) n_b \exp(-qV_g/kT)$$

(Equation 2-22)

This equation developed by Lagowski *et.al.* for the chemisorption of oxygen on ZnO, utilized values of  $n\beta = 1.8$  and  $(-q\phi/kT) = 0.72$  eV, such that the values of  $n_{emp}$  and  $A_n$  are  $10^{15}$  cm<sup>-2</sup> and  $10^{-16}$  cm<sup>2</sup>, respectively, are obtained. This equation is developed from chemical kinetics and is different from charge trapping via Shockley-Read recombination theory<sup>74</sup>, which yields unrealistically small capture cross sections, in that a thermal activation energy appears.

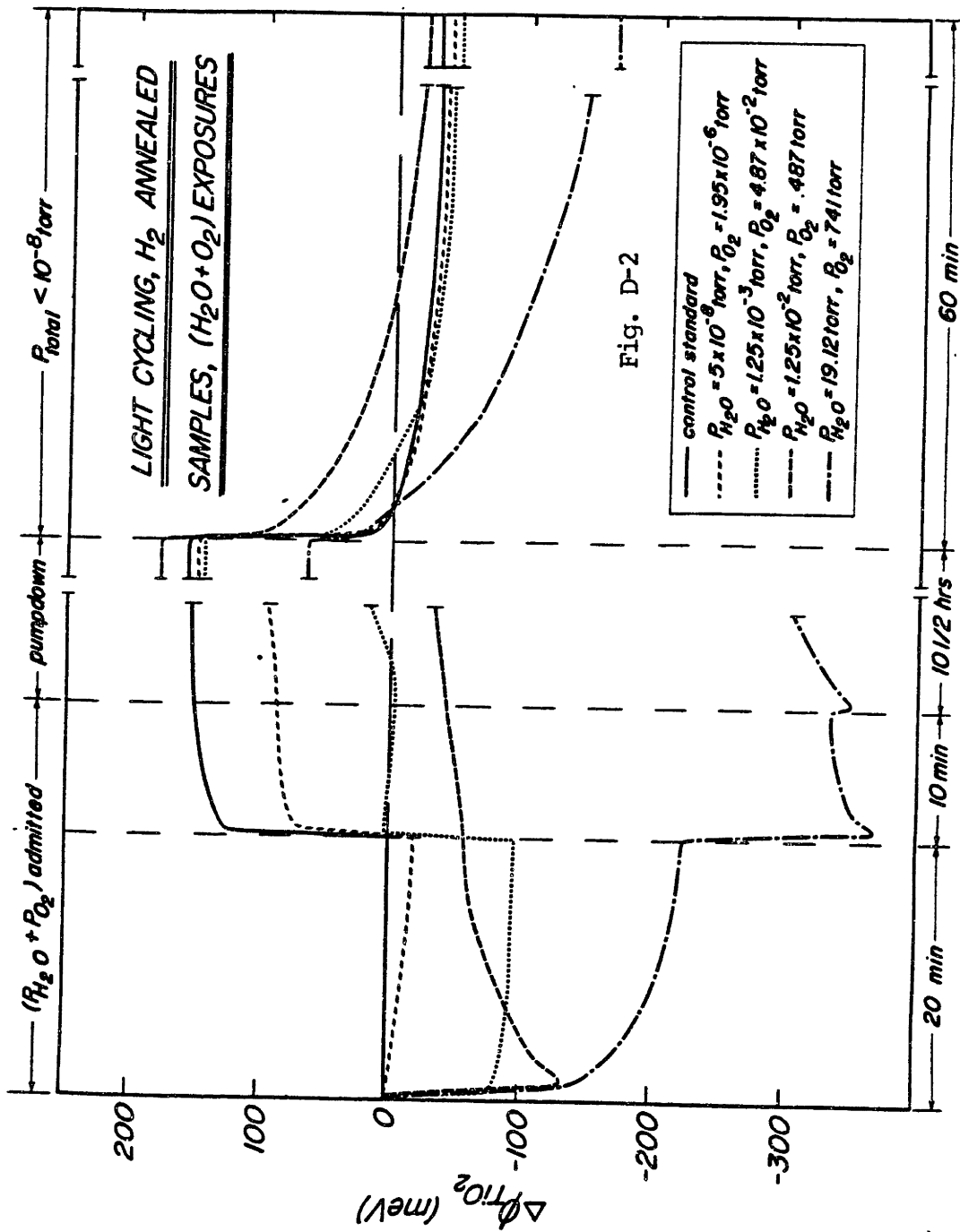
#### D. CPD Ambient Cycling Data

In this appendix, data derived from light and dark ambient cycling, as depicted in Figures 4.11 and 4.12, are presented. The volume of data precludes the possibility of presenting this information in the body of this work. Data concerned with the "hydrogen annealed" samples, reduced at 400°C in 1 atm of H<sub>2</sub> for 48 hours, is presented first. Data from the "vacuum annealed" samples, reduced at 400°C in 10<sup>-7</sup> atm H<sub>2</sub> for 48 hours, is then presented. The bulk donor densities associated with these samples are 4 x 10<sup>17</sup> cm<sup>-3</sup> and 2 x 10<sup>17</sup> cm<sup>-3</sup>, respectively. Ambient cycling was done under three different sets of ambients: O<sub>2</sub>, H<sub>2</sub>O and (O<sub>2</sub> + H<sub>2</sub>O). The ambient pressures used in the cycling procedures and the resulting exposures are listed in Table 5.1. The data presented in figures D-1 through D-24 do not represent all of the data from experimentation. For the sake of clarity, those data which do not exhibit some change in the cycling transients do not appear. The phenomenological work function differences reflect the measured CPD variations through the relationship  $\Delta \phi_{TiO_2} = -\Delta CPD$  according to the discussion in section 4.3.4. The changes in  $\phi_{TiO_2}$  with ambient cycling are presented here. Also presented are changes in the surface charge,  $\Delta n_s$ , with ambient cycling. These data are generated through the use of equation (4-6), knowing the changes in the nulling voltage.



LIGHT CYCLING, H<sub>2</sub> ANNEALED  
SAMPLES, O<sub>2</sub> EXPOSURES

Fig. D-1



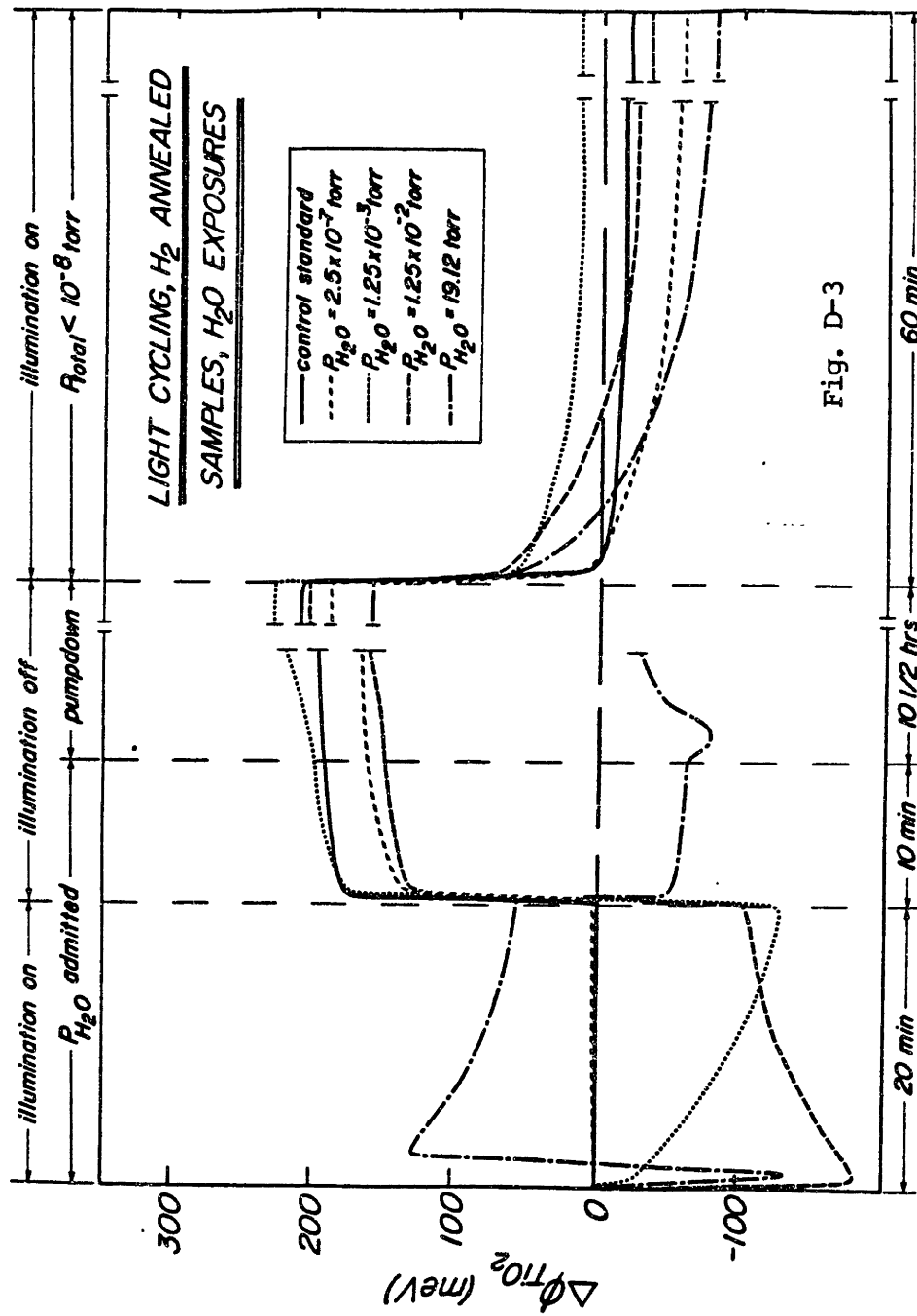


Fig. D-3

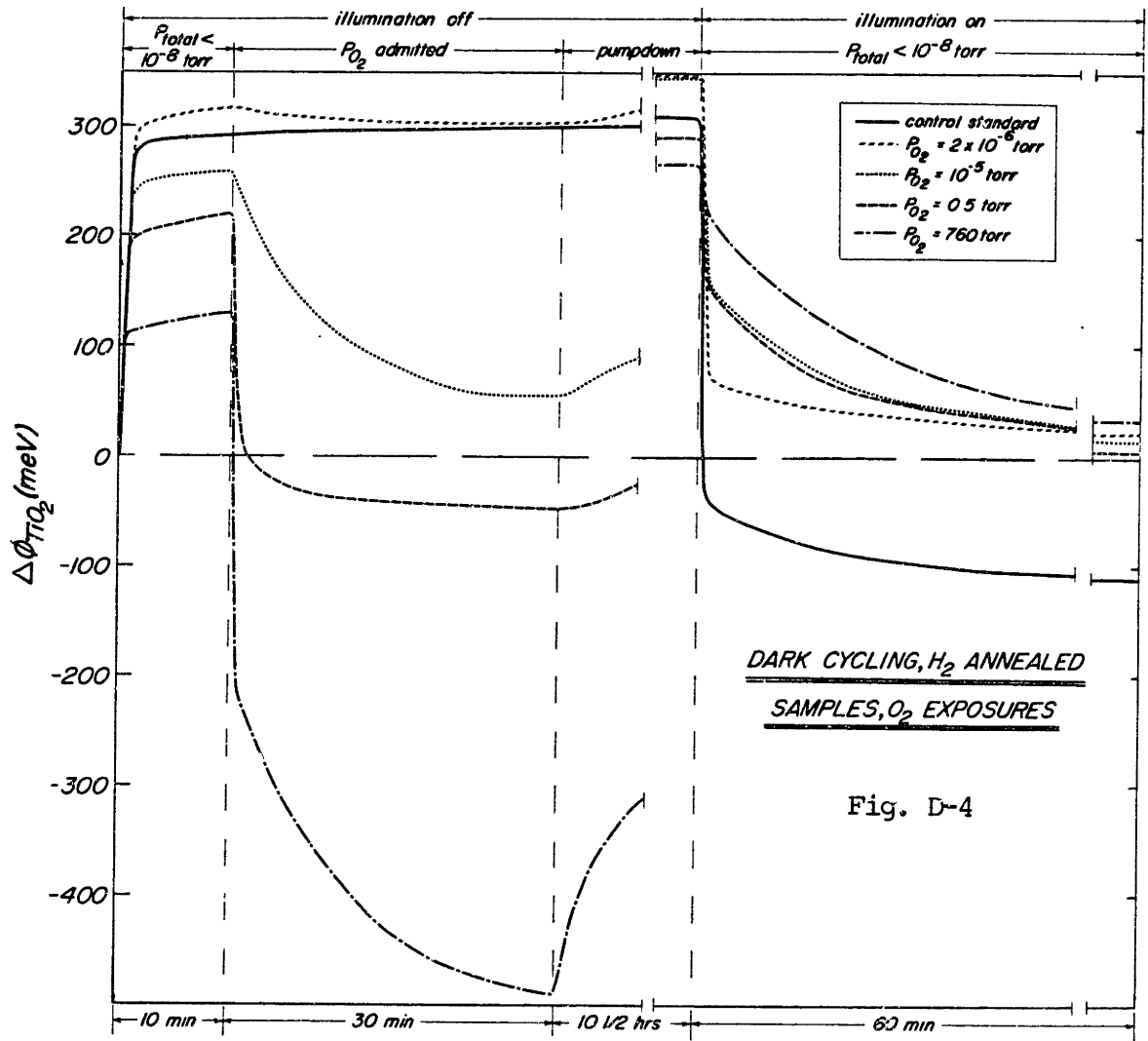


Fig. D-4

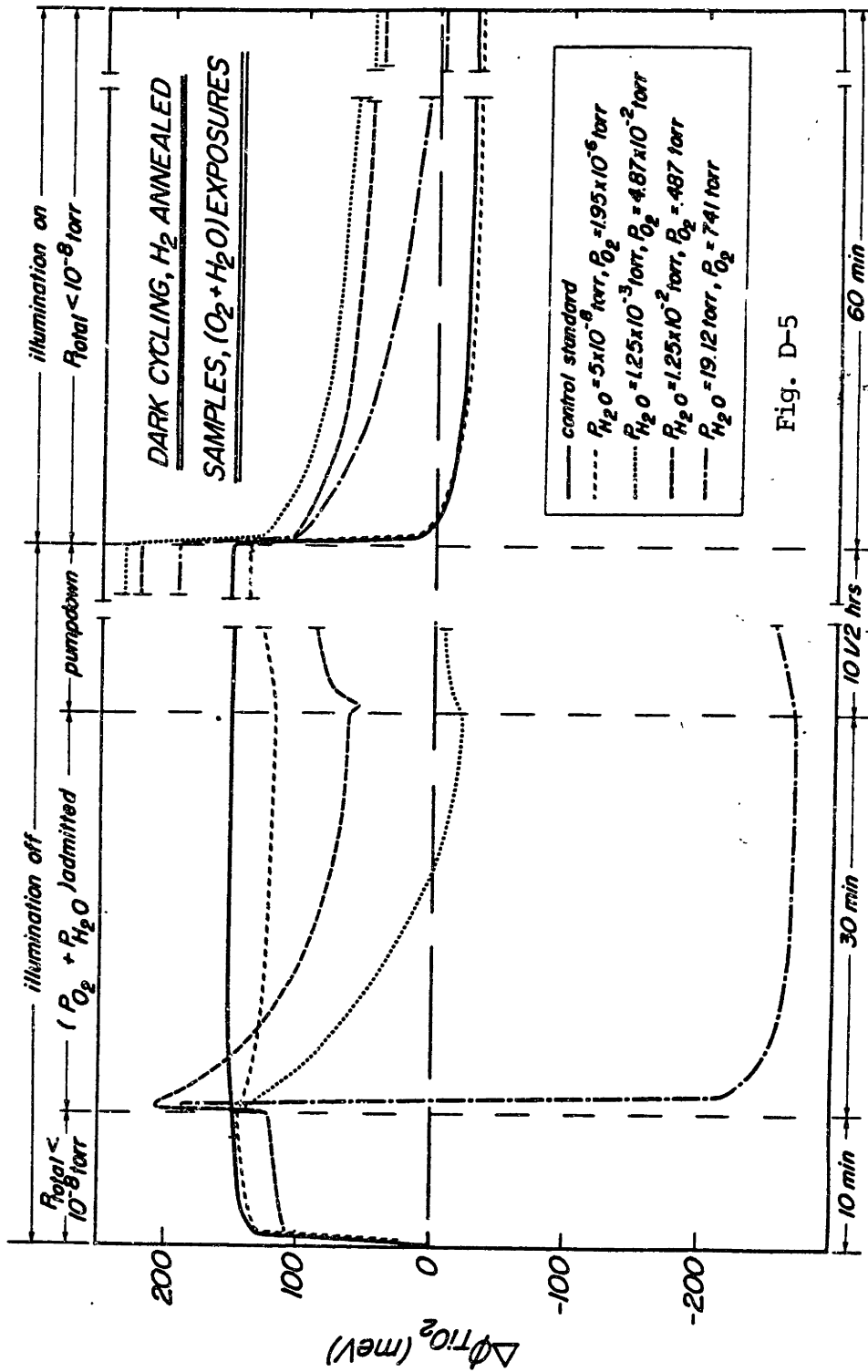
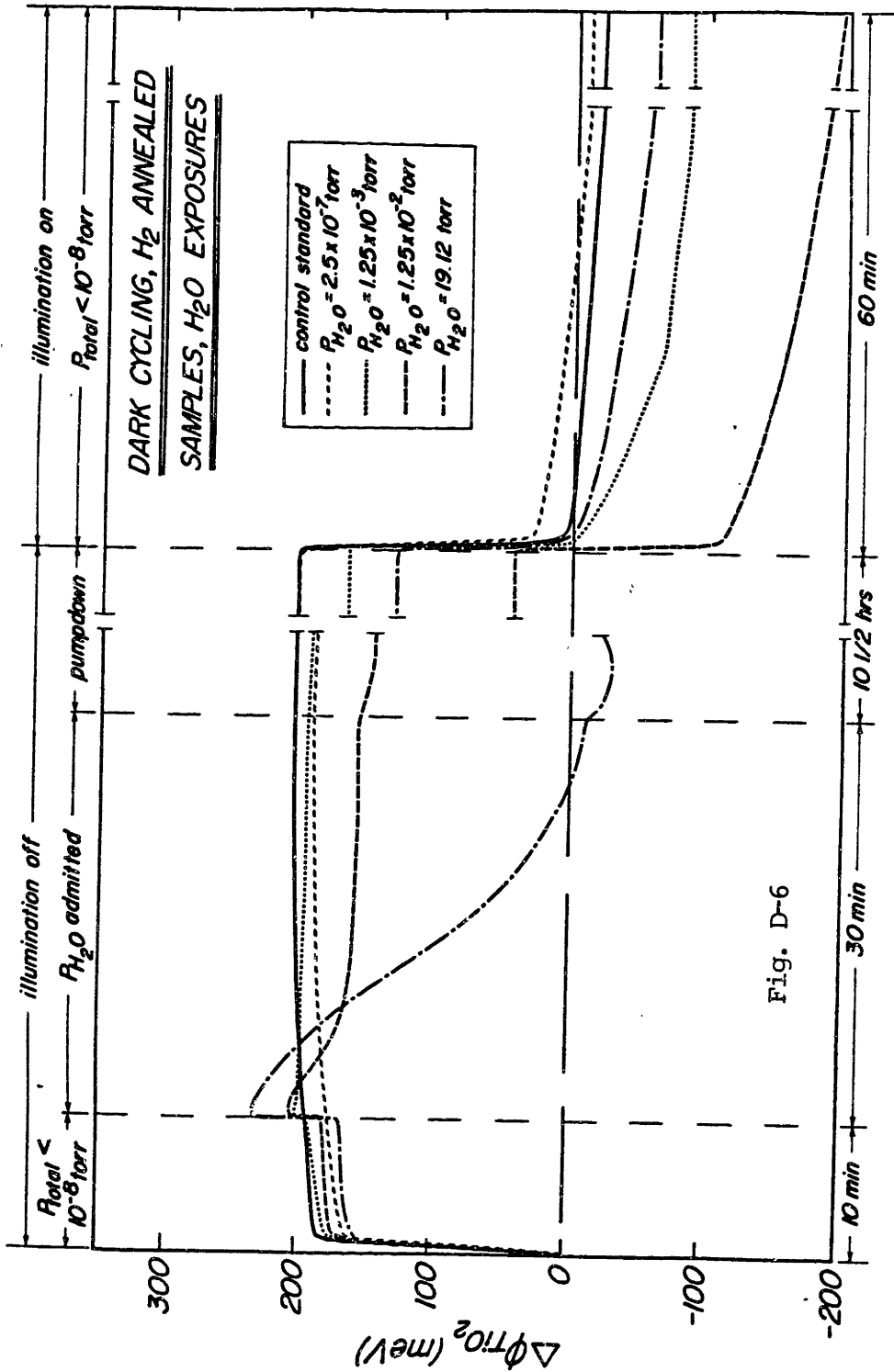


Fig. D-5





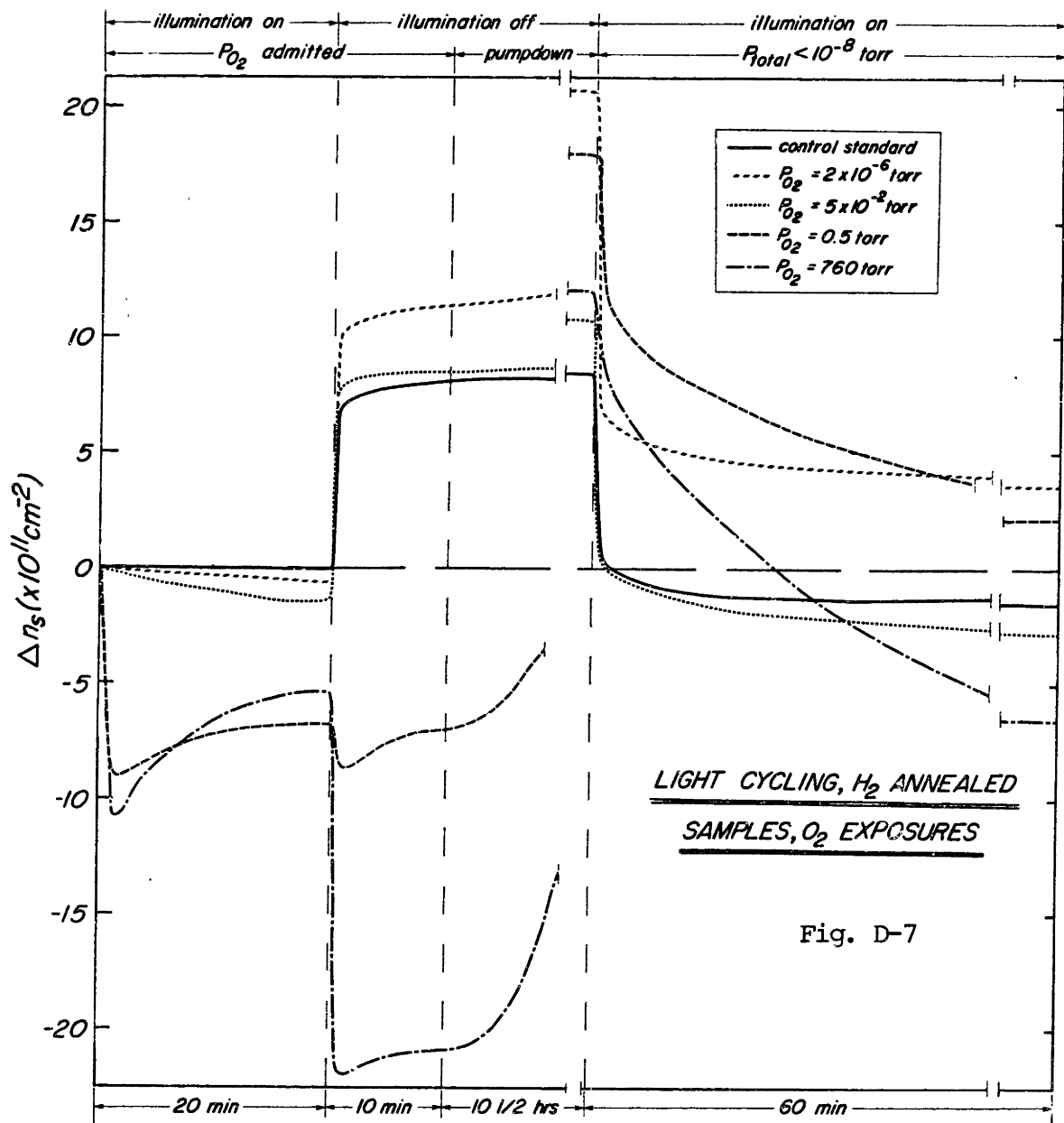
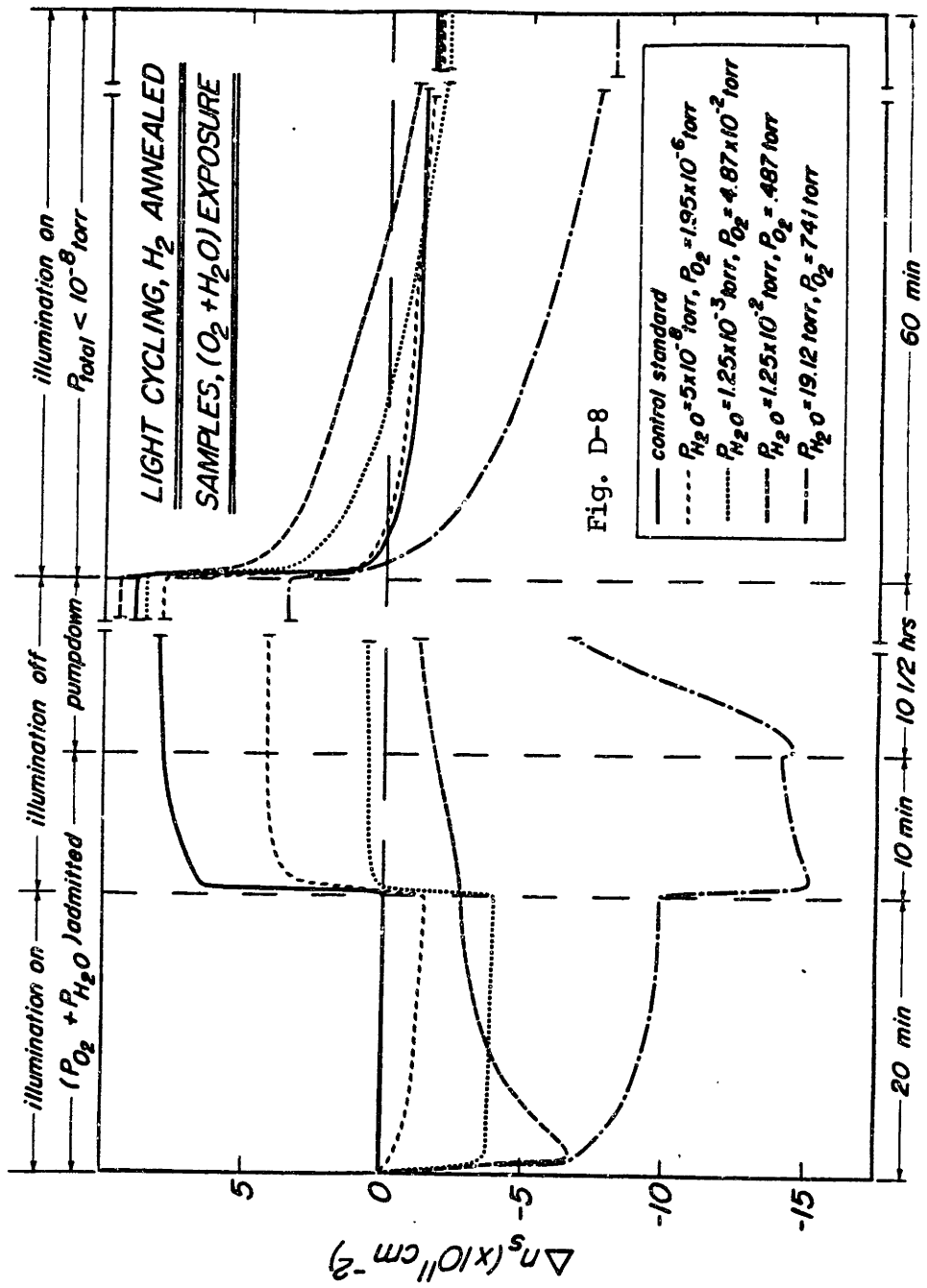
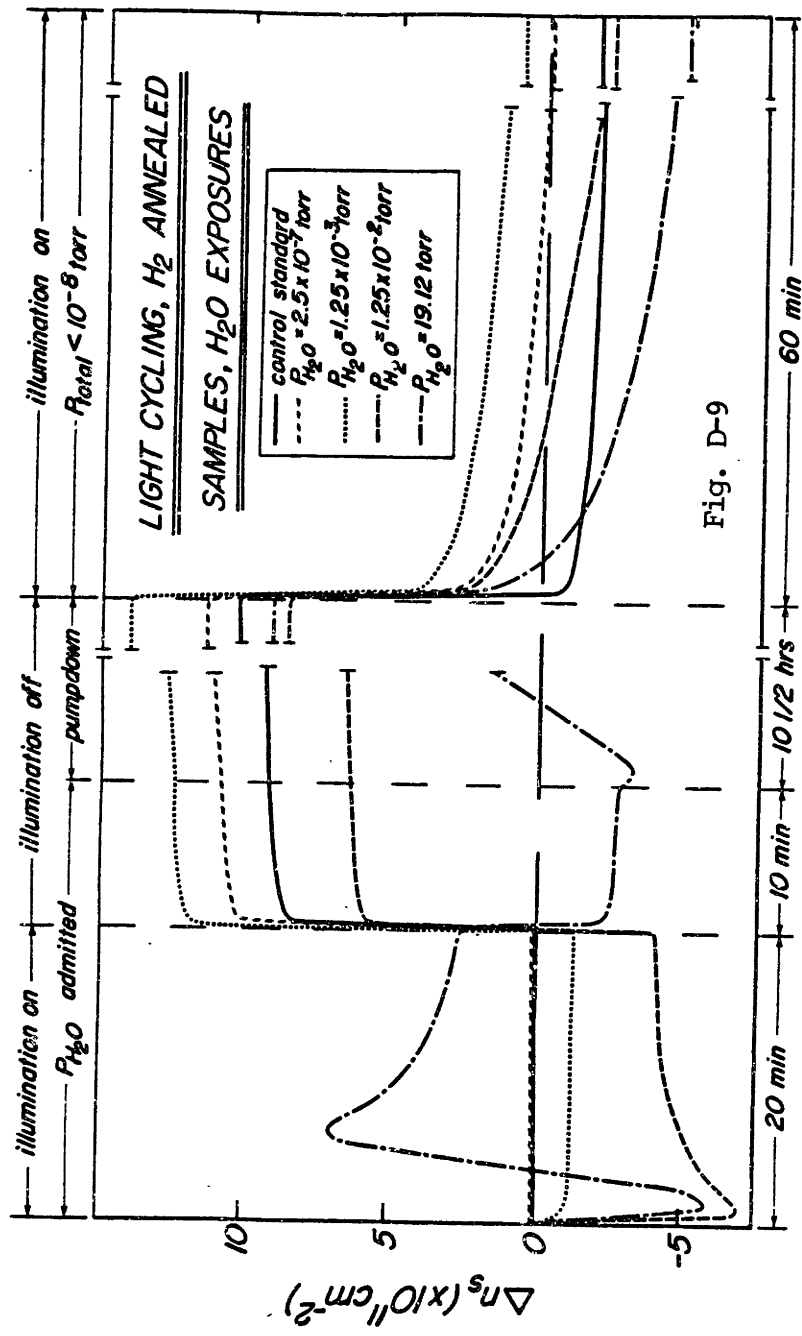


Fig. D-7





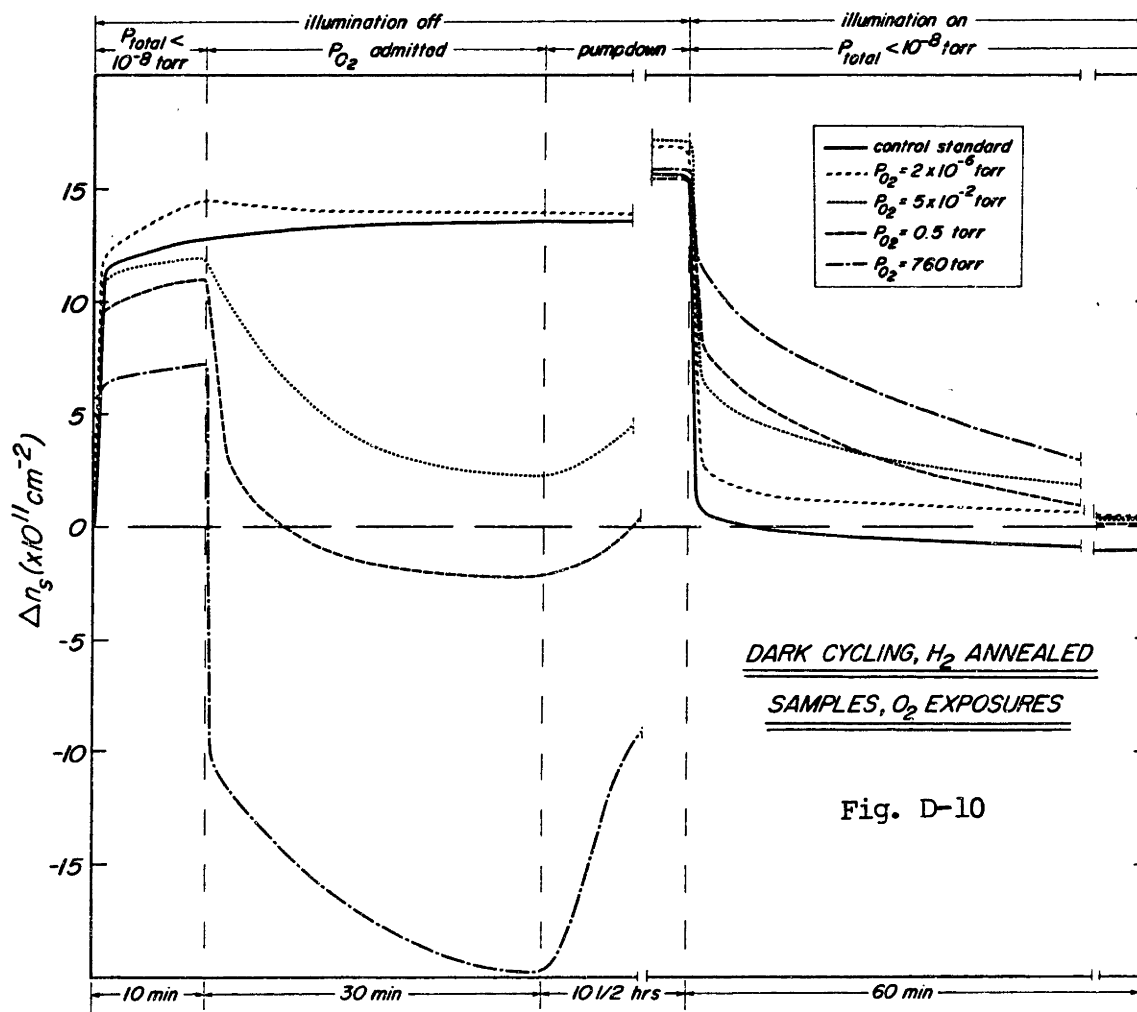
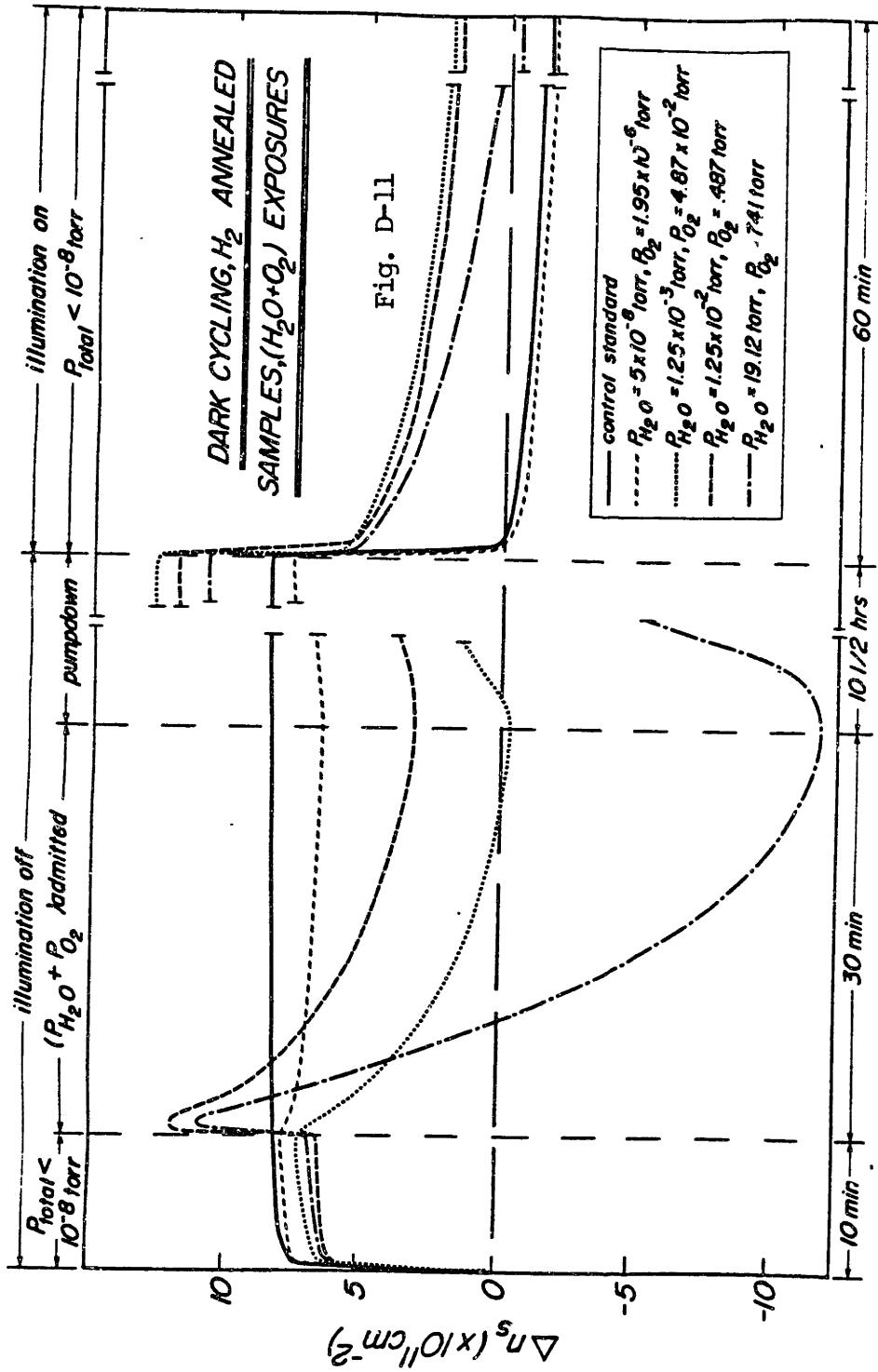


Fig. D-10



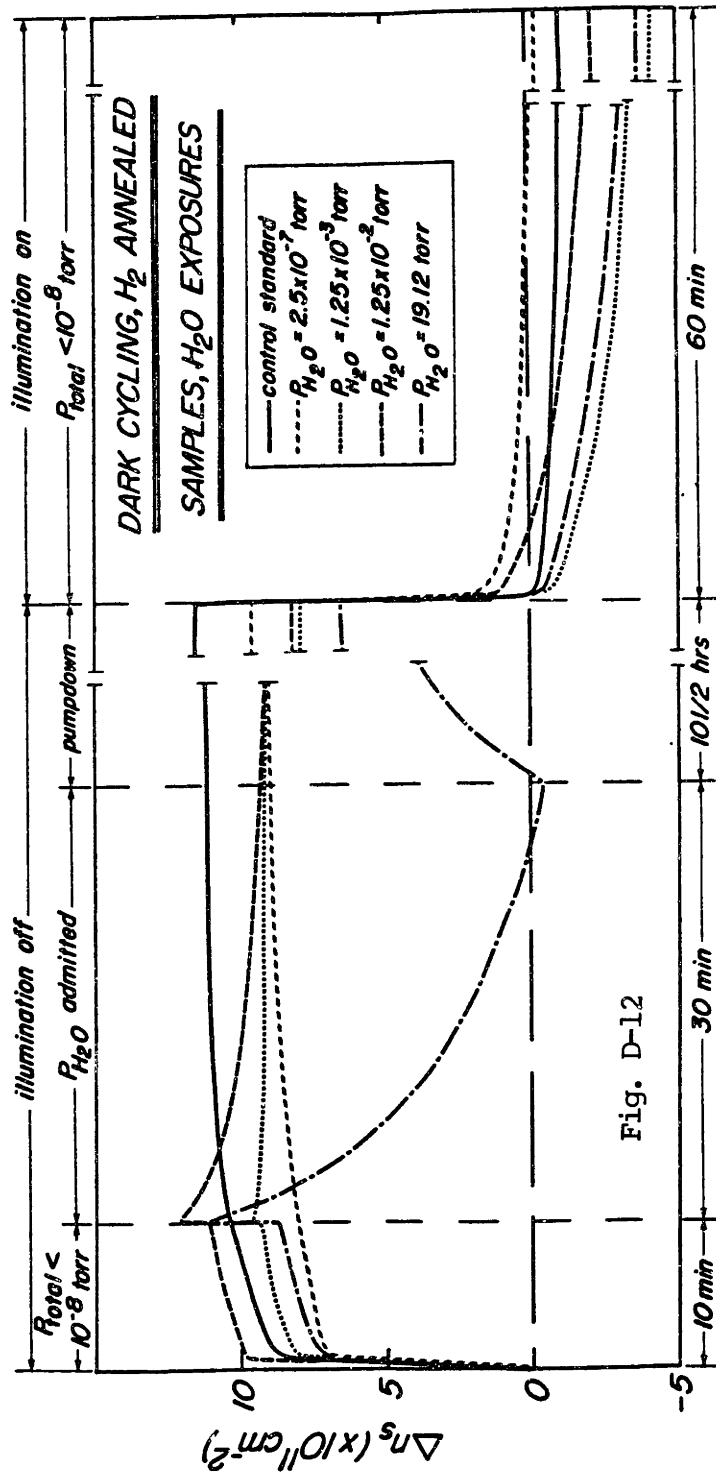
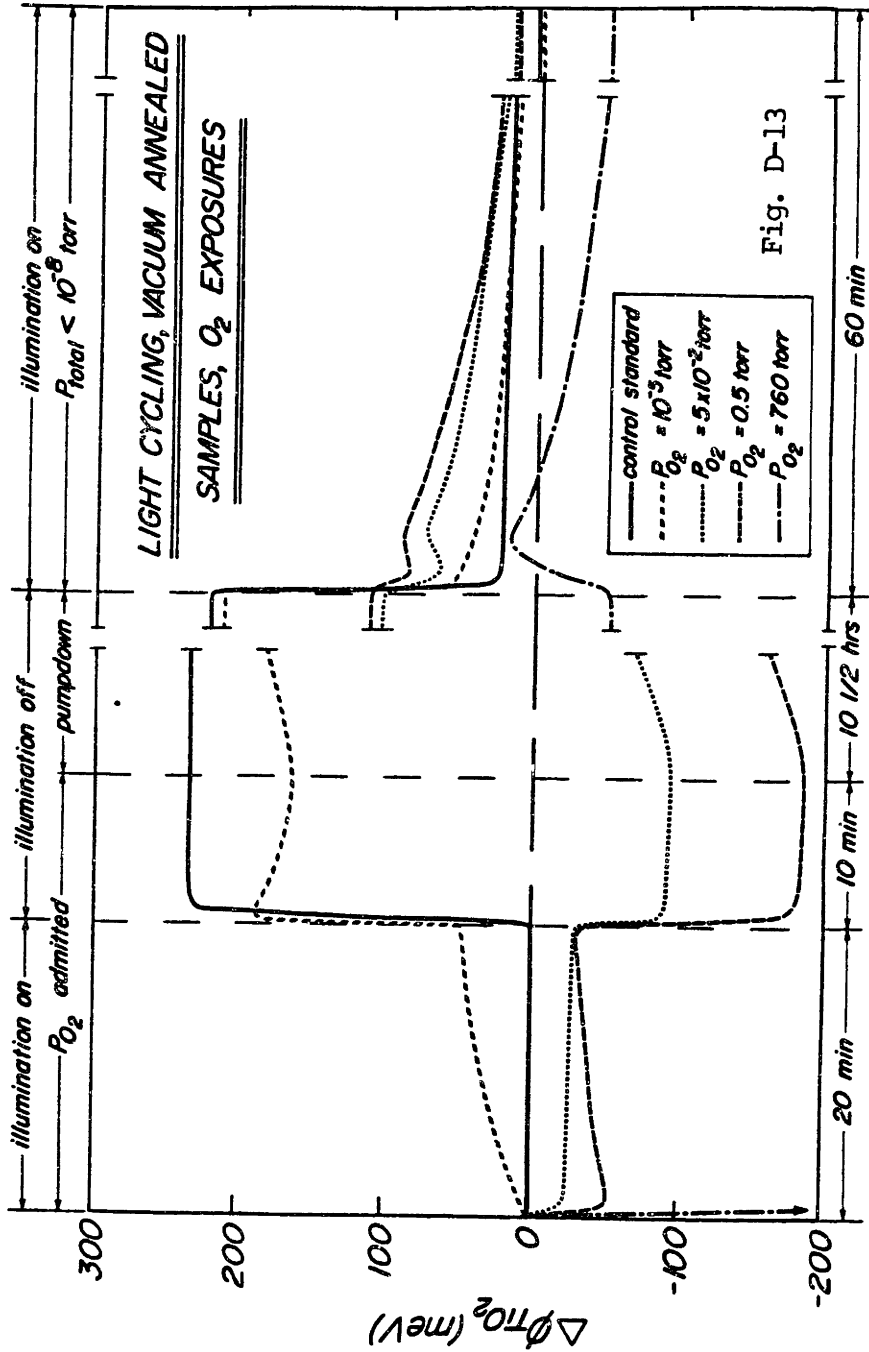
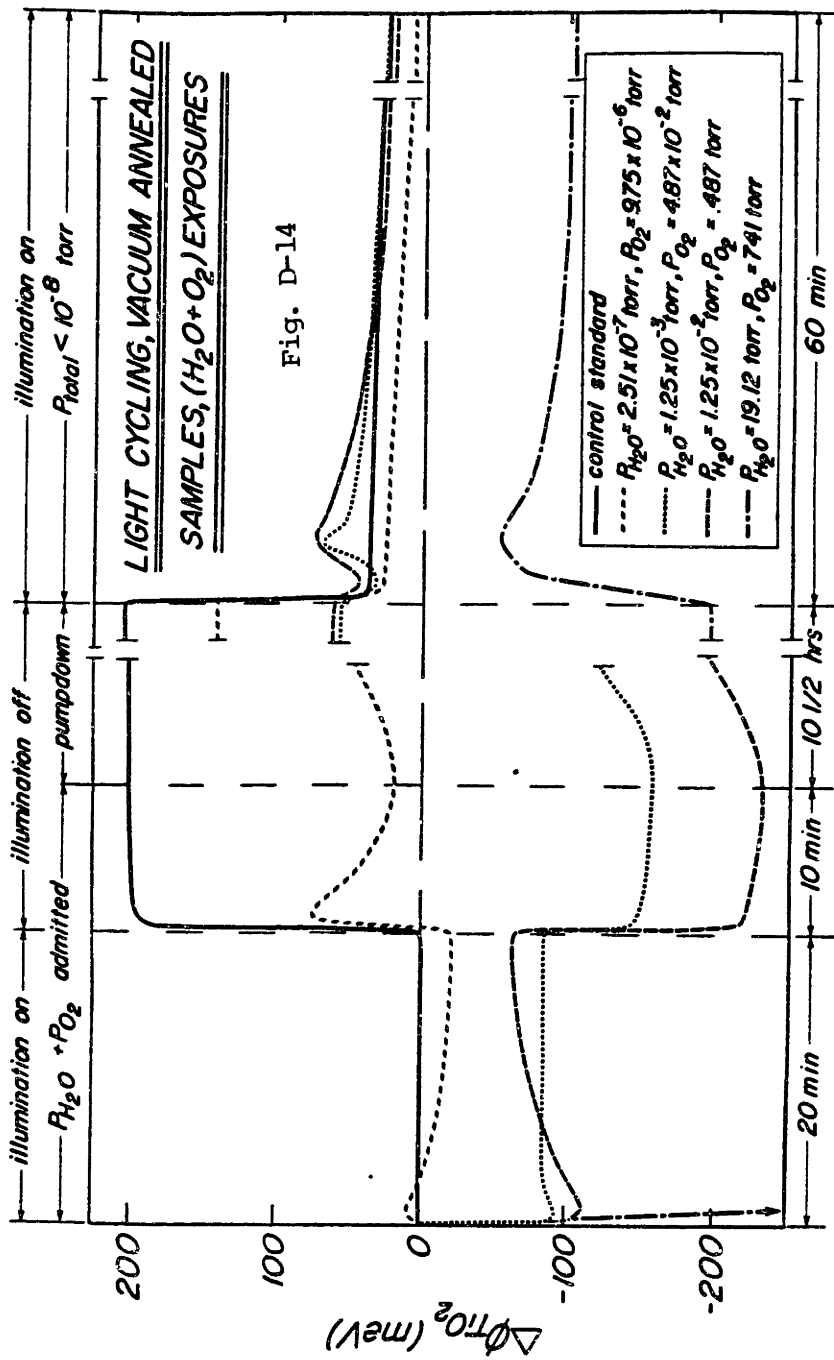
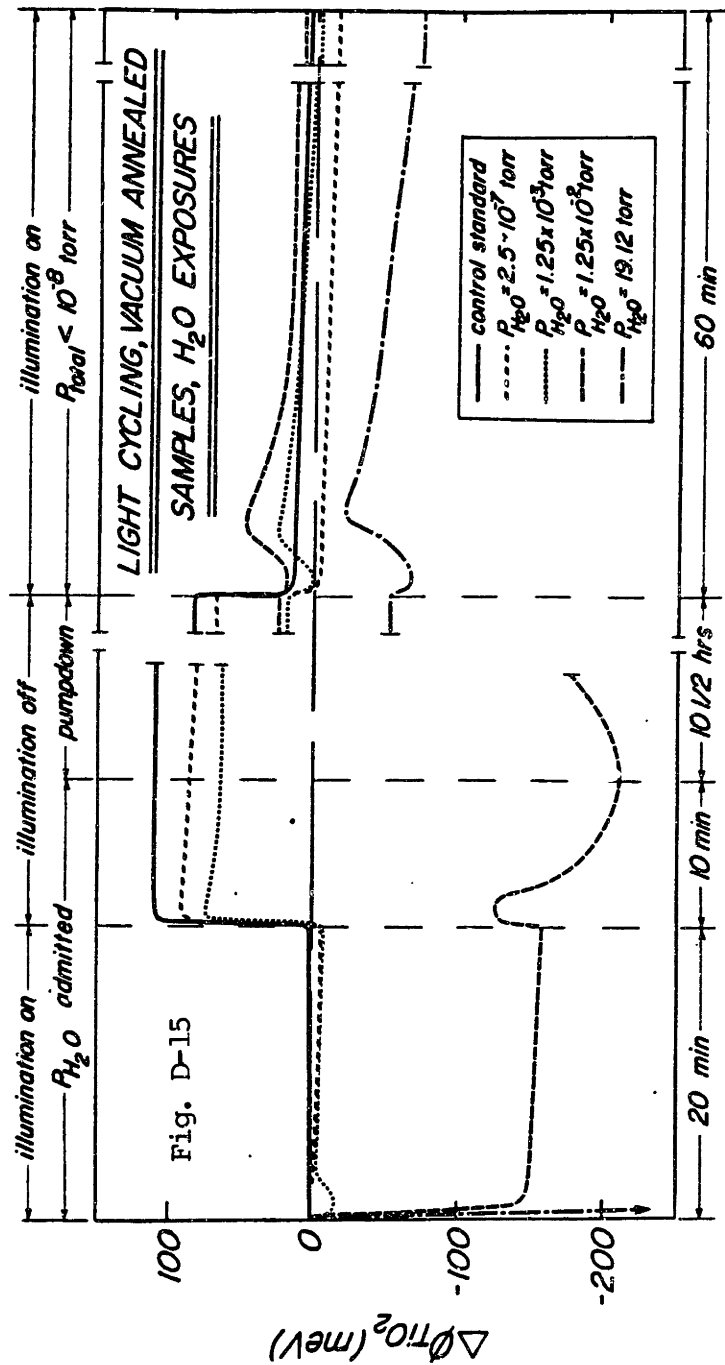


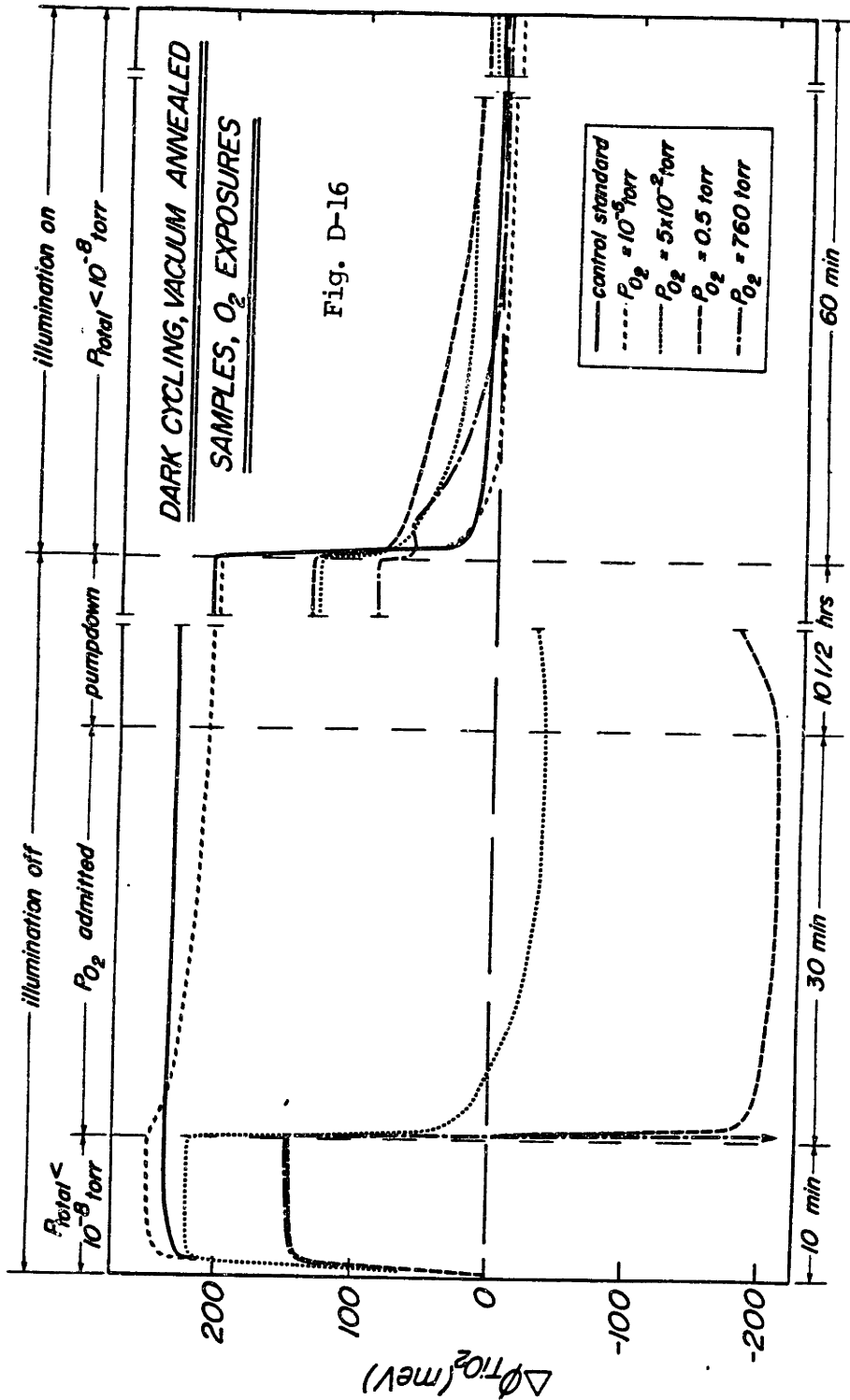
Fig. D-12

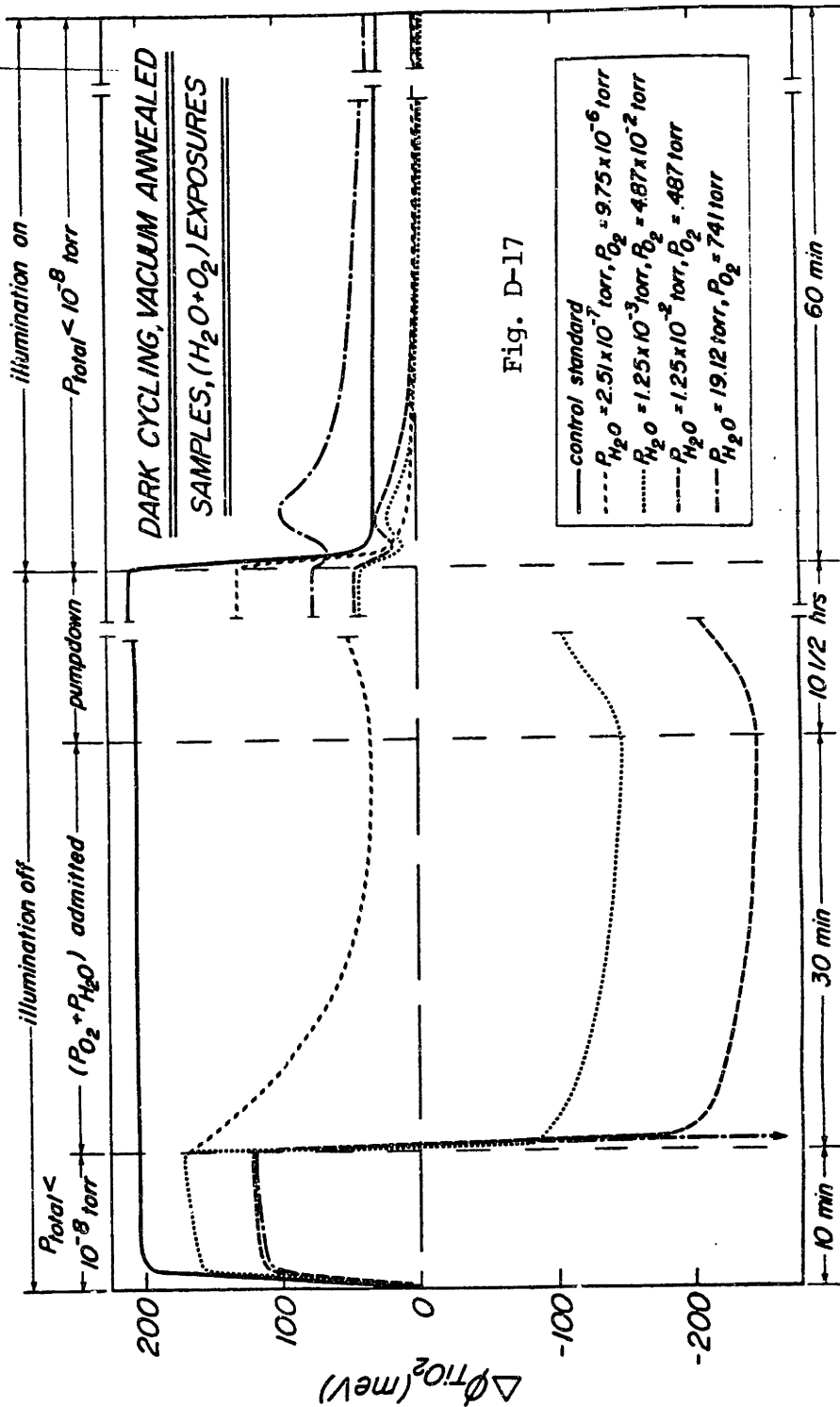












DARK CYCLING, VACUUM ANNEALED SAMPLES, H<sub>2</sub>O EXPOSURES

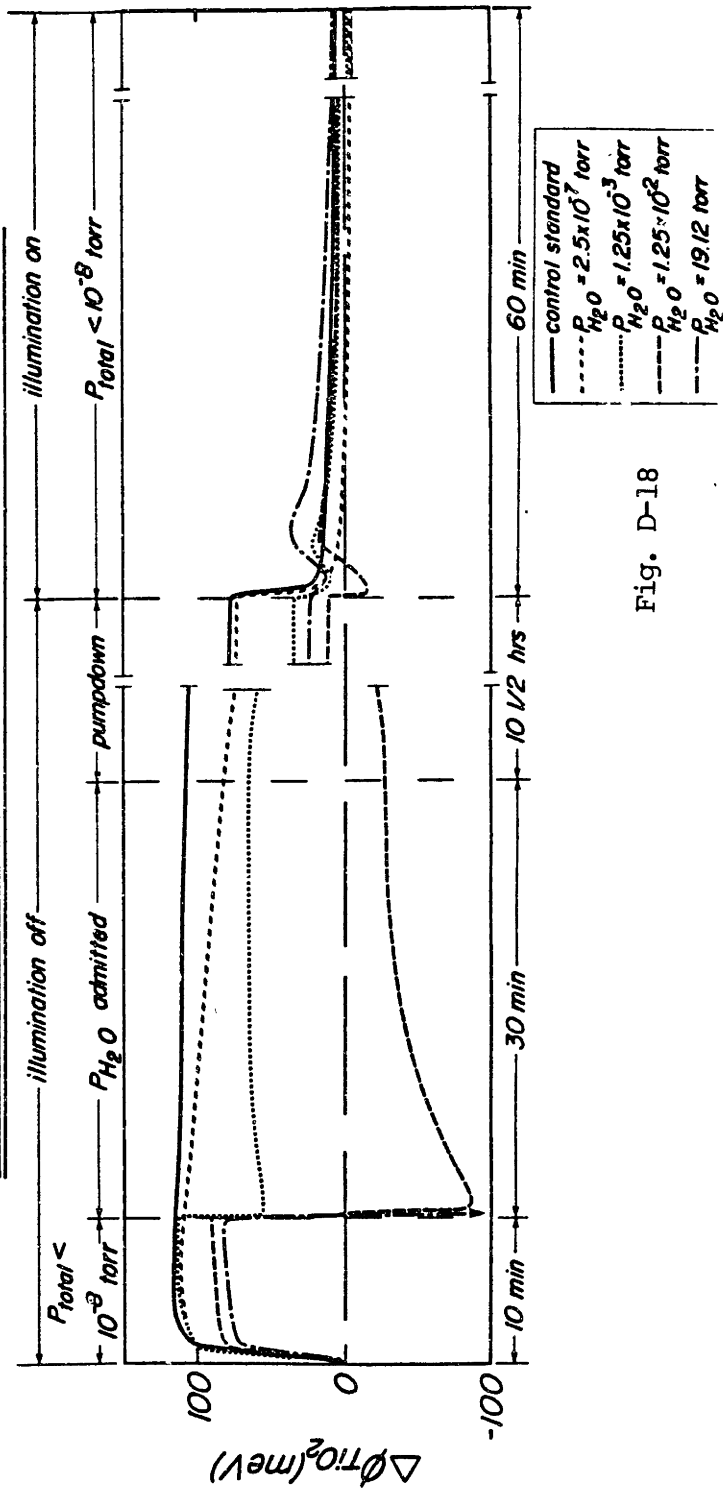


Fig. D-18

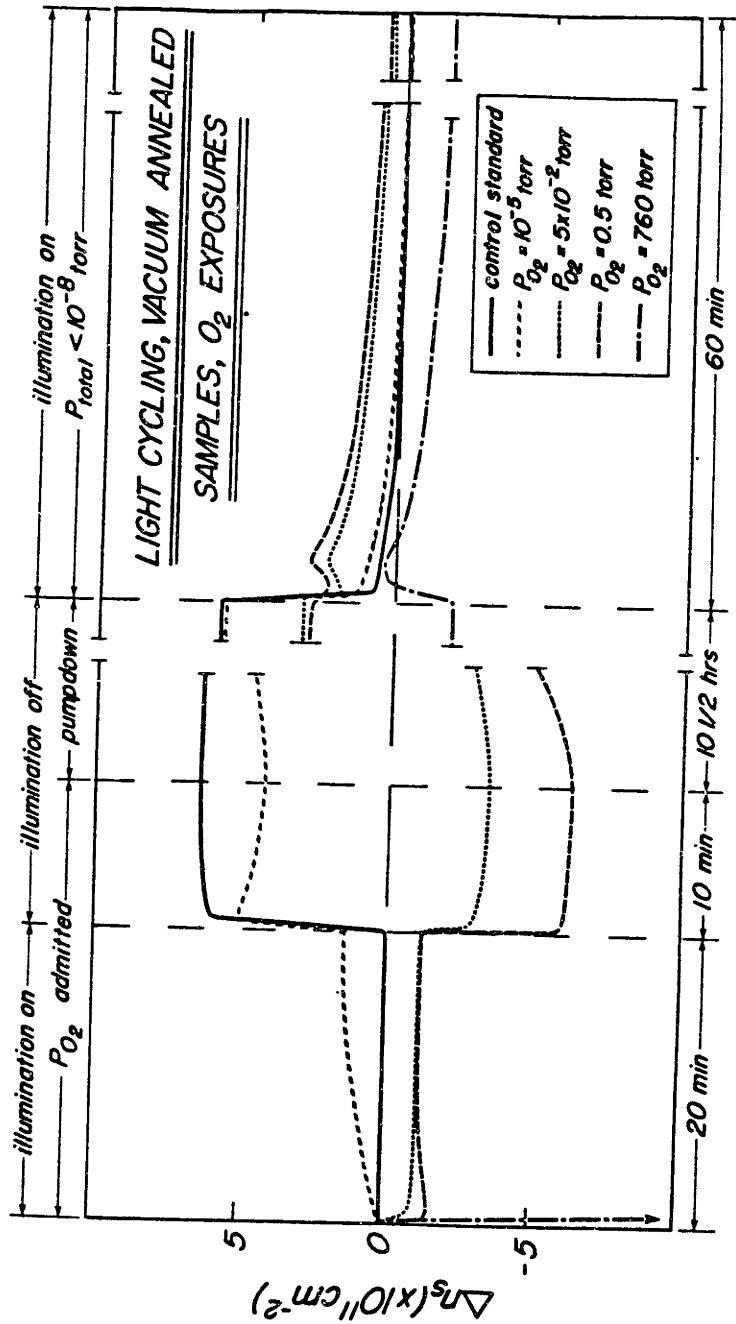


Fig. D-19

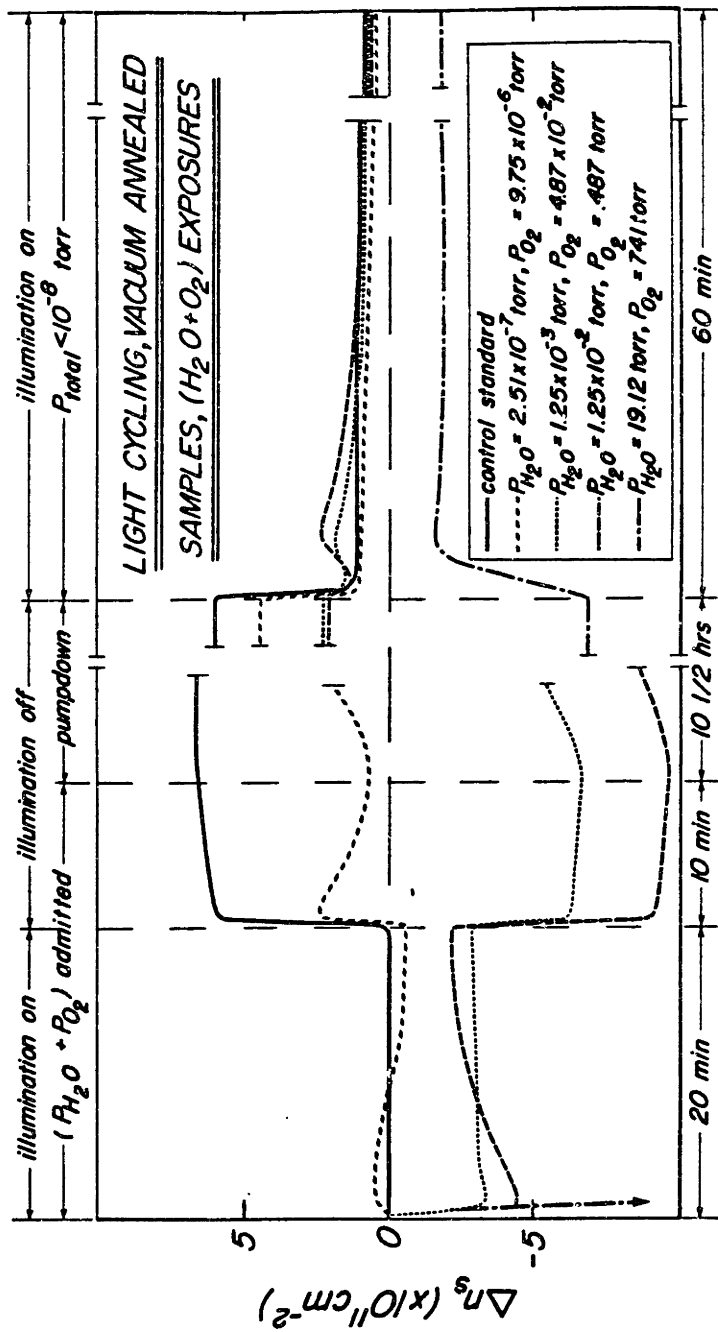


Fig. D-20

**LIGHT CYCLING, VACUUM ANNEALED SAMPLES, H<sub>2</sub>O EXPOSURES**

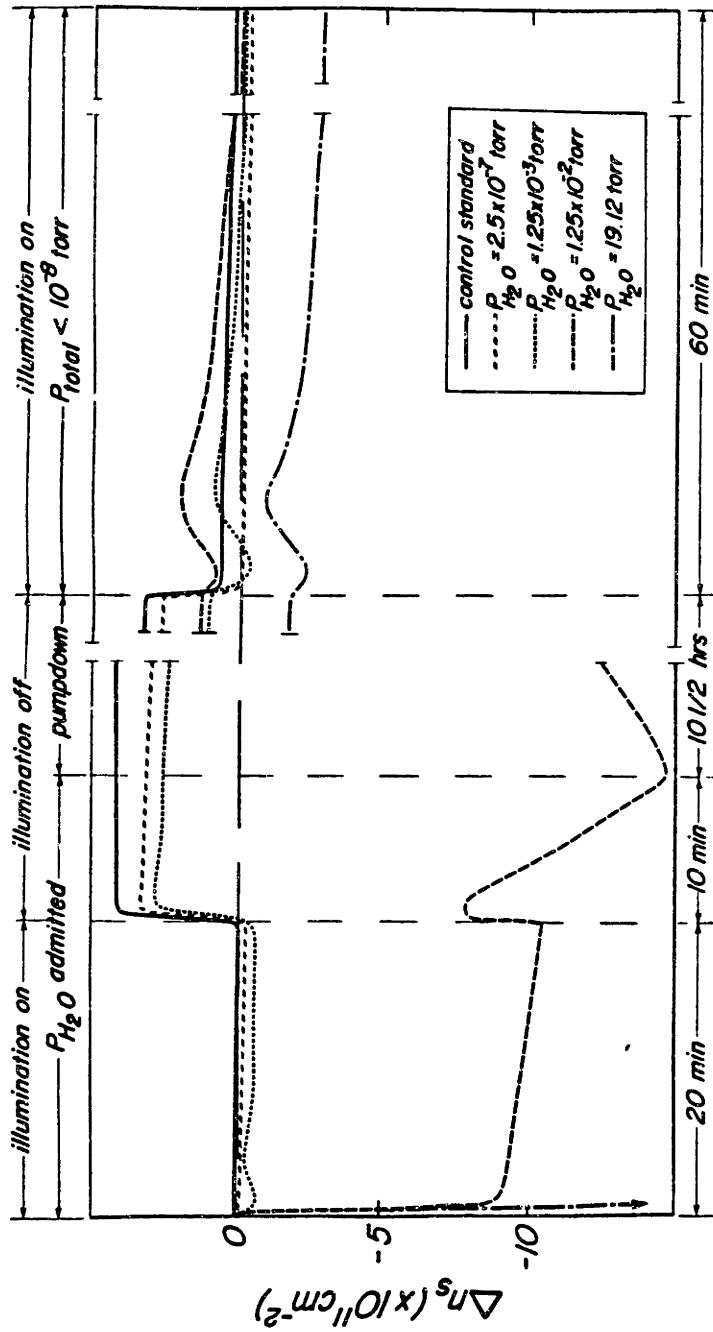


Fig. D-21

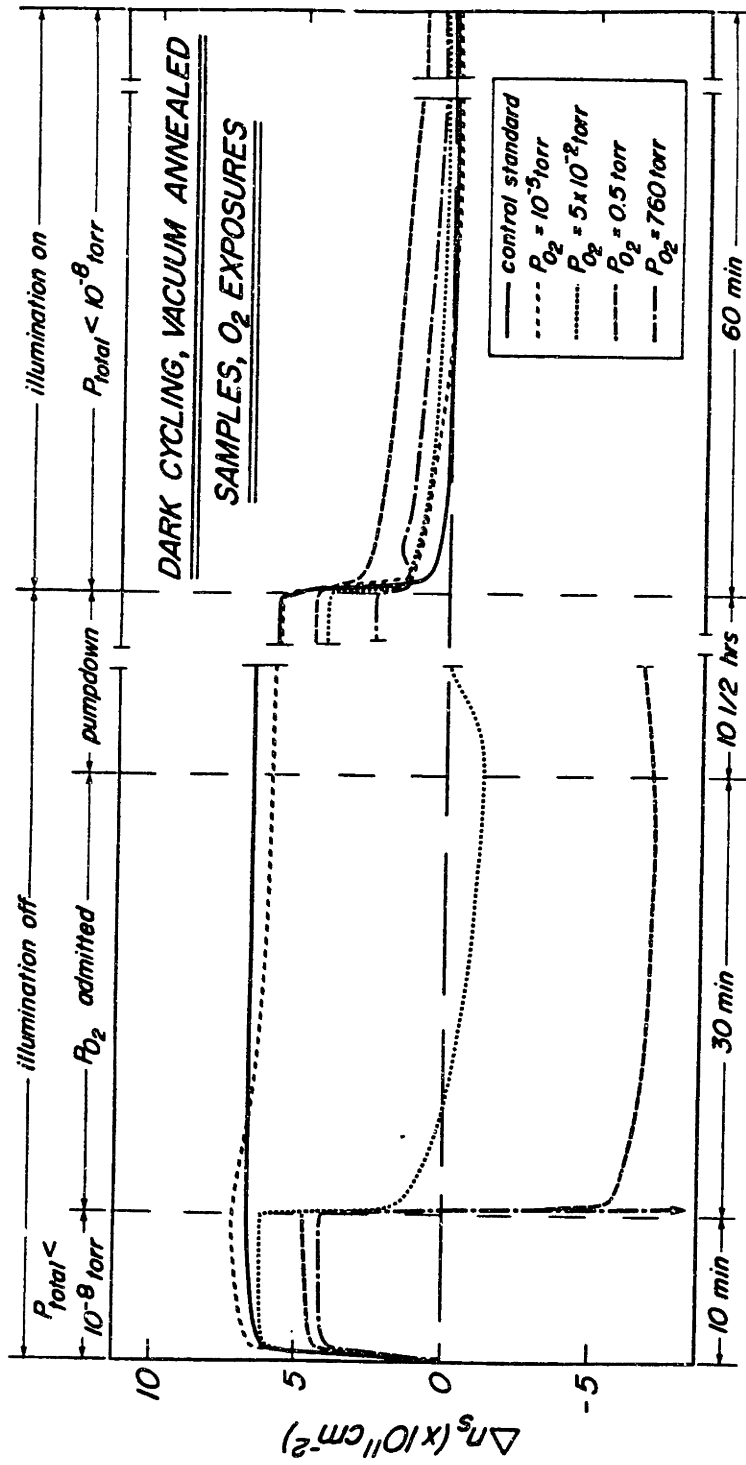


Fig. D-22



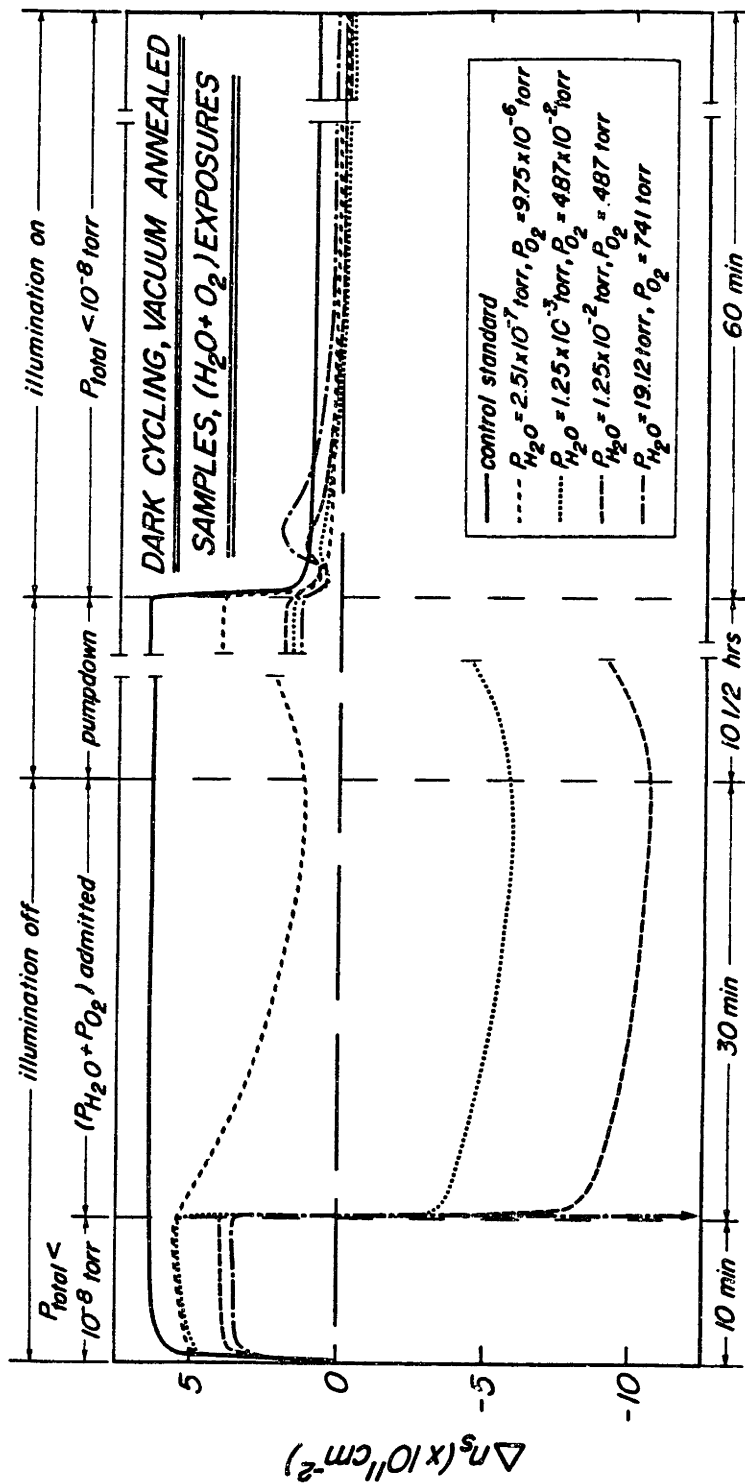


Fig. D-23

**DARK CYCLING, VACUUM ANNEALED SAMPLES, H<sub>2</sub>O EXPOSURES**

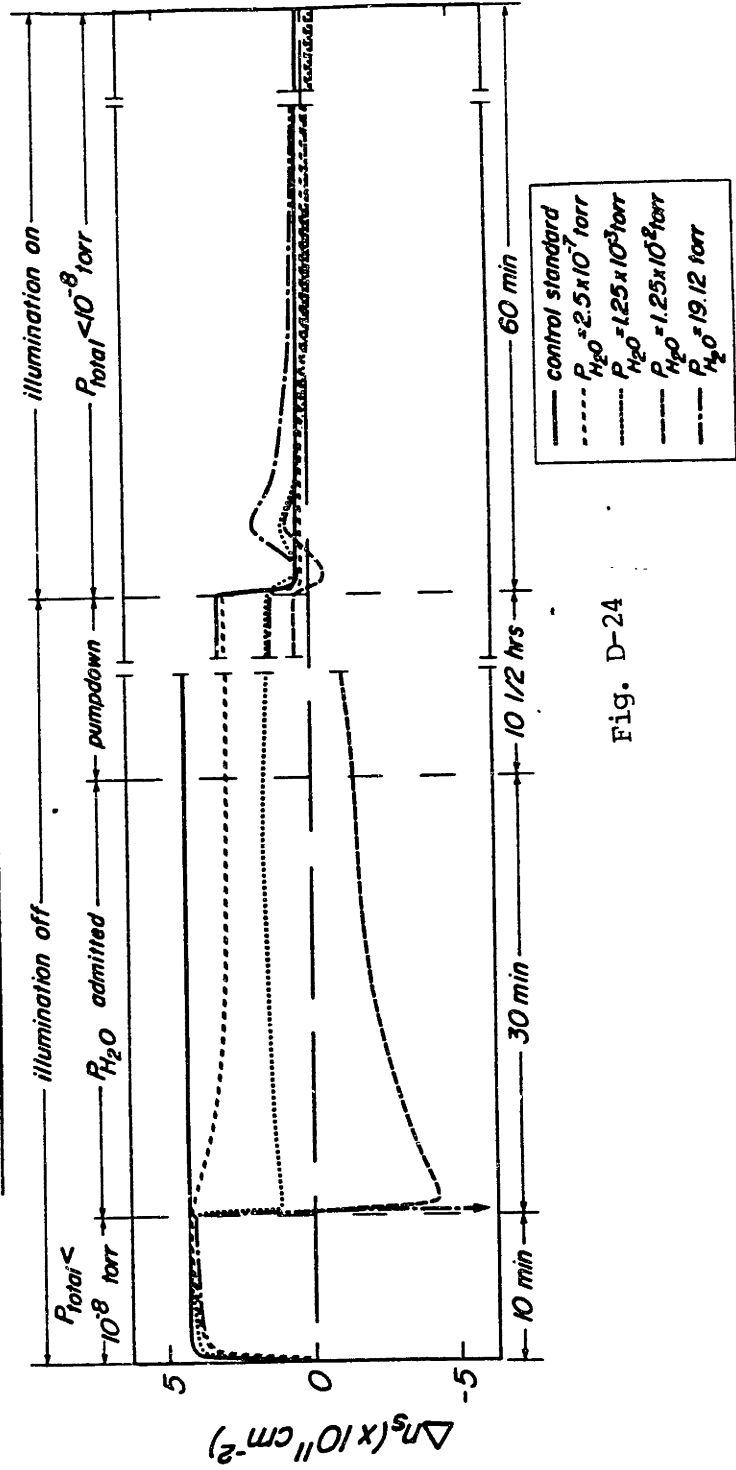


Fig. D-24

## BIBLIOGRAPHY

1. A. Fujishima and K. Honda, *Nature*, **238**, 37 (1972).
2. A. Fujishima, K. Kohayakawa and K. Honda, *J. Electrochem. Soc.*, **122** (11), 1487 (1975).
3. H. Morisaki, T. Watanabe, M. Iwase and K. Yazawa, *Appl. Phys. Lett.*, **29** (6), 338 (1976).
4. D. Laser and A.J. Bard, *J. Electrochem Soc.*, **123** (7), 1027 (1976).
5. R. Williams, *J. Vac. Sci. Tech.*, **13**, 12 (1976).
6. A.J. Nozik, *Appl. Phys. Lett.*, **29**, 150 (1976).
7. W.A. Gerrard and L.M. Rouse, *J. Vac. Sci. Tech.*, **15**, 1155 (1978).
8. L.A. Harris and R.H. Wilson, *Ann. Rev. Mat. Sci.*, **8**, 99 (1978).
9. J.G. Mavroides, *Mat. Sci. Bull.*, **13**, 1379 (1978).
10. A.J. Bard, *Science*, **207**, 139 (1980).
11. H. Gerischer in "Proc. Semiconductor Liquid Junction Solar Cells", 1 (ed. by A. Heller), *Electrochem. Soc.* (1977).
12. H. Gerischer in "Proc. Internat'l Conf. on Photochemical Conversion and Storage of Solar Energy", 77 (ed. by J. Bolton), *Academic Press* (1977).
13. R. Memming, *Electrochim. Acta*, **25**, 77 (1980).
14. D.E. Scaife, *Solar Energy*, **25**, 41 (1980).
15. M.A. Butler and D.S. Ginley, *J. Mat Sci.*, **15**, 1 (1980).
16. H.H. Kung, J.S. Jarett, A.W. Sleight and A. Ferritti, *J. Appl. Phys.*, **48** (6), 2463 (1977).
17. J.G. Mavroides, D.I. Tchernev, J.A. Kafalas and D.F. Kolesar, *Mat. Res. Bull.*, **10**, 1023 (1980).
18. A.J. Nozik, *Nature*, **237**, 383 (1975).
19. F. Mollers, H.J. Tolle and R. Memming, *J. Electrochem. Soc.*, **121**, 1160 (1974).

20. K.L. Hardee and A.J. Bard, J. Electrochem. Soc., 122, (6), 739 (1975).
21. J. Augustynski, J. Hinden, and C. Stalder, J. Electrochem. Soc., 124 (7), 1063 (1977).
22. H. Gerischer, J. Vac. Sci. Tech., 15 (4), 1422 (1978).
23. S.R. Morrison, "The Chemical Physics of Surfaces", Plenum Press (1977).
24. S.R. Morrison, "Electrochemistry at Semiconductor and Oxidized Metal Electrodes", Plenum Press (1980).
25. H.P. Boehme, Discuss. Faraday Soc., 52, 264 (1971).
26. H.S. Ritter, "Pigment Handbook", Vol. III, ed. T.C. Patton, Wiley-Interscience (1973).
27. H. Morisaki, M. Hariya and K. Yazawa, Appl. Phys. Lett., 30 (1), 7 (1977).
28. J. O'M. Bockris and K. Uosaki, Int. J. Hydrogen Energy, 2, 123 (1977).
29. R.N. Noufi, P.A. Kohl, S.N. Frank, and A.J. Bard, J. Electrochem. Soc., 125 (2), 246 (1978).
30. L.A. Harris, D.R. Cross and M.E. Gerstner, J. Electrochem. Soc., 124 (6), 839 (1977).I
31. S.N. Frank and A.J. Bard, J. Am. Chem. Soc., 97 (26), 7428(1975).
32. J. Schoonman, K. Vos and G. Blasse, J. Electrochem. Soc., 128 (5), 1154 (1981).
33. G. Cooper, J.A. Turner and A.J. Nozik, J. Electrochem. Soc., 129 (9), 1973 (1982).
34. H.O. Finklea, J. Electrochem. Soc., 129 (9), 2003 (1982).
35. M. Tomkiewicz, J. Electrochem. Soc., 126 (9), 1505 (1979).

36. M. Tomkiewicz, J. Electrochem. Soc., **127** (7), 1518 (1980).
37. M. Tomkiewicz, Surf. Sci., **101**, 286 (1980).
38. D.C. Cronemeyer, Phys. Rev., **87** (5), 876 (1952).
39. R.G. Breckenridge and W.R. Hosler, Phys. Rev., **91** (4), 793 (1953).
40. D.C. Cronemeyer, Phys. Rev., **113** (5), 1222 (1959).
41. R.R. Addiss, A.K. Ghosh and F.G. Wakim, Appl. Phys. Lett., **12** (11), 397 (1968).
42. A.K. Ghosh, F.G. Wakim and R.R. Addiss, Phys. Rev., **184** (3), 979 (1969).
43. A.K. Ghosh, R.B. Lauer and R.R. Addiss, Phys. Rev. B, **8** (10), 4842 (1973).
44. A.K. Ghosh and H.P. Maruska, J. Electrochem. Soc., **124** (10), 1516 (1977).
45. L.A. Harris and R. Schumaker, J. Electrochem. Soc., **127** (5), 1186 (1980).
46. L.A. Harris and R.H. Wilson, J. Electrochem. Soc., **123** (7), 1010 (1976).
47. M.A. Butler, J. Electrochem. Soc., **126** (2), 338 (1979).
48. J.O'M. Bockris and K. Uosaki, J. Electrochem. Soc., **124** (1), 98 (1977).
49. D.S. Ginley and M.L. Knotek, J. Electrochem. Soc., **126** (12), 2163 (1979).
50. V.E. Henrich, Prog. in Surf. Sci., **9**, 143 (1979).
51. V.E. Henrich, G. Dresselhaus and H.J. Zieger, Solid State Comm., **24**, 623 (1977).
52. M.L. Knotek and P.J. Feibelman, Surf. Sci., **90**, 78 (1979).
53. Y.W. Chung, W.J. Lo and G.A. Somorjai, Surf. Sci., **64**, 588 (1977).
54. R.H. Tait and R.V. Kasowski, Phys. Rev. B, **20** (12), 5178 (1979).

55. C.N. Sayers and N.R. Armstrong, *Surf. Sci.*, **77**, 301 (1978).
56. V.E. Henrich, G. Dresselhaus and H.J. Zeiger, *Phys. Rev. Lett.*, **36** (22), 1335 (1976).
57. V.E. Henrich, G. Dresselhaus and H.J. Zeiger, *J. Vac. Sci. and Tech.*, **15**, 534 (1978).
58. W.J. Lo, Y.W. Chung and G.A. Somorjai, *Surf. Sci.*, **71**, 199 (1978).
59. V.E. Henrich and R.L. Kurtz, *Phys. Rev. B*, **23** (12), 6280 (1981).
60. R.V. Kasowski and R.H. Tait, *Phys. Rev. B*, **20** (12), 5168 (1979).
61. J. M. Kowalski, K.H. Johnson and H.L. Tuller, *J. Electrochem. Soc.*, **127** (9), 1969 (1980).
62. M. Tsukada, C. Satoko and H. Adachi, *J. Phys. Soc. Japan*, **47** (5), 1610 (1979).
63. R.D. Iyengar and M. Codell, *Adv. Coll. Interface Sci.*, **3**, 365 (1972).
64. J. Cunningham and A.L. Penny, *J. Phys. Chem.*, **78** (9), 870 (1974).
65. R.R. Addiss and F.G. Wakim, *Photo. Sci. and Eng.*, **13** (3), 111 (1969).
66. P. Vohl, *Photo. Sci. and Eng.*, **13** (3), 120 (1969).
67. N. Van Hieu and D. Lichtman, *Surf. Sci.*, **103**, 535 (1981).
68. W.W. Gartner, *Phys. Rev.*, **116** (1), 84 (1959).
69. M.A. Butler, *J. App. Phys.*, **48** (5), 1914 (1977).
70. R.H. Wilson, *J. App. Phys.*, **48** (10), 4292 (1977).
71. J. Reichman, *App. Phys. Lett.*, **36** (7), 574 (1980).
72. S.M. Sze, "Physics of Semiconductor Devices", 2nd ed., 248, Wiley-Interscience (1981).
73. H. Gerischer, *J. Electrochem. Soc.*, **13** (11), 1174 (1966).
74. A. Many, Y. Goldstein and N.B. Grover, "Semiconductor Surfaces",

- North Holland (1965).
75. C. Wagner and K. Hauffe, *Z. Electrochem.*, **44**, 172 (1938).
  76. P.B. Weiss, *J. Chem. Phys.*, **20** (9), 1483 (1952).
  77. H.J. Krusmeyer and D.G. Thomas, *J. Phys. Chem. Solids*, **4**, 78 (1958).
  78. C.G.B. Garrett, *J. Chem. Phys.*, **33** (4), 966 (1960).
  79. R.P. Holmstrom, Ph.D. thesis, MIT, Materials Science (1979).
  80. E.H. Weber, *Phys. Stat. Solidi (a)*, **1** (1970).
  81. J. Lagowski, E.S. Sproles and H.C. Gatos, *J. App. Phys.*, **48** (8), 3566 (1977).
  82. Commercial Crystal Laboratories, Inc., South Amboy, NJ.
  83. B.D. Cullity, "Elements of X-Ray Diffraction", Addison-Wesley (1956).
  84. Nalco Chemical Company, Chicago, IL.
  85. W.R. Runyon, "Semiconductor Measurements and Instrumentation", McGraw-Hill (1975).
  86. W.H. Brattain and C.G.B. Garrett, from "Methods of Experimental Physics", Vol. 6b, ed. by V. Lark-Horovitz and V.A. Johnson, Academic Press (1959).
  87. F.A. Kroger, "The Chemistry of Imperfect Crystals", Vol. 2, North Holland (1974).
  88. C.L. Balestra, Sc.D. thesis, MIT, Materials Science (1972).
  89. J. Lagowski and H.C. Gatos, *J. Vac. Sci. Tech.*, **10** (1), 130 (1973).
  90. C.D. Wagner, W.M. Riggs, L.E. Davis, J.F. Moulder and J.E. Muilenberg, "Handbook of X-Ray Photoelectron Spectroscopy", Perkin Elmer, Physical Electronics Division (1979).
  91. C.D. Wagner, L.E. Davis, M.V. Zeller, J.A. Taylor, R.H. Raymond

- and L.H Gale, J. Surf. Interface Anal., 3, 211 (1981).
92. T.A. Carlson, J. Surf. Interface Anal., 4, 125 (1982).
  93. W.J. Landis and J.R. Martin, J. Vac. Sci. Tech., 22 (3) (1984),  
in press.
  94. D.A. Stephenson and N.J. Binkowski, J. Non-Crystalline Solids, 22,  
399 (1976).
  95. "The Oxide Handbook", 2nd ed., G.V. Samsonov, ed., IFI/Plenum  
Publishing (1982).
  96. P. Kofstad, "Nonstoichiometry, Diffusion and Electrical  
Conductivity in Binary Metal Oxides", Wiley-Interscience (1972).
  97. J.F. Baumard, Sol. State Comm., 20, 859 (1976).
  98. V.I. Barbanel and V.N. Bogomolov, Sov. Phys., Sol. State, 11 (9),  
2160 (1970).
  99. H.L. Tuller, in private communication, 5/84.
  100. V. Cristea and V. Babes, Phys. Stat. Sol. (a), 45, 617 (1978).
  101. P.I. Kingsbury, W.D. Olson and O.W. Johnson, Phys.Rev., 175 (3),  
1091 (1968).
  102. O.W. Johnson, W.D. Ohlson and P.I. Kingsbury, Phys.Rev., 175 (3),  
1102 (1968).
  103. R.H. Wilson, L.A. Harris and M.E. Gerstner, J. Electrochem. Soc.,  
126 (4), 844 (1979).
  104. Data for the partial pressure of water vapor in Ar bubbled through  
water from CRC Handbook of Chemistry and Physics, 48th ed.,  
Chemical Rubber Company (1967).
  105. N.B. Hannay, "Semiconductors", Reinhold Publishing Company,  
(1960).
  106. J. Shappir and A. Many, Surf. Sci., 141, 169 (1968).



107. F.A. Grant, Rev. of Mod. Phys., **31**, 646 (1959).
108. C. Palace, H. Berman and C. Frondel, "Dana's System of Mineralogy," Vol. I, 7th ed., p. 544, John Wiley and Sons (1944).
109. R.W.G. Wycoff, "Crystal Structure," p. 5, Interscience (1948).
110. P.D.S. St. Pierre, J. Am. Ceramic Soc., **35**, 188 (1952).
111. A. von Hippel, K. Kalnajs, and W.B. Westphal, J. Phys. Chem. Solids, **23**, 779 (1962).
112. M. Cardona and G. Harbeke, Phys. Rev., **137**, 5A, 1467 (1965).
113. D.M. Eagles, Phys. Chem. Solids, **25**, 1243 (1964).
114. D.C. Cronmeyer, Phys. Rev., **113**, 1222 (1959).
115. G.A. Acket and J. Volger, Phys. Lett., **8**, 245 (1964).
116. H.P.R. Frederiske, J. Appl. Phys. **32**, 2211 (1961).
117. E. Tani and J.F. Baumard, J. Sol. State Chem., **32**, 105 (1980).
118. J. Gautron, J.F. Marucco and P. Lemasson, Mat. Res. Bull., **16**, 575 (1981).
119. J.F. Baumard and F. Gervais, Phys. Rev. B, **13** (4), 2316 (1977).

## BIOGRAPHIC NOTE

The author was born in St. Louis, Missouri on May 2, 1955. He was raised and educated in Salinas, California, graduating from Palma High School. He attended the University of California at San Diego (Revelle College) from 1973 to 1977, receiving a B.A. degree in Applied Mechanics and Engineering Science in June, 1977.

In the fall of 1977, he entered the University of California, Berkeley, in the Department of Materials Science and Engineering. Under the tutelage of Prof. Gareth Thomas, he pursued a master's degree in the T.E.M. and mechanical metallurgy studies of duplex ferritic-martensitic steels. In April, 1979, the author received a M.Sc. degree for his thesis "Duplex Ferritic-Martensitic Low Carbon Steels Containing Silicon, Aluminum and Molybdenum". He also received teaching experience in metallurgy and failure analysis.

From April, 1979, until September, 1980, the author was employed at the Central Engineering Laboratories of FMC Corporation as a Consultant Materials Engineer. In this work he devised, conducted and reported on testing programs for proposed components and failure analyses on production equipment.

In September, 1980 he joined the Electronic Materials Group in MIT's Department of Materials Science and Engineering. He has pursued doctoral studies in semiconductor bulk and surface characterization under the guidance of Prof. Harry Gatos and Dr. Jacek Lagowski.